

# **The state of phytoplankton and bacterioplankton in the Labrador Sea: Atlantic Zone Off-Shelf Monitoring Program 1994-2013**

W.K.W. Li and W.G. Harrison

Ocean and Ecosystem Sciences Division  
Maritimes Region  
Fisheries and Oceans Canada

Bedford Institute of Oceanography  
P.O. Box 1006  
Dartmouth, Nova Scotia  
Canada B2Y 4A2

2014

**Canadian Technical Report of  
Hydrography and Ocean Sciences 302**



Fisheries and Oceans  
Canada

Pêches et Océans  
Canada

**Canada**

## **Canadian Technical Report of Hydrography and Ocean Sciences**

Technical reports contain scientific and technical information of a type that represents a contribution to existing knowledge but which is not normally found in the primary literature. The subject matter is generally related to programs and interests of the Oceans and Science sectors of Fisheries and Oceans Canada.

Technical reports may be cited as full publications. The correct citation appears above the abstract of each report. Each report is abstracted in the data base *Aquatic Sciences and Fisheries Abstracts*.

Technical reports are produced regionally but are numbered nationally. Requests for individual reports will be filled by the issuing establishment listed on the front cover and title page.

Regional and headquarters establishments of Ocean Science and Surveys ceased publication of their various report series as of December 1981. A complete listing of these publications and the last number issued under each title are published in the *Canadian Journal of Fisheries and Aquatic Sciences*, Volume 38: Index to Publications 1981. The current series began with Report Number 1 in January 1982.

## **Rapport technique canadien sur l'hydrographie et les sciences océaniques**

Les rapports techniques contiennent des renseignements scientifiques et techniques qui constituent une contribution aux connaissances actuelles mais que l'on ne trouve pas normalement dans les revues scientifiques. Le sujet est généralement rattaché aux programmes et intérêts des secteurs des Océans et des Sciences de Pêches et Océans Canada.

Les rapports techniques peuvent être cités comme des publications à part entière. Le titre exact figure au-dessus du résumé de chaque rapport. Les rapports techniques sont résumés dans la base de données *Résumés des sciences aquatiques et halieutiques*.

Les rapports techniques sont produits à l'échelon régional, mais numérotés à l'échelon national. Les demandes de rapports seront satisfaites par l'établissement auteur dont le nom figure sur la couverture et la page de titre.

Les établissements de l'ancien secteur des Sciences et Levés océaniques dans les régions et à l'administration centrale ont cessé de publier leurs diverses séries de rapports en décembre 1981. Vous trouverez dans l'index des publications du volume 38 du *Journal canadien des sciences halieutiques et aquatiques*, la liste de ces publications ainsi que le dernier numéro paru dans chaque catégorie. La nouvelle série a commencé avec la publication du rapport numéro 1 en janvier 1982.

Canadian Technical Report of  
Hydrography and Ocean Sciences 302

2014

The state of phytoplankton and bacterioplankton  
in the Labrador Sea:  
Atlantic Zone Off-Shelf Monitoring Program 1994-2013

by

W.K.W. Li and W.G. Harrison

Ocean and Ecosystem Sciences Division  
Maritimes Region  
Fisheries and Oceans Canada

Bedford Institute of Oceanography  
P.O. Box 1006  
Dartmouth, Nova Scotia  
Canada B2Y 4A2  
E-mail: [Bill.Li@dfo-mpo.gc.ca](mailto:Bill.Li@dfo-mpo.gc.ca)

© Her Majesty the Queen in Right of Canada, 2014

Cat. No. Fs97-18/302E ISBN 978-1-100-25283-4 ISSN 0711-6764 (print version)

Cat. No. Fs97-18/302E-PDF ISBN 978-1-100-25284-1 ISSN 1488-5417 (PDF version)

Correct citation for this publication:

Li, W.K.W. and W.G. Harrison 2014. The state of phytoplankton and bacterioplankton in the Labrador Sea: Atlantic Zone Off-Shelf Monitoring Program 1994-2013. Can. Tech. Rep. Hydrogr. Ocean. Sci. 302: xviii + 181 p.



## TABLE OF CONTENTS

LIST OF TABLES .....	v
LIST OF FIGURES .....	vi
ABSTRACT .....	xvi
RÉSUMÉ .....	xvii
PREFACE.....	xviii
1. INTRODUCTION .....	1
1.1 AIMS AND STRATEGY .....	1
1.2 BACKGROUND .....	1
1.3 PURPOSE .....	2
2. METHODS .....	3
2.1 SAMPLING AND ANALYSES.....	3
2.2 DATA HANDLING .....	4
2.3 SATELLITE REMOTE SENSING .....	5
2.4 DATA PRESENTATION .....	5
2.5 DATA SUMMARY .....	7
2.6 DATA AVAILABILITY .....	8
3. RESULTS .....	8
3.1 TEMPERATURE .....	8
3.2 SALINITY .....	9
3.3 STRATIFICATION ( $\Delta$ SIGMA-THETA).....	9
3.4 OXYGEN .....	9
3.5 NITRATE.....	10
3.6 PHOSPHATE .....	10
3.7 SILICATE.....	10
3.8 EXCESS PHOSPHATE .....	11
3.9 EXCESS SILICATE .....	11
3.10 BACTERIA.....	12
3.11 CHLOROPHYLL <i>a</i> .....	13
3.12 <i>SYNECHOCOCCUS</i> .....	14
3.13 PICOEUKARYOTES .....	14

3.14 PICOPHYTOPLANKTON .....	15
3.15 NANOPHYTOPLANKTON.....	15
3.16 PHYTOPLANKTON PIGMENTS.....	15
3.17 PARTICULATE ORGANIC MATTER.....	21
3.18 SPATIAL PATTERNS.....	22
4. DISCUSSION.....	24
4.1 SCIENTIFIC METHOD.....	24
4.2 ANNUAL CYCLES OF SST AND SSC .....	25
4.3 MEAN DISTRIBUTION .....	26
4.4 MULTIYEAR CHANGE .....	27
4.5 IMPLICATIONS .....	29
ACKNOWLEDGMENTS .....	30
REFERENCES .....	31
TABLES .....	34
FIGURES.....	38

**LIST OF TABLES**

Table 1: List of AZOMP Labrador Sea cruises 1994-2013.

Table 2: Location, ocean bottom depth, and section distance for standard AR7W stations in 3 nominal regions of the Labrador Sea.

Table 3: Climatological depth-averaged mean values on AR7W in spring/summer: temperature, salinity, stratification, oxygen, nutrients, chlorophyll *a*, microbial cells.

Table 4: Climatological near-surface mean values on AR7W in spring/summer: POC, PON, phytoplankton pigments.

## LIST OF FIGURES

- Figure 1: Map of the Labrador Sea area showing 28 hydrographic stations on the Atlantic Repeat Hydrography Line 7 West (AR7W).
- Figure 2: Semi-monthly SST record on a 511-pixel virtual AR7W transect for 1998, 1999, 2000, and 2001.
- Figure 3: Semi-monthly SST record on a 511-pixel virtual AR7W transect for 2002, 2003, 2004, and 2005.
- Figure 4: Semi-monthly SST record on a 511-pixel virtual AR7W transect for 2006, 2007, 2008, and 2009.
- Figure 5: Semi-monthly SST record on a 511-pixel virtual AR7W transect for 2010, 2011, 2012, and 2013.
- Figure 6: Semi-monthly SST climatology (1998-2013) on a 511-pixel virtual AR7W transect: contour plot (upper) and 3D-surface plot (lower).
- Figure 7: Semi-monthly SST climatology (1998-2013) in 3 regions: Labrador Shelf and Slope (LSS), Central Labrador Basin (CLB), and Greenland Shelf and Slope (GSS).
- Figure 8: Slope of multiyear change (1998-2013) in SST on a virtual 511-pixel AR7W transect for individual months (May, June, July), for spring/summer (combined May-June-July), and for the whole year (January to December).
- Figure 9: Semi-monthly SSC record on a 511-pixel virtual AR7W transect for 2003, 2004, 2005, and 2006.
- Figure 10: Semi-monthly SSC record on a 511-pixel virtual AR7W transect for 2007, 2008, 2009, and 2010.
- Figure 11: Semi-monthly SSC record on a 511-pixel virtual AR7W transect for 2011, 2012, and 2013.
- Figure 12: Semi-monthly SSC climatology (2003-2013) on a 511-pixel virtual AR7W transect: contour plot (upper) and 3D-surface plot (lower).
- Figure 13: Semi-monthly SSC climatology (2003-2013) in 3 regions: Labrador Shelf and Slope (LSS), Central Labrador Basin (CLB), and Greenland Shelf and Slope (GSS).
- Figure 14: Slope of multiyear change (2003-2013) in SSC on a virtual 511-pixel AR7W transect for individual months (May, June, July), for spring/summer (combined May-June-July), and for the whole year as available (March to October).

Figure 15: Temperature profiles of time-averaged depth-binned values in the upper 100 m layer at Stations 1-8.

Figure 16: Temperature profiles of time-averaged depth-binned values in the upper 100 m layer at Stations 9-16.

Figure 17: Temperature profiles of time-averaged depth-binned values in the upper 100 m layer at Stations 17-24.

Figure 18: Temperature profiles of time-averaged depth-binned values in the upper 100 m layer at Stations 25-28; and averaged over stations at LSS, CLB, and GSS. Lower right panel is the along transect distribution of time-averaged and depth-averaged temperature.

Figure 19: Temperature time series of depth-averaged values at Stations 1-8.

Figure 20: Temperature time series of depth-averaged values at Stations 9-16.

Figure 21: Temperature time series of depth-averaged values at Stations 17-24.

Figure 22: Temperature time series of depth-averaged values at Stations 25-28; and averaged over stations at LSS, CLB, and GSS. Lower right panel is the along transect distribution of standardised multiyear change in depth-averaged temperature.

Figure 23: Salinity profiles of time-averaged depth-binned values in the upper 100 m layer at Stations 1-8.

Figure 24: Salinity profiles of time-averaged depth-binned values in the upper 100 m layer at Stations 9-16.

Figure 25: Salinity profiles of time-averaged depth-binned values in the upper 100 m layer at Stations 17-24.

Figure 26: Salinity profiles of time-averaged depth-binned values in the upper 100 m layer at Stations 25-28; and averaged over stations at LSS, CLB, and GSS. Lower right panel is the along transect distribution of time-averaged and depth-averaged salinity.

Figure 27: Salinity time series of depth-averaged values at Stations 1-8.

Figure 28: Salinity time series of depth-averaged values at Stations 9-16.

Figure 29: Salinity time series of depth-averaged values at Stations 17-24.

Figure 30: Salinity time series of depth-averaged values at Stations 25-28; and averaged over stations at LSS, CLB, and GSS. Lower right panel is the along transect distribution of standardised multiyear change in depth-averaged salinity.

Figure 31: Density profiles of time-averaged depth-binned values in the upper 100 m layer at Stations 1-8.

Figure 32: Density profiles of time-averaged depth-binned values in the upper 100 m layer at Stations 9-16.

Figure 33: Density profiles of time-averaged depth-binned values in the upper 100 m layer at Stations 17-24.

Figure 34: Density profiles of time-averaged depth-binned values in the upper 100 m layer at Stations 25-28; and averaged over stations at LSS, CLB, and GSS. Lower right panel is the along transect distribution of time-averaged values for the difference between maximum and minimum density ( $\sigma_{\theta_{max}} - \sigma_{\theta_{min}}$ ) in the upper 100m layer.

Figure 35: Density-difference ( $\sigma_{\theta_{max}} - \sigma_{\theta_{min}}$ ) time series at Stations 1-8.

Figure 36: Density-difference ( $\sigma_{\theta_{max}} - \sigma_{\theta_{min}}$ ) time series at Stations 9-16.

Figure 37: Density-difference ( $\sigma_{\theta_{max}} - \sigma_{\theta_{min}}$ ) time series at Stations 17-24.

Figure 38: Density-difference ( $\sigma_{\theta_{max}} - \sigma_{\theta_{min}}$ ) time series at Stations 25-28; and averaged over stations at LSS, CLB, and GSS. Lower right panel is the along transect distribution of standardised multiyear change in density-difference.

Figure 39: Dissolved oxygen profiles of time-averaged depth-binned values in the upper 100 m layer at Stations 1-8.

Figure 40: Dissolved oxygen profiles of time-averaged depth-binned values in the upper 100 m layer at Stations 9-16.

Figure 41: Dissolved oxygen profiles of time-averaged depth-binned values in the upper 100 m layer at Stations 17-24.

Figure 42: Dissolved oxygen profiles of time-averaged depth-binned values in the upper 100 m layer at Stations 25-28; and averaged over stations at LSS, CLB, and GSS. Lower right panel is the along transect distribution of time-averaged and depth-averaged dissolved oxygen.

Figure 43: Dissolved oxygen time series of depth-averaged values at Stations 1-8.

Figure 44: Dissolved oxygen time series of depth-averaged values at Stations 9-16.

Figure 45: Dissolved oxygen time series of depth-averaged values at Stations 17-24.

Figure 46: Dissolved oxygen time series of depth-averaged values at Stations 25-28; and averaged over stations at LSS, CLB, and GSS. Lower right panel is the along

transect distribution of standardised multiyear change in depth-averaged dissolved oxygen.

Figure 47: Nitrate profiles of time-averaged depth-binned values in the upper 100 m layer at Stations 1-8.

Figure 48: Nitrate profiles of time-averaged depth-binned values in the upper 100 m layer at Stations 9-16.

Figure 49: Nitrate profiles of time-averaged depth-binned values in the upper 100 m layer at Stations 17-24.

Figure 50: Nitrate profiles of time-averaged depth-binned values in the upper 100 m layer at Stations 25-28; and averaged over stations at LSS, CLB, and GSS. Lower right panel is the along transect distribution of time-averaged and depth-averaged nitrate.

Figure 51: Nitrate time series of depth-averaged values at Stations 1-8.

Figure 52: Nitrate time series of depth-averaged values at Stations 9-16.

Figure 53: Nitrate time series of depth-averaged values at Stations 17-24.

Figure 54: Nitrate time series of depth-averaged values at Stations 25-28; and averaged over stations at LSS, CLB, and GSS. Lower right panel is the along transect distribution of standardised multiyear change in depth-averaged nitrate.

Figure 55: Phosphate profiles of time-averaged depth-binned values in the upper 100 m layer at Stations 1-8.

Figure 56: Phosphate profiles of time-averaged depth-binned values in the upper 100 m layer at Stations 9-16.

Figure 57: Phosphate profiles of time-averaged depth-binned values in the upper 100 m layer at Stations 17-24.

Figure 58: Phosphate profiles of time-averaged depth-binned values in the upper 100 m layer at Stations 25-28; and averaged over stations at LSS, CLB, and GSS. Lower right panel is the along transect distribution of time-averaged and depth-averaged phosphate.

Figure 59: Phosphate time series of depth-averaged values at Stations 1-8.

Figure 60: Phosphate time series of depth-averaged values at Stations 9-16.

Figure 61: Phosphate time series of depth-averaged values at Stations 17-24.

Figure 62: Phosphate time series of depth-averaged values at Stations 25-28; and averaged over stations at LSS, CLB, and GSS. Lower right panel is the along transect distribution of standardised multiyear change in depth-averaged phosphate.

Figure 63: Silicate profiles of time-averaged depth-binned values in the upper 100 m layer at Stations 1-8.

Figure 64: Silicate profiles of time-averaged depth-binned values in the upper 100 m layer at Stations 9-16.

Figure 65: Silicate profiles of time-averaged depth-binned values in the upper 100 m layer at Stations 17-24.

Figure 66: Silicate profiles of time-averaged depth-binned values in the upper 100 m layer at Stations 25-28; and averaged over stations at LSS, CLB, and GSS. Lower right panel is the along transect distribution of time-averaged and depth-averaged silicate.

Figure 67: Silicate time series of depth-averaged values at Stations 1-8.

Figure 68: Silicate time series of depth-averaged values at Stations 9-16.

Figure 69: Silicate time series of depth-averaged values at Stations 17-24.

Figure 70: Silicate time series of depth-averaged values at Stations 25-28; and averaged over stations at LSS, CLB, and GSS. Lower right panel is the along transect distribution of standardised multiyear change in depth-averaged silicate.

Figure 71: Excess phosphate profiles of time-averaged depth-binned values in the upper 100 m layer at Stations 1-8.

Figure 72: Excess phosphate profiles of time-averaged depth-binned values in the upper 100 m layer at Stations 9-16.

Figure 73: Excess phosphate profiles of time-averaged depth-binned values in the upper 100 m layer at Stations 17-24.

Figure 74: Excess phosphate profiles of time-averaged depth-binned values in the upper 100 m layer at Stations 25-28; and averaged over stations at LSS, CLB, and GSS. Lower right panel is the along transect distribution of time-averaged and depth-averaged excess phosphate.

Figure 75: Excess phosphate time series of depth-averaged values at Stations 1-8.

Figure 76: Excess phosphate time series of depth-averaged values at Stations 9-16.

Figure 77: Excess phosphate time series of depth-averaged values at Stations 17-24.



Figure 78: Excess phosphate time series of depth-averaged values at Stations 25-28; and averaged over stations at LSS, CLB, and GSS. Lower right panel is the along transect distribution of standardised multiyear change in depth-averaged excess phosphate.

Figure 79: Excess silicate profiles of time-averaged depth-binned values in the upper 100 m layer at Stations 1-8.

Figure 80: Excess silicate profiles of time-averaged depth-binned values in the upper 100 m layer at Stations 9-16.

Figure 81: Excess silicate profiles of time-averaged depth-binned values in the upper 100 m layer at Stations 17-24.

Figure 82: Excess silicate profiles of time-averaged depth-binned values in the upper 100 m layer at Stations 25-28; and averaged over stations at LSS, CLB, and GSS. Lower right panel is the along transect distribution of time-averaged and depth-averaged excess silicate.

Figure 83: Excess silicate time series of depth-averaged values at Stations 1-8.

Figure 84: Excess silicate time series of depth-averaged values at Stations 9-16.

Figure 85: Excess silicate time series of depth-averaged values at Stations 17-24.

Figure 86: Excess silicate time series of depth-averaged values at Stations 25-28; and averaged over stations at LSS, CLB, and GSS. Lower right panel is the along transect distribution of standardised multiyear change in depth-averaged excess silicate.

Figure 87: Bacteria profiles of time-averaged depth-binned values in the upper 100 m layer at Stations 1-8.

Figure 88: Bacteria profiles of time-averaged depth-binned values in the upper 100 m layer at Stations 9-16.

Figure 89: Bacteria profiles of time-averaged depth-binned values in the upper 100 m layer at Stations 17-24.

Figure 90: Bacteria profiles of time-averaged depth-binned values in the upper 100 m layer at Stations 25-28; and averaged over stations at LSS, CLB, and GSS. Lower right panel is the along transect distribution of time-averaged and depth-averaged bacteria.

Figure 91: Bacteria time series of depth-averaged values at Stations 1-8.

Figure 92: Bacteria time series of depth-averaged values at Stations 9-16.

Figure 93: Bacteria time series of depth-averaged values at Stations 17-24.

Figure 94: Bacteria time series of depth-averaged values at Stations 25-28; and averaged over stations at LSS, CLB, and GSS. Lower right panel is the along transect distribution of standardised multiyear change in depth-averaged bacteria.

Figure 95: Chlorophyll *a* profiles of time-averaged depth-binned values in the upper 100 m layer at Stations 1-8.

Figure 96: Chlorophyll *a* profiles of time-averaged depth-binned values in the upper 100 m layer at Stations 9-16.

Figure 97: Chlorophyll *a* profiles of time-averaged depth-binned values in the upper 100 m layer at Stations 17-24.

Figure 98: Chlorophyll *a* profiles of time-averaged depth-binned values in the upper 100 m layer at Stations 25-28; and averaged over stations at LSS, CLB, and GSS. Lower right panel is the along transect distribution of time-averaged and depth-averaged chlorophyll *a*.

Figure 99: Chlorophyll *a* time series of depth-averaged values at Stations 1-8.

Figure 100: Chlorophyll *a* time series of depth-averaged values at Stations 9-16.

Figure 101: Chlorophyll *a* time series of depth-averaged values at Stations 17-24.

Figure 102: Chlorophyll *a* time series of depth-averaged values at Stations 25-28; and averaged over stations at LSS, CLB, and GSS. Lower right panel is the along transect distribution of standardised multiyear change in depth-averaged chlorophyll *a*.

Figure 103: *Synechococcus* profiles of time-averaged depth-binned values in the upper 100 m layer at Stations 1-8.

Figure 104: *Synechococcus* profiles of time-averaged depth-binned values in the upper 100 m layer at Stations 9-16.

Figure 105: *Synechococcus* profiles of time-averaged depth-binned values in the upper 100 m layer at Stations 17-24.

Figure 106: *Synechococcus* profiles of time-averaged depth-binned values in the upper 100 m layer at Stations 25-28; and averaged over stations at LSS, CLB, and GSS. Lower right panel is the along transect distribution of time-averaged and depth-averaged *Synechococcus*.

Figure 107: *Synechococcus* time series of depth-averaged values at Stations 1-8.

Figure 108: *Synechococcus* time series of depth-averaged values at Stations 9-16.

Figure 109: *Synechococcus* time series of depth-averaged values at Stations 17-24.

Figure 110: *Synechococcus* time series of depth-averaged values at Stations 25-28; and averaged over stations at LSS, CLB, and GSS. Lower right panel is the along transect distribution of standardised multiyear change in depth-averaged *Synechococcus*.

Figure 111: Picoeukaryotes profiles of time-averaged depth-binned values in the upper 100 m layer at Stations 1-8.

Figure 112: Picoeukaryotes profiles of time-averaged depth-binned values in the upper 100 m layer at Stations 9-16.

Figure 113: Picoeukaryotes profiles of time-averaged depth-binned values in the upper 100 m layer at Stations 17-24.

Figure 114: Picoeukaryotes profiles of time-averaged depth-binned values in the upper 100 m layer at Stations 25-28; and averaged over stations at LSS, CLB, and GSS. Lower right panel is the along transect distribution of time-averaged and depth-averaged picoeukaryotes.

Figure 115: Picoeukaryotes time series of depth-averaged values at Stations 1-8.

Figure 116: Picoeukaryotes time series of depth-averaged values at Stations 9-16.

Figure 117: Picoeukaryotes time series of depth-averaged values at Stations 17-24.

Figure 118: Picoeukaryotes time series of depth-averaged values at Stations 25-28; and averaged over stations at LSS, CLB, and GSS. Lower right panel is the along transect distribution of standardised multiyear change in depth-averaged picoeukaryotes.

Figure 119: Nanophytoplankton profiles of time-averaged depth-binned values in the upper 100 m layer at Stations 1-8.

Figure 120: Nanophytoplankton profiles of time-averaged depth-binned values in the upper 100 m layer at Stations 9-16.

Figure 121: Nanophytoplankton profiles of time-averaged depth-binned values in the upper 100 m layer at Stations 17-24.

Figure 122: Nanophytoplankton profiles of time-averaged depth-binned values in the upper 100 m layer at Stations 25-28; and averaged over stations at LSS, CLB, and GSS. Lower right panel is the along transect distribution of time-averaged and depth-averaged nanophytoplankton.

Figure 123: Nanophytoplankton time series of depth-averaged values at Stations 1-8.

Figure 124: Nanophytoplankton time series of depth-averaged values at Stations 9-16.

Figure 125: Nanophytoplankton time series of depth-averaged values at Stations 17-24.

Figure 126: Nanophytoplankton time series of depth-averaged values at Stations 25-28; and averaged over stations at LSS, CLB, and GSS. Lower right panel is the along transect distribution of standardised multiyear change in depth-averaged nanophytoplankton.

Figure 127: Along transect distribution of time-averaged near-surface phytoplankton pigments: But-fuco, Hex-fuco, Allo, Chla, Chlb, Chlc1c2, Chlc3, Diadino.

Figure 128: Along transect distribution of time-averaged near-surface phytoplankton pigments: Diato, Fuco, Peri, Zea, DiagPig; and particulate organic matter: POC, PON, POC:PON.

Figure 129: Along transect distribution of standardised multiyear change in near-surface phytoplankton pigments: But-fuco, Hex-fuco, Allo, Chla, Chlb, Chlc1c2, Chlc3, Diadino.

Figure 130: Along transect distribution of standardised multiyear change in near-surface phytoplankton pigments: Diato, Fuco, Peri, Zea, DiagPig; and particulate organic matter: POC, PON, POC:PON.

Figure 131: Full-depth vertical section plots of bacteria in 1999 and 2000.

Figure 132: Full-depth vertical section plots of bacteria in 2001 and 2002.

Figure 133: Full-depth vertical section plots of bacteria in 2003 and 2004.

Figure 134: Full-depth vertical section plots of bacteria in 2005 and 2006.

Figure 135: Full-depth vertical section plots of bacteria in 2007 and 2008.

Figure 136: Full-depth vertical section plots of bacteria in 2009 and 2010.

Figure 137: Full-depth vertical section plots of bacteria in 2011 and 2012.

Figure 138: Full-depth vertical section plot of bacteria, 1999-2012 average.

Figure 139: Full-depth profiles of bacteria at Station 17, 1999-2006. Depth scale is square root meters, showing boundaries between epipelagic, mesopelagic, and bathypelagic zones.

Figure 140: Full-depth profiles of bacteria at Station 17, 2007-2012. Depth scale is square root meters, showing boundaries between epipelagic, mesopelagic, and bathypelagic zones. Bottom middle panel shows ensemble of profiles from 1999-2012.

Figure 141: Time series of bacterial depth profiles at Station 17. Depth scale is square root meters, showing boundaries between epipelagic, mesopelagic, and bathypelagic zones.

Figure 142: Time series of bacterial inventories integrated within depth layers of epipelagic, mesopelagic, and bathypelagic zones at Station 17; and showing standardised multiyear change.

Figure 143: Pattern of spatial coherence in mean distribution of physical, chemical, and biological variables adjusted to zero-mean and unit deviation; variables are ranked by the loading of the first principal component.

Figure 144: Pattern of spatial coherence in multiyear change of physical, chemical, and biological variables expressed in the common unit of standard deviates per year; variables are ranked by the loading of the first principal component.

**ABSTRACT**

Li, W.K.W. and W.G. Harrison 2014. The state of phytoplankton and bacterioplankton in the Labrador Sea: Atlantic Zone Off-Shelf Monitoring Program 1994-2013. Can. Tech. Rep. Hydrogr. Ocean. Sci. 302: xviii + 181 p.

Since the early 1990s, the Atlantic Zone Off-Shelf Monitoring Program has undertaken dedicated oceanographic sampling in the Labrador Sea in spring or early summer, which regularly includes 28 stations on the Atlantic Repeat Hydrography Line 7 West (AR7W). This report presents a detailed record of microbial plankton in the context of their immediate physical and chemical environment at these 28 stations from 1994 to 2013. It provides information on microbes that is supplementary to annual data of the core program reported to the Canadian Science Advisory Secretariat. Descriptions are given for both the climatological mean state and the rate of multiyear change for picophytoplankton, nanophytoplankton, bacterioplankton, and associated phytoplankton pigments. Year-round remote sensing data on sea surface temperature and sea surface chlorophyll establish the annual cycles which provide seasonal context to the *in situ* observations. The physical (temperature, salinity, stratification), chemical (nitrate, phosphate, silicate, oxygen), and biological variables are compared on the common basis of dimensionless standard anomalies. The results of such comparisons are ordered sequences of variables ranked by relative spatial coherence across AR7W. A key biological observation arising from the 20-year time series of spring/summer *in situ* measurements is that bulk phytoplankton biomass has increased at almost all 28 stations, and most strongly on the Greenland Shelf and Slope where the biomass is normally highest.

## RÉSUMÉ

Li, W.K.W. and W.G. Harrison 2014. Situation du phytoplancton et du bactérioplancton dans la mer du Labrador: Programme de monitoring de la zone Atlantique au large du plateau continental 1994-2013. Rapp. tech. can. hydrogr. sci. océan. 302: xviii + 181 p.

Depuis le début des années 1990, le Programme de monitoring de la zone Atlantique au large du plateau continental a entrepris un échantillonnage océanographique dédié dans la mer du Labrador au printemps ou au début de l'été effectué régulièrement à 28 stations réparties le long du transect 7 ouest utilisé pour des observations hydrographiques répétées dans l'Atlantique (AR7W). Ce rapport présente un dossier détaillé sur le plancton microbien dans le contexte de son environnement physique et chimique immédiat à ces 28 stations de 1994 à 2013. Il fournit des renseignements sur les microbes qui viennent compléter les données annuelles du programme de base déclarées au Secrétariat canadien de consultation scientifique. Les descriptions sont fournies pour l'état moyen du climat et le taux de variation pluriannuelle du picophytoplancton, du nanophytoplancton, du bactérioplancton ainsi que des pigments phytoplanctoniques associés. Toute l'année, les données de télédétection de la température de la surface de la mer et de la chlorophylle à la surface de la mer établissent les cycles annuels qui fournissent un contexte saisonnier pour les observations in situ. Les variables physiques (température, salinité, stratification), chimiques (nitrate, phosphate, silicate, oxygène) et biologiques sont comparées sur une base commune d'anomalies adimensionnelles standard. Les résultats de ces comparaisons sont des séquences ordonnées de variables classées par cohérence spatiale relative le long d'AR7W. L'une des principales observations biologiques découlant de la série chronologique s'étendant sur 20 ans des mesures réalisées in situ au printemps et à l'été est que la biomasse globale du phytoplancton a augmenté à presque toutes les 28 stations, et plus fortement sur le plateau du Groenland et le talus où la biomasse est généralement plus élevée.

**PREFACE**

This is one in a set of three reports that document the mean state and interannual change of phytoplankton and bacterioplankton in the ocean waters of Atlantic Canada from program inception to the end of 2013. This report documents the observations made in the Labrador Sea in the Atlantic Zone Off-Shelf Monitoring Program. The companion reports document observations made in the Scotian Shelf and Slope in the Atlantic Zone Monitoring Program<sup>1</sup>, and at the Compass Buoy Station in the Bedford Basin Monitoring Program<sup>2</sup>. Together, this set of three reports comprises an integrated technical output of the core non-research component of microbial oceanographic activity in Ocean and Ecosystem Sciences Division aligned to the DFO hierarchical program architecture of Sustainable Aquatic Ecosystems / Oceans Management / Ecosystem Assessments / Aquatic Ecosystems Science.

---

<sup>1</sup> Li, W.K.W. 2014. The state of phytoplankton and bacterioplankton on the Scotian Shelf and Slope: Atlantic Zone Monitoring Program 1997-2013. Can. Tech. Rep. Hydrogr. Ocean. Sci. 303: xx + 140 p.

<sup>2</sup> Li, W.K.W. 2014. The state of phytoplankton and bacterioplankton at the Compass Buoy Station : Bedford Basin Monitoring Program 1992-2013. Can. Tech. Rep. Hydrogr. Ocean. Sci. 304: xiv + 122p.



## 1. INTRODUCTION

### 1.1 AIMS AND STRATEGY

The Atlantic Zone Off-Shelf Monitoring Program (AZOMP) aims to monitor variability in the ocean climate and plankton affecting regional climate and ecosystems off Atlantic Canada and the global climate system. To this end, the objective is to collect and analyse physical, chemical and biological oceanographic observations from the continental slope and deeper waters of the Northwest Atlantic<sup>3</sup>. The largest component of AZOMP is the Labrador Sea Monitoring Program (Hendry and Harrison 2007) which conducts annual observations on an oceanographic section across the Labrador Sea, referred to as the Atlantic Repeat Hydrography Line 7 West (AR7W)<sup>4</sup>.

In aspiring towards a goal of monitoring climate and plankton variability, AZOMP has ostensibly adopted an analytic strategy to link cause and effect - a focus on mechanistic oceanographic processes over indeterminate complex environmental history, which, arguably, may be a useful alternative to a synthetic approach for managing ecological futures. With this strategy, AZOMP is firmly grounded in phenomenological description of the cumulative oceanographic data collection. The ensuing data reduction and statistical predictions are not explicitly referenced to a null hypothesis in the tradition of hypothetico-deductive science amenable to strong test. Instead, AZOMP collects circumstantial evidence that corroborates (or not) the alternative hypothesis of biological change produced by a physical or chemical cause of interest. In this reductionist heuristic, we accept that the reification of statistics constructs the knowledge representation which enables us to understand and explain, at least in a probabilistic manner.

### 1.2 BACKGROUND

Every year since the early 1990s, the Labrador Sea Monitoring Program has undertaken dedicated oceanographic sampling on AR7W in spring, sometimes extending into summer. The ~900 km section extends from Hamilton Bank on the Labrador Shelf, over the Labrador Slope, across the deep central Labrador Basin, over the narrow Greenland Slope, to Cape Desolation on the Greenland Shelf. Local ocean conditions permitting, a total of 28 fixed stations are occupied for hydrographic sampling of plankton and related variables. The standard measurements are of conductivity, temperature, pressure, dissolved oxygen, red fluorescence, and photosynthetically active radiation (all in continuous profiling mode); nitrate, phosphate, silicate, and bulk

---

<sup>3</sup> <http://www.bio.gc.ca/science/monitoring-monitorage/azomp-pmzao/azomp-pmzao-eng.php>

<sup>4</sup> <http://www.bio.gc.ca/science/monitoring-monitorage/azomp-pmzao/labrador/labrador-eng.php>

chlorophyll *a* (all from selected discrete depths); and mesozooplankton (integrated vertical haul).

At these stations, the core measurement of the primary trophic level is bulk chlorophyll *a*, which is a cellular biomarker indicating the photosynthetically-capable portion of the plankton community. Although potentially rich in information, this bulk descriptor is nevertheless no more than a high level aggregate of the extensive biological diversity contributing to oxygenic photolithotrophic primary production. To disaggregate the bulk, the component organisms can be classified in a number of different ways: by their systematic names (taxonomy), by their evolutionary lineage (phylogeny), by their metabolism (trophic mode), by their biological attributes and habits (functional traits), by their chemical composition (stoichiometry), or by their physical size (allometry). These and other classifications reflect different facets of life: arguably, no facet is inherently pre-eminent in ecological enquiry; rather, each facet can be more or less useful in particular contexts. These measurements, when made, supplement the information provided by the core measurement of chlorophyll *a*.

With respect to organism size, the unicellular forms of plankton in the ocean span three orders of magnitude (a thousand-fold) in linear dimension, which is equivalent to nine orders of magnitude (a billion-fold) in volume or mass dimension. By convention (Sieburth et al. 1978), unicellular plankton are grouped into three size classes that are designated by linear dimensions of equivalent spherical diameter but adhere to a nomenclature that corresponds approximately to the live weights of the organisms at the upper end of their range. Thus, picoplankton, nanoplankton, and microplankton occupy the respective size windows of 0.2-2.0  $\mu\text{m}$ , 2-20  $\mu\text{m}$ , and 20-200  $\mu\text{m}$ ; and they have respective live weights of approximately unit picogram, nanogram, and microgram. In each of these microbial size classes, there are members that are primary producers (picophytoplankton, nanophytoplankton, microphytoplankton), members that are primary consumers (bacterioplankton, nanoheterotrophic protists, microheterotrophic protists), and members that are mixotrophic, contributing to both primary and secondary production (Flynn et al. 2013).

### **1.3 PURPOSE**

The present report has a two-fold purpose. First, it describes both the climatological mean state and the interannual change for core variables (chlorophyll *a*, nutrients, temperature, salinity, oxygen) as well as for supplementary variables (bacteria, picophytoplankton, nanophytoplankton, and associated phytoplankton pigments) at the aforementioned 28 stations over the 20 year period (1994-2013). As these *in situ* observations only describe the state of the ocean in spring and summer, we complement

them with the annual cycle of sea surface temperature and sea surface chlorophyll recorded by year-round satellite remote sensing.

Second, this report relates the multiyear change of microbial plankton variables to their physical and chemical environment. We compare the rate of change over time of all variables on the common basis of dimensionless standard anomalies. The result is a visual pattern of spatial coherence (or anti-coherence) in multiyear change of physical, chemical, and biological variables along the entire oceanographic section. This report is a detailed evidentiary record of microbial plankton and their environment in the Labrador Sea, against which scientific hypotheses may be tested.

## 2. METHODS

### 2.1 SAMPLING AND ANALYSES

Data reported in this document were collected on 20 cruises in the Labrador Sea from 1994 to 2013 (Table 1). The earliest start of a cruise was day 126 (May 6, 2011), and the latest start was day 194 (July 13, 2003). On average, the cruises started on day  $149 \pm 21$  and lasted for  $20 \pm 5$  days. The actual dates on which AR7W stations were occupied can be extracted from the datasets made available. Other cruises in the fall (1996-026) and winter (2002-075) are not included in this report.

The locations of the 28 standard AR7W stations are mapped in Figure 1 and listed in Table 2. In this report, we group the stations into 3 nominal regions: the Labrador Shelf and Slope (LSS) for stations 1-10; the Central Labrador Basin (CLB) for stations 11-23; the Greenland Shelf and Slope (GSS) for stations 24-28. According to this nominal assignment, CLB extends over a region where ocean bottom depth exceeds 2900 m; LSS covers the region of shallower depths to the west, and GSS covers the region of shallower depths to the east.

Samples for nutrients, chlorophyll *a*, picophytoplankton, and nanophytoplankton were collected at nominal 10 m depth intervals from the surface to 100 m. Samples for heterotrophic bacteria (which are not limited to the euphotic zone) were collected from each one of 24 Niskin bottles on full hydrographic casts from sea surface down to near the ocean bottom. For POC/PON and phytoplankton pigments, only near-surface samples were collected.

Standard method protocols were used to record hydrographic profiles, to collect water samples, and to analyse nutrients and chlorophyll *a* (Mitchell et al. 2002). Particulate organic carbon (POC) and nitrogen (PON) were measured by Perkin Elmer

Series II CHNS/O Analyzer 2400. For picophytoplankton (picoeukaryotic algae and *Synechococcus* cyanobacteria), nanophytoplankton, and bacterioplankton, the protocols for fixing and analysing samples by flow cytometry have been previously described (Li and Dickie 2001).

For phytoplankton pigments, the method of high performance liquid chromatography (Stuart and Head 2005) was used to estimate concentrations of the following pigments:

- 19'-butanoyloxyfucoxanthin [But-fuco]
- 19'-hexanoyloxyfucoxanthin [Hex-fuco]
- alloxanthin [Allo]
- chlorophyll *a* [Chl*a*]
- chlorophyll *b* [Chl*b*]
- chlorophyll *c*<sub>1</sub>+*c*<sub>2</sub> [Chl*c*<sub>1</sub>*c*<sub>2</sub>]
- chlorophyll *c*<sub>3</sub> [Chl*c*<sub>3</sub>]
- diadinoxanthin [Diadino]
- diatoxanthin [Diato]
- fucoxanthin [Fuco]
- peridinin [Peri]
- zeaxanthin [Zea]

Following Uitz et al. (2006), we constructed a weighted sum of diagnostic pigments [DiagPig] as a quasi-measure of total chlorophyll *a*:

$$[\text{DiagPig}] = 1.41[\text{Fuco}] + 1.41[\text{Peri}] + 1.27[\text{Hex-fuco}] + 0.35[\text{But-fuco}] + 0.60[\text{Allo}] + 1.01[\text{Chl}b] + 0.86[\text{Zea}]$$

## 2.2 DATA HANDLING

At the time of collection, each water sample was assigned a unique 6-digit identification number that served to link all variously-measured physical, chemical, and biological variables to the date, time, geographic location, and depth of sampling. Metadata included cruise number and station name.

Hydrographic data (temperature, salinity, pressure, density, oxygen) were extracted from continuous vertical profiles to match the actual depths from which water samples were collected. A measure of stratification ( $\Delta$  sigma-theta) was calculated by taking the arithmetic difference between maximum and minimum values of water density (sigma-theta) in the upper 100 m.

All data were compiled and consolidated into a single flat file. For ease of manipulation, all data (which were pressure-referenced) were assigned to 10 m depth bins using the Microsoft Excel built-in function “mround”. Data manipulations were handled using an Excel pivot table created from the flat file.

## 2.3 SATELLITE REMOTE SENSING

Sea surface temperature (SST) and sea surface chlorophyll (SSC) are recorded by satellite remote sensing on a year-round basis, but there are periods when radiance is masked by ice, cloud and fog. We use the data products made available by the Bedford Institute of Oceanography Operational Remote Sensing Unit<sup>5</sup> to establish the annual cycle so that *in situ* measurements made in spring/summer are placed in local seasonal context. The annual records of SST (1998-2013) from the Advanced Very High Resolution Radiometer (AVHRR) and those of SSC (2003-2013) from the Moderate Resolution Imaging Spectroradiometer (MODIS) are composited to 24 sequential semi-monthly periods on a virtual transect from 53.684°N, 55.551°W to 60.564°N, 48.237°W, comprised of 511 pixels, which give a spatial resolution of less than 2 km.

## 2.4 DATA PRESENTATION

### 2.4.1 Annual cycle of remote variables

The annual cycles of SST and SSC in each year for which data are available are plotted as contoured sections from January to December in the horizontal aspect and from 55.551°W to 48.237°W longitude in the vertical aspect. We used the kriging algorithm of Surfer<sup>6</sup> to grid and display the data.

Climatological annual cycles are presented in 2 formats: first, as a contoured section which is the average over all years of the individual year sections; second, as a simple x-y line plot of SST or SSC versus semi-month number for which the variables are averaged into the 3 regions LSS, CLB, and GSS.

### 2.4.2 Interannual change of remote variables

At each of the 511 pixels of the virtual ocean transect, the multiyear time series of SST (1998-2013) and SSC (2003-2013) are constructed for each month separately, and also for the year as a whole (by combining the months together). The rate of interannual change of SST and SSC is given by the slope of the linear regression of the variables on

<sup>5</sup> <http://www.bio.gc.ca/science/newtech-technouvelles/sensing-teledetection/index-eng.php>

<sup>6</sup> Surfer Surface Mapping System, Version 8.05, Golden Software Inc, Golden, Colorado

year (degrees Celsius per year, and milligrams chlorophyll *a* per year). Thus, for example, the interannual rate of SST change for the month of May at pixel 1 (representing 55.551°W) requires the extraction of May SST values at pixel 1 successively for each of the 16 years in the available AVHRR time series. This procedure is repeated for each month and at every pixel to display the month-specific rate of change across the entire AR7W section.

### ***2.4.3 Climatological mean state of in situ variables***

2.4.3.1 Vertical distribution: For each *in situ* variable at each station, we plot the 10 m depth-resolved vertical profile by taking the average of all appropriate measurements within each depth-bin made over the entire 20-year time series. POC/PON and phytoplankton pigment variables are excluded because these were only sampled near-surface.

2.4.3.2 AR7W section gradient: We plot the 28-station AR7W section gradient by taking the depth-average (0-100 m) of each time-averaged variable (from 2.4.3.1), or the time-averaged surface values in the case of POC/PON and phytoplankton pigment variables.

### ***2.4.4 Interannual change of in situ variables***

2.4.4.1 Time series: For each *in situ* variable at each station, we plot the 20-year (or shorter) time series of the depth-average (0-100 m) of each variable. For plankton variables, a base-10 logarithmic transform was first applied to the measurements. The first-order multiyear trend is indicated by simple linear regression in the plots by a dashed line.

2.4.4.2 Rate of change: The interannual departure from climatological mean state for each *in situ* variable is reported using the dimensionless standardised (or normalised) anomaly, as follows. From each time series (in 2.4.4.1), the mean ( $M$ ) and standard deviation ( $S$ ) are calculated over the entire period. The standard anomaly  $A$  for any year  $y$  of the measured value  $X$  is given by  $A_y = (X_y - M)/S$ . Thus, for  $y$  extending over the entire period of observation, the rate of multiyear change is reported as the slope of the linear regression of  $A_y$  on  $y$ . We refer to this quantity as the “slope of change”, and because it has the same units (standard deviates per year) for all variables, it is a common basis for comparison across physics, chemistry, and biology. For each variable at each station, we plot the “slope of change” to indicate locations along the AR7W section where the variables are increasing, decreasing, or not changing.

### ***2.4.5 Distribution of bacteria***

2.4.5.1 Distribution along AR7W: For each year from 1999-2012, the spatial distribution of bacteria is plotted as contoured sections of logarithmic cell concentration from sea surface to ocean bottom in the vertical aspect, and from station 1 to station 28 in the horizontal aspect. We used the VG gridding algorithm of Ocean Data View<sup>7</sup> suitable for variable resolution in a rectangular grid.

2.4.5.2 Distribution in depth zones: Selecting the deepest station (L3-17) for representation, depth profiles of bacterial concentration are plotted for each year from 1999-2012 to highlight differences in 3 depth zones: the epipelagic (0-200m), the mesopelagic (200-2000m), and the bathypelagic (2000-3680m). For visual clarity, cell concentration is expressed in logarithmic units, and depth is expressed in square root units.

2.4.5.3 Times series in depth zones: Selecting the deepest station (L3-17) for representation, depth-integrated bacterial abundance (cells m<sup>-2</sup>) within each of the 3 depth zones for each year from 1999-2012 was calculated by trapezoidal integration of bacterial concentrations (cells m<sup>-3</sup>) at depth. Within each depth zone, the rate of multiyear change in depth-integrated abundance is given by the “slope of change” (standard deviates per year) as in Section 2.4.4.2.

## 2.5 DATA SUMMARY

We use a colour-coded 2-dimensional visual display to summarise (i) the distribution of climatological mean values, and (ii) the direction (positive or negative) and intensity (strong or weak) of multiyear change in all of the *in situ* variables at all 28 stations. We first performed principal component analysis on (i) the climatological values adjusted to zero mean and unit deviation (see Section 3.18.1), and on (ii) the calculated “slope of change” of standard anomalies for the variables (see Section 3.18.2). We then used the loading of the first component to rank the variables. A visual summary displays the variables in a vertical sequence ranked (separately for climatology and for multiyear change) from the highest positive loading to the highest negative loading, arrayed along a horizontal sequence of ascending station number. This method is similar in construction to that introduced by Frank (2003), but differs in intent. Whereas Frank sought to discern the ordinated pattern of how standardised anomalies of ecosystem variables are changing over time from year-to-year, we instead seek to discern the ordinated pattern of how (i) the mean values, and (ii) the standardised rate of change are manifesting over space, namely from west-to-east on AR7W. In other words, in our application, the element of time-change is incorporated into the variable expression, and we are seeking the spatial coherence of this expression amongst the physical, chemical,

---

<sup>7</sup> Schilitzer, R. Ocean Data View. <http://odv.awi.de>

and biological variables. Thus, variables close to each other in component ranking reflect a degree of similarity in their spatial dynamics. Vice versa, variables far apart from each other in rank with opposite signs reflect a degree of inverse similarity. This allows the visualisation of any coherence in the manner in which suites of these variables are distributed and change over the AR7W section.

## 2.6 DATA AVAILABILITY

The data in this report are available from the BioChem database maintained by DFO Integrated Science Data Management<sup>8</sup>. The data have also been submitted to the International Council for the Exploration of the Sea (ICES) Working Group on Phytoplankton and Microbial Ecology (WGMPE)<sup>9</sup>, as well as the UNESCO Intergovernmental Oceanographic Commission (IOC) International Group for Marine Ecological Time Series (IGMETS)<sup>10</sup>.

## 3. RESULTS

The description of salient results is based on Figures 2-144 and Tables 3 and 4.

### 3.1 TEMPERATURE

#### 3.1.1 Sea Surface Temperature (AVHRR)

[Figures 2-8]

The annual cycles of SST show rapid spring temperature increase in May and June through the entire AR7W section, reaching a peak in mid-August everywhere. The annual range of SST is large in LSS (min -1.4°C, max 8.2°C), moderate in CLB (min 2.2°C, max 9.3°C), and small in GSS (min 0.9°C, max 5.3°C).

Over the length of the AVHRR record (1998-2013), for the combined months of May, June, and July (which is the period of AZOMP at sea *in situ* observations), SST has been increasing everywhere on AR7W except at the western and eastern edges of CLB. This 3-month pattern across the entire transect is a net result of opposing SST trends for May and June on the one hand, and July on the other hand.

---

<sup>8</sup> <http://www.meds-sdmm.dfo-mpo.gc.ca/biochem/biochem-eng.htm>

<sup>9</sup> <http://wgpme.net>

<sup>10</sup> <http://igmets.net>



On an annual basis (January to December), SST is decreasing on LSS and into the western edge of CLB. However, SST is increasing almost everywhere east of the central CLB.

### ***3.1.2 In Situ Temperature***

[Figures 15-22, Table 3]

In spring/summer, depth-averaged and time-averaged temperature (0-100m) is sub-zero on the Labrador Shelf, rises sharply on the Labrador Slope, remains fairly constant ( $4.28 \pm 0.20^{\circ}\text{C}$ ) across the Central Labrador Basin, and decreases from the Greenland Slope to slightly above zero on the Greenland Shelf.

Over the length of the *in situ* record, the spring/summer depth-averaged temperature has a rate of change that is slightly negative (or virtually zero) across the entire AR7W section.

## **3.2 SALINITY**

[Figures 23-30, Table 3]

In spring/summer, depth-averaged and time-averaged salinity (0-100m) exhibits a west-to-east change that parallels that of depth-averaged temperature. Salinity is low (<33 psu) on the Labrador Shelf, rises sharply on the Labrador Slope, remains fairly constant ( $34.63 \pm 0.09$  psu) across the Central Labrador Basin, and decreases from the Greenland Slope to slightly above 33 psu on the Greenland Shelf.

Over the length of the *in situ* record, the spring/summer depth-averaged salinity has a rate of change that is slightly negative on much of LSS, but slightly positive on much of CLB and GSS.

## **3.3 STRATIFICATION ( $\Delta$ SIGMA-THETA)**

[Figures 31-38, Table 3]

In spring/summer, stratification in the upper 100 m is strongest in LSS where surface waters are fresh and cold, weakest in CLB where surface waters are salty and warm, and intermediate in GSS where waters are not as fresh nor as cold as in LSS.

Over the length of the *in situ* record, the spring/summer stratification has a rate of change that is negative at almost all stations.

## **3.4 OXYGEN**

[Figures 39-46, Table 3]

In spring/summer, depth-averaged and time-averaged dissolved oxygen concentration (0-100m) is highest in LSS where waters are fresh and cold, lowest in CLB where waters are salty and warm, and intermediate in GSS where waters are not as fresh nor as cold as in LSS.

Over the length of the *in situ* record, the spring/summer depth-averaged dissolved oxygen has a rate of change that is positive at all stations in CLB and GSS, and at half of the stations in LSS.

### 3.5 NITRATE

[Figures 47-54, Table 3]

In spring/summer, depth-averaged and time-averaged nitrate concentration (0-100m) is highest in CLB, intermediate in LSS, and lowest in GSS. At this time of year, nitrate is not depleted<sup>11</sup> anywhere, even at the shallowest depths. Concentrations ( $\text{mmol m}^{-3}$ ) at the surface (nominal zero meter depth) are 3.8 (average), 0.8 (minimum), 6.7 (maximum) at LSS; they are 6.8 (average), 3.6 (minimum), 8.7 (maximum) at CLB; and they are 3.6 (average), 1.2 (minimum), and 5.5 (maximum) at GSS.

Over the length of the *in situ* record, the spring/summer depth-averaged nitrate concentration has a rate of change that is generally positive, except for negative values at the stations near the western end of LSS and the eastern end of GSS.

### 3.6 PHOSPHATE

[Figures 55-62, Table 3]

In spring/summer, depth-averaged and time-averaged phosphate concentration (0-100m) is largely uniform across most of LSS and CLB, except near the eastern edge of CLB where values are lower, and become even lower eastward onto GSS. As with nitrate, at this time of year there is no depletion of phosphate anywhere, even at the shallowest depths.

Over the length of the *in situ* record, the spring/summer depth-averaged phosphate concentration has a rate of change similar to that of nitrate: namely, generally positive everywhere, except negative at the western end of LSS and the eastern end of GSS.

### 3.7 SILICATE

---

<sup>11</sup> In reference to nutrients, “depleted” is taken to mean reduced to a concentration below analytical detection.

[Figures 63-70, Table 3]

In spring/summer, depth-averaged and time-averaged silicate concentration (0-100m) decreases from west to east. It is highest at mid-shelf stations in LSS, at intermediate and fairly uniform levels across most of CLB, and lowest in GSS at the eastern end. As with nitrate and phosphate, at this time of year there is no depletion of silicate anywhere, even at the shallowest depths.

Over the length of the *in situ* record, the spring/summer depth-averaged silicate concentration has a rate of change whose direction (positive or negative) is similar to those of nitrate and phosphate. Of the 28 stations on AR7W, 12 stations exhibit concomitant positive change in all 3 nutrients, and 6 stations exhibit concomitant negative change in all 3 nutrients. In the remaining 10 stations, the direction of change was not the same for all 3 nutrients, but in none of these cases is there a strong (i.e. above average) magnitude of change.

### 3.8 EXCESS PHOSPHATE

[Figures 71-78, Table 3]

Both phosphorous and nitrogen are essential macro-nutrients for phytoplankton, but they are needed in different molar amounts. The stoichiometric elemental composition of average phytoplankton (Redfield composition) is given by the canonical molar ratio of 16N:1P. Under an idealised balanced demand for the 2 nutrients, the quantity  $P^*$  (termed “excess phosphate”, and defined as  $[P] - [N/16]$ ) is an indicator of excess P when its value is positive, and deficit P when its value is negative.

In spring/summer, depth-averaged and time averaged  $P^*$  (0-100m) is positive everywhere, but there are strong regional differences. It is highest on the Labrador Shelf, progressively decreasing to low positive values on the Labrador Slope and the western portion of CLB, thence increasing eastwards to GSS. The maximum  $P^*$  in GSS ( $0.20 \text{ mmol m}^{-3}$ ) is less than half the maximum  $P^*$  in LSS ( $0.44 \text{ mmol m}^{-3}$ ).

Over the length of the *in situ* record, the spring/summer depth-averaged  $P^*$  has a rate of change that is negative in LSS. That is to say, the excess amount of phosphate is decreasing, but remains surplus to the stoichiometric requirement set by nitrogen demand of phytoplankton. Elsewhere (CLB and GSS),  $P^*$  has a rate of change that varies between low positive and low negative values at different stations.

### 3.9 EXCESS SILICATE

[Figures 79-86, Table 3]

Both silicon and nitrogen are essential macro-nutrients for diatoms, and they are needed in similar molar amounts on average. Under an idealised balanced demand for the 2 nutrients, the quantity  $Si^*$  (termed “excess silicate”, and defined as  $[Si] - [N]$ ) is an indicator of excess Si when its value is positive, and deficit Si when its value is negative.

In spring/summer, depth-averaged and time averaged  $Si^*$  (0-100m) is positive only on the Labrador Shelf. Everywhere else,  $Si^*$  is negative, indicating a condition of silicon insufficiency for diatoms when nitrogen requirements have been met.

Over the length of the *in situ* record, the spring/summer depth-averaged  $Si^*$  has a rate of change that varies between low positive and low negative values at different stations.

### **3.10 BACTERIA**

#### ***3.10.1 Upper Ocean***

[Figures 87-94, Table 3]

In spring/summer, depth-averaged and time-averaged bacterial concentration (0-100m) is about half-million cells per ml on the shelves, about one-million cells per ml in CLB, and at intermediate values on the slopes in the transition regions.

Over the length of the *in situ* record, the spring/summer depth-averaged upper ocean bacterial concentration has a rate of change that is positive on the Labrador Shelf, switching to negative on the Labrador Slope and the western portion of CLB, switching back to positive on the eastern portion of CLB and the Greenland Slope, and finally becoming negative again on the Greenland Shelf.

#### ***3.10.2. Epipelagic, Mesopelagic, Bathypelagic Zones***

[Figures 131-142]

The concentration of bacteria decreases exponentially from the upper ocean to the abyss. Although there is considerable inter-annual variability in this vertical distribution, concentrations (in units of  $\log_{10}$  cells  $ml^{-1}$ ) are usually 5.5-6.5 in the epipelagic zone, 4.5-5.5 in the mesopelagic zone, and 4.0-5.0 in the bathypelagic zone. Of particular note is that in CLB, bacterial concentration is often slightly higher immediately near the ocean bottom, which is the location of Denmark Strait Overflow Water.

At station L3-17, which is the deepest station on AR7W, the depth-integrated inventory of bacterial abundance (in units of  $10^{13}$  cells  $m^{-2}$ ) is  $12.9 \pm 4.9$ ,  $20.7 \pm 5.5$ , and  $8.9 \pm 4.6$  in the epipelagic, mesopelagic, and bathypelagic zones respectively. The

year-to-year variability (coefficient of variation) is greatest in the bathypelagic (51%), least in the mesopelagic (26%), and intermediate in the epipelagic (38%). Over the length of the *in situ* record, bacterial inventory has decreased in the epipelagic and mesopelagic, but has increased in the bathypelagic zone. For the entire water-column at L3-17 from the upper ocean to the abyss, total bacterial inventory has not changed significantly, except for a marked decrease in 2012.

### 3.11 CHLOROPHYLL *a*

#### 3.11.1 Sea Surface Chlorophyll (MODIS)

[Figures 9-14]

The annual cycles of SSC show the strongest ( $>3 \text{ mg chl m}^{-3}$ ) and the earliest spring blooms (April) in GSS. In both LSS and CLB, the spring blooms are weaker ( $<2 \text{ mg chl m}^{-3}$ ) and attain their peak later, in May. It is only in LSS that a secondary, much less intense bloom appears in fall (September, October). In CLB, a distinct bloom in summer (July, August) is sometimes evident (e.g. 2006, 2010).

Over the length of the MODIS record (2003-2013), for the combined months of May, June, and July (which is the period of AZOMP at sea *in situ* observations), SSC has generally been increasing in LSS, but decreasing in CLB and GSS, with an exceptional increase at the junction between CLB and GSS.

On an annual basis during the ice-free season (March to October), the transect pattern in the direction (positive or negative) of multiyear SSC change is generally similar to that in the May-June-July period, except that the exceptional increase at the junction of CLB and GSS is subsumed, and that the magnitude of change (in both directions) is attenuated, almost to zero.

#### 3.11.2 In Situ Chlorophyll

[Figures 95-102, Table 3]

The quantity reported in this section is determined by fluorometric assay (Mitchell et al. 2002) and is therefore analytically independent of the quantity determined by HPLC analysis (Section 3.16.4).

In spring/summer, there is indication that at some stations, total chlorophyll *a* is slightly higher subsurface than at the shallowest depth-bin.

The depth-averaged and time-averaged chlorophyll *a* (0-100m) is virtually the same throughout LSS ( $1.86 \pm 0.28$  mg chl  $m^{-3}$ ) and CLB ( $1.87 \pm 0.51$  mg chl  $m^{-3}$ ), but increases markedly across GSS (from 2.47 to 5.84 mg chl  $m^{-3}$ ).

Over the length of the *in situ* record, the spring/summer depth-averaged chlorophyll has a relative rate of change that is positive across almost the entire AR7W section. The strongest absolute increases occur in GSS, where, averaging over the 5 stations (L3-24 to L3-28), the slope of positive change has a value of  $0.36 \pm 0.15$  mg chl  $m^{-3} y^{-1}$  that is statistically significant ( $p = 0.03$ ). The absolute increases of chlorophyll in CLB and LSS are less strong ( $0.06 \pm 0.03$  and  $0.08 \pm 0.05$  mg chl  $m^{-3} y^{-1}$  respectively) and statistically weaker ( $p = 0.06$  and  $0.15$  respectively).

### 3.12 SYNECHOCOCCUS

[Figures 103-110, Table 3]

*Synechococcus*, a cyanobacterium, constitutes the prokaryotic component of the photosynthetic picoplankton in these waters. In spring/summer, the depth-averaged and time-averaged cell concentration is distributed along the transect in almost exactly the same pattern as depth-averaged and time-averaged temperature: namely low on the Labrador Shelf, rising sharply on the Labrador Slope, remaining fairly constant across the Central Labrador Basin, and decreasing from the Greenland Slope to the Greenland Shelf. Indeed, the correlation between depth-averaged and time-averaged station values for temperature and  $\log_{10}$  *Synechococcus* concentration is extremely strong ( $r = 0.96$ ) and significant ( $p < 0.0001$ ). It should be noted that absolute concentrations range from order  $10^1$  to  $10^3$  cells  $ml^{-1}$ , which are orders less than in lower latitude waters (Li et al. 2013).

Over the length of the *in situ* record, the depth-averaged concentration of *Synechococcus* has a positive rate of change on the Labrador Shelf, but a negative rate of change almost everywhere else.

### 3.13 PICOEUKARYOTES

[Figures 111-118, Table 3]

Picoeukaryotic algae constitute the polyphyletic eukaryotic component of the photosynthetic picoplankton. In spring/summer, the depth-averaged and time-averaged cell concentration is highest in central CLB, and the values decrease both westwards and eastwards. In LSS to the west, average concentrations are only 2/3 those in CLB; and in GSS to the east, this fraction is 1/3.

Over the length of the *in situ* record, the depth-averaged concentration of picoeukaryotes exhibits a rate of change that has no apparent remarkable pattern across the transect, with generally weak positive and negative trends in all 3 regions. Out of 28 stations, there are more that show a negative trend (17) than a positive one (11).

### 3.14 PICOPHYTOPLANKTON

[Table 3, no figure plots]

Picophytoplankton is simply the sum of the two photosynthetic picoplankton components: *Synechococcus* (Section 3.12) and picoeukaryotic algae (Section 3.13). It is useful to combine the 2 components into a single ataxonomic size class because the polyphyletic members can be considered as one ecological functional group. Although the patterns over depth, space, and time can, in principle, be deduced for the whole from the parts, we have carried out the calculations as if picophytoplankton were a separate entity for the sake of checking internal consistency in the dataset.

In spring/summer, the depth-averaged and time-averaged picophytoplankton is dominated by the eukaryotic component across the entire transect. Thus, the distribution of picophytoplankton is essentially the same as that of picoeukaryotes (Section 3.13): highest concentrations in CLB ( $6778 \pm 2043$  cells ml<sup>-1</sup>), intermediate in LSS ( $3546 \pm 1037$  cells ml<sup>-1</sup>), and lowest in GSS ( $2271 \pm 1911$  cells ml<sup>-1</sup>).

Over the length of the *in situ* record, the depth-averaged concentration of picophytoplankton exhibits a rate of change that is essentially the same as that of its dominant component, the picoeukaryotes (Section 3.13).

### 3.15 NANOPHYTOPLANKTON

[Figures 119-126, Table 3]

In spring/summer, the depth-averaged and time-averaged cell concentration of nanophytoplankton increases steadily from west to east, with low values in LSS ( $893 \pm 173$  cells ml<sup>-1</sup>), intermediate values in CLB ( $2111 \pm 654$  cells ml<sup>-1</sup>), and high values in GSS ( $3431 \pm 773$  cells ml<sup>-1</sup>). Solitary cells of the commonly occurring arctoboreal prymnesiophyte *Phaeocystis pouchetii* belong to this size class.

Over the length of the *in situ* record, the depth-averaged concentration of nanophytoplankton has a rate of change that is generally negative on the western half of the transect (LSS and western CLB), but generally positive on the eastern half of the transect (eastern CLB and GSS).

### 3.16 PHYTOPLANKTON PIGMENTS

In this section, we use Roy et al. (2011) as our reference monograph on phytoplankton pigments, especially the chapters by Jeffrey et al. (2011) on microalgal classes and their signature pigments, and by Higgins et al. (2011) on the quantitative interpretation of chemotaxonomic pigment data.

### **3.16.1 19'-Butanoyloxyfucoxanthin**

[Figures 127,129; Table 4]

The xanthophyll 19'-butanoyloxyfucoxanthin is dominant in Dictyophyceae and Pelagophyceae; it is significant but not always present in Prymnesiophyceae; and it is minor or variable in Dinophyceae. Of particular note is that this pigment was not detected in GSS during intense blooms of the prymnesiophyte *Phaeocystis pouchetii* (Stuart et al. 2000).

In spring/summer, the time-averaged near-surface concentration of But-fuco is highest in CLB, very low in LSS and GSS, and entirely absent on the Greenland Shelf.

Over the length of the *in situ* record, But-fuco has a rate of change that is mostly positive in the western half of the transect, and mostly negative in the eastern half.

### **3.16.2 19'-Hexanoyloxyfucoxanthin**

[Figures 127,129; Table 4]

The xanthophyll 19'-hexanoyloxyfucoxanthin is dominant in Prymnesiophyceae and Dinophyceae. Of particular note is that this pigment was also not detected in GSS during intense blooms of the prymnesiophyte *Phaeocystis pouchetii* (Stuart et al. 2000).

In spring/summer, the time-averaged near-surface concentration of Hex-fuco is distributed across the transect in the essential manner as But-fuco: high in CLB, lower in LSS, lowest in GSS, and entirely absent on the Greenland Shelf.

Over the length of the *in situ* record, Hex-fuco has a rate of change that is generally negative everywhere, except for positive values on the Labrador Shelf.

### **3.16.3 Alloxanthin**

[Figures 127,129; Table 4]

The xanthophyll alloxanthin is dominant in Cryptophyta, including cryptophycean symbionts of the ciliate *Myrionecta rubra*. Alloxanthin also occurs in some dinoflagellates, and has been reported in 2 chlorophytes that show no evidence of a cryptomonad endosymbiont.



In spring/summer, the time-averaged near-surface concentration of Allo declines steadily from the western CLB eastwards to the end of the transect on the Greenland Shelf. Allo is essentially absent on the Labrador Shelf.

Over the length of the *in situ* record, Allo has a rate of change that is mostly positive in CLB.

#### **3.16.4 Chlorophyll a**

[Figures 127,129; Table 4]

Chlorophyll *a* is universal pigment found in all taxa. The quantity reported in this section is determined by HPLC analysis, and is therefore analytically independent from the quantity reported in Section 3.11

In spring/summer, the time-averaged near-surface concentration of Chl*a* has a “U-shaped” distribution across the transect: namely, high in the west (LSS) and east (GSS), lower in CLB – with a notable exception that the 2 most westerly stations (L3-01, L3-02) have slightly lower concentrations than stations immediately to their east.

Over the length of the *in situ* record, Chl*a* has a rate of change that is positive everywhere in LSS and GSS. Within CLB, the rate of change switches from being negative in the west to being positive in the east. The transect pattern resembles a “V-shape”.

#### **3.16.5 Chlorophyll b**

[Figures 127,129; Table 4]

Chlorophyll *b* is dominant in the green algal lineage – Chlorophyceae, Prasinophyceae, Trebouxiophyceae, Mesostigmatophyceae, Euglenophyceae, and Chlorarachniophyceae.

In spring/summer, the time-averaged near-surface concentration of Chl*b* increases steadily from west to east on the Labrador Shelf, but decreases eastwards from the Labrador Slope, through the entire CLB, to the Greenland Shelf. On the Greenland Slope, some patches of high concentration appear to be present.

Over the length of the *in situ* record, Chl*b* has a rate of change that gradually switches from being negative in the west to being positive in the east – with a notable exception that the 2 most westerly stations (L3-01, L3-02) have positive rates of change.

### 3.16.6 Chlorophyll $c_1+c_2$

[Figures 127,129; Table 4]

Chlorophyll  $c_1+c_2$  (unresolved) is dominant and widespread across 4 divisions (Heterokontophyta, Haptophyta, Cryptophyta, Dinophyta) with a distribution in 11 classes (Bacillariophyceae, Chrysophyceae, Dictyochophyceae, Pelagophyceae, Phaeothamniophyceae, Raphidophyceae, Synurophyceae, Pavlovophyceae, Prymnesiophyceae, Cryptophyceae, and Dinophyceae).

In spring/summer, the time-averaged near-surface concentration of  $Chlc_{1c_2}$  has a “U-shaped” distribution across the transect: namely, high in the west (LSS) and east (GSS), lower in CLB – with a notable exception that the 2 most westerly stations (L3-01, L3-02) have slightly lower concentrations than stations immediately to their east. This is the same pattern as  $Chla$  (Section 3.16.4).

Over the length of the *in situ* record,  $Chlc_{1c_2}$  has a rate of change that is positive almost everywhere in LSS and GSS. Within CLB, the rate of change switches from being negative in the west to being positive in the east. This is a pattern similar to  $Chla$  (Section 3.16.4).

### 3.16.7 Chlorophyll $c_3$

[Figures 127,129; Table 4]

Chlorophyll  $c_3$  is dominant in Bacillariophyceae, Bolidophyceae, Prymnesiophyceae, and Dinophyceae; the pigment is significant but not always present in Dictyophyceae and Pelagophyceae.

In spring/summer, the time-averaged near-surface concentration of  $Chlc_3$  is an “inverted U-shaped” distribution across the transect: namely, high in CLB, low in GSS, and extremely low (but not absent) in LSS.

Over the length of the *in situ* record, the transect pattern for the rate of change in  $Chlc_3$  is similar to that of  $Chla$  (Section 3.16.4), but statistically more noisy.

### 3.16.8 Diadinoxanthin

[Figures 127,129; Table 4]

The xanthophyll diadinoxanthin is dominant in Bacillariophyceae, Bolidophyceae, Dictyochophyceae, Pelagophyceae, Phaeothamniophyceae, Pavlovophyceae, Prymnesiophyceae, Dinophyceae, and Euglenophyceae. It is a minor pigment in Xanthophyceae.

In spring/summer, the time-averaged near-surface concentration of Diadino shows a general decrease from west to east – with a notable exception that the 2 most westerly stations (L3-01, L3-02) have slightly lower concentrations than stations immediately to their east.

Over the length of the *in situ* record, the transect pattern for the rate of change in Diadino is similar to that of Chla (Section 3.16.4), but statistically more noisy.

### **3.16.9 Diatoxanthin**

[Figures 128,130; Table 4]

Diatoxanthin is the de-epoxidation product of diadinoxanthin. Thus, the distribution of diatoxanthin in algal classes is exactly that of diadinoxanthin, except that diatoxanthin is a minor pigment throughout.

In spring/summer, the time-averaged near-surface concentration of Diato shows a transect pattern similar to that of Diadino (Section 3.16.8). The ratio Diadino:Diato is  $12 \pm 3$  in LSS,  $12 \pm 4$  in CLB, and  $36 \pm 29$  in GSS.

Over the length of the *in situ* record, the rate of change in Diato is positive at most of the stations.

### **3.16.10 Fucoxanthin**

[Figures 128,130; Table 4]

The xanthophyll fucoxanthin is dominant and widespread in Bacillariophyceae, Bolidophyceae, Chrysophyceae, Dictyochophyceae, Pelagophyceae, Phaeothamniophyceae, Pinguiphyceae, Raphidophyceae, Synurophyceae, Pavlovophyceae, Prymnesiophyceae, and Dinophyceae.

In spring/summer, the time-averaged near-surface concentration of Fuco has a highly-attenuated “U-shaped” distribution across the transect. Concentrations ( $\text{mg m}^{-3}$ ) are lowest in CLB ( $0.96 \pm 0.25$ ), only marginally higher in LSS ( $1.15 \pm 0.31$ ), but substantially higher in GSS ( $1.43 \pm 0.32$ ).

Over the length of the *in situ* record, the transect pattern for the rate of change in Fuco is similar to that of Chla (Section 3.16.4) – a “V-shape” with generally positive rates in LSS and GSS, and a switch from negative to positive rates going eastward within CLB.

### **3.16.11 Peridinin**

[Figures 128,130; Table 4]

Peridinin is a diagnostic marker for dinoflagellates.

In spring/summer, the time-averaged near-surface concentration of Peri progressively increases from west to east within LSS, reaching a maximum at the junction with CLB. Eastward of this junction, concentrations decrease, eventually to zero in GSS, but not before attaining a secondary (lower) maximum at station L3-20.

Over the length of the *in situ* record, the rate of change in Peri is strongly positive in LSS, and weakly positive in most of CLB. Peri is absent in GSS.

### **3.16.12 Zeaxanthin**

[Figures 128,130; Table 4]

The xanthophyll zeaxanthin is widespread in cyanobacteria, and also present in the classes of the green lineage – Prasinophyceae, Chlorophyceae, Trebouxiophyceae, and Chlorarachniophyceae.

In spring/summer, the time-averaged near-surface concentration of Zea decreases from west to east, in a pattern not greatly dissimilar from Chl*b* (Section 3.16.5).

Over the length of the *in situ* record, the transect pattern of the rate of change in Zea appears unique amongst all the pigments considered. The rate of change is negative in LSS and GSS, but near zero at many stations in CLB.

### **3.16.13 Diagnostic Pigments**

[Figures 128,130; Table 4]

The weighted sum of diagnostic pigments (DiagPig) is a quasi-measure of total phytoplankton chlorophyll *a*. This quasi-measure is based on the weighted contribution of 7 phytoplankton pigments used as chemotaxonomic markers for constituent members of the phytoplankton community. In principle, the salient patterns of DiagPig should corroborate those of Chl*a* (Section 3.16.4). However, because we have not tuned the Uitz global formula with weighting factors derived from local calibration, the comparison between DiagPig and Chl*a* cannot be taken as a validation exercise. Notwithstanding the lack of calibration, because Fuco occurs at high concentrations in these waters, and also because Fuco is weighted heavily in the Uitz global formula, it can be deduced that the results of DiagPig and Fuco are necessarily similar in pattern. These deductions are confirmed.

In spring/summer, time-averaged surface concentrations of DiagPig are generally similar across the transect, but perhaps a little bit higher in LSS ( $2.03 \pm 0.42 \text{ mg m}^{-3}$ ) and GSS ( $2.28 \pm 0.45 \text{ mg m}^{-3}$ ) than in CLB ( $1.71 \pm 0.41 \text{ mg m}^{-3}$ ).

Over the length of the *in situ* record, the transect pattern for the rate of change in DiagPig is similar to that of Fuco (Section 3.16.10), both of which appear as statistically noisy versions of the “V-shape” in Chl*a* (Section 3.16.4).

### 3.17 PARTICULATE ORGANIC MATTER

#### 3.17.1 *Particulate organic carbon*

[Figures 128,130; Table 4]

POC measures both living and non-living carbon in seston. A linear regression of the time-averaged near-surface concentrations of POC versus Chl*a* yields  $POC = (103 \pm 37) + [(68 \pm 9) \times Chl a]$  ( $p < 0.0001$ ), implying that the non-phytoplankton component of seston is  $103 \text{ mgC m}^{-3}$ ; and that the carbon-to-chlorophyll ratio for phytoplankton is  $68 \text{ mgC mgChl}^{-1}$ .

Strong correlation between POC and Chl*a* ( $r = 0.83$ ) indicates similar “U-shaped” patterns of distribution across the transect: high POC in the west (LSS) and east (GSS), lower in CLB – with a notable exception, once again, that the 2 most westerly stations (L3-01, L3-02) have slightly lower concentrations than stations immediately to their east.

Over the length of the *in situ* record, the rate of change in time-averaged POC is positive in 21 out of 28 stations.

#### 3.17.2 *Particulate organic nitrogen*

[Figures 128,130; Table 4]

PON is highly correlated with POC ( $r = 0.86$ ), but in comparing the time-averaged station values across the transect, the range of variation for PON is slightly less than that of POC. An indication of this relative difference is that the ratio of maximum to minimum is slightly lower for PON (2.8) than for POC (3.4). We can deduce from this relative difference that the ratio of POC:PON (Section 3.17.3) is not constant across the transect.

Over the length of the *in situ* record, the rate of change in time-averaged PON is positive in 22 out of 28 stations.

#### 3.17.3 *POC:PON*

[Figures 128,130; Table 4]

POC:PON is the stoichiometric molar ratio of organic carbon to organic nitrogen in seston. Its value in the Labrador Sea is different from the canonical Redfield ratio for living phytoplankton ( $6.6 \text{ molC molN}^{-1}$ ), as expected because of non-phytoplankton

components in the seston, and also because ecological elemental ratios do not merely reflect physiology and biochemistry, but are now understood to emerge from complex nested hierarchical processes.

In spring/summer, POC:PON of time-averaged near-surface seston is lowest and least-variable in CLB ( $7.6 \pm 0.4 \text{ mol mol}^{-1}$ ) compared to LSS ( $9.2 \pm 1.5$ ) and to GSS ( $8.4 \pm 1.3$ ).

Over the length of the *in situ* record, the rate of change in time-averaged POC:PON is negative in 16, and positive in 12 out of 28 stations. Of the 16 stations at which POC:PON is decreasing, 11 of these stations are ones at which both POC and PON are separately increasing. Conversely, of the 12 stations at which POC:PON is increasing, 2 of these stations are ones at which both POC and PON are separately decreasing.

### 3.18 SPATIAL PATTERNS

#### 3.18.1 Climatological Means

[Figure 143]

We examine the spatial pattern across AR7W of climatological (1994-2013) mean values for 30 variables in physics, chemistry, and biology. For each variable, we computed the mean and standard deviation over 28 stations, and then adjusted each individual station value to zero-mean and unit-deviation by subtraction of mean followed by division by standard deviation. With an array of 30 adjusted variables and 28 stations, a spatial pattern is constructed by ranking the adjusted variables in ascending order according to the loading of the first principal component, which explains 48% of the variance.

A comparison is made of 4 classes of standard values, defined (and colour-coded) as follows: (i) strong positive (dark red) for a standard value greater than the mean of all positive standard values; (ii) weak positive (light red) for a standard value less than the mean of all positive standard values; (iii) weak negative (light blue) for a standard value greater (i.e. less negative) than the mean of all negative standard values; and (iv) strong negative (dark blue) for a standard value less (i.e. more negative) than the mean of all negative standard values. These 4 colour-coded classes provide a visual summary of spatial coherence and anti-coherence amongst clusters of variables.

At one end of the ordination (high negative loadings), the variables are characterised by low mean values in LSS and GSS but high values in CLB – the so-called inverted U-shape or inverted V-shape distributions along AR7W. These include temperature, salinity, nitrate, bacteria, picoeukaryotes, alloxanthin, *Synechococcus*, hex-fuco, Chlc3, but-fuco, and peridinin. At the other end of the ordination (high positive loadings), the

variables are characterised in the anti-sense of high mean values in LSS and GSS but low values in CLB – the so-called U-shape or V-shape distributions along AR7W. These include excess silicate, Chl $a$ , stratification, oxygen, Chl $c1c2$ , POC, PON, POC:PON, fucoxanthin, and diagnostic pigments. In between the 2 ends of the ordination is a mix of various patterns. For example, a west-to-east increase in nanophytoplankton concentration (low negative loading) is closely juxtaposed against a west-to-east decrease in silicate concentration (low positive loading).

### 3.18.2 *Multiyear Change*

[Figure 144]

We examine the spatial pattern across AR7W of the rate of multiyear change for 30 variables in physics, chemistry, and biology. The rates of multiyear change expressed as standard deviates per year have already been presented (Sections 3.1 - 3.17). With an array of 30 standardised rate variables and 28 stations, a spatial pattern is constructed by ranking the variables in ascending order according to the loading of the first principal component, which explains 35% of the variance.

A comparison is made of 4 classes of multiyear change, defined (and colour-coded) as follows: (i) strong positive change (dark red) for a regression slope greater than the mean of all positive-valued slopes; (ii) weak positive change (light red) for a regression slope less than the mean of all positive-valued slopes; (iii) weak negative change (light blue) for a regression slope greater (i.e. less negative) than the mean of all negative-valued slopes; and (iv) strong negative change (dark blue) for a regression slope less (i.e. more negative) than the mean of all negative-valued slopes.

With the 30 variables ranked and displayed in the manner described, the upper ocean ( $z \leq 100\text{m}$ ) of the Labrador Sea in spring/summer for the 1994-2013 period can be characterised as follows.

- Nutrients (nitrate, phosphate, silicate, excess phosphate) and physical conditions (temperature, salinity, stratification) have a high degree of spatial similarity in their pattern of change, all being ranked closely at one end of the ordination. The multiyear change in these variables is mostly weak everywhere, but in the few places where change is strong, it is mostly negative.
- In sharp contrast at the other end of the ordination, many variables representing the bulk portion of the phytoplankton community (Chl $a$ , DiagPig, Fuco, Chl $c1c2$ , Total chlorophyll  $a$ , Chl $c3$ , Diadino, POC) have a high degree of spatial similarity of a different character: these variables are strongly increasing on the shelves and slopes (LSS, GSS), but decreasing or not changing much in CLB.
- Microbial cells (bacteria, *Synechococcus*, picoeukaryotes, nanophytoplankton) have a first-component pattern that is characterised by very few strong changes

throughout CLB and GSS, and a mix of positive and negative change in LSS. The second principal component separates *Synechococcus* from the other microbes on the basis of strong increase on the Labrador Shelf.

## 4. DISCUSSION

### 4.1 SCIENTIFIC METHOD

This report presents a detailed evidentiary record of microbial plankton and their environment in the Labrador Sea from 1994 to 2013. It provides information on microbes that is supplementary to annual data of the core program reported to the Canadian Science Advisory Secretariat (Yashayaev et al. 2014a) and the Northwest Atlantic Fisheries Organization (Yashayaev et al. 2014b). In this respect, the microbial data broaden AZOMP ecosystem considerations to include all size classes of the phytoplankton and also the prokaryotic secondary producers. Amongst the small number of long-term oceanographic observation programs in the world carried out in support of ecosystem assessment and management, AZOMP is one of the very few that includes direct measurements in explicit recognition of the new microbial paradigm (now 40-years old) of the ocean's food web (Pomeroy 1974).

The distribution of selected properties of the phytoplankton in the Northwest Atlantic subpolar region is variously monitored: by direct sampling (*in vitro* and *in vivo* red fluorescence), by satellite remote sensing (ocean colour), and by Continuous Plankton Recorder on ships of opportunity (Phytoplankton Colour Index, diatoms, dinoflagellates). Due to different scales of sampling (Head and Pepin 2010), and importantly, due to differences in the fundamental characteristics of the measured variables, the results are not redundant, but are complementary. As Cullen (1982) once remarked: "It should not be assumed, *a priori* that fluorescence represents chlorophyll, chlorophyll represents biomass, or even that biomass represents acceptable food for herbivores".

To put a finer point on this important distinction, we note how, even within the unitary field of oceanography, there are differences amongst the sub-disciplines on how phytoplankton are tokened. To physical oceanographers, phytoplankton may be synonymous with fluorescence: the release of photons as electrons return to ground state after excitation. To optical oceanographers, phytoplankton may be synonymous with visible spectral radiometric signatures. To chemical oceanographers, phytoplankton may be synonymous with  $C_{55}H_{72}O_5N_4Mg$  (chlorophyll *a*), a diagnostic molecule that can be measured with great analytical precision by absorption or chromatography when disaggregated from its native state in a test tube. To fisheries



oceanographers, phytoplankton may be synonymous with green colouration on a silk mesh towed behind a vessel-of-opportunity. However, to biological oceanographers, phytoplankton are known in a myriad of ways (Section 1.2) representing the two great classes of biological processes: matter and energy transfer on the one hand, and the maintenance, transmission, and modification of genetically based information on the other hand (Eldredge 1986). The nexus of this dual hierarchy in ecology (elements to molecules to organelles to organisms to populations to communities to meta-communities) and in evolution (genes to transcripts to organisms to species to phyla to domain) is the individual free-living organismal entity. To view mechanistic AZOMP at this nexus of individual entities of algae and bacteria affirms the complementarity of reductionism and organicism (Hull 1974).

Towards meeting the expressed goals and objectives of AZOMP (Section 1.1), we offer in this report the multidisciplinary data sets that can be used to establish relationships among the organismal (phytoplankton and bacteria), chemotaxonomic (diagnostic pigments), chemical (nutrients and oxygen), and physical (temperature, salinity, stratification) variables. We use the method of hierarchical coarse-graining to progressively enlarge the scale of analysis to discern macroscopic pattern (Li and López-Urrutia 2013). Starting with point measurements in space and time, we progressively averaged over depth, over stations, and over years. Phytoplankton and bacterioplankton interact at the short scales of microbial generation times and cellular distances which are below the detection capabilities of AZOMP; but temporal and spatial averaging to increasingly large scales allows the detection of climate-related signals (Li et al. 2006; Li 2009).

Notwithstanding the short length of the time series, the relationships amongst variables presented in this report offer insight on putative changes in the state of the Labrador Sea. However, we note carefully that phenomenological ecology offers, at best, circumstantial evidence which corroborates one particular alternative hypothesis, but does not and cannot constitute a strong test of a null hypothesis (Strong 1980). Essentially, in ecological systems, causes are usually neither severally necessary nor jointly sufficient for their effects (Hull 1974). This means that although we may be able to explain (in statistical form), we may not always be able to predict. This is an ineluctable constraint.

## 4.2 ANNUAL CYCLES OF SST AND SSC

Year-round satellite observations of SST and SSC provide the seasonal context to AZOMP *in situ* measurements made in May, June, and July. Satellite observations are made at space and time scales (kilometers, 2-week composites) that are exceedingly large in comparison to shipboard CTD measurements of temperature and chlorophyll

(meters, minutes). Therefore, there is no expectation that variables should necessarily be precisely matched. Nevertheless, it is evident that the 3-month window of *in situ* observation in spring/summer is the period of most rapid temperature increase and most rapid chlorophyll change in the Labrador Sea.

The matter of seasonal context can be posed as a question: to what extent do the multiyear changes in SST and SSC during the 3-month period reflect the multiyear change for the entire 12-month period? Analyses (Figures 8 and 14) show that a substantial portion of multiyear annual change is indeed captured in the 3-month period. For example, increasing SST in the central CLB is evident for much of the year (except July and October). Notably however, for SST, the trend of spring/summer increase in LSS reverses to become a trend of decrease when assessed over a 12-month period. For SSC, the strong trend of spring/summer increase in a narrow longitudinal band on the Greenland Slope is subsumed over a 12-month period.

The 20 AZOMP cruises (Table 1) have an average duration of about 3 weeks; therefore, for practical purpose, this is deemed to be the duration for a set of quasi-synoptic observations. In constructing the climatology (i.e. average condition over the years of observation) or the time series (i.e. change in condition) of an *in situ* variable at each station, the variance includes not only natural interannual variability (which is that of interest), but also point-sampling variability, as well as the distortion of temporal aliasing - as the nominal 3-week cruise duration is shifted earlier or later in successive years. With almost 20 years of measurement for many *in situ* variables, aliasing distortion is presumably averaged out to a considerable extent. Given a mismatch between trends of SST and *in situ* temperature change, and between SSC and *in situ* chlorophyll change, logical explanations may lie in different scales of measurement, in the thickness of the water layer under consideration, and in length of the observational records.

### **4.3 MEAN DISTRIBUTION**

The mean state of the upper ocean in the Labrador Sea is strongly related to regional ocean circulation and water mass characteristics. The distribution of temperature and salinity along AR7W can be attributed to: (i) transport of warm and salty water from the north Atlantic Current to the central Labrador Sea; (ii) transport of cold and low-salinity water from the Arctic to the Labrador and Greenland Shelves; (iii) progressive loss of heat and greater excess of precipitation over evaporation as the counter-clockwise gyre circulation transports water around the northern and western boundaries of the deep basin, with rapid transition between the less-saline water over the shelves and the more-saline waters over the deep basin (Yashayaev and Clarke 2008).

The mean distributions of nutrients and oxygen along AR7W are also related to water mass characteristics (Yeats et al. 2010). The signatures of stoichiometric phosphorus excess in Arctic waters (Yamamoto-Kawai et al. 2006) and stoichiometric silicon deficit in Atlantic waters remain evident, even as phytoplankton assimilate (but do not deplete) the nutrients during the spring/summer window of observation (Harrison and Li 2008).

Here in this report, for the first time, it is evident that the mean distributions of microbial plankton in the Labrador Sea are also spatially coherent with the mean distributions of physical and chemical characteristics related to water mass transports (Figure 143). The large bulk of phytoplankton biomass (e.g. *Chla*, diagnostic pigments, *Chlc1c2*, fucoxanthin, POC) on the continental shelves receiving cold low-salinity Arctic waters is relatively sparse in the smaller microbial components (e.g. bacteria, piceoeukaryotes, *Synechococcus*, hex-fuco, but-fuco, *Chlc3*). Conversely, the smaller bulk of phytoplankton biomass in the central Basin receiving warm high-salinity Atlantic waters is relatively abundant in these picoplankton and nanoplankton.

The assignment of pigment types to size classes of the phytoplankton is not without ambiguity, especially in polar and sub-polar waters where cyanobacteria are a minor fraction at best of the picophytoplankton. In general, prasinophytes, bolidophytes, pelagophytes, chrysophytes, haptophytes, and dictyochophytes may all be represented in the piceoeukaryotes (Jeffrey et al. 2011). The diversity of taxa comprising this polyphyletic group renders it difficult to validate pigment-based size classification of picophytoplankton, which assigns only *Chlb* and zeaxanthin to this group (Uitz et al. 2006). For the spring/summer period, the mean inverted V-shaped distribution of picophytoplankton across the Labrador Sea (Section 3.14) appears to be a strong characteristic feature related to source waters that is not reflected in the distributions of *Chlb* or zeaxanthin.

#### **4.4 MULTIYEAR CHANGE**

Temperature and salinity in the 150-2000m layer (~mesopelagic zone) of the central Labrador Sea have unequivocally increased since 1994, although the trend is at times punctuated by sharp reversals due to deep winter convection (Yashayaev 2007; Yashayaev et al. 2014a,b). However, in the seasonally active surface layer (~epipelagic zone), multiyear trends in temperature, salinity, and density are more difficult to discern because of at least three factors contributing to short and long term variability: heat exchange with the atmosphere, heat and salt gain from Atlantic source waters, and freshwater input from ice, melt-water, continental runoff, and precipitation.

The short record of SST from 1998-2013 (Figure 8) confirms a temperature increase in most of CLB, but the *in situ* record of depth-averaged (0-100m) spring/summer hydrographic conditions in CLB are equivocal: salinity is increasing as expected (Figure 30), but temperature is not (Figure 22). As a consequence, the difference in seawater density between the bottom and top of this 100 m layer is decreasing (Figure 38), leading to a weak increase in the depth-averaged concentration of nitrate (Figure 54), phosphate (Figure 62), and silicate (Figure 70) in CLB.

Elsewhere (Harrison and Li 2008), we have suggested that light is the principal limiting factor of phytoplankton production and growth for much of the year in the Labrador Sea. At times during mid to late summer when surface irradiance is at its seasonal peak, nutrients may be a limiting factor, either by themselves or in conjunction with light as co-limiting resources. In other words, during the spring/summer window of *in situ* sampling on AR7W, contemporaneous measurements of dissolved nutrient concentrations and phytoplankton standing biomass provide little predictive information on the production of organic matter from the availability of inorganic substrates.

A key biological observation arising from our 20-year time series of spring/summer *in situ* measurements is that bulk phytoplankton biomass has increased at almost all 28 stations (Figure 102), and most strongly on the Greenland Shelf and Slope where the biomass is normally highest (Section 3.11.2). The increase is, in principle, an algebraic sum of weighted positive and negative changes in the constituent pigment groups (Figures 129, 130), or in the constituent size classes (Figures 118, 126), emphasising that the members of the community do not all change in the same direction or to the same extent. The pigment groups that exhibit a pattern of change with the strongest spatial coherence to bulk phytoplankton are those of the red algal lineage, not those of the green algal or cyanobacterial lineages (which tend to be picoplankton). Notably however, *Synechococcus* seems to be increasing on the Labrador Shelf (Figure 110) where it is normally at very low concentrations (Figure 106). Since this cyanobacterium is normally at even lower concentrations in upstream polar waters (Nelson et al. 2014), enhanced transport of this picoplankton from the Arctic Ocean seems unlikely. On the other hand, we might admit Atlantic water as a possible source (Gradinger and Lenz 1989).

Generally, it is not evident what factor, or set of factors, is the proximate driver of any of the noted changes. In an ultimate sense, the local standing stock of phytoplankton builds up to the extent that its fundamental ecological niche is realised, constrained by limiting resources, and removed by loss processes (e.g. zooplankton grazing, viral lysis, automortality, advection, sinking). These ecological processes are dynamic and because they operate at sub-annual time scales, the link of proximate cause

to observed effect requires examination of the system at the relevant time scales (days to weeks) of the putative processes, for which the inter-annual observations we have are inappropriately scaled.

#### 4.5 IMPLICATIONS

In principle, the response of an ecosystem to climate variability can be mediated by microbial plankton as an intermediary between the physical/chemical environment and the higher trophic levels. As an example of such cause-and-effect, on the Newfoundland and Labrador Shelves, a higher-than-normal air temperature in springtime not only results in a shallower mixed layer depth, but also a higher water temperature, a higher rate of ice melt releasing more freshwater, a smaller ice extent and a more northerly ice edge – all of which result in an early and prolonged spring phytoplankton bloom (Wu et al. 2007), which, in turn is correlated with body size of individual shrimp, presumably through the availability of phytoplankton, detritus, copepod eggs, nauplii, and copepodites as food items (Fuentes-Yaco et al. 2007). Although this propagation of signal from air temperature to shrimp size through the phytoplankton is highly plausible and compelling, it is the nature of open ecosystems that causes are neither severally necessary nor jointly sufficient for their effects (Hull 1974). In other words, we cannot say that each of the causes (e.g. higher air temperature, higher water temperature, greater ice melt, fresher surface waters, stronger stratification, greater phytoplankton biomass, more copepods) taken separately is necessary for shrimp to have larger body size; and neither can we say that all of them taken together is sufficient for the effect. For good or bad, the metaphor of signal propagation is a reification<sup>12</sup> (Slobodkin 2001), but it remains a cornerstone of predicting ecosystem response to climate variability and change. The unstated premise of these conjectures is linearity in response that links cause to effect, which is seldom the case in highly-connected complex and adaptive systems. Evidence to test these conjectures lie beyond the scope of this report.

---

<sup>12</sup> Slobodkin explains that “[r]eification consists of accepting a designation as if it has empirical meaning when, in fact, its existence has either never been tested or it has been found empty...reification is taken as an untestable axiom...To reify consists of assigning to a word, quantity or image an illegitimate ontological status”.

## ACKNOWLEDGMENTS

We thank DFO Maritimes Science sector management, the AZOMP Coordinating Committee, and the Canadian Coast Guard for supporting and enabling this work. The great many dedicated DFO staff persons who have served on these bodies since program inception are too numerous to list completely here: Greenan (Blair) and Loder (John) made large contributions. We also thank the many members of the Ocean and Ecosystem Science Division and the Program Coordination and Support Division who manage, coordinate, administer, and undertake the work at-sea, in the laboratory, and in the office. We especially thank our at-sea colleagues who have directly contributed to and supported the sample collecting and analysis activities of the Labrador Sea cruises, including Anning (Jeff), Anstey (Carol), Azetsu-Scott (Kumiko), Caverhill (Carla), Childs (Darlene), Clarke (Allyn), Dickie (Paul), Geshelin (Yuri), Harris (Les), Head (Erica), Lazier (John), Nelson (Rick), Perry (Tim), Punshon (Steve), Ringuette (Marc), and Yashayaev (Igor). We are also grateful to those who have worked in the flow cytometry laboratory over the years: Forbes (Gillian), Giroux (Chantal), Haussler (Kelly), Horn (Diane), Scarcella (Karen), and Sykes (Peter). The remote sensing data products were prepared by Caverhill (Carla), Maass (Heidi), and Porter (Cathy). We thank Erica Head and César Fuentes-Yaco for their review of this report.

**REFERENCES**

- Cullen, J.J. 1982. The deep chlorophyll maximum: comparing vertical profiles of chlorophyll *a*. *Can. J. Fish. Aquat. Sci.* 39: 791-803.
- Eldredge, N. 1986. Information, economics, and evolution. *Ann. Rev. Ecol. Syst.* 17: 351-369.
- Flynn, K.J., Stoecker, D.K., Mitra, A., Raven, J.A., Glibert, P.M., Hansen, P.J., Granéli, E., and Burkholder, J.M. 2013. Misuse of the phytoplankton-zooplankton dichotomy: the need to assign organisms as mixotrophs within plankton functional types. *J. Plankton Res.* 35:3-11.
- Frank, K.T. 2003. State of the Eastern Scotian Shelf Ecosystem. Department of Fisheries and Oceans, Canadian Science Advisory Secretariat, Ecosystem Status Report 2003/004.
- Fuentes-Yaco, C., Koeller, P.A., Sathyendranath, S., and Platt, T. 2007. Shrimp (*Pandalus borealis*) growth and timing of the spring phytoplankton bloom on the Newfoundland-Labrador Shelf. *Fish. Oceanogr.* 16:116-129.
- Gradinger, R. and Lenz, J. 1989. Picocyanobacteria in the high Arctic. *Mar Ecol Prog Ser* 52:99–101
- Harrison, W.G. and Li, W.K.W. 2008. Phytoplankton growth and regulation in the Labrador Sea: light and nutrient limitation. *J. Northwest Atl. Fish. Sci.* 39:71-82.
- Head, E.J.H. and Pepin P. 2010. Monitoring changes in phytoplankton abundance and composition in the Northwest Atlantic: a comparison of results obtained by continuous plankton recorder sampling and colour satellite imagery. *J. Plankton Res.* 32: 1649–1660.
- Hendry, R. and Harrison, W.G. 2007. Status of the Labrador Sea. *AZMP Bulletin* 6:11-15.
- Higgins, H.W., Wright, S.W., and Schluter, L. 2011. Quantitative interpretation of chemotaxonomic pigment data. In: *Phytoplankton Pigments: Characterization, Chemotaxonomy and Applications in Oceanography*. Cambridge University Press, pp. 257-313. <http://dx.doi.org/10.1017/CBO9780511732263.010>
- Hull, D.L. 1974. *Philosophy of Biological Science*. Prentice-Hall, New Jersey, 148p.
- Jeffrey, S.W., Wright, S.W., and Zapata, M. 2011. Microalgal classes and their signature pigments. In: *Phytoplankton Pigments: Characterization, Chemotaxonomy*

and Applications in Oceanography. Cambridge University Press, pp. 3-77.  
<http://dx.doi.org/10.1017/CBO9780511732263.004>

- Li, W.K.W. 2009. From cytometry to macroecology: a quarter century quest in microbial oceanography. *Aquat. Microb. Ecol.* 57: 239-251.
- Li, W.K.W., Carmack, E.C., McLaughlin, F.A., Nelson, R.J., and Williams, W.J. 2013. Space-for-time substitution in predicting the state of picoplankton and nanoplankton in a changing Arctic Ocean. *J. Geophys. Res. Oceans* 118, 1-10, doi:10.1002/jgrc.20417.
- Li, W.K.W. and Dickie, P.M. 2001. Monitoring phytoplankton, bacterioplankton, and virioplankton in a coastal inlet (Bedford Basin) by flow cytometry. *Cytometry* 44:236-246.
- Li, W.K.W., Harrison, W.G., and Head, E.J.H. 2006. Coherent sign switching in multiyear trends of microbial plankton. *Science* 311: 1157-1160.
- Li, W.K.W. and López-Urrutia, A. 2013. Macroscopic patterns in marine plankton. *In: Encyclopedia of Biodiversity, Volume 4.* Edited by S.A. Levin. Academic Press, Waltham, MA. pp. 667-680.
- Nelson, R.J. et al. 2014. Biodiversity and biogeography of the lower trophic taxa of the Pacific Arctic Region: Sensitivities to climate change. *In: J.M. Grebmeier and W. Maslowski (eds.), The Pacific Arctic Region: Ecosystem Status and Trends in a Rapidly Changing Environment, DOI 10.1007/978-94-017-8863-2\_10, Springer Science+Business Media Dordrecht 2014, pp. 269-336.*
- Mitchell, M.R., G. Harrison, K. Pauley, A. Gagné, G. Maillet, and P. Strain. 2002. Atlantic Zonal Monitoring Program Sampling Protocol. *Can. Tech. Rep. Hydrogr. Ocean Sci.* 223: iv + 23 pp.
- Pomeroy, L.R. 1974. The ocean's food web, a changing paradigm. *Bioscience* 24: 499-504.
- Roy, S., Llewellyn, C.A., Egeland, E.S., and Johnsen, G. [Eds.] 2011. *Phytoplankton Pigments: Characterization, Chemotaxonomy and Applications in Oceanography.* Cambridge University Press. <http://dx.doi.org/10.1017/CBO9780511732263>
- Sieburth, J.McN., Smetacek, V., and Lenz, J. 1978. Pelagic ecosystem structure: Heterotrophic compartments of the plankton and their relationship to plankton size fractions. *Limnol. Oceanogr.* 23:1256-1263.
- Slobodkin, L.B. 2001. The good, the bad and the reified. *Evolutionary Ecological Research* 3:1-13.



- Strong, D.R. Jr. 1980. Null hypothesis in ecology. *In* *Conceptual Issues in Ecology*. Edited by E. Saarinen. D. Reidel Publishing, Dordrecht. pp. 245-259.
- Stuart, V. and Head, E.J.H. 2005. The BIO method. In: *The Second SeaWiFS HPLC Analysis Round-Robin Experiment (SeaHARRE-2)*. NASA/TM-2005-212785. National Aeronautics and Space Administration, Goddard Space Flight Center, Maryland, pp. 78-80.
- Stuart, V., Sathyendranath, S., Head, E.J.H., Platt, T., Irwin, B., and Maass, H. 2000. Bio-optical characteristics of diatom and prymnesiophyte populations in the Labrador Sea. *Mar. Ecol. Prog. Ser.* 201:91-106.
- Uitz, J., Claustre, H., Morel, A., and Hooker, S.B. 2006. Vertical distribution of phytoplankton communities in open ocean: An assessment based on surface chlorophyll. *J. Geophys. Res.* 111, C08005, doi:10.1029/2005JC003207.
- Wu, Y., Peterson, I.K., Tang, C.L., Platt, T., Sathyendranath, S., and Fuentes-Yaco, C. 2007. The impact of sea ice on the initiation of the spring bloom on the Newfoundland and Labrador Shelves. *J. Plankton Res.* 29:509-514.
- Yamamoto-Kawai, M., Carmack, E., and McLaughlin, F. 2006. Nitrogen balance and Arctic throughflow. *Nature* 443: 43.
- Yashayaev, I. 2007. Hydrographic changes in the Labrador Sea, 1960-2005. *Prog. Oceanogr.* 73:242-276.
- Yashayaev, I., Head, E.J.H., Azetsu-Scott, K., Ringuette, M., Wang, Z., Anning, J., and Punshon, S. 2014a. Environmental conditions in the Labrador Sea during 2013. *DFO Can. Sci. Advis. Sec. Res. Doc.* 2014/nnn. v +35 p.
- Yashayaev, I., Head, E.J.H., Azetsu-Scott, K., Ringuette, M., Wang, Z., Anning, J., and Punshon, S. 2014b. Environmental conditions in the Labrador Sea during 2013. *Northwest Atlantic Fisheries Organisation Serial No. N6302, NAFO SCR Doc.* 14/011.
- Yashayaev, I., and Clarke, A. 2008. Evolution of North Atlantic water masses inferred from Labrador Sea salinity series. *Oceanography* 21(1):30-45.
- Yeats, P., Ryan, S., and Harrison, G. 2010. Temporal trends in nutrient and oxygen concentrations in the Labrador Sea and on the Scotian Shelf. *AZMP Bulletin* 9:23-27.

## TABLES

TABLE 1. List of AZOMP Labrador Sea cruises 1994-2013.

YEAR	CRUISE	DATE		DAY OF YEAR		# OF DAYS
		START	END	START	END	
1994	94-008	24-May-1994	12-Jun-1994	144	163	20
1995	95-016	6-Jul-1995	23-Jul-1995	187	204	18
1996	96-006	12-May-1996	1-Jun-1996	133	153	21
1997	97-009	9-May-1997	11-Jun-1997	129	162	34
1998	98-023	22-Jun-1998	9-Jul-1998	173	190	18
1999	99-022	27-Jun-1999	13-Jul-1999	178	194	17
2000	00-009	20-May-2000	8-Jun-2000	141	160	20
2001	01-022	30-May-2001	15-Jun-2001	150	166	17
2002	02-032	23-Jun-2002	19-Jul-2002	174	200	27
2003	03-038	13-Jul-2003	4-Aug-2003	194	216	23
2004	04-016	15-May-2004	30-May-2004	136	151	16
2005	05-016	26-May-2005	7-Jun-2005	146	158	13
2006	06-019	24-May-2006	8-Jun-2006	144	159	16
2007	07-011	10-May-2007	27-May-2007	130	147	18
2008	08-009	20-May-2008	4-Jun-2008	141	156	16
2009	09-015	17-May-2009	1-Jun-2009	137	152	16
2010	10-014	13-May-2010	30-May-2010	133	150	18
2011	11-009	6-May-2011	28-May-2011	126	148	23
2012	12-001	1-Jun-2012	17-Jun-2012	153	169	17
2013	13-008	6-May-2013	28-May-2013	126	148	23
<b>Average</b>				<b>149</b>	<b>167</b>	<b>20</b>
<b>Std Dev</b>				<b>21</b>	<b>21</b>	<b>5</b>
<b>Minimum</b>				<b>126</b>	<b>147</b>	<b>13</b>
<b>Maximum</b>				<b>194</b>	<b>216</b>	<b>34</b>

TABLE 2. Location, ocean bottom depth, and section distance for standard AR7W stations in 3 nominal regions of the Labrador Sea.

Nominal Region*	AR7W Station	Latitude (North)	Longitude (West)	Bottom Depth (m)	Section distance (km)
LSS	1	53.68	55.55	160	0
LSS	2	53.80	55.44	210	15
LSS	3	53.99	55.25	148	40
LSS	4	54.22	55.02	170	69
LSS	5	54.49	54.76	202	105
LSS	6	54.76	54.49	239	140
LSS	7	54.96	54.30	364	165
LSS	8	55.11	54.14	1567	188
LSS	9	55.26	53.98	2053	205
LSS	10	55.42	53.83	2718	225
CLB	11	55.61	53.63	2950	250
CLB	12	55.85	53.40	3164	280
CLB	13	56.11	53.12	3370	315
CLB	14	56.54	52.68	3541	370
CLB	15	56.96	52.24	3568	426
CLB	16	57.38	51.79	3588	484
CLB	17	57.80	51.34	3679	535
CLB	18	58.22	50.88	3605	585
CLB	19	58.64	50.42	3576	648
CLB	20	59.07	49.95	3517	705
CLB	21	59.48	49.48	3334	760
CLB	22	59.75	49.17	3268	797
CLB	23	59.98	48.90	2968	828
GSS	24	60.18	48.68	2899	853
GSS	25	60.29	48.54	2703	870
GSS	26	60.37	48.45	738	878
GSS	27	60.45	48.36	145	890
GSS	28	60.57	48.23	128	906

\* **Nominal Region**

LSS = Labrador Shelf and Slope

CLB = Central Labrador Basin

GSS = Greenland Shelf and Slope

TABLE 3. Climatological depth-averaged mean values on AR7W in spring/summer. Units: Celsius (temperature); psu (salinity);  $\text{kg m}^{-3}$  (sigma-theta,  $\Delta$  sigma-theta);  $\text{ml l}^{-1}$  (oxygen);  $\text{mmol m}^{-3}$  (nitrate, phosphate, silicate, excess phosphate, excess silicate);  $\text{cells ml}^{-1}$  (bacteria, *Synechococcus*, picoeukaryotes, picophytoplankton, nanophytoplankton);  $\text{mg m}^{-3}$  (chlorophyll *a*). P\* = phosphate excess relative to Redfield is [P-N/16]; Si\* = silicate excess relative to diatom requirement is [Si-N].

REGION	STATION	DEPTH AVERAGE (0-100M)				DEPTH AVERAGE (0-100M)											
		TEMPERATURE	SALINITY	SIGMA-THETA	$\Delta$ SIGMA-THETA	OXYGEN	NITRATE	PHOSPHATE	SILICATE	P*	Si*	CHLOROPHYLL	BACTERIA	SYNECHO	PICOEUK	PICOPHYTO	NANOPHYTO
LSS	L3-01	-0.18	32.31	25.92	1.73	8.17	5.18	0.73	6.43	0.44	1.64	2.13	517777	45	3076	3095	717
LSS	L3-02	-0.11	32.44	26.02	1.24	8.31	5.04	0.72	6.14	0.43	1.41	2.28	595852	50	3251	3290	783
LSS	L3-03	-0.23	32.59	26.17	1.29	8.04	6.10	0.74	6.74	0.41	1.17	1.97	527930	34	2436	2469	854
LSS	L3-04	-0.35	32.64	26.20	1.20	7.94	6.06	0.73	6.51	0.39	1.02	2.22	476731	39	2770	2807	712
LSS	L3-05	-0.38	32.69	26.25	1.08	7.76	6.32	0.77	7.45	0.40	1.39	1.91	465881	38	3049	3087	858
LSS	L3-06	-0.39	32.77	26.33	1.16	7.84	7.04	0.80	7.43	0.38	0.65	1.57	426967	38	2937	2975	796
LSS	L3-07	-0.09	33.19	26.65	1.10	7.81	7.48	0.77	7.40	0.32	0.15	1.61	521273	36	3138	3172	812
LSS	L3-08	1.95	33.93	27.10	0.91	7.30	8.85	0.76	6.63	0.21	-2.18	1.59	618730	98	3642	3740	1100
LSS	L3-09	3.09	34.28	27.29	0.76	7.44	10.06	0.78	6.43	0.15	-3.64	1.75	636779	180	5136	5315	1158
LSS	L3-10	3.61	34.42	27.33	0.60	7.49	9.82	0.76	5.81	0.15	-4.01	1.56	712803	331	5181	5512	1144
LSS	AVERAGE	0.69	33.13	26.53	1.11	7.81	7.20	0.75	6.70	0.33	-0.24	1.86	550072	89	3462	3546	893
CLB	L3-11	3.79	34.50	27.40	0.56	7.24	10.21	0.76	5.78	0.12	-4.37	1.60	866664	406	4654	4929	1980
CLB	L3-12	4.17	34.49	27.36	0.46	7.25	9.56	0.69	5.34	0.11	-4.22	2.41	1050803	981	5874	6854	1707
CLB	L3-13	4.14	34.64	27.49	0.25	7.40	10.23	0.75	5.37	0.11	-4.87	1.75	898638	1530	7417	8947	1551
CLB	L3-14	4.40	34.69	27.50	0.25	7.34	9.82	0.73	4.84	0.12	-4.98	1.58	885394	1472	5790	7157	1404
CLB	L3-15	4.39	34.70	27.50	0.20	7.35	10.47	0.78	5.34	0.12	-5.14	1.54	974087	1853	7096	8919	1734
CLB	L3-16	4.30	34.70	27.51	0.23	7.10	10.47	0.75	5.44	0.10	-5.03	1.36	816321	1822	4838	6242	1485
CLB	L3-17	4.32	34.71	27.52	0.24	7.36	9.86	0.76	5.40	0.15	-4.45	1.95	1058854	1601	7007	8608	2224
CLB	L3-18	4.46	34.72	27.51	0.22	7.21	10.27	0.75	5.66	0.10	-4.64	1.66	1065268	1450	6566	7910	1761
CLB	L3-19	4.62	34.74	27.51	0.22	7.38	10.33	0.77	5.70	0.12	-4.63	1.42	1218711	1648	8232	9880	1892
CLB	L3-20	4.28	34.64	27.46	0.29	7.31	8.90	0.71	5.21	0.15	-3.68	1.42	1075596	1128	5024	6390	2776
CLB	L3-21	4.23	34.60	27.43	0.32	7.31	8.14	0.68	5.15	0.16	-2.99	2.21	1118184	628	4046	4675	2609
CLB	L3-22	4.18	34.51	27.36	0.29	7.37	6.44	0.55	4.20	0.17	-2.24	2.35	1231469	377	3884	4229	2635
CLB	L3-23	4.31	34.57	27.39	0.34	7.50	7.94	0.65	4.70	0.15	-3.24	3.11	1018147	769	2600	3369	3679
CLB	AVERAGE	4.28	34.63	27.46	0.30	7.32	9.43	0.72	5.24	0.13	-4.19	1.87	1021395	1205	5618	6778	2111
GSS	L3-24	4.43	34.59	27.39	0.33	7.41	8.44	0.70	5.26	0.17	-3.18	2.47	927612	1042	3940	4982	3532
GSS	L3-25	3.69	34.32	27.23	0.54	7.67	7.87	0.65	4.43	0.16	-3.45	3.64	676766	895	2707	3602	4517
GSS	L3-26	2.31	34.03	27.14	0.67	7.37	7.21	0.63	4.11	0.18	-3.10	3.75	475144	136	673	774	2339
GSS	L3-27	1.12	33.57	26.90	0.80	7.83	5.75	0.54	3.56	0.20	-2.18	4.10	471927	64	1013	1075	3357
GSS	L3-28	0.75	33.26	26.67	0.90	8.14	3.73	0.43	2.34	0.20	-1.40	5.84	563983	43	881	924	3410
GSS	AVERAGE	2.46	33.95	27.07	0.65	7.68	6.60	0.59	3.94	0.18	-2.66	3.96	623086	436	1843	2271	3431

TABLE 4. Climatological near-surface mean values on AR7W in spring/summer. Units:  $\text{mg m}^{-3}$  (POC, PON, 19'-butanoyloxyfucoxanthin [BUT], 19'-hexanoyloxyfucoxanthin [HEX], alloxanthin [ALLO], chlorophyll *a* [CHL*a*], chlorophyll *b* [CHL*b*], chlorophyll  $c_1+c_2$  [CHL*c*<sub>1+c<sub>2</sub></sub>], chlorophyll  $c_3$  [CHL*c*<sub>3</sub>], diadinoxanthin [DIADINO], diatoxanthin [DIATO], fucoxanthin [FUCO], peridinin [PERI], zeaxanthin [ZEA], diagnostic pigments [DIAGPIG]);  $\text{mol mol}^{-1}$  (POC:PON).

		NEAR-SURFACE VALUE															
REGION	STATION	POC	PON	POC:PON	BUT	HEX	ALLO	CHL <i>a</i>	CHL <i>b</i>	CHL <i>c</i> <sub>1+c<sub>2</sub></sub>	CHL <i>c</i> <sub>3</sub>	DIADINO	DIATO	FUCO	PERI	ZEA	DIAGPIG
LSS	L3-01	399	42	11.60	0.013	0.095	0.000	4.31	0.13	0.53	0.02	0.15	0.010	0.93	0.030	0.014	1.63
LSS	L3-02	358	44	9.64	0.012	0.075	0.000	4.06	0.14	0.53	0.04	0.15	0.012	1.25	0.010	0.014	2.03
LSS	L3-03	629	72	10.31	0.028	0.071	0.004	6.71	0.17	0.84	0.01	0.30	0.031	1.66	0.034	0.039	2.69
LSS	L3-04	471	51	10.47	0.004	0.070	0.000	5.81	0.21	0.64	0.00	0.22	0.020	1.30	0.014	0.023	2.17
LSS	L3-05	677	77	10.34	0.017	0.078	0.000	6.37	0.30	0.76	0.01	0.20	0.014	1.41	0.021	0.013	2.44
LSS	L3-06	447	59	8.69	0.017	0.091	0.000	6.10	0.34	0.71	0.02	0.20	0.014	1.33	0.019	0.035	2.39
LSS	L3-07	228	33	8.32	0.004	0.100	0.000	2.90	0.34	0.26	0.02	0.15	0.014	0.62	0.029	0.026	1.42
LSS	L3-08	258	46	6.95	0.015	0.092	0.011	3.24	0.17	0.37	0.04	0.21	0.013	1.23	0.033	0.014	2.10
LSS	L3-09	301	49	8.03	0.025	0.120	0.020	2.87	0.16	0.29	0.05	0.16	0.027	0.76	0.074	0.018	1.53
LSS	L3-10	244	41	7.71	0.028	0.174	0.025	2.94	0.13	0.34	0.11	0.21	0.021	1.01	0.067	0.009	1.91
LSS	AVERAGE	401	51	9.21	0.016	0.097	0.006	4.53	0.21	0.53	0.03	0.19	0.017	1.15	0.033	0.020	2.03
CLB	L3-11	264	41	7.96	0.039	0.185	0.024	3.32	0.13	0.46	0.15	0.21	0.029	1.05	0.077	0.011	1.99
CLB	L3-12	321	49	7.30	0.044	0.228	0.030	3.48	0.12	0.45	0.22	0.29	0.035	1.43	0.057	0.018	2.56
CLB	L3-13	342	57	7.52	0.028	0.222	0.020	2.71	0.09	0.38	0.16	0.24	0.016	1.01	0.050	0.011	1.90
CLB	L3-14	234	38	8.28	0.025	0.132	0.020	2.95	0.10	0.40	0.16	0.17	0.015	1.12	0.038	0.010	1.93
CLB	L3-15	282	49	7.51	0.036	0.104	0.021	2.00	0.11	0.28	0.08	0.16	0.010	0.94	0.029	0.010	1.65
CLB	L3-16	197	31	7.54	0.038	0.140	0.014	1.52	0.08	0.22	0.11	0.12	0.009	0.54	0.024	0.005	1.07
CLB	L3-17	295	42	8.27	0.019	0.116	0.014	2.33	0.09	0.33	0.16	0.14	0.015	0.86	0.034	0.012	1.53
CLB	L3-18	326	55	7.76	0.026	0.121	0.012	3.09	0.10	0.43	0.17	0.16	0.008	1.27	0.049	0.010	2.14
CLB	L3-19	307	46	7.92	0.030	0.149	0.012	2.05	0.07	0.36	0.12	0.14	0.026	0.74	0.035	0.014	1.37
CLB	L3-20	216	32	7.83	0.022	0.115	0.016	1.90	0.09	0.25	0.09	0.11	0.011	0.57	0.051	0.008	1.14
CLB	L3-21	370	63	6.98	0.010	0.143	0.011	3.10	0.06	0.42	0.16	0.14	0.011	0.98	0.047	0.009	1.71
CLB	L3-22	378	68	6.82	0.016	0.125	0.014	2.41	0.13	0.33	0.12	0.14	0.009	0.82	0.029	0.010	1.51
CLB	L3-23	512	81	7.55	0.020	0.087	0.005	4.10	0.06	0.47	0.09	0.10	0.006	1.09	0.018	0.003	1.74
CLB	AVERAGE	311	50	7.63	0.027	0.144	0.016	2.69	0.09	0.37	0.14	0.16	0.015	0.96	0.041	0.010	1.71
GSS	L3-24	242	37	7.68	0.048	0.165	0.007	3.87	0.35	0.45	0.12	0.11	0.007	0.97	0.020	0.004	1.98
GSS	L3-25	344	56	7.60	0.015	0.099	0.006	5.26	0.05	0.60	0.13	0.14	0.006	1.41	0.000	0.004	2.18
GSS	L3-26	524	86	7.27	0.000	0.031	0.005	6.95	0.40	0.84	0.14	0.17	0.002	1.86	0.000	0.000	3.06
GSS	L3-27	450	57	9.44	0.000	0.000	0.003	5.76	0.02	0.63	0.04	0.11	0.003	1.37	0.000	0.004	1.96
GSS	L3-28	620	74	10.10	0.000	0.000	0.004	5.99	0.04	0.68	0.06	0.13	0.007	1.52	0.000	0.026	2.21
GSS	AVERAGE	436	62	8.42	0.013	0.059	0.005	5.57	0.17	0.64	0.10	0.13	0.005	1.43	0.004	0.008	2.28

Figure 1

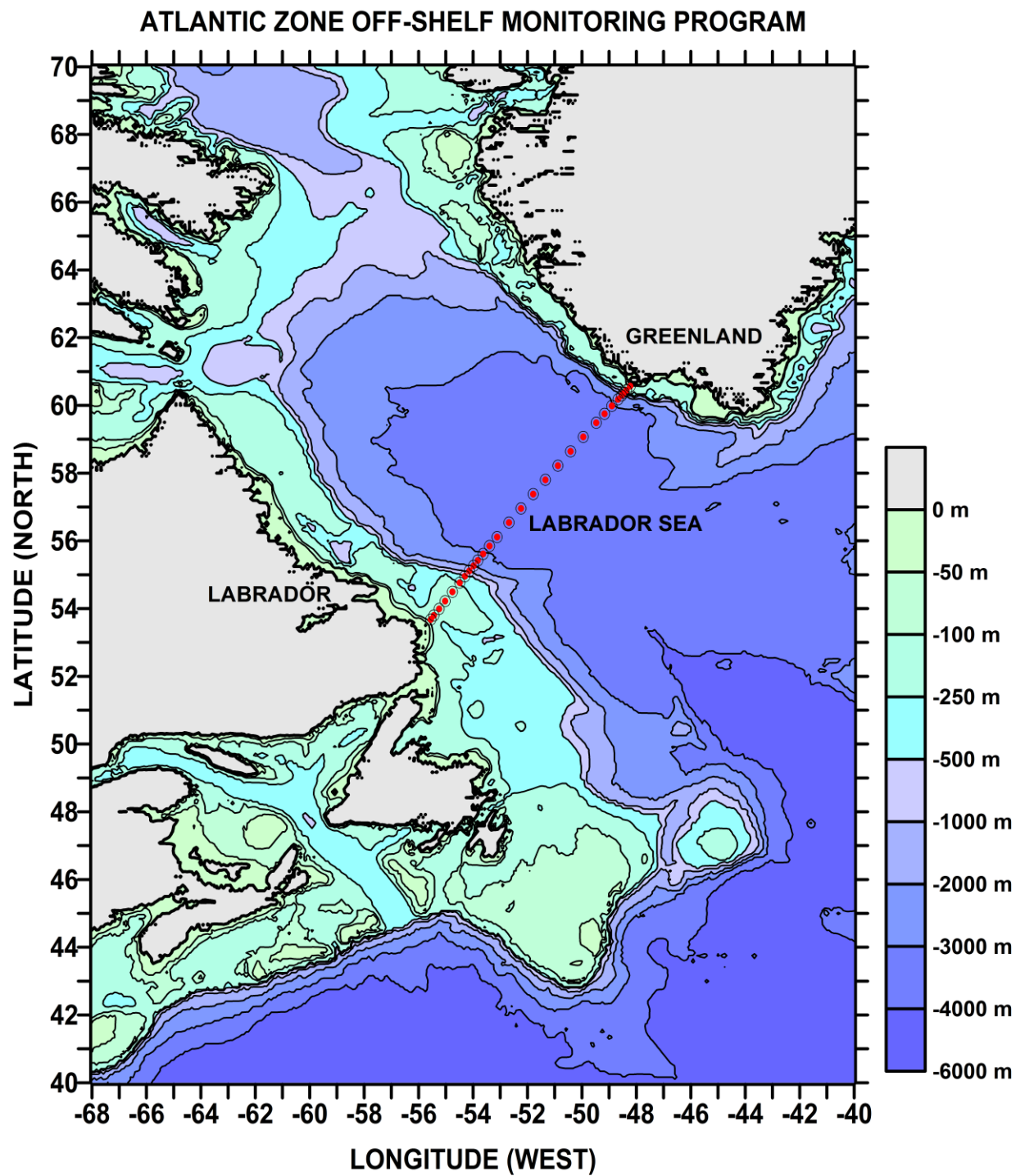




Figure 2

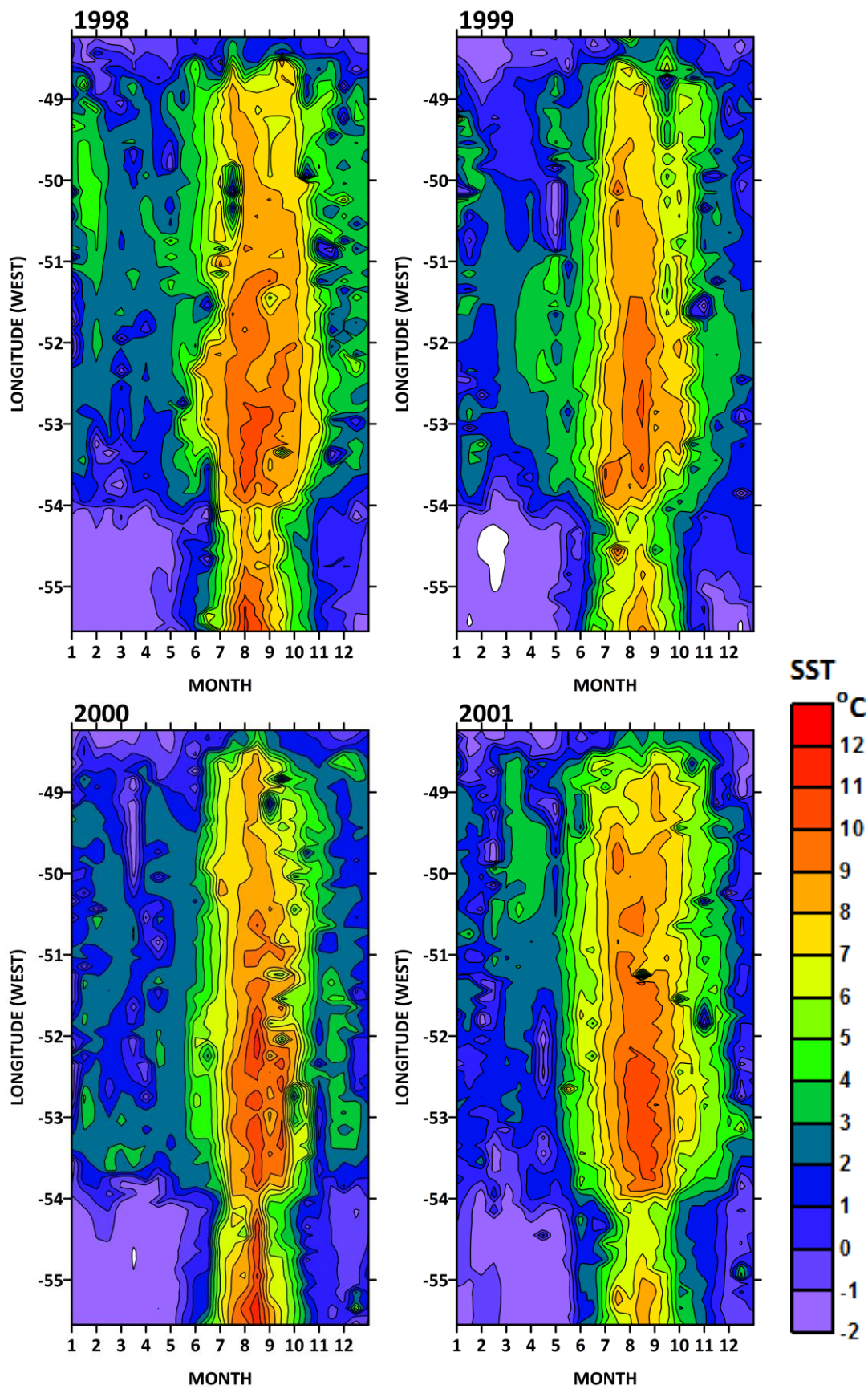


Figure 3

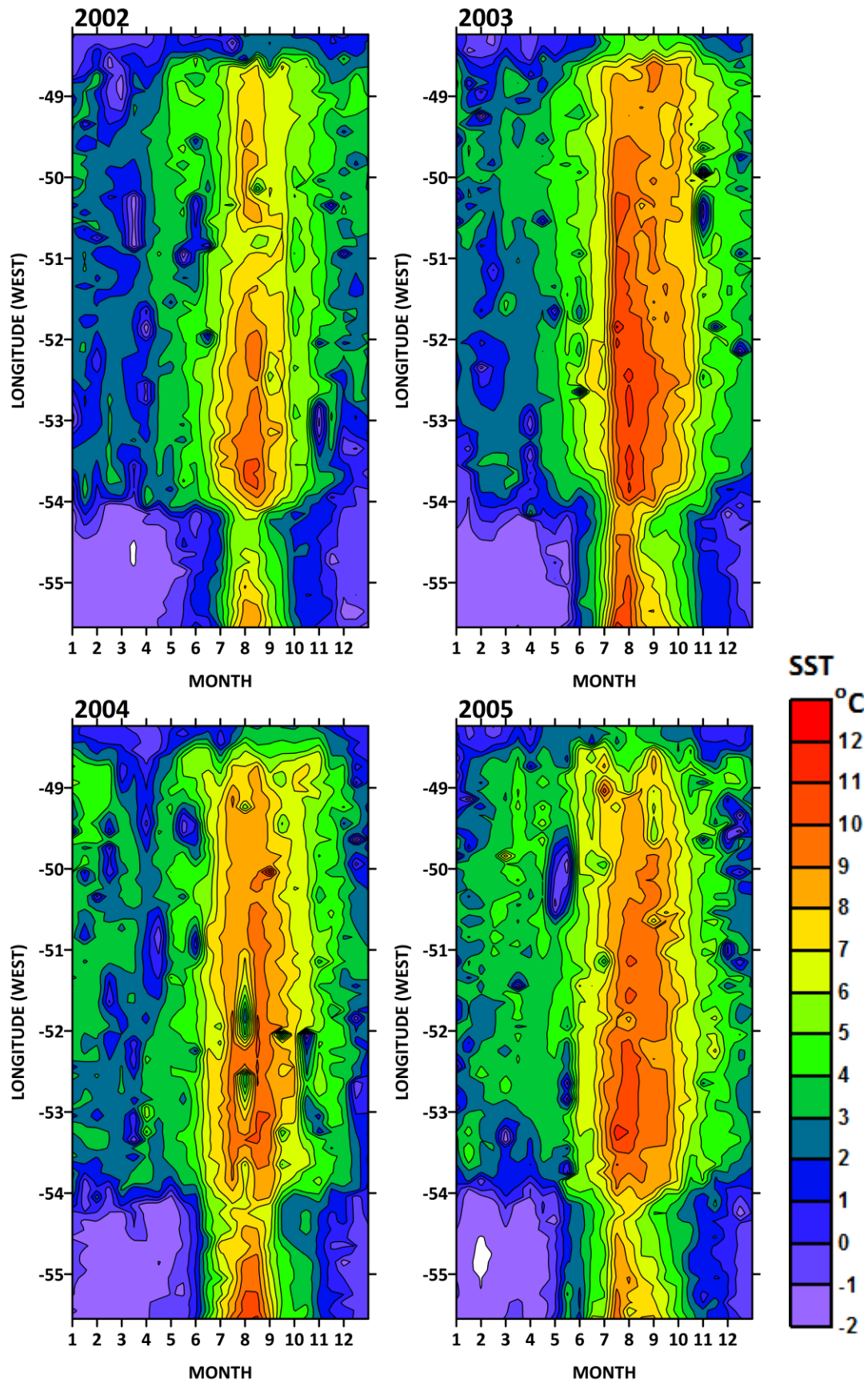




Figure 4

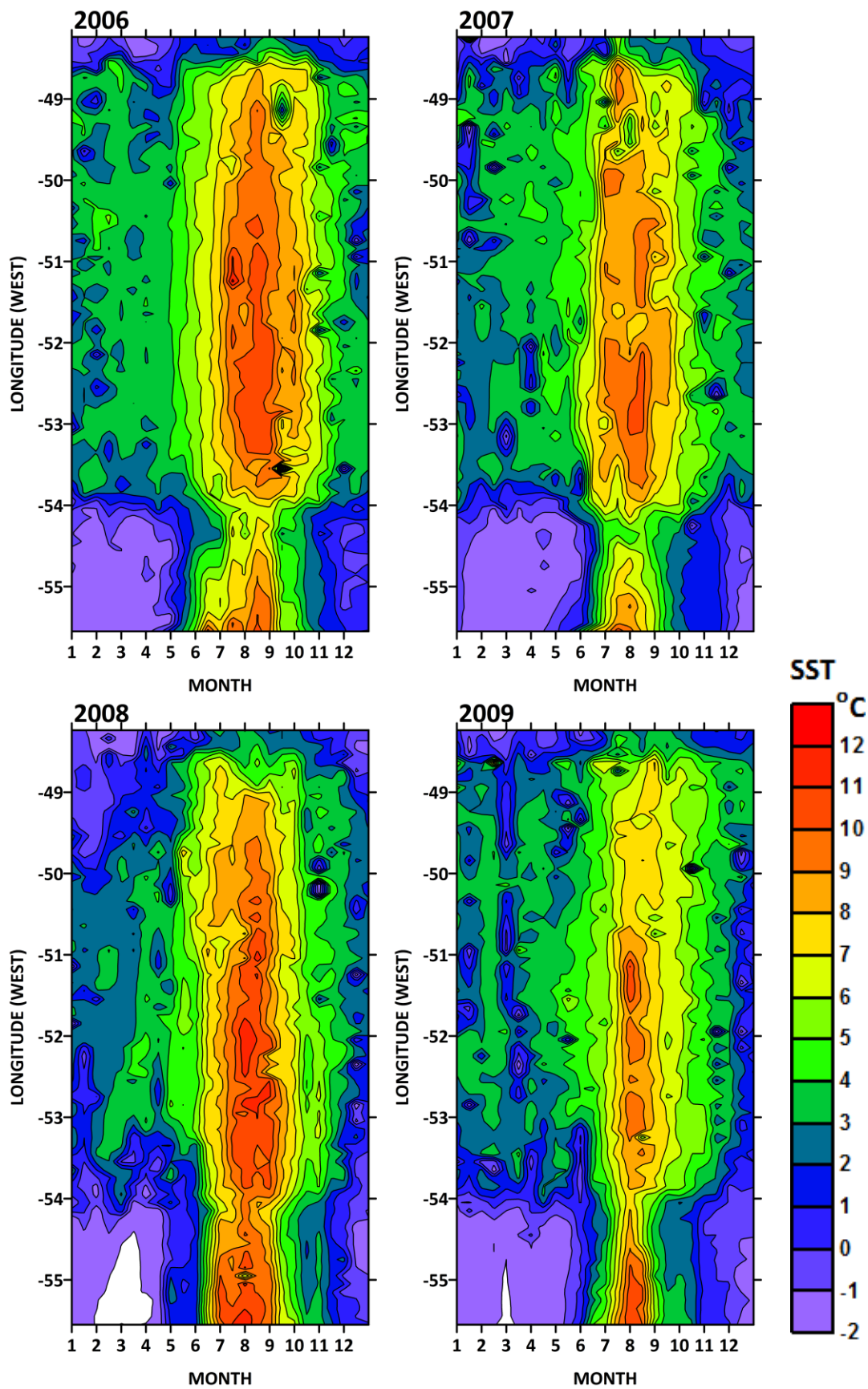


Figure 5

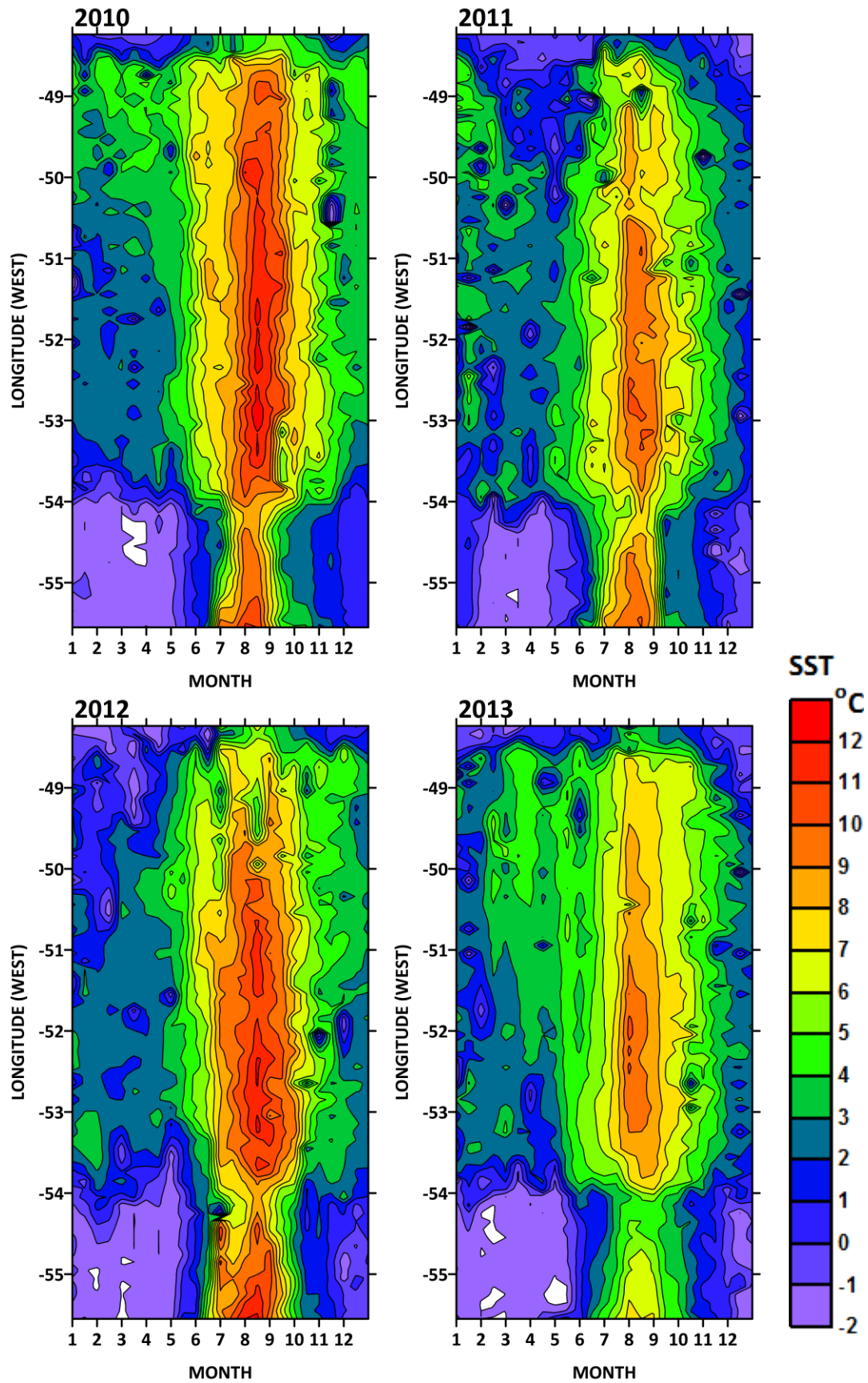


Figure 6

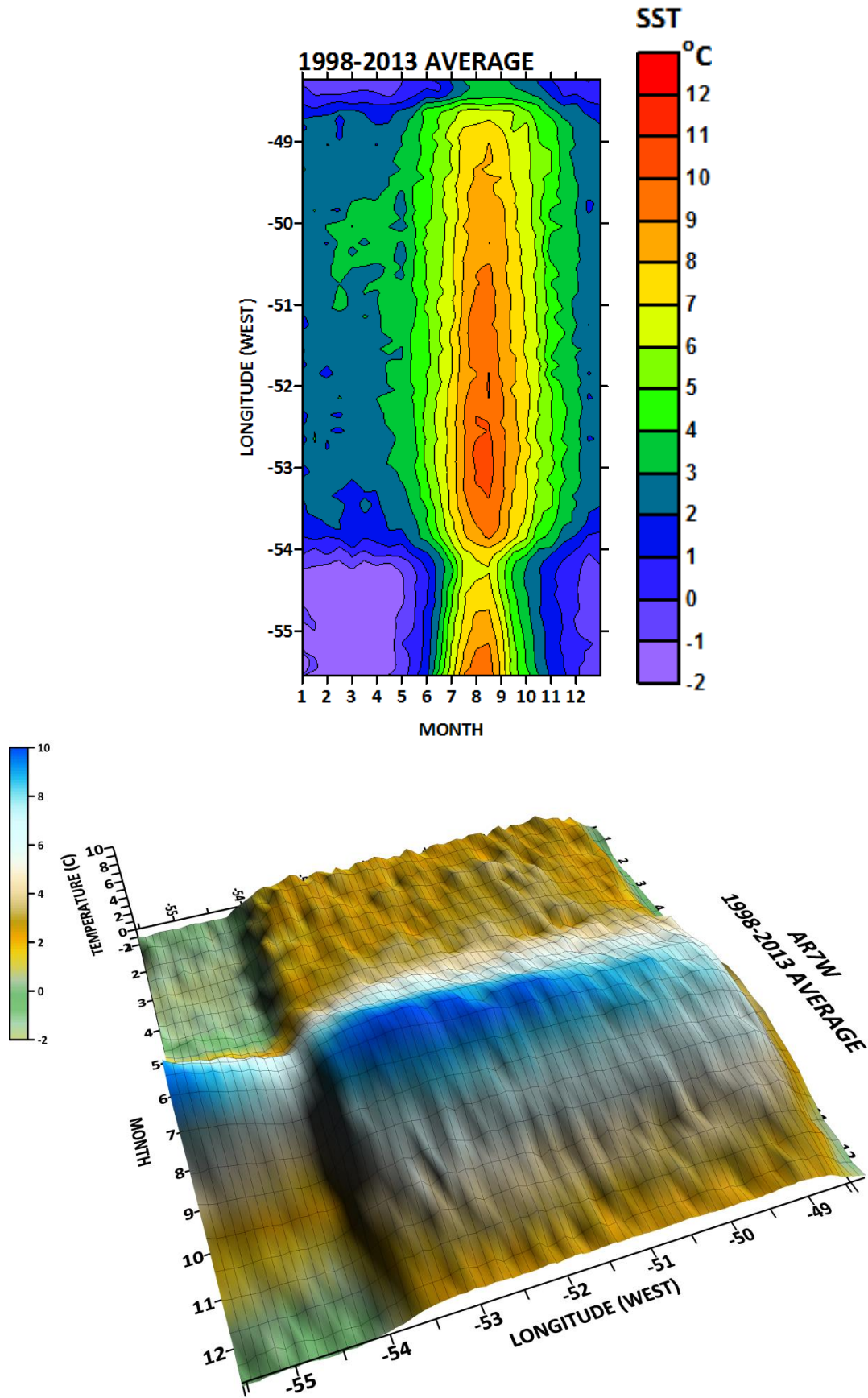


Figure 7

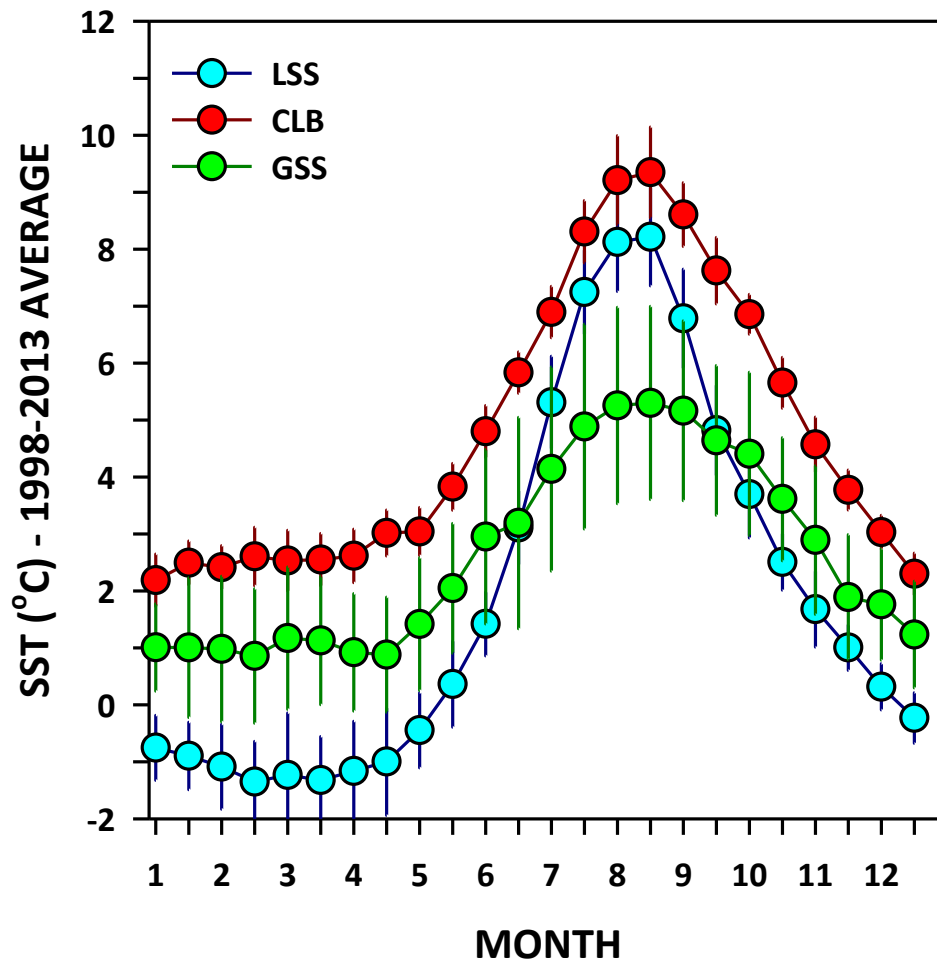


Figure 8

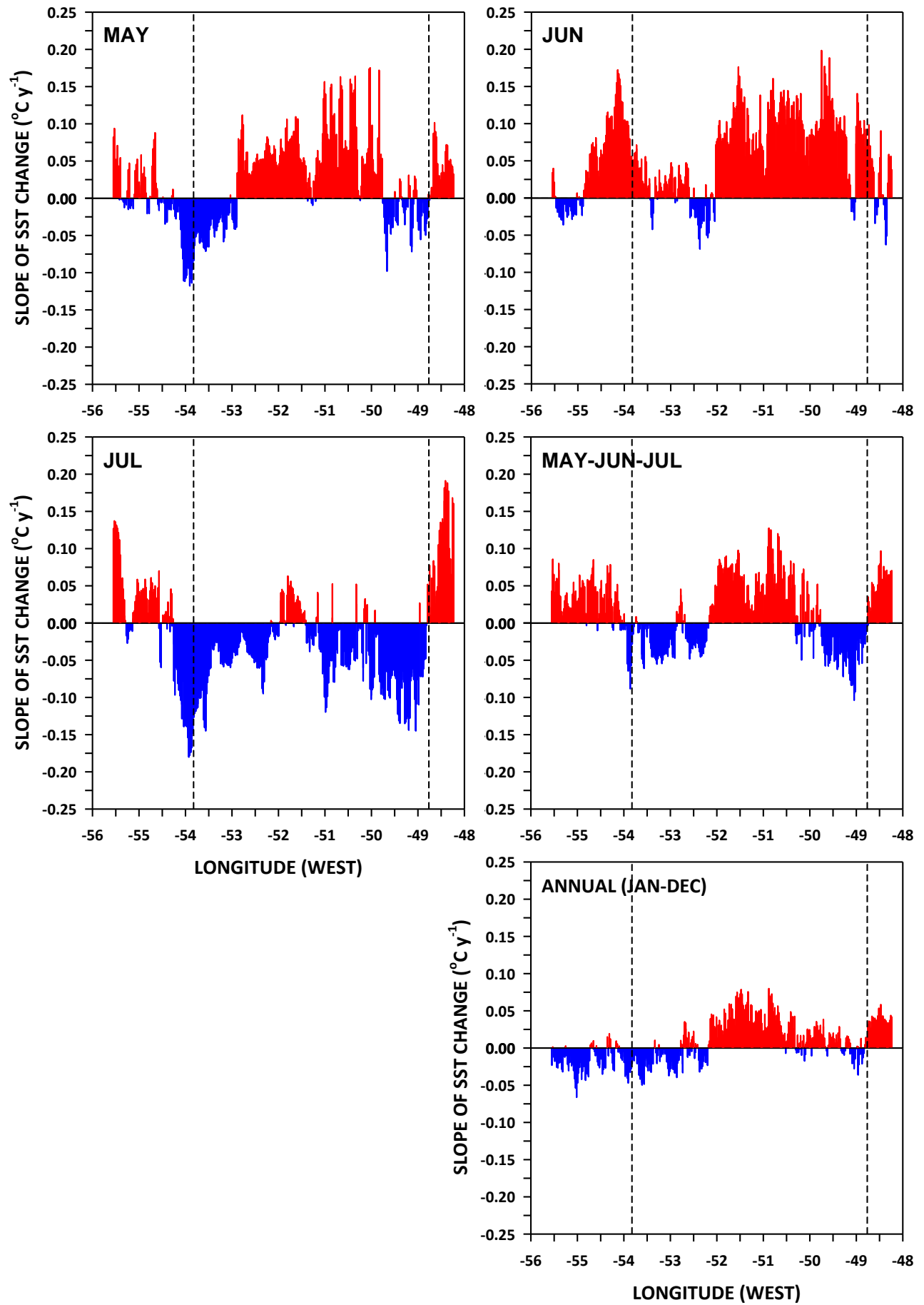


Figure 9

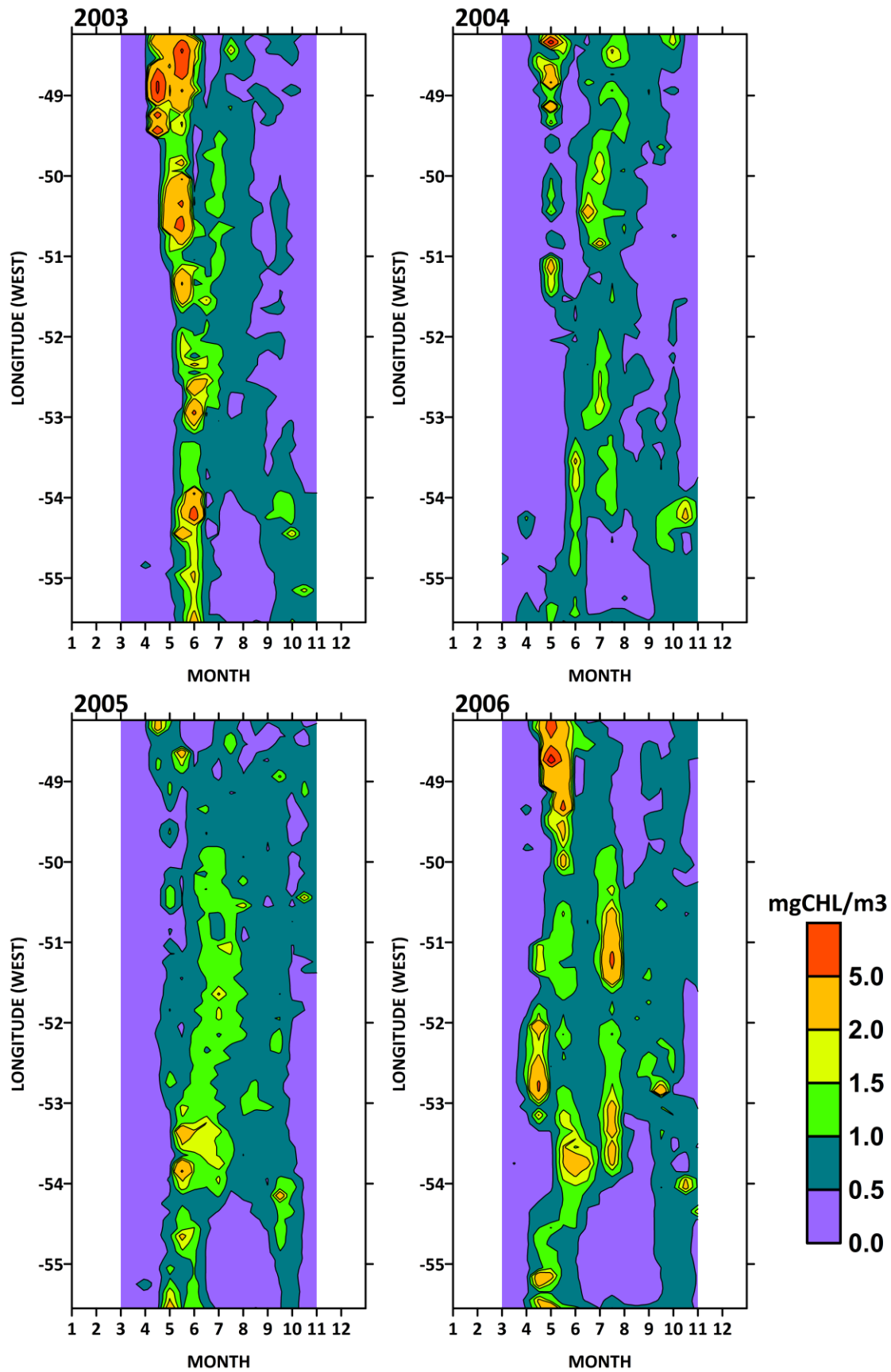




Figure 10

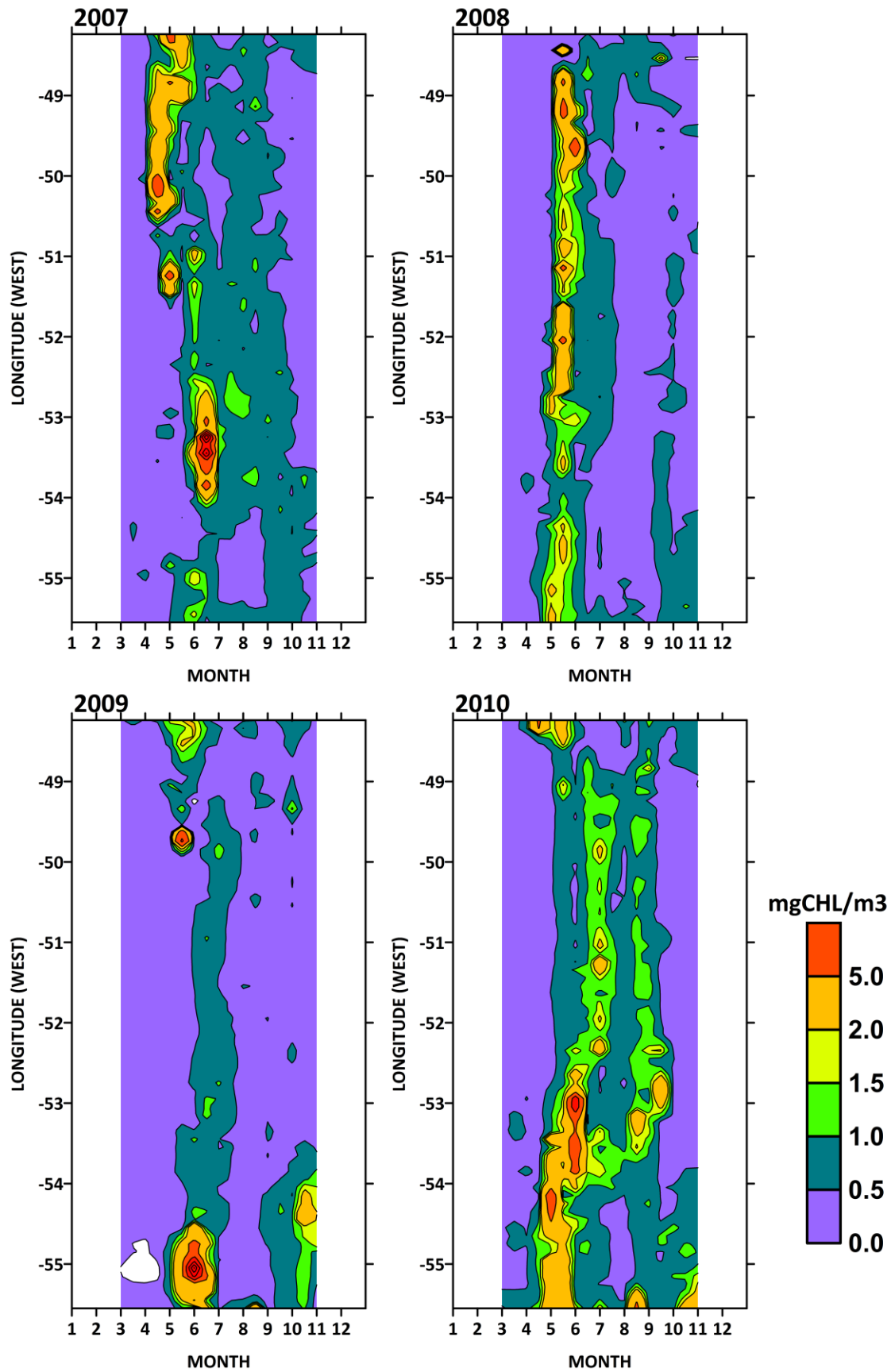


Figure 11

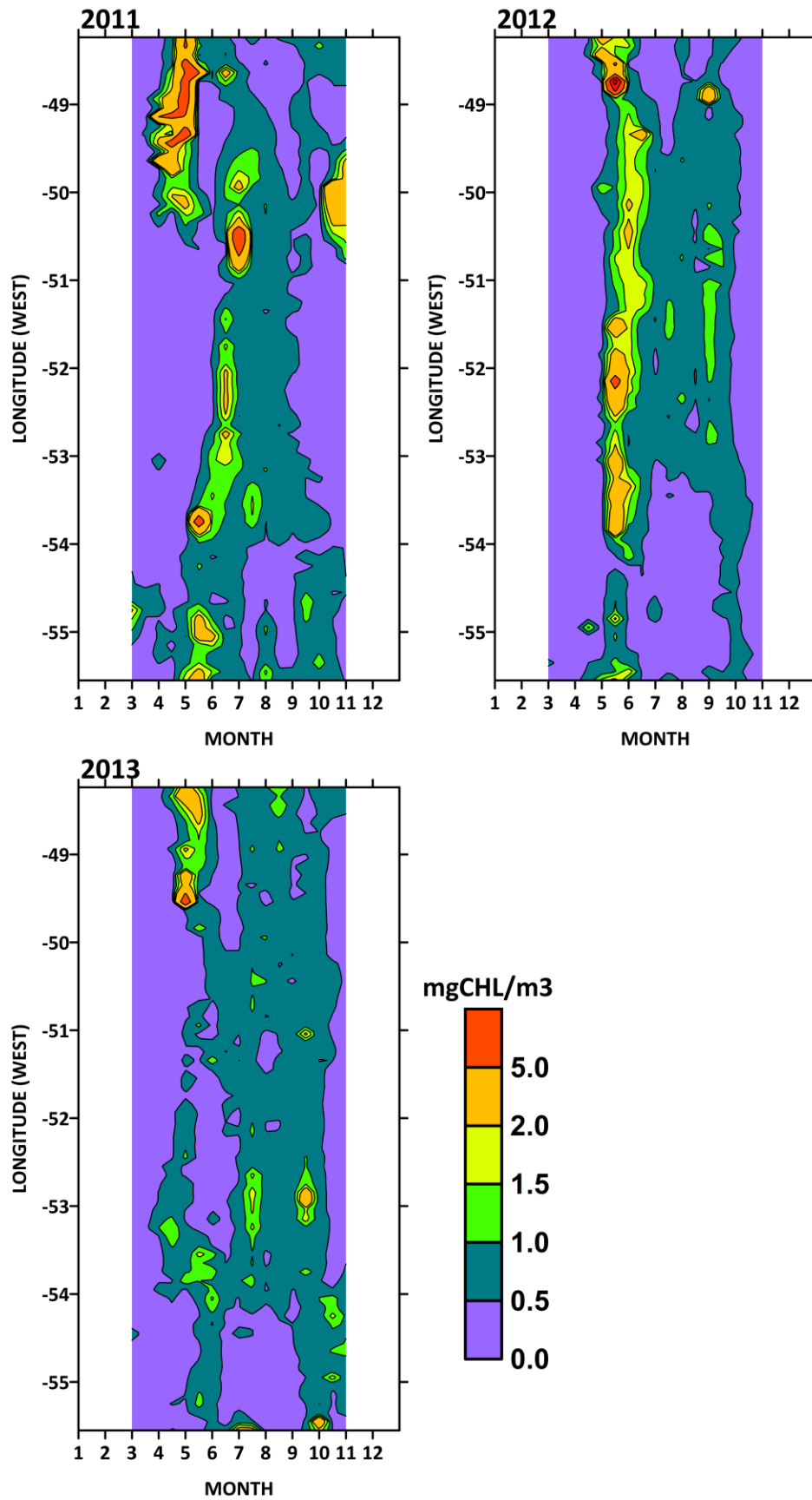




Figure 12

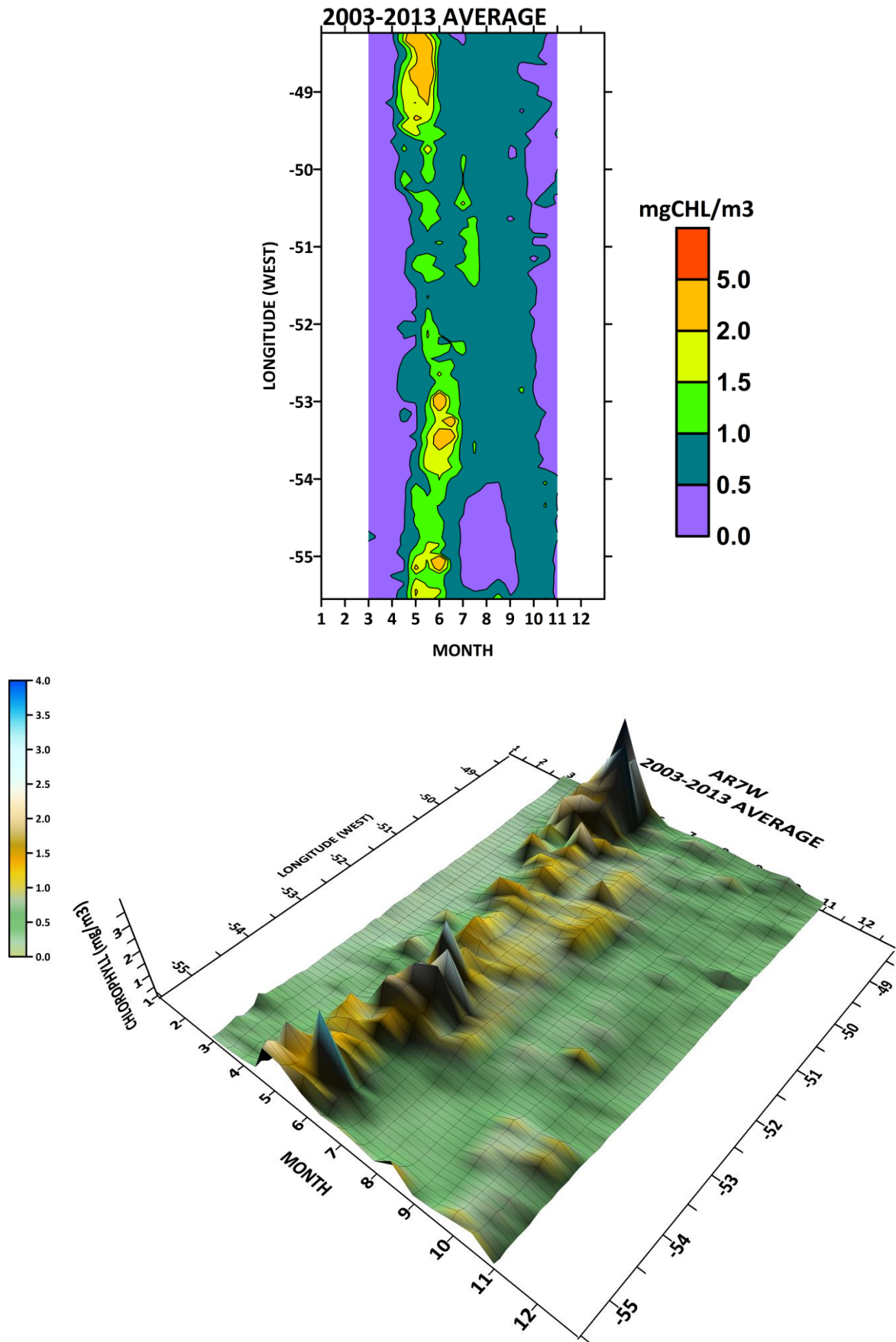


Figure 13

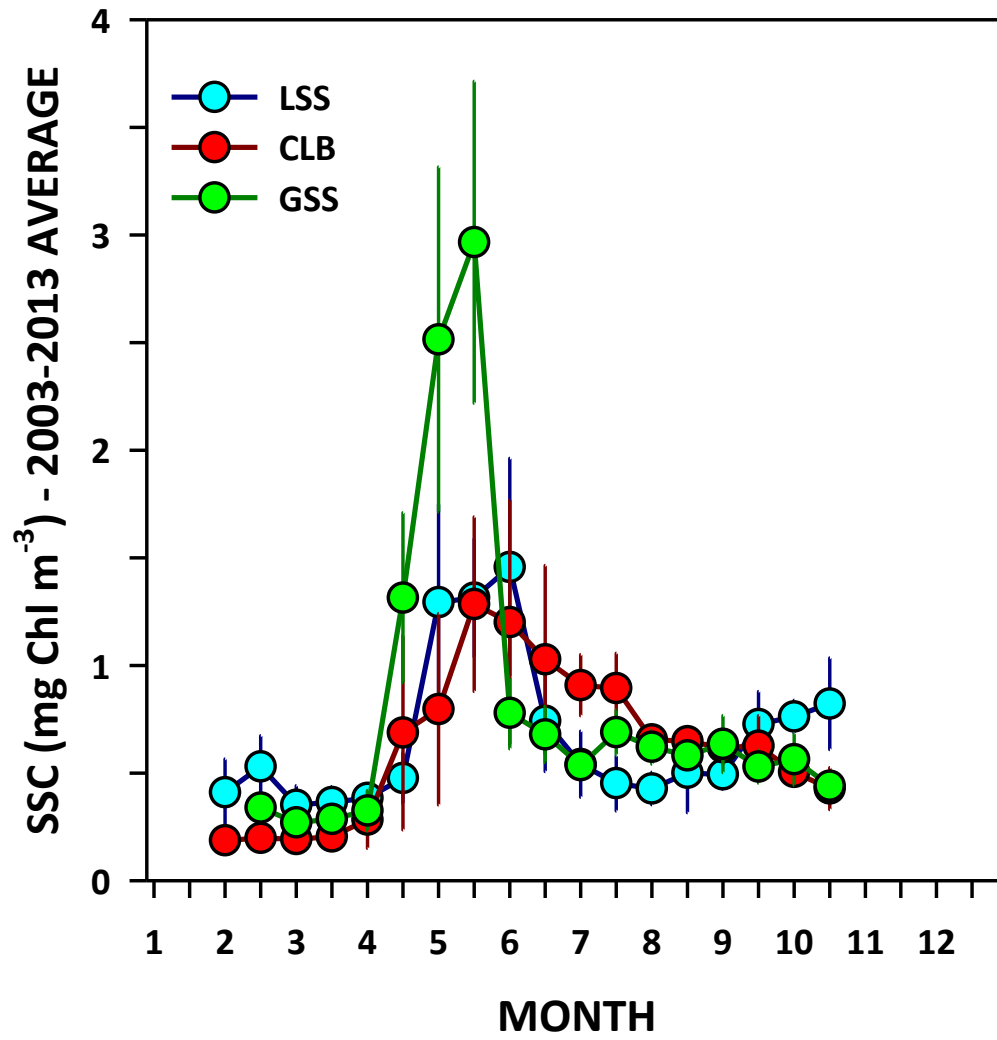


Figure 14

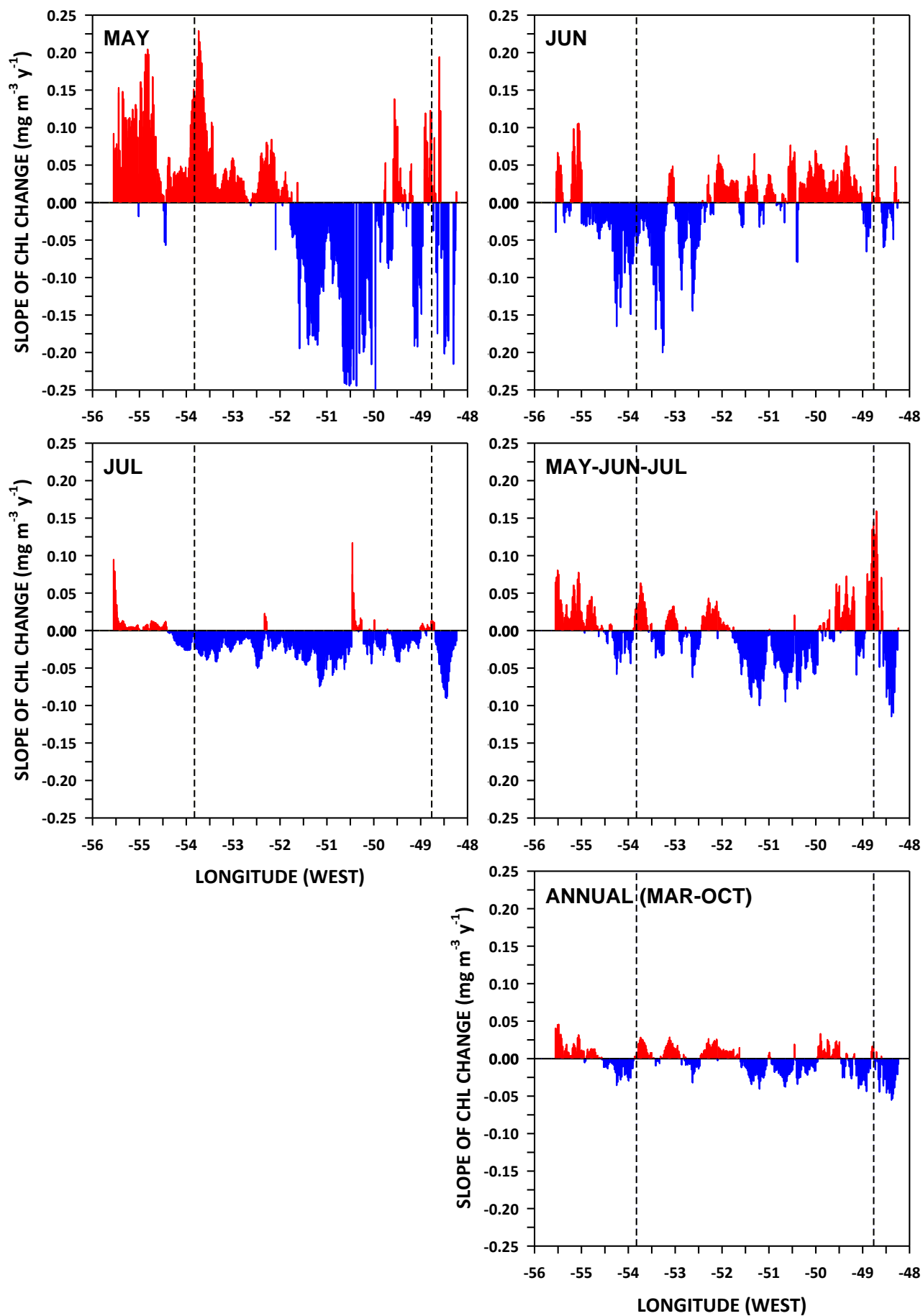


Figure 15

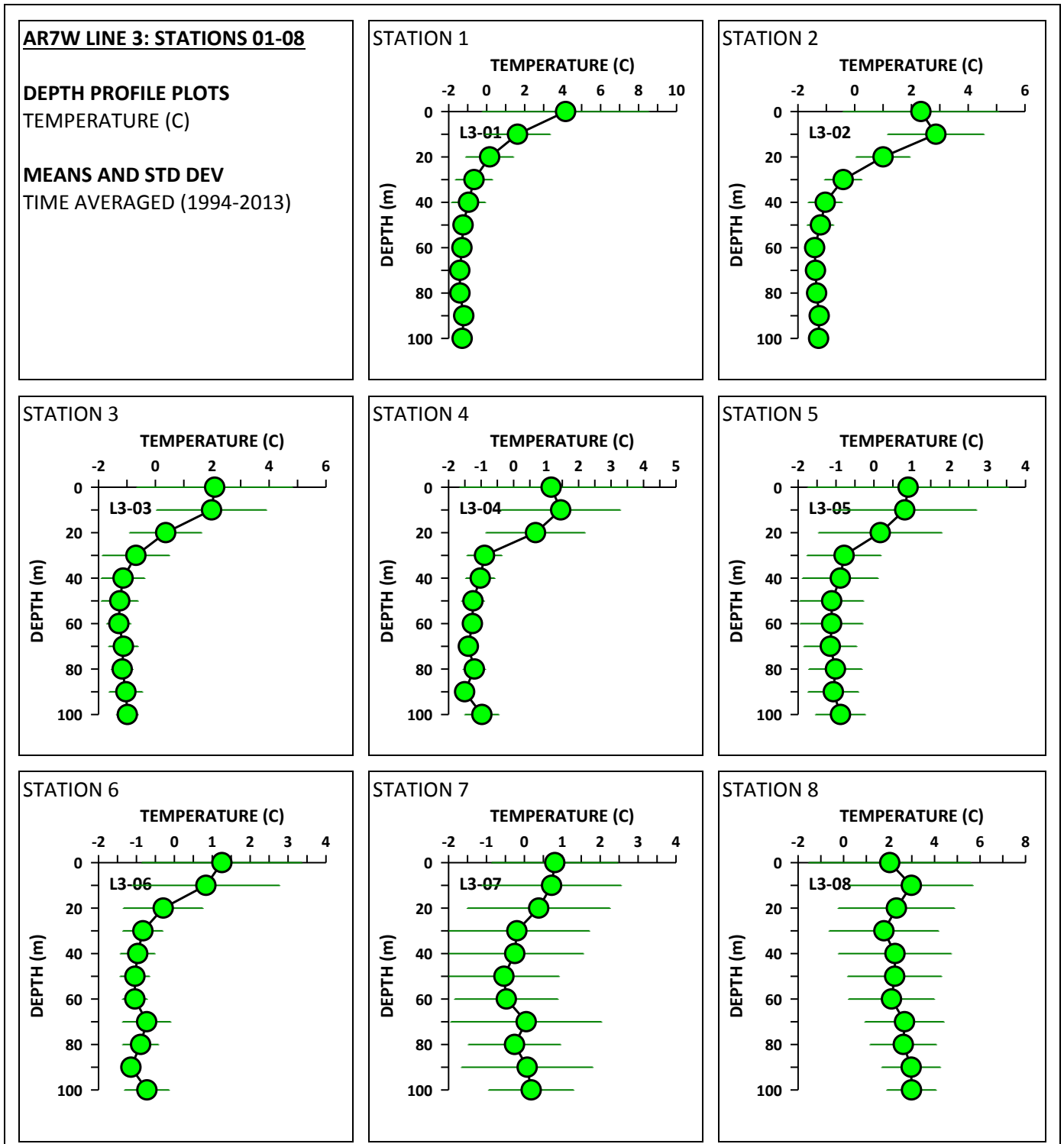




Figure 17

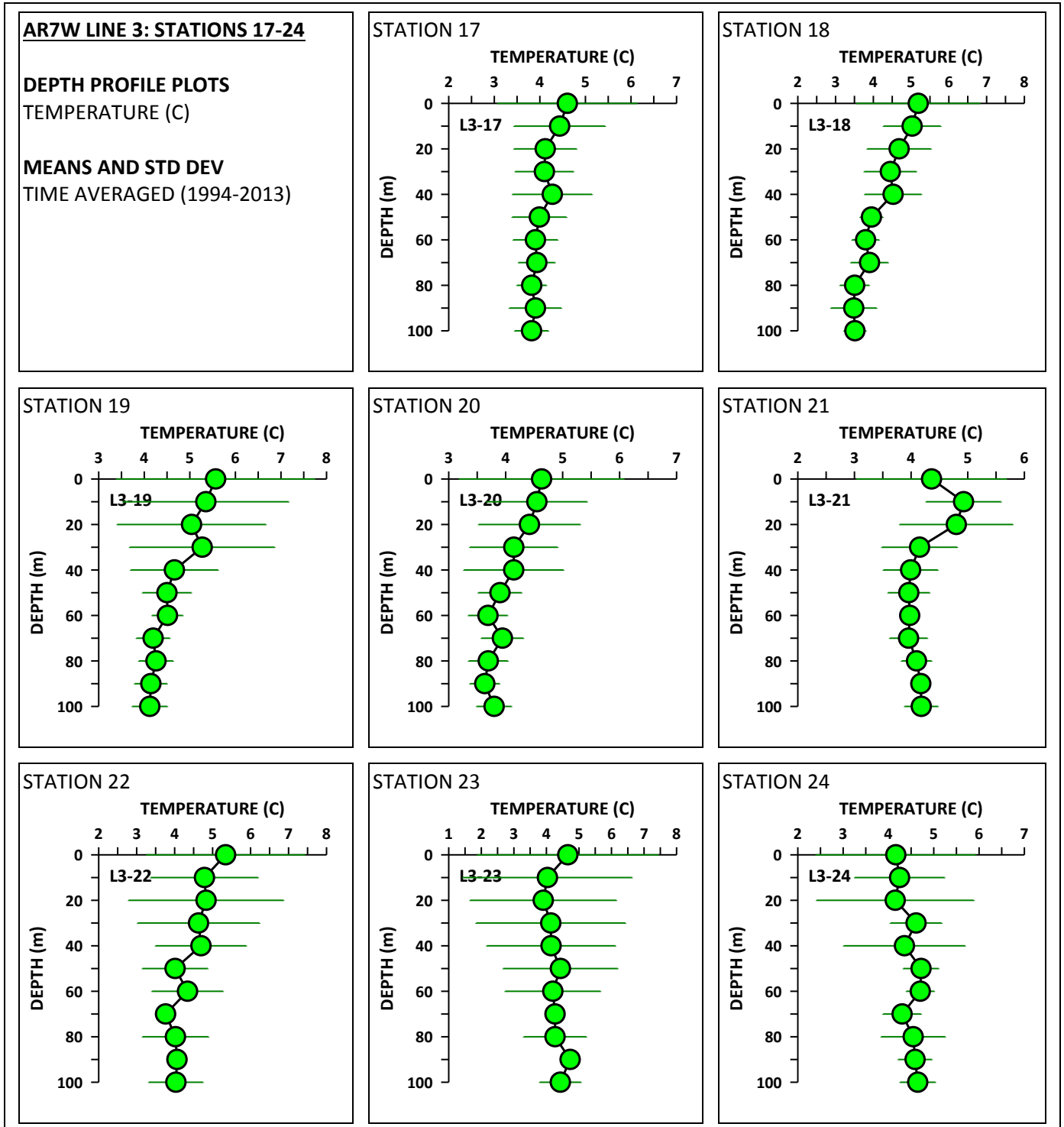


Figure 18

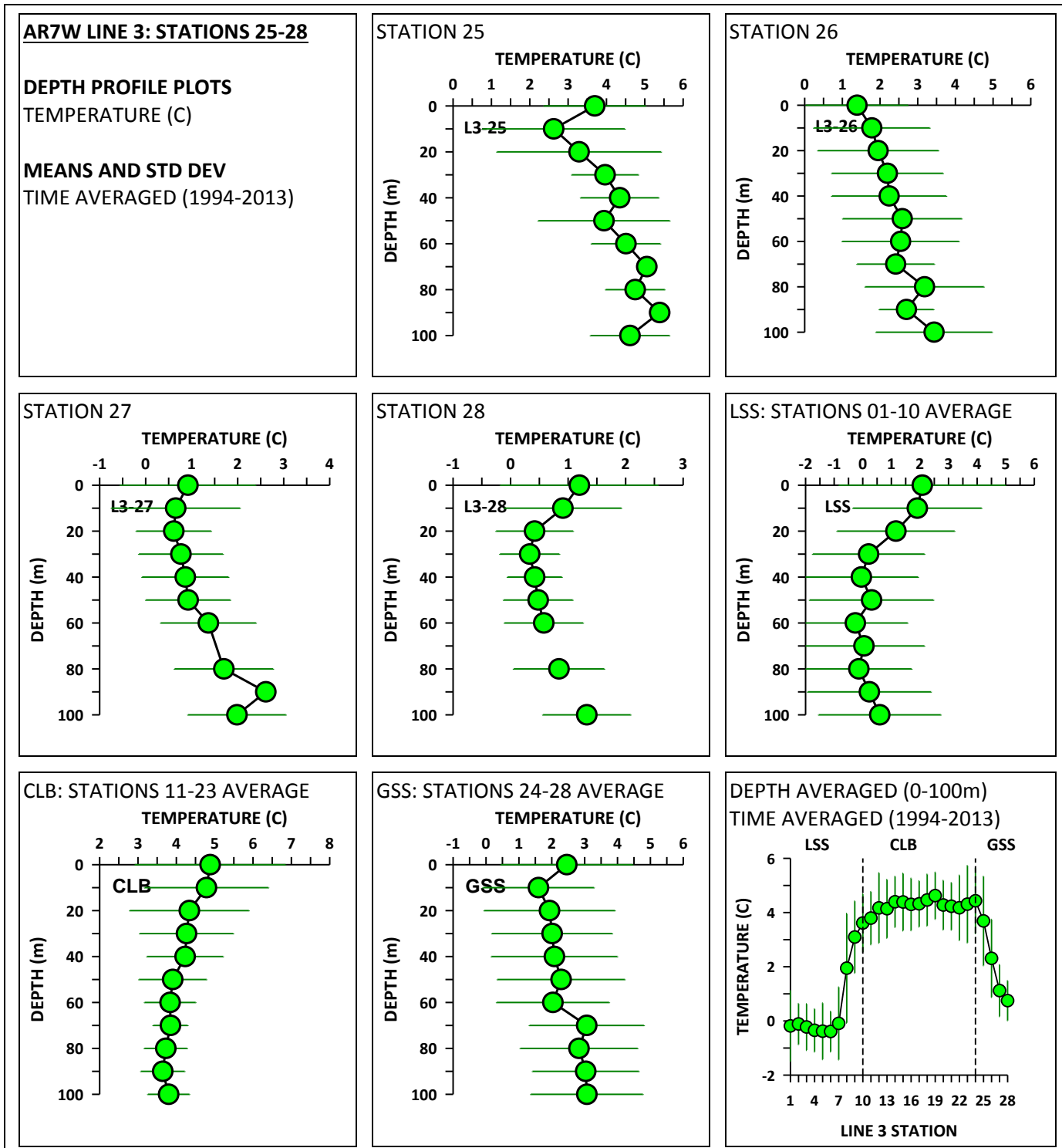


Figure 19

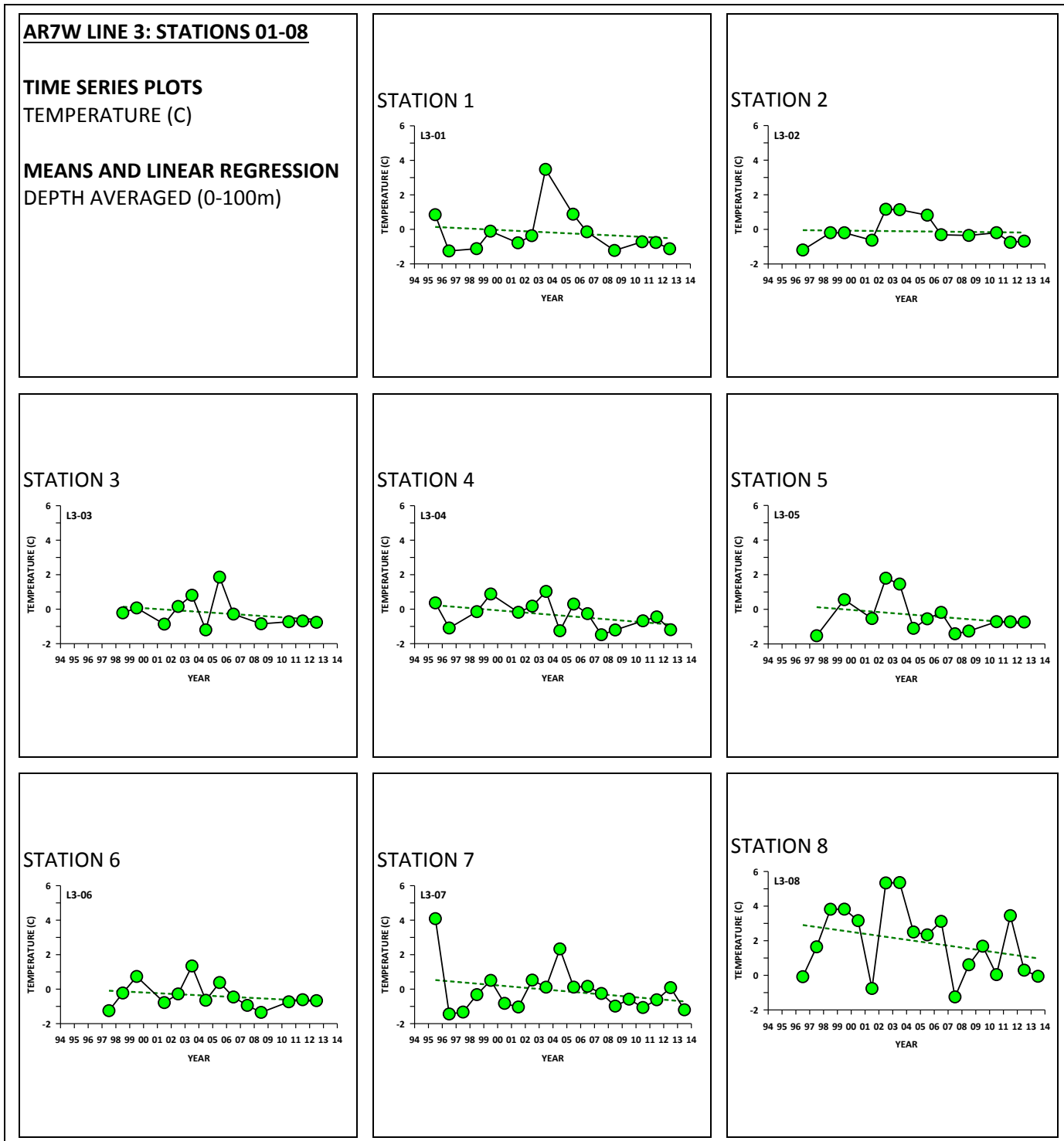




Figure 20

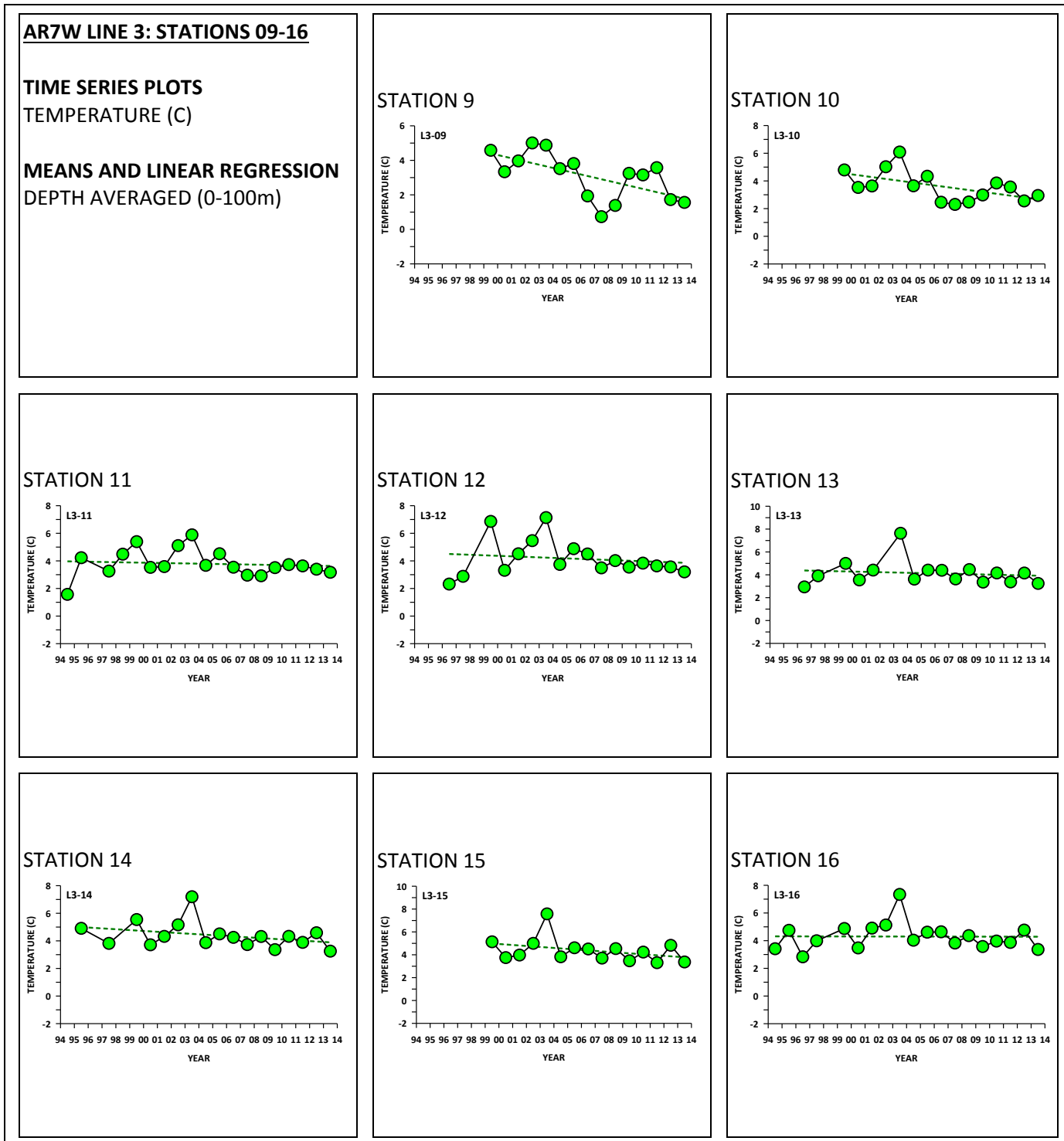


Figure 21

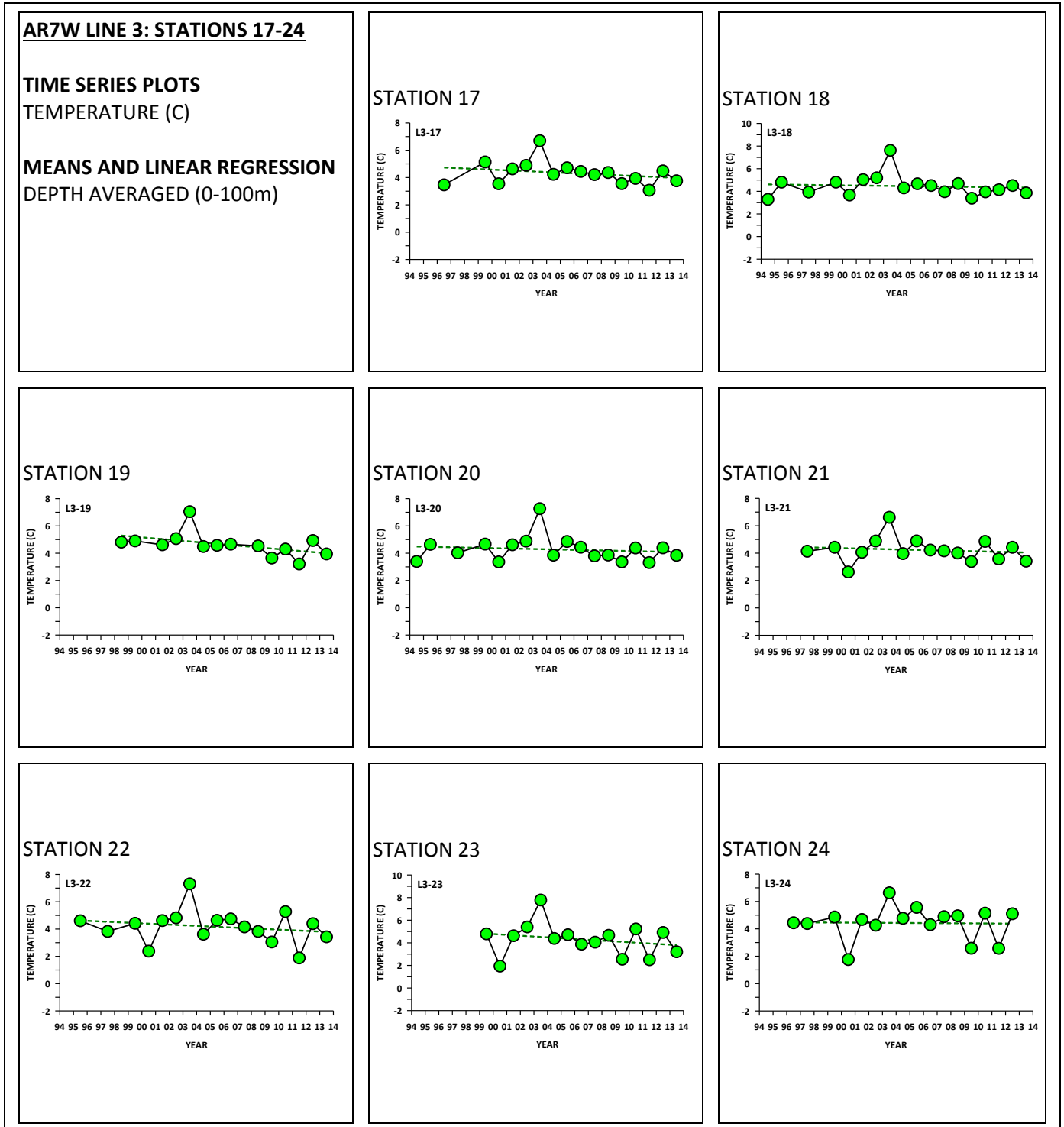


Figure 22

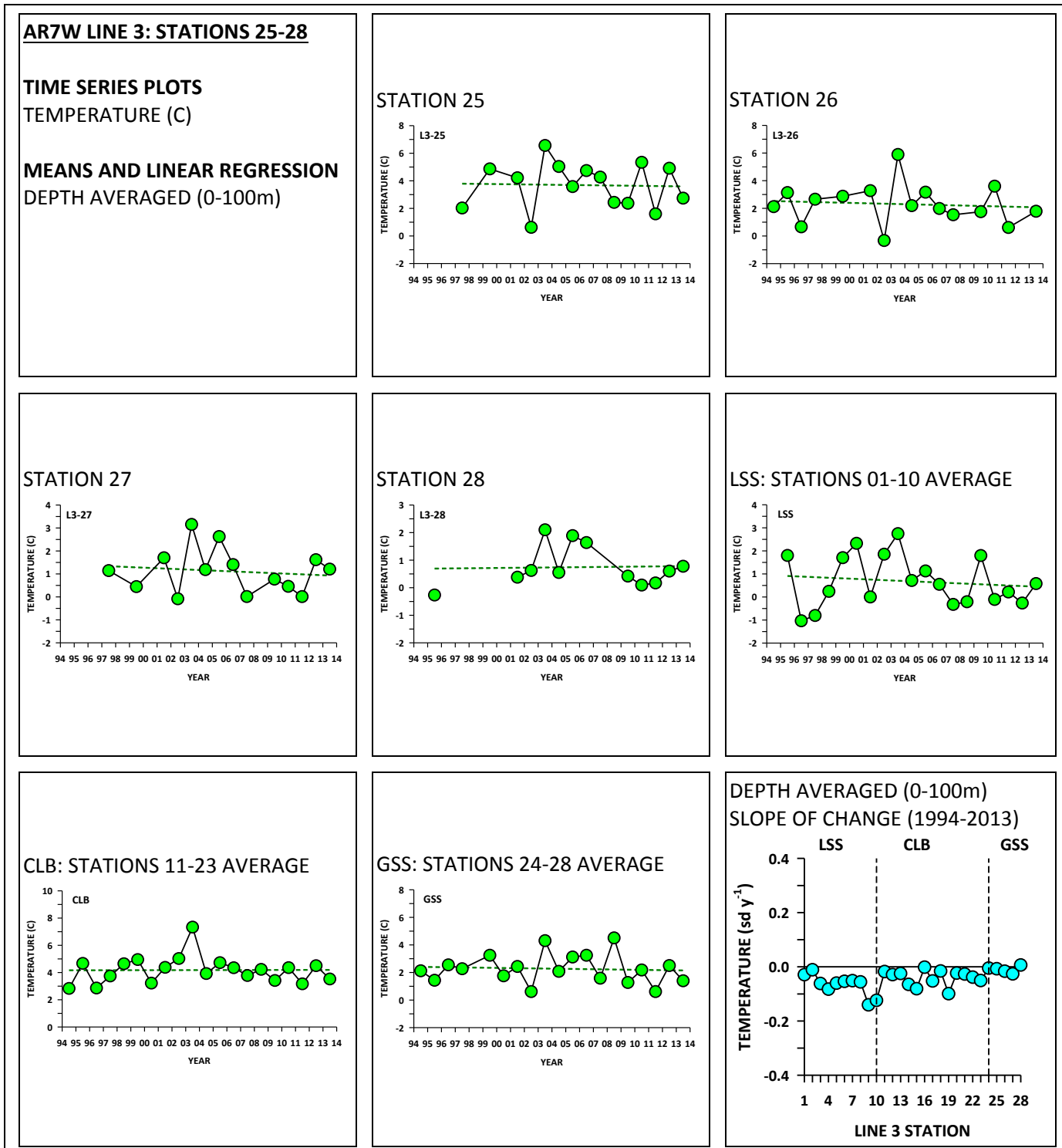


Figure 23

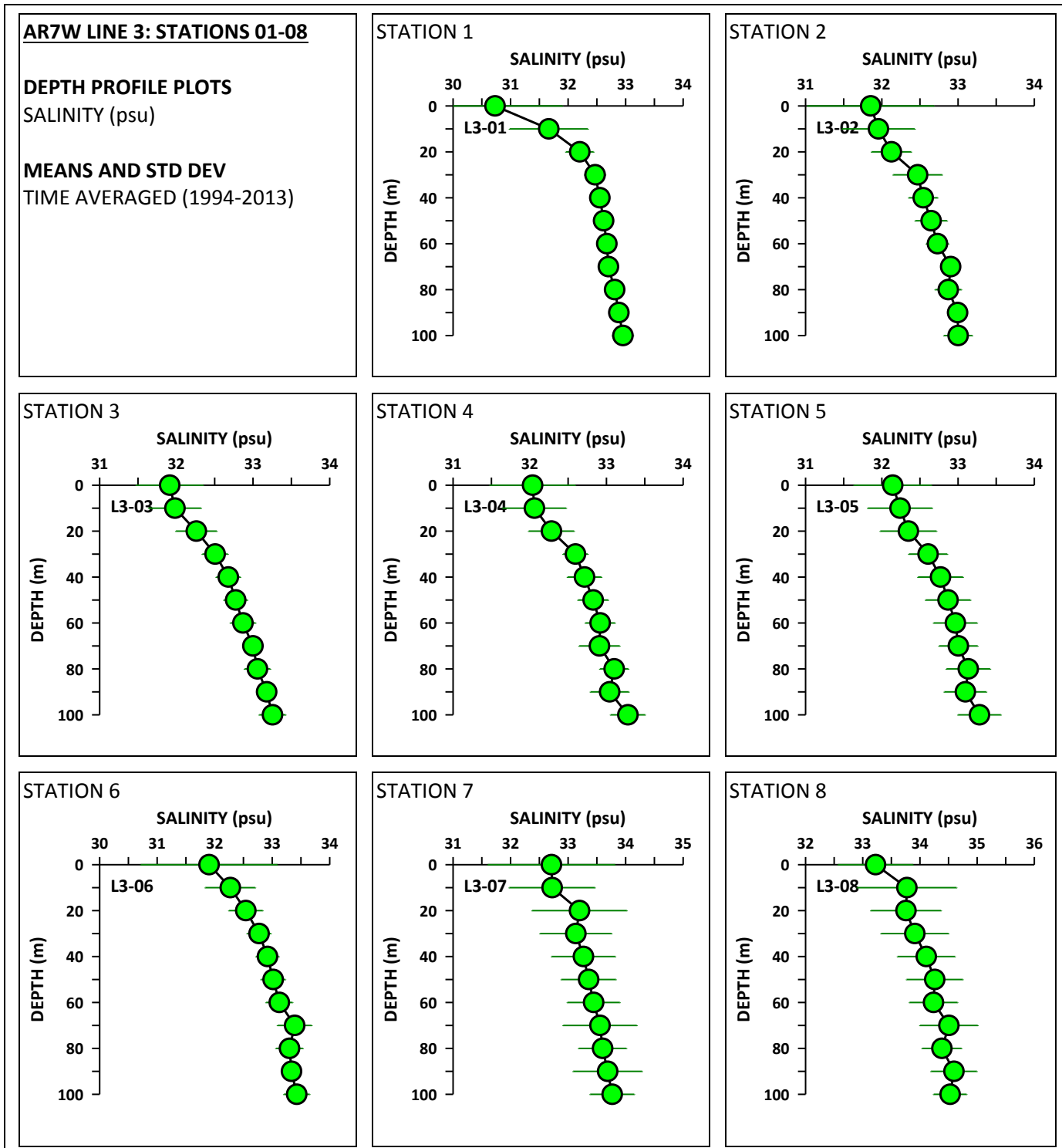


Figure 24

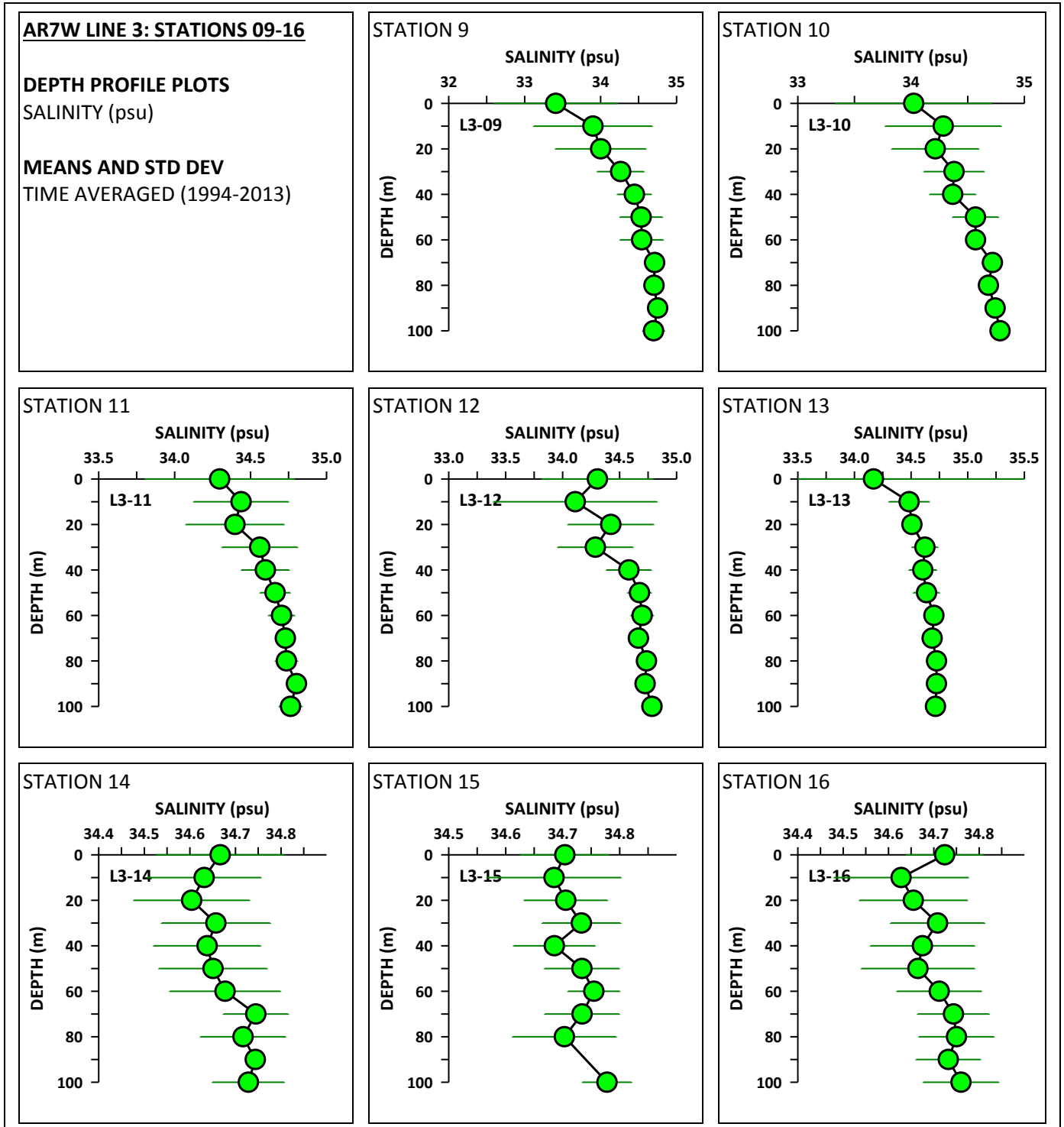


Figure 25

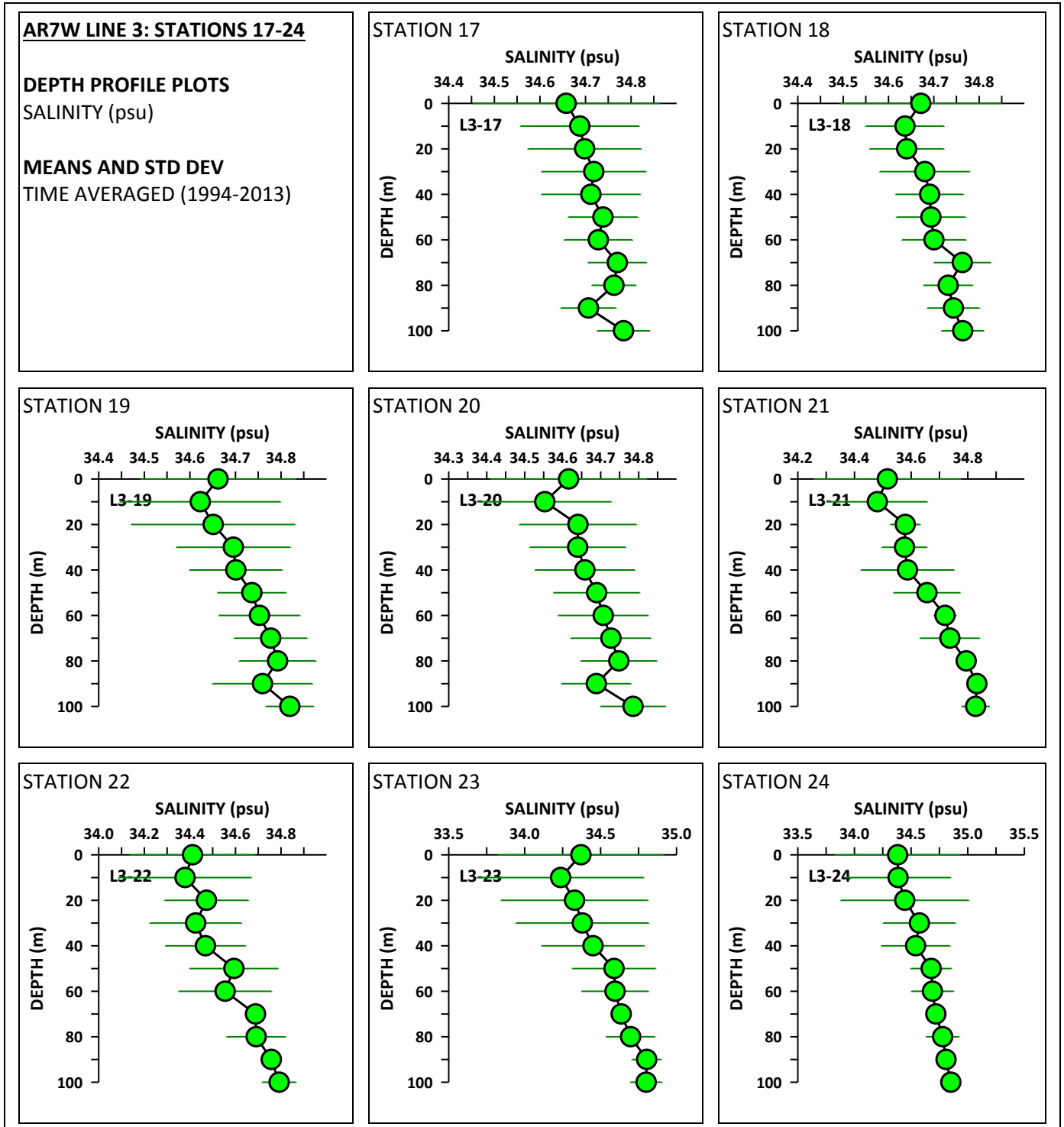


Figure 26

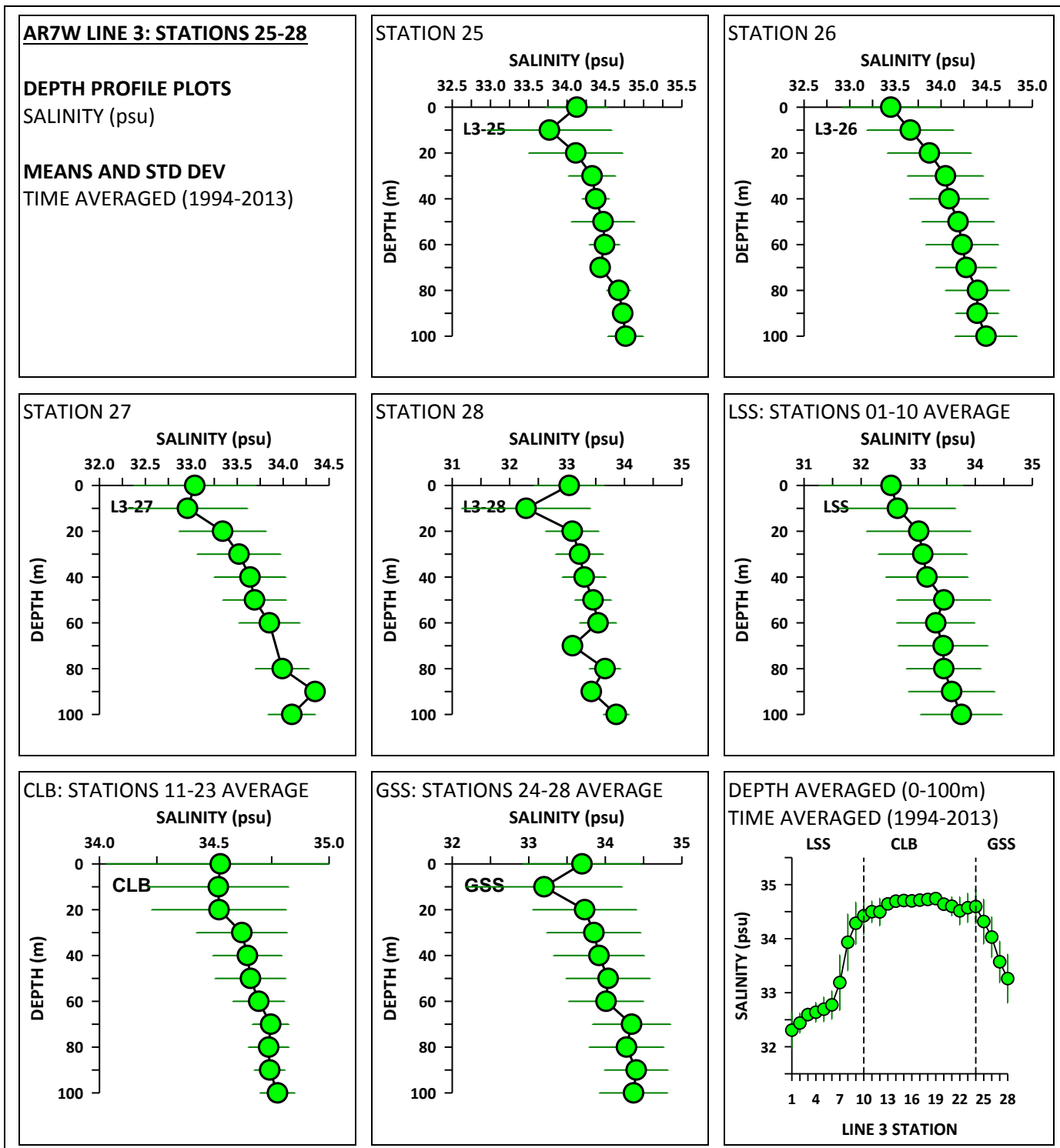


Figure 27

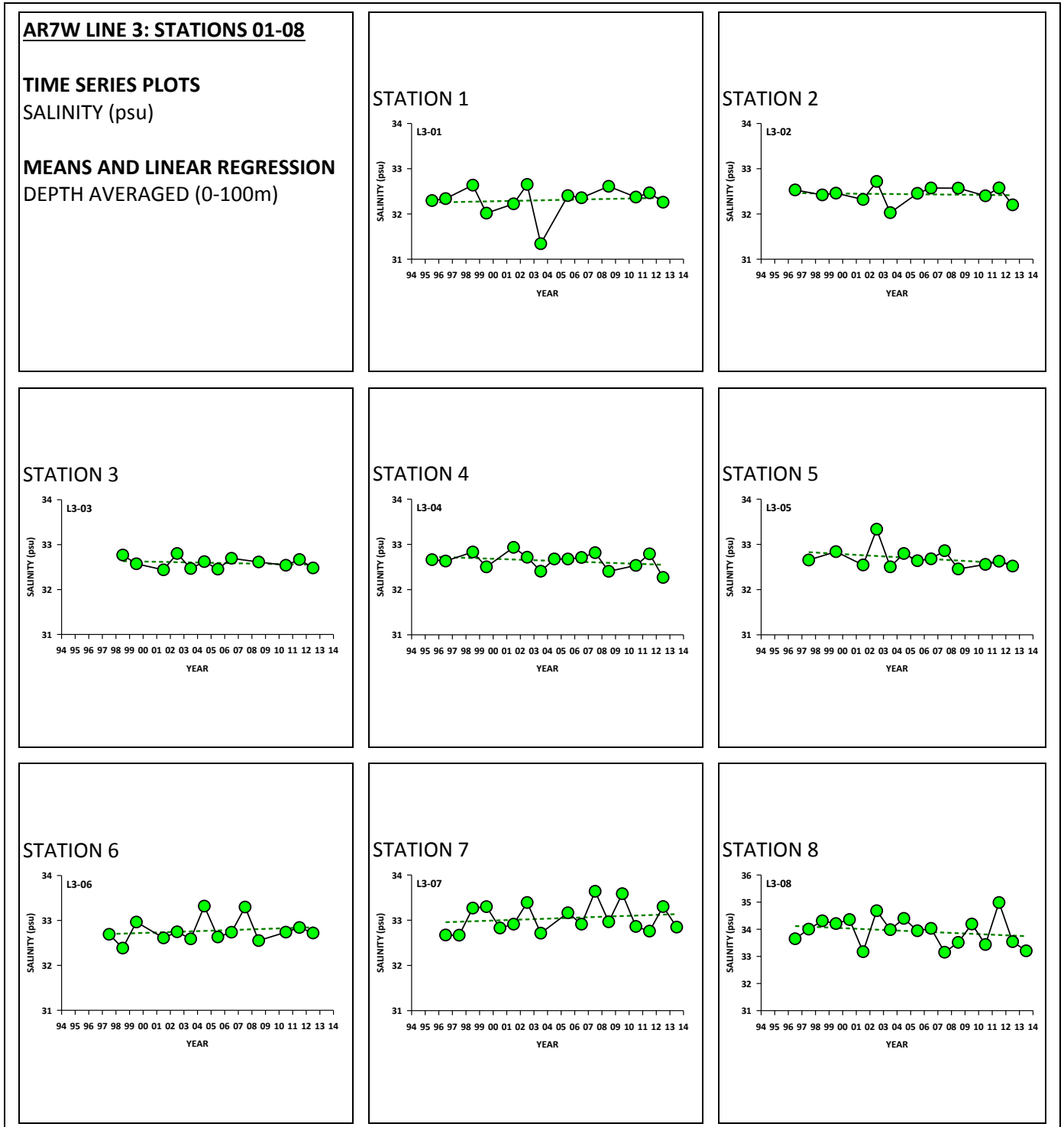




Figure 28

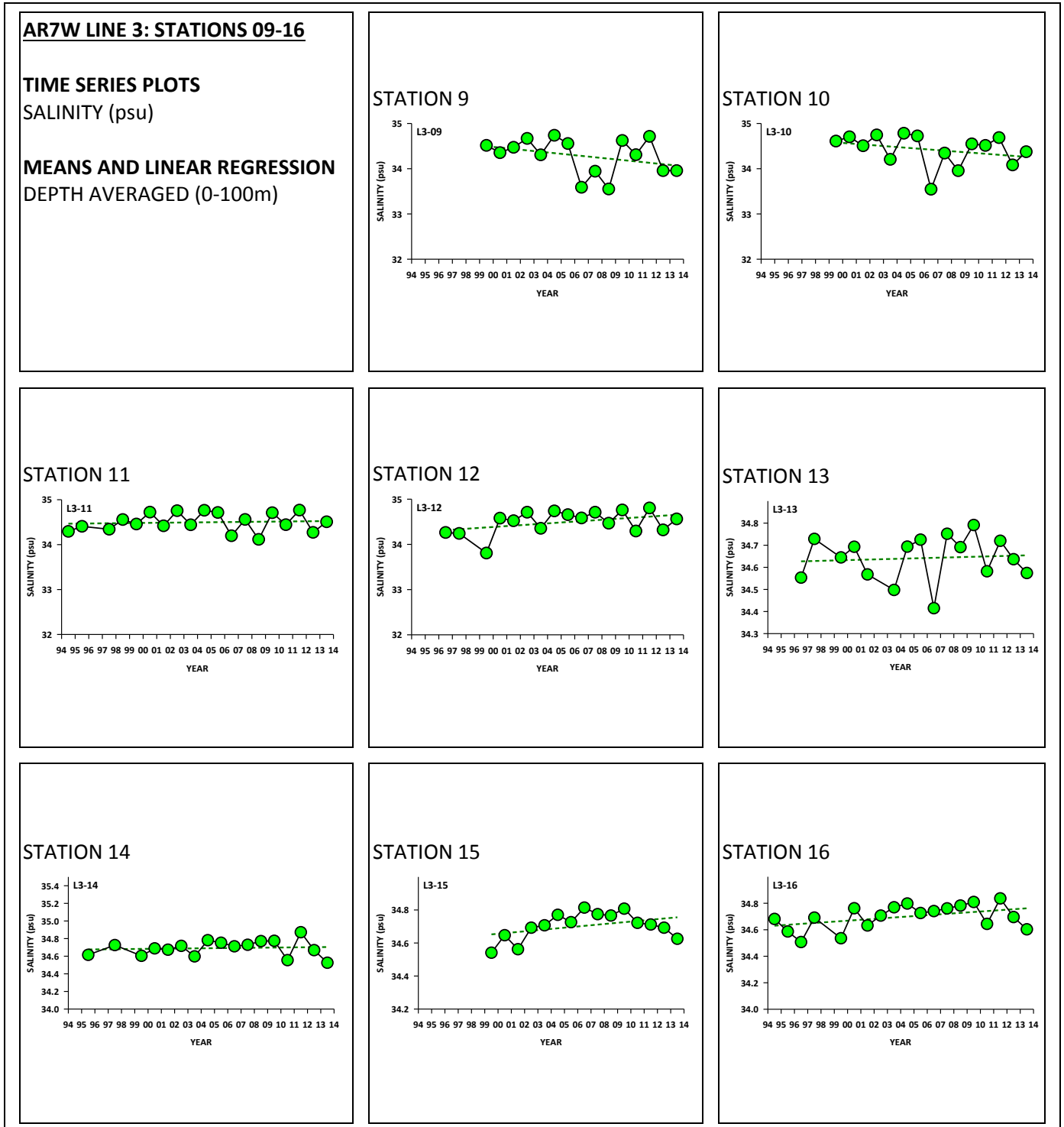


Figure 29

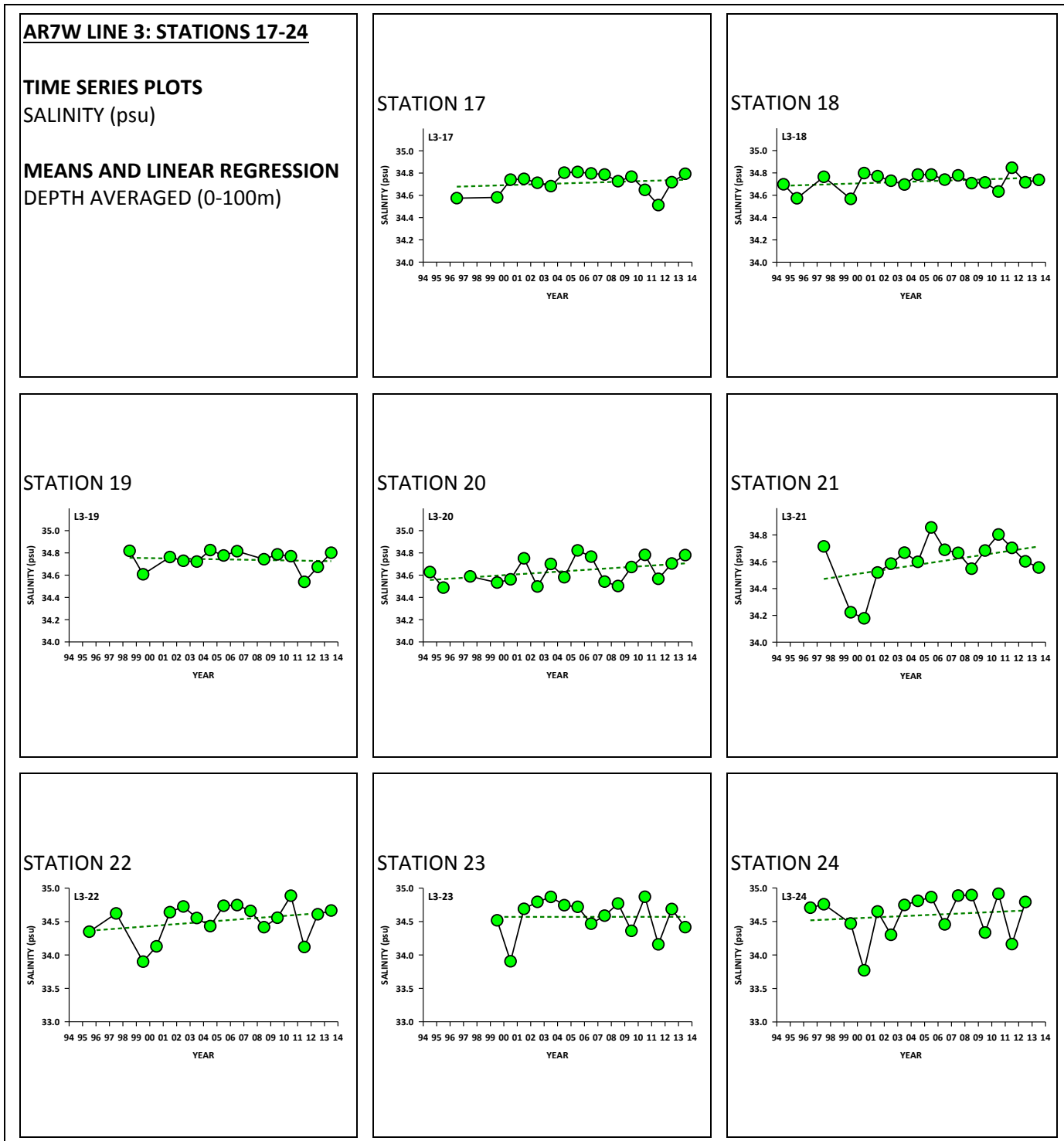


Figure 30

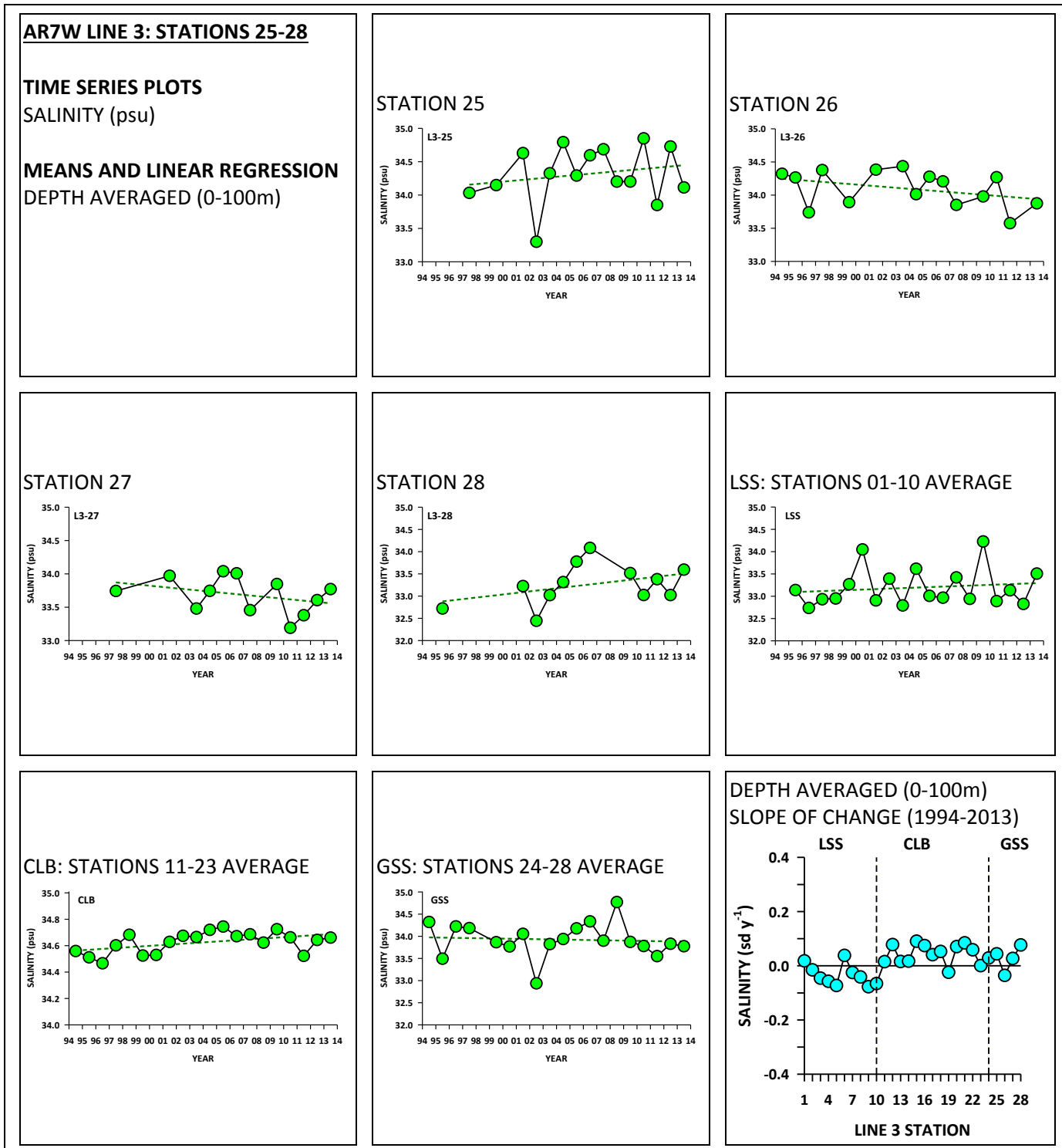


Figure 31

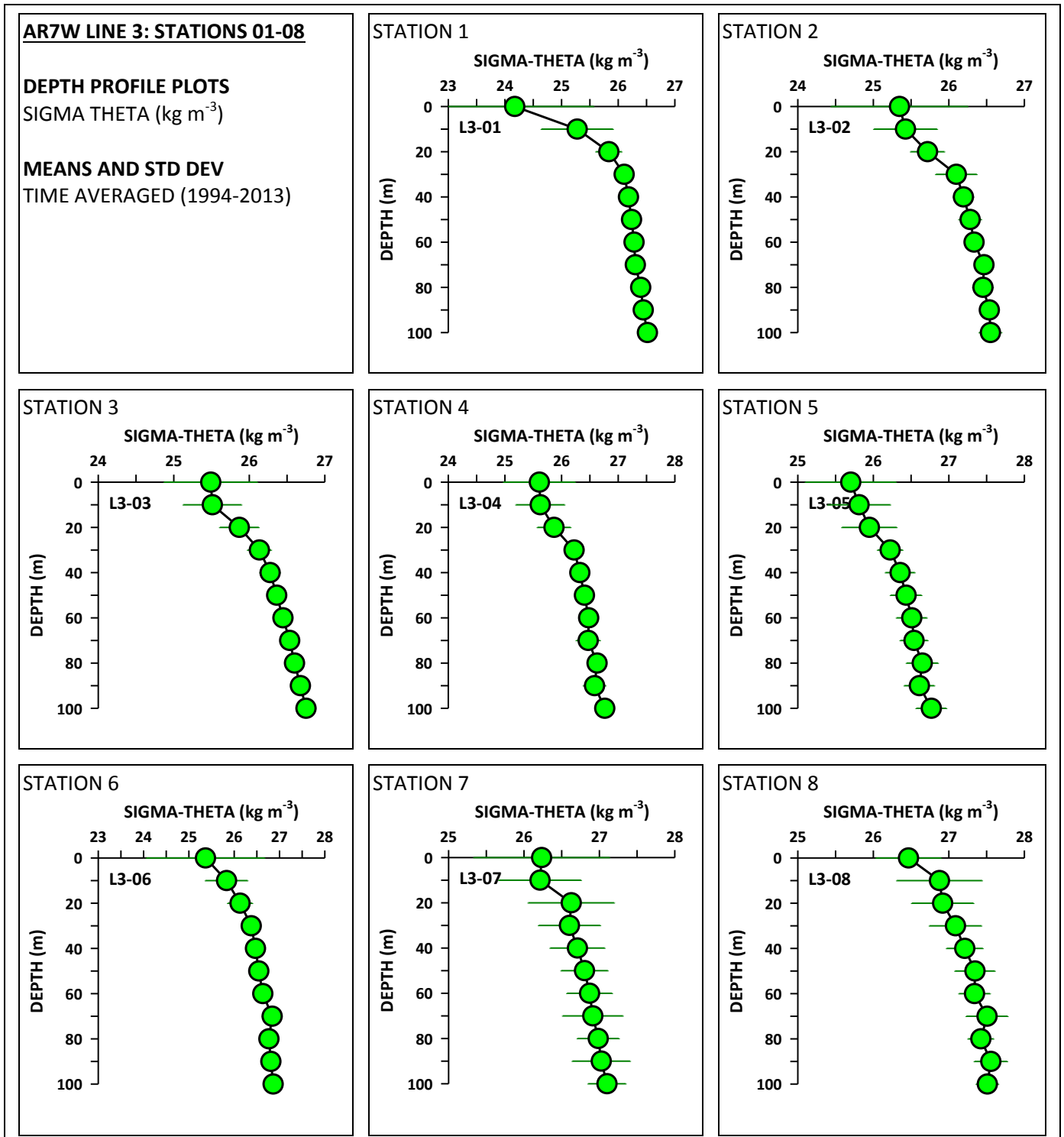


Figure 32

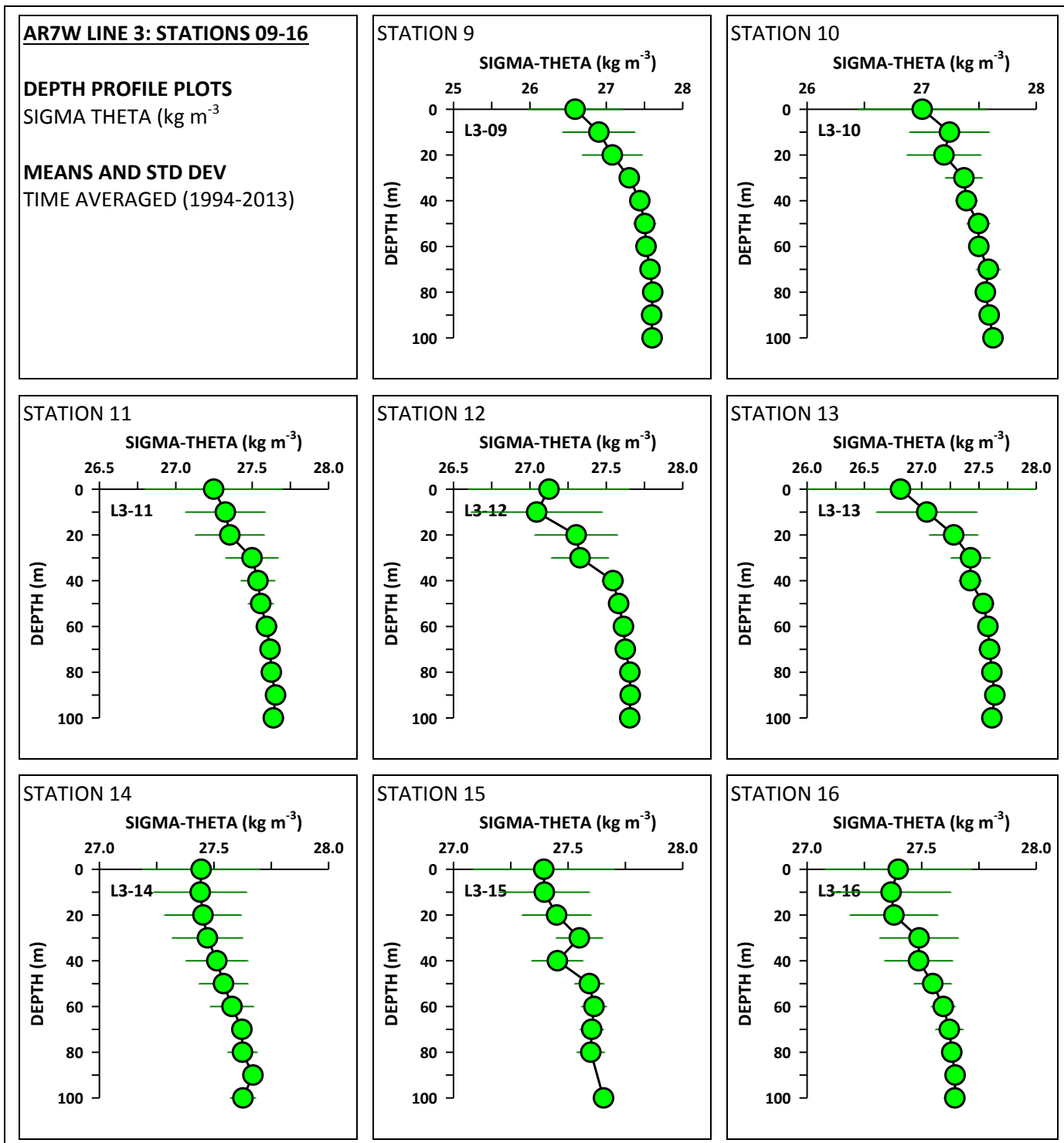


Figure 33

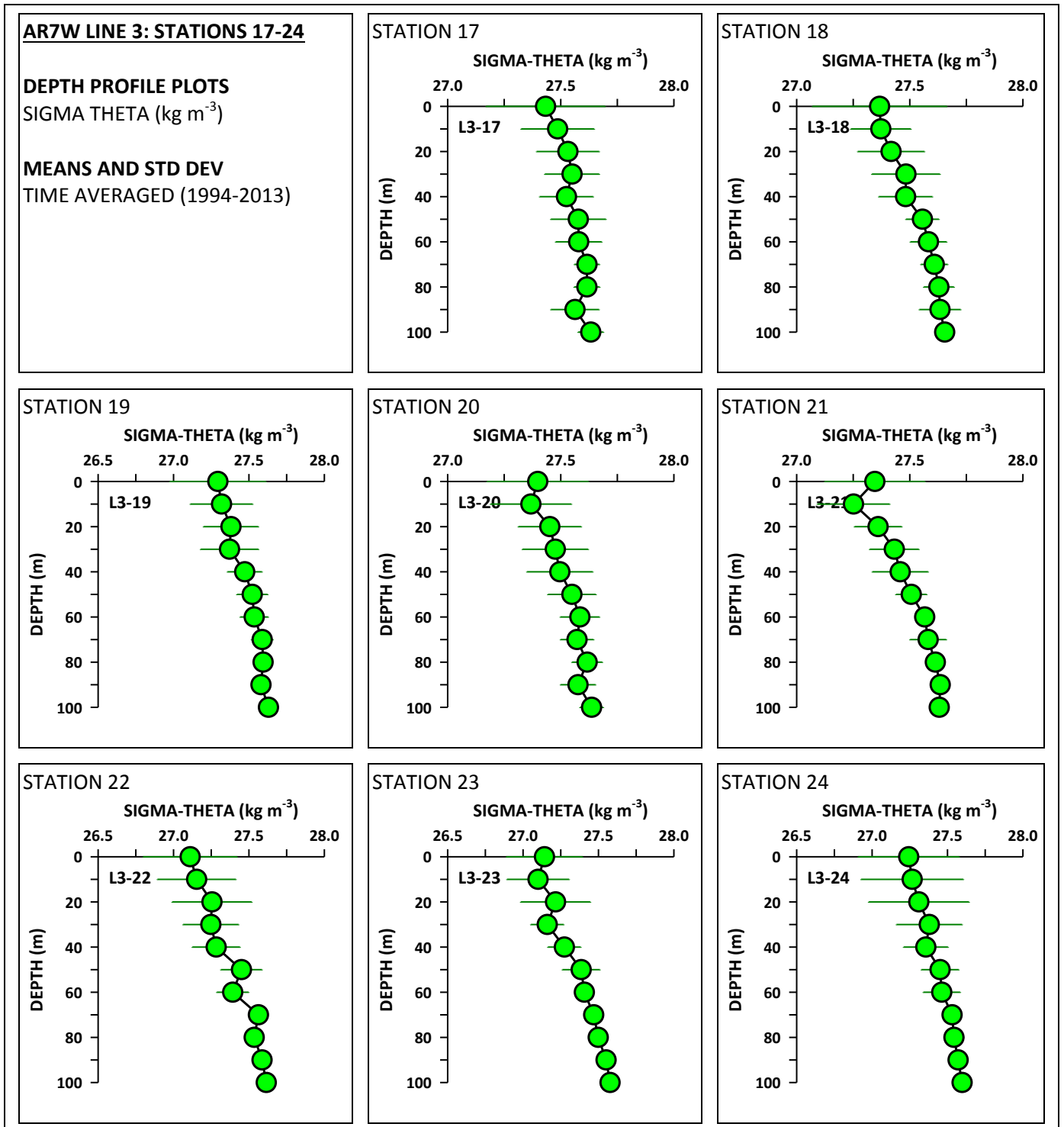


Figure 34

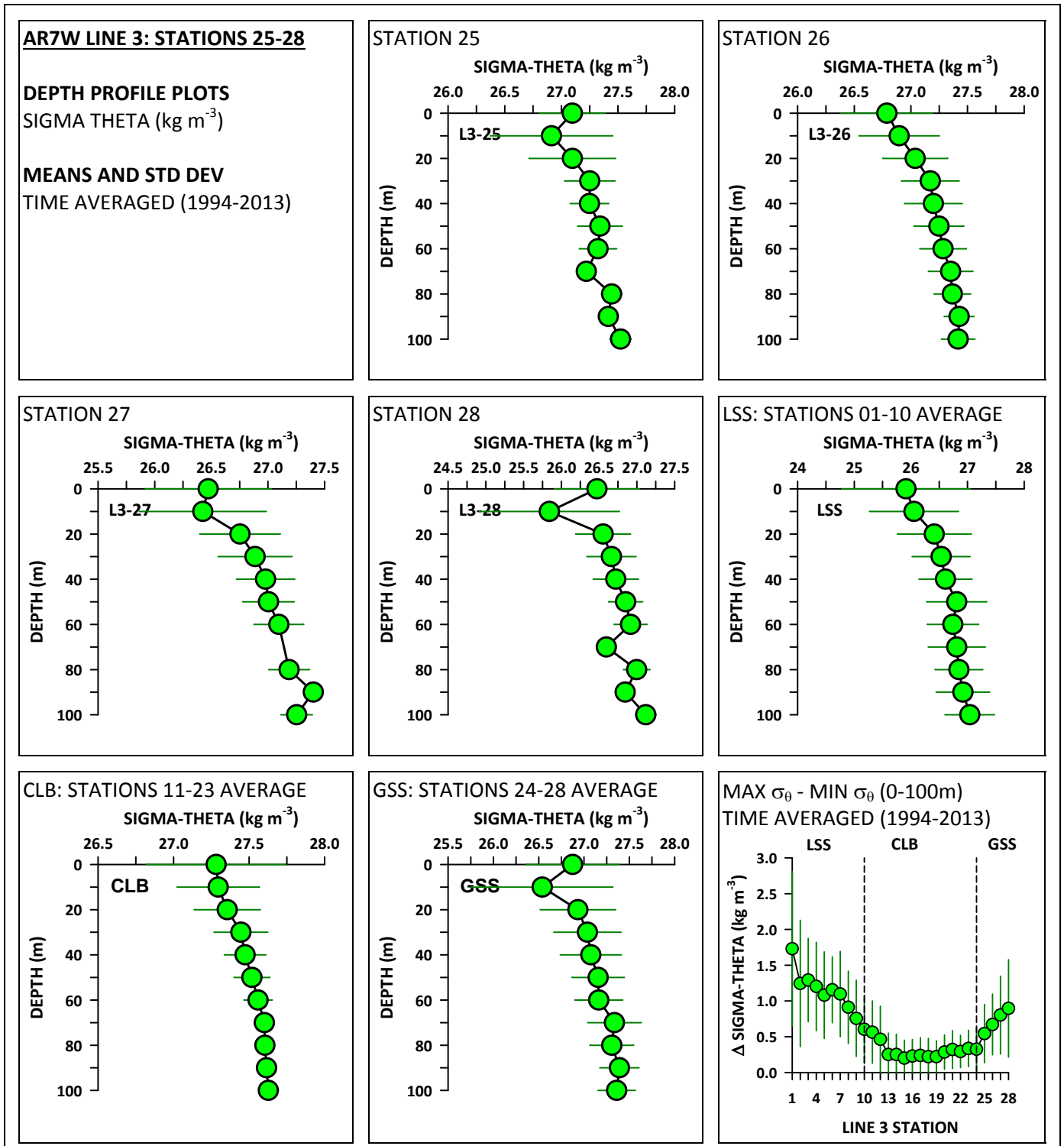


Figure 35

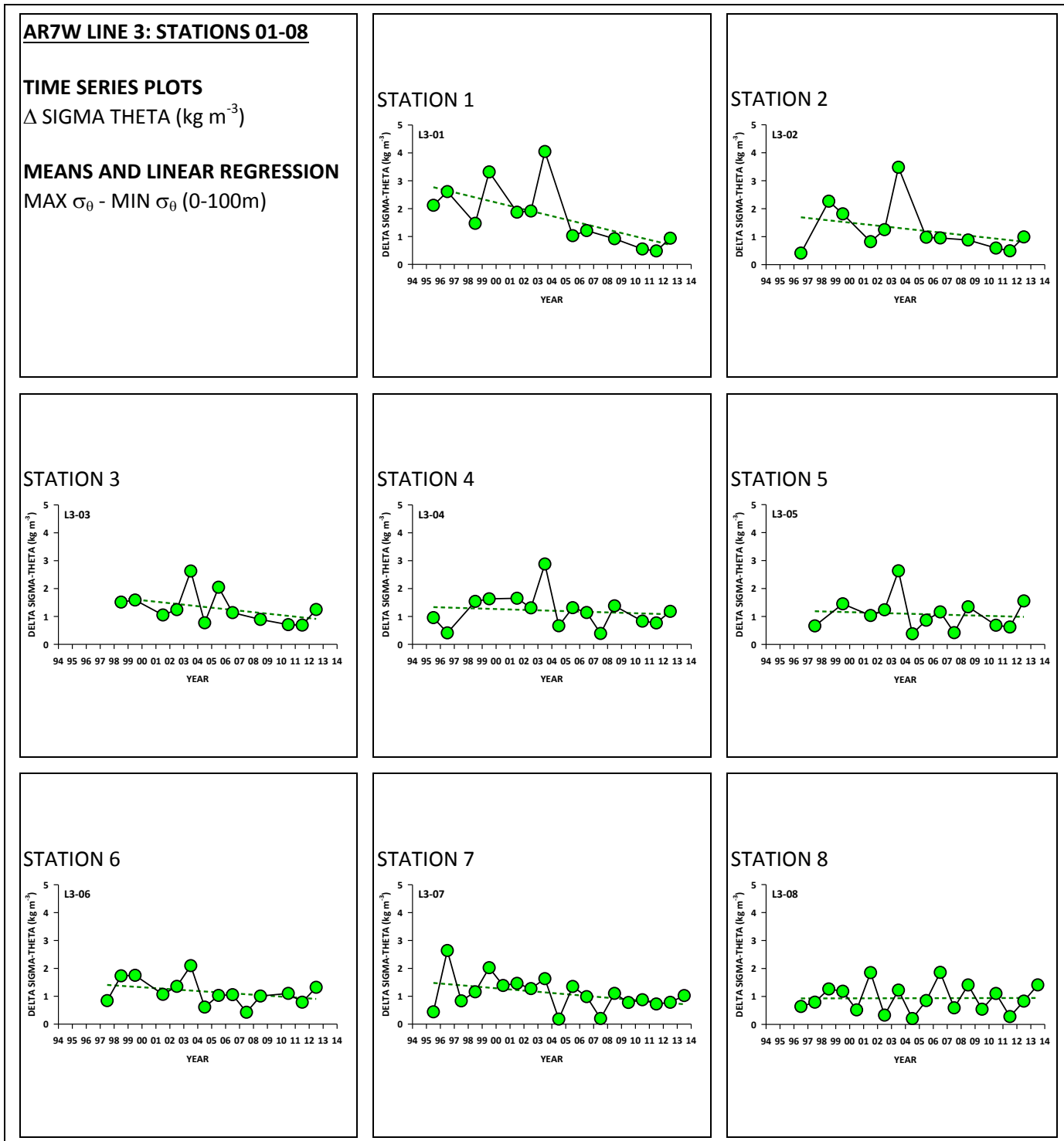




Figure 36

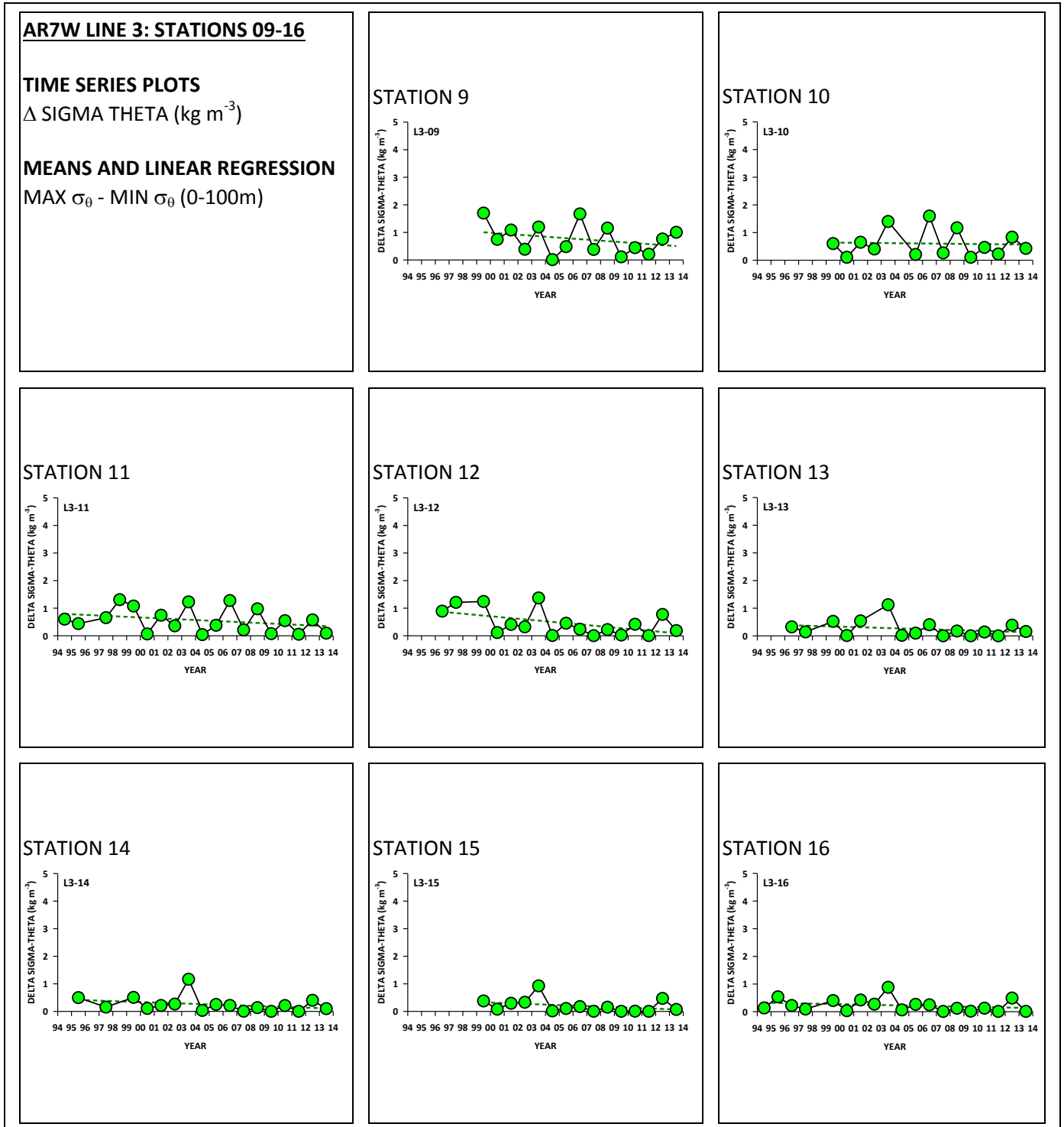


Figure 37

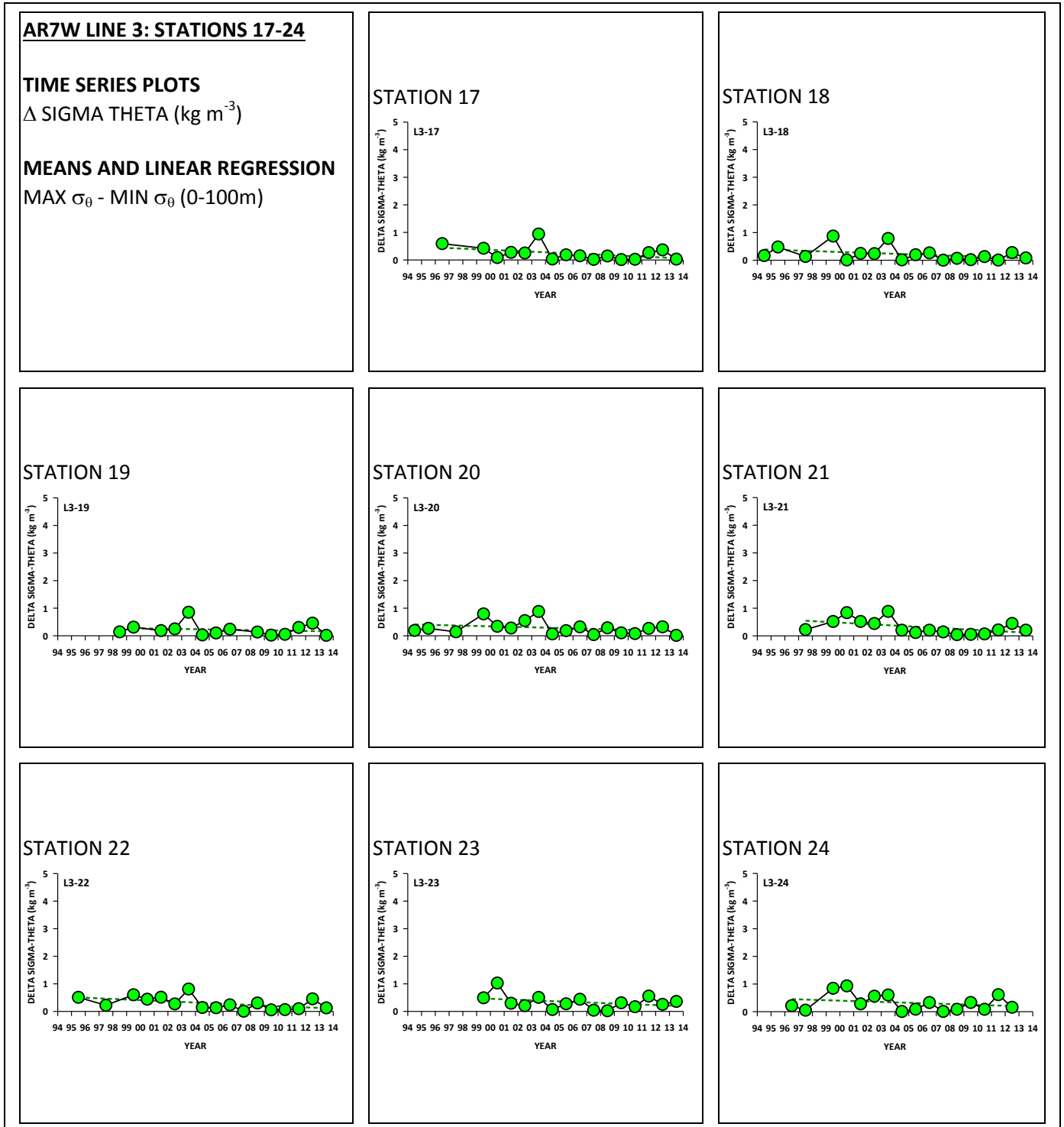


Figure 38

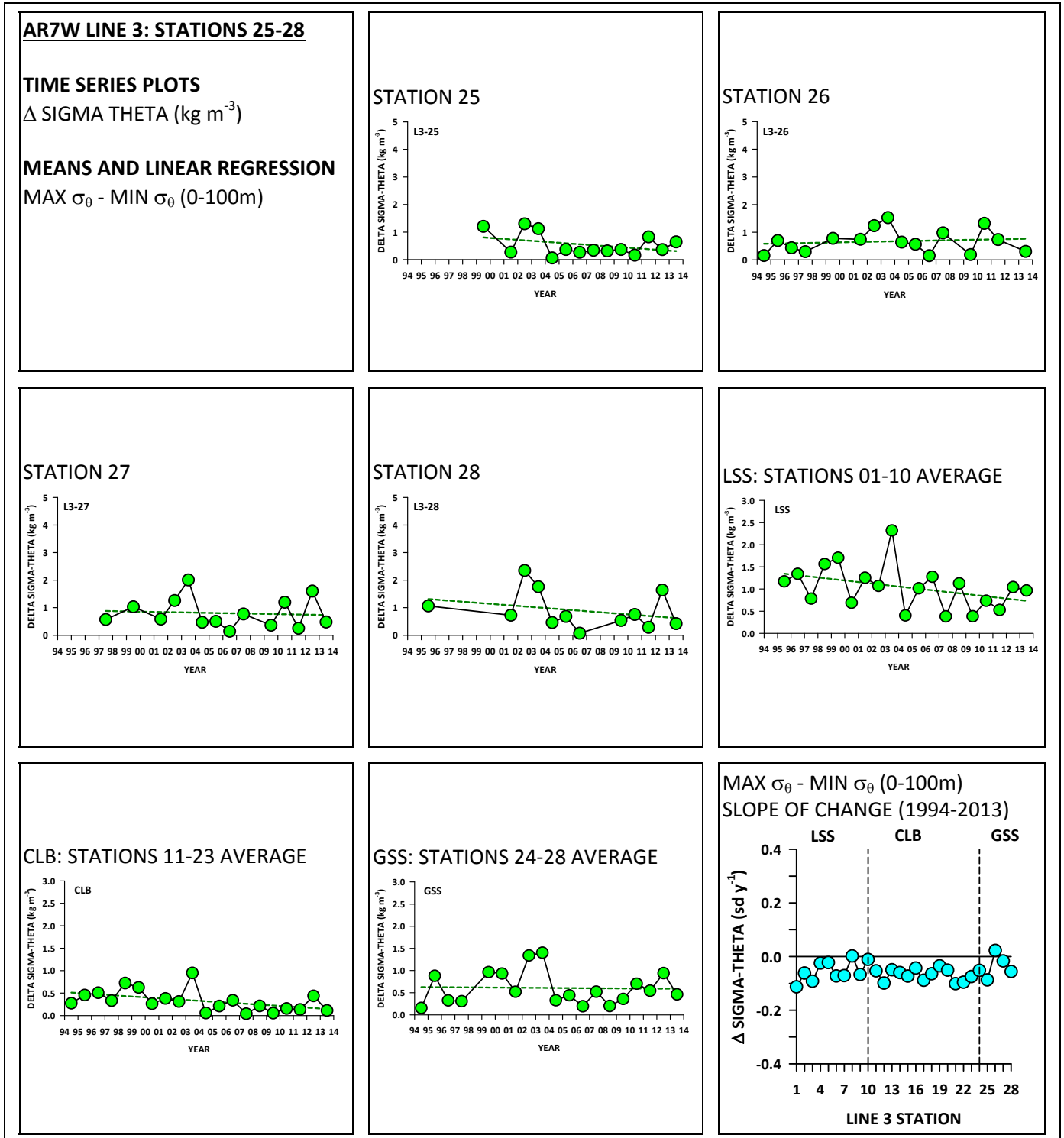




Figure 40

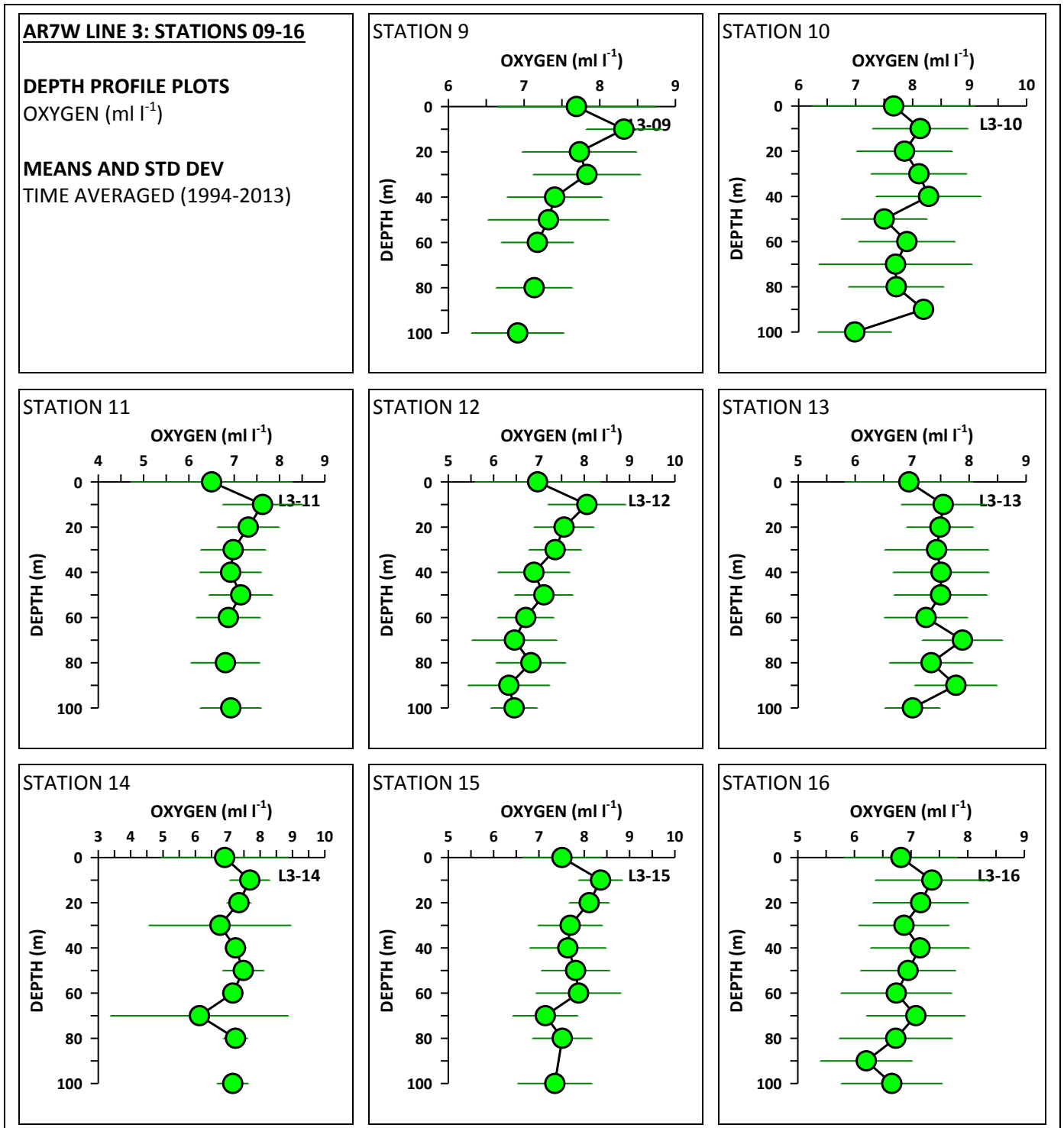


Figure 41

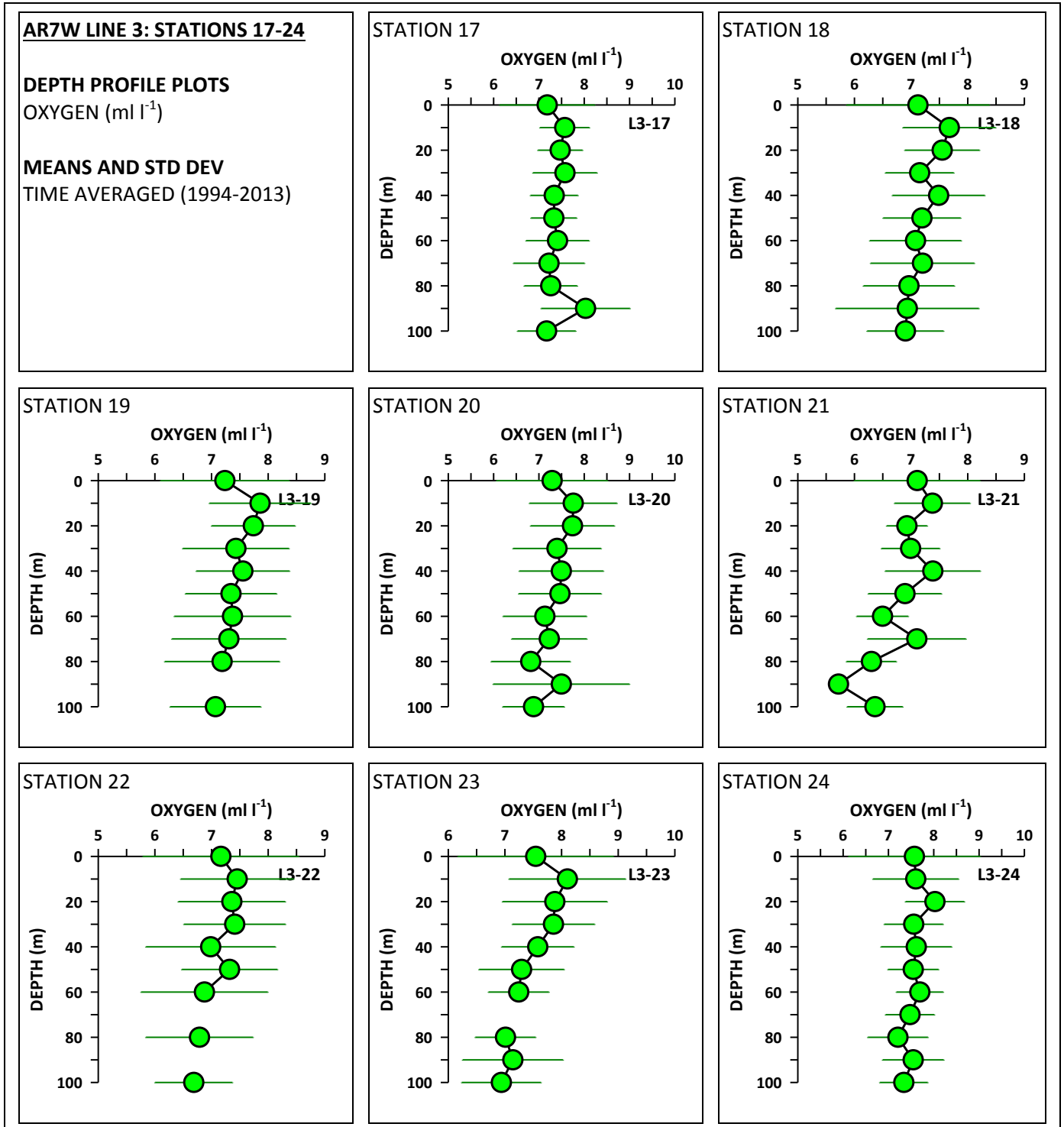


Figure 42

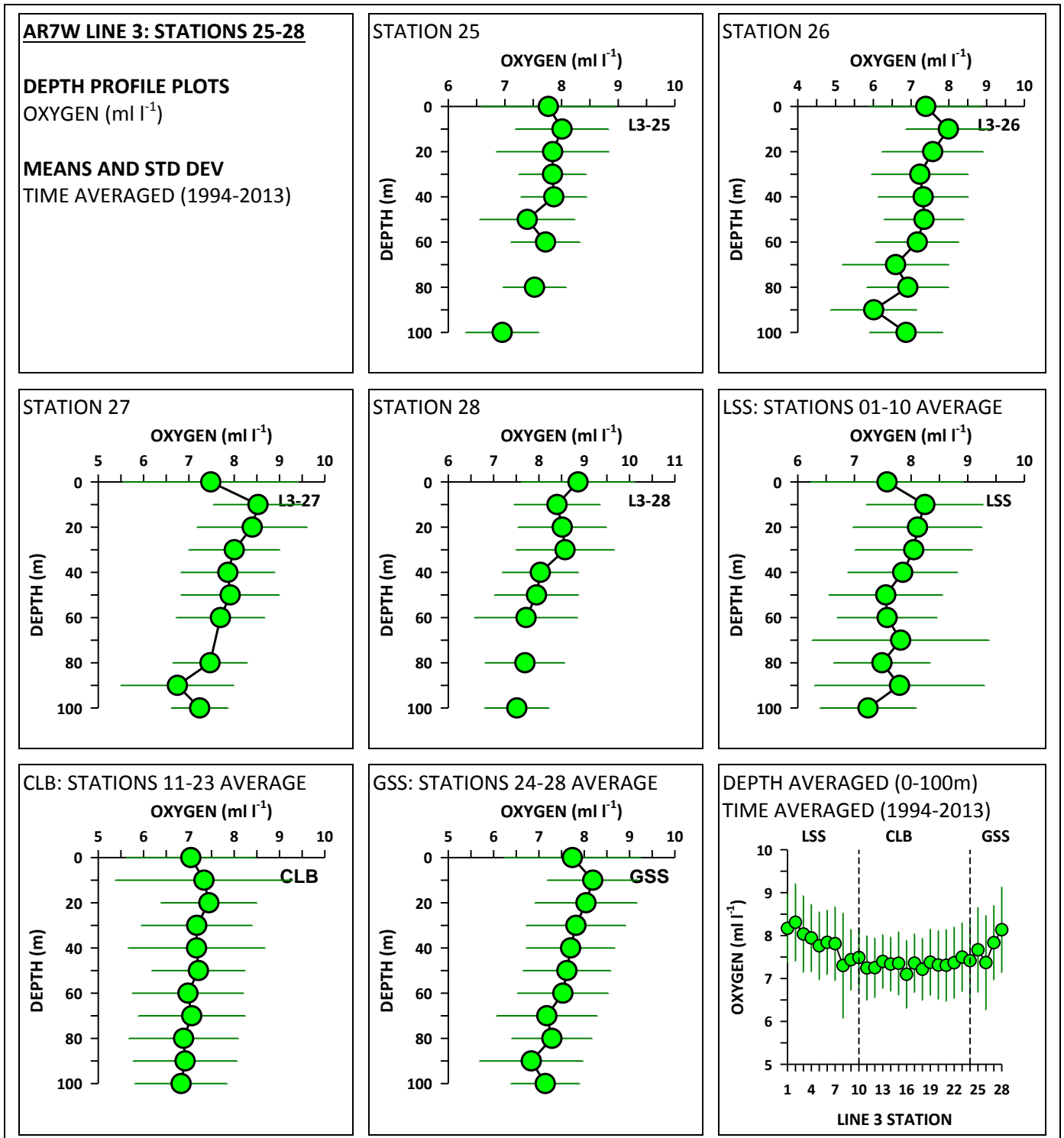


Figure 43

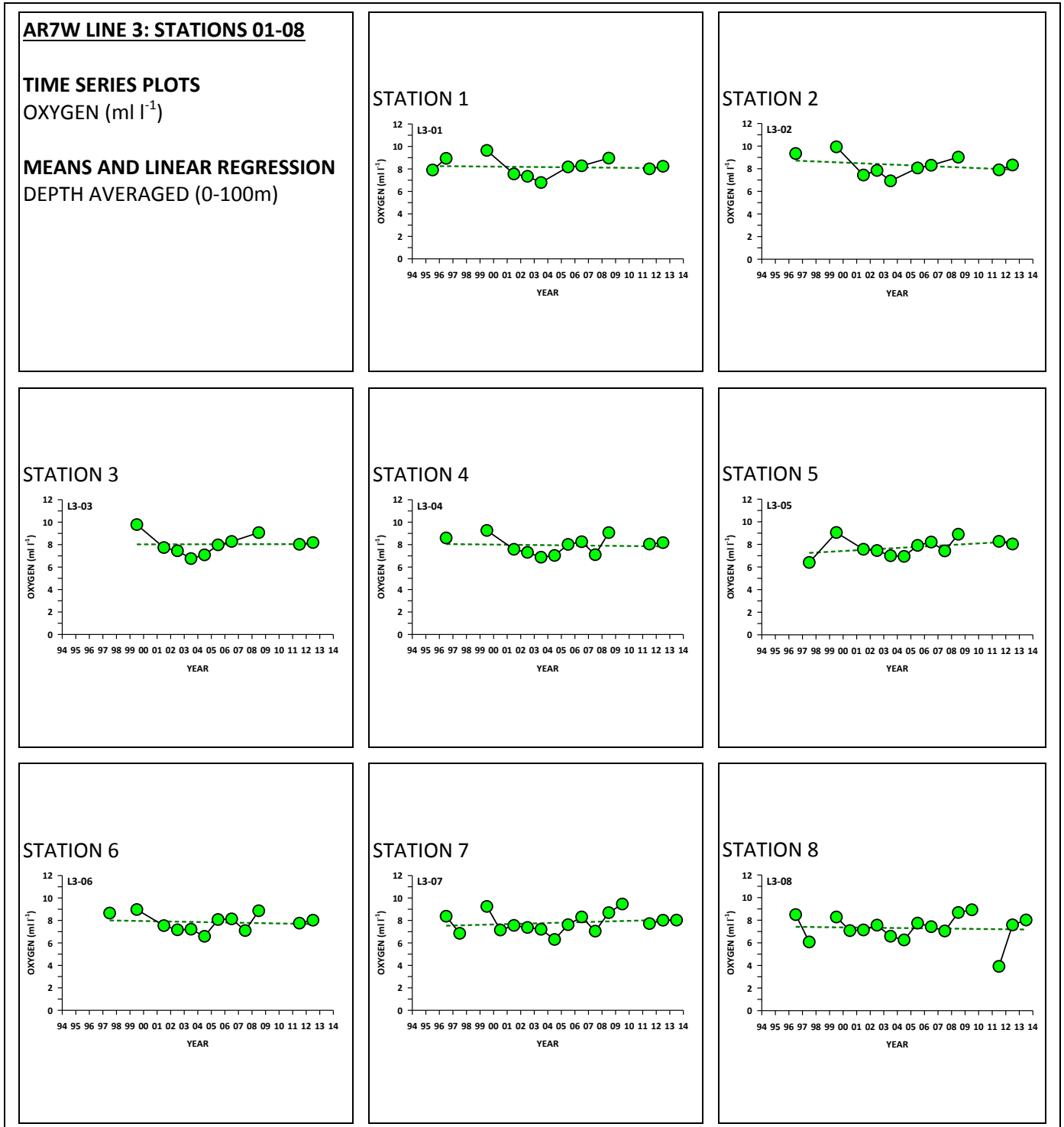




Figure 44

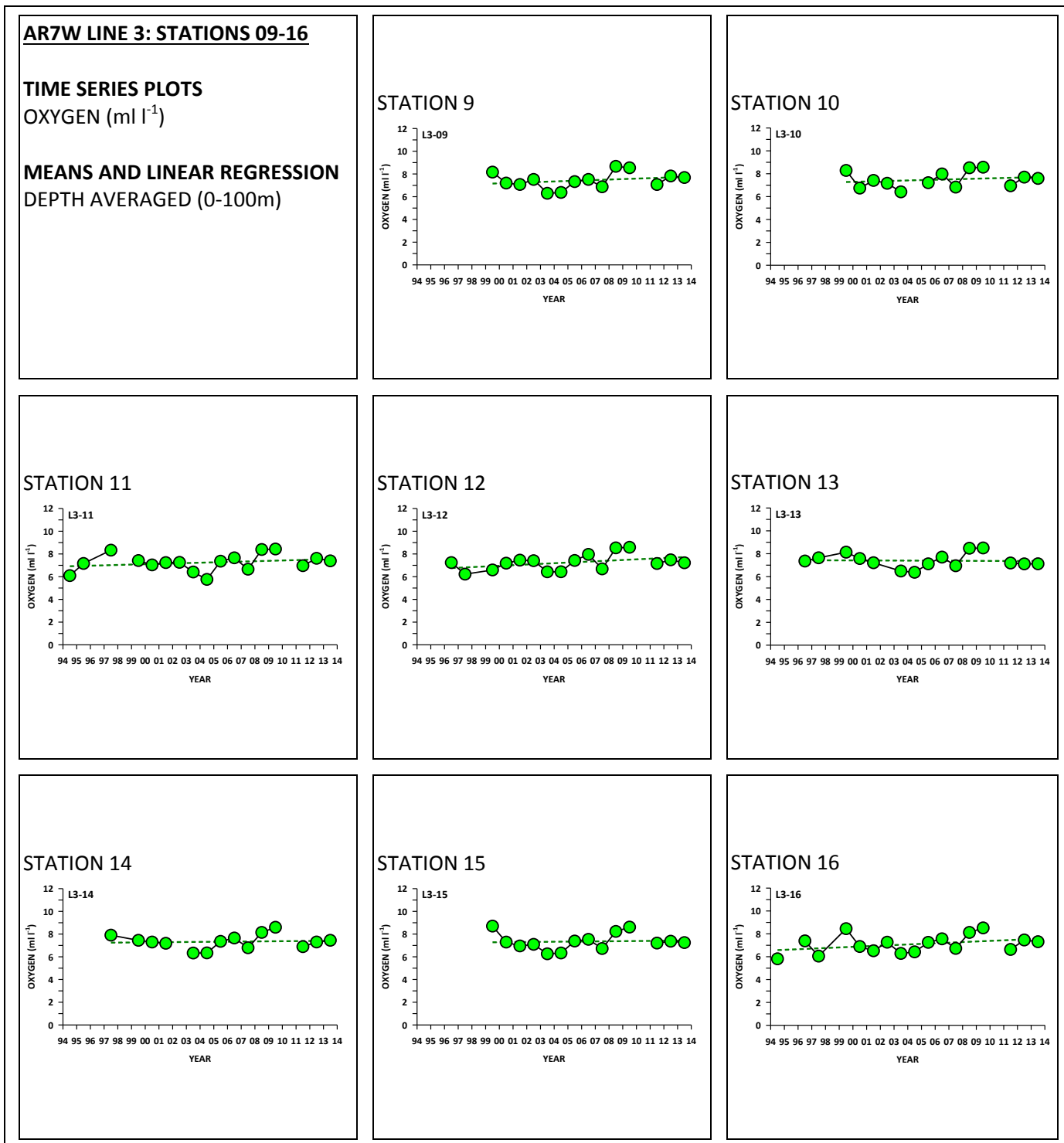


Figure 45

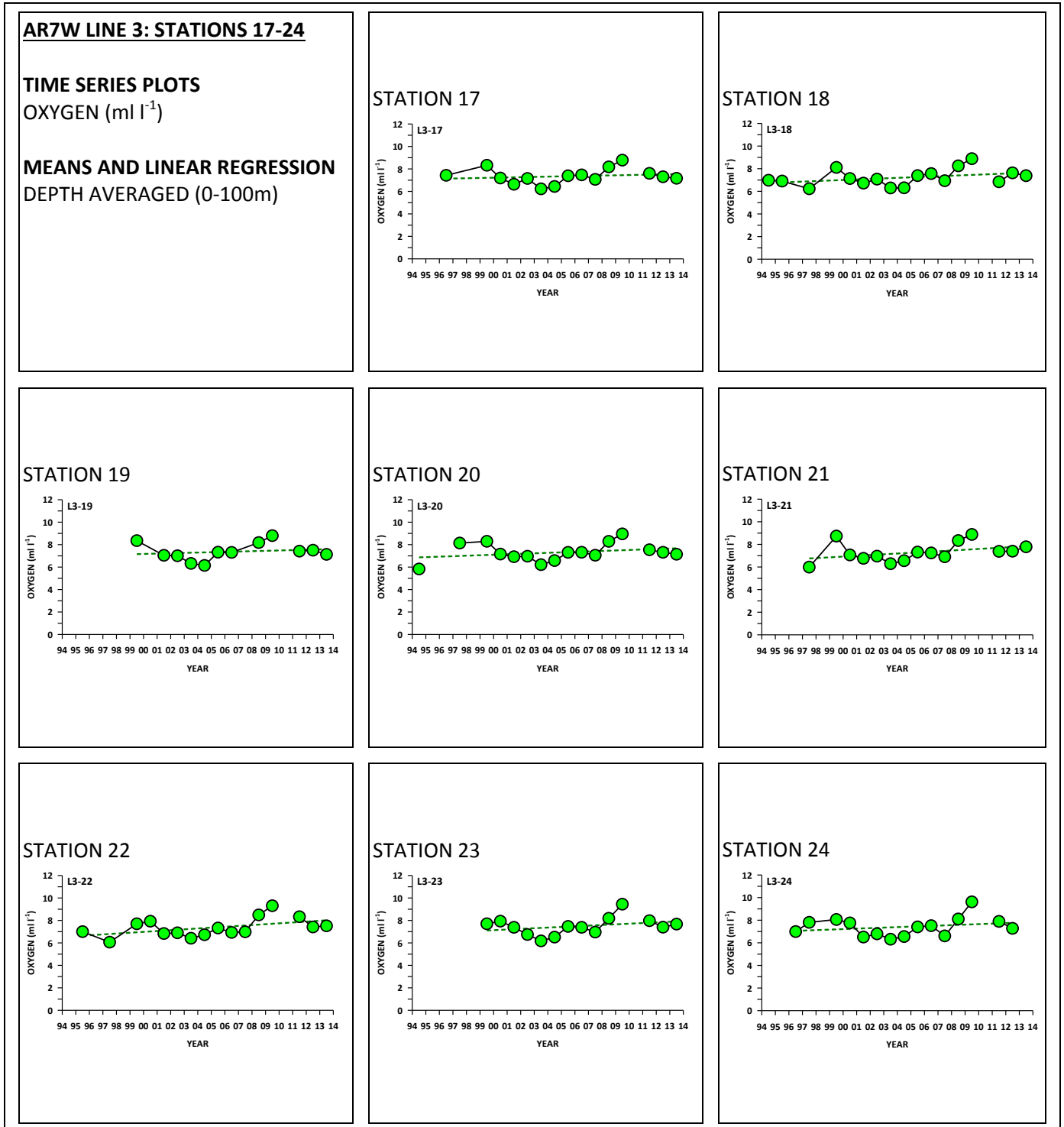


Figure 46

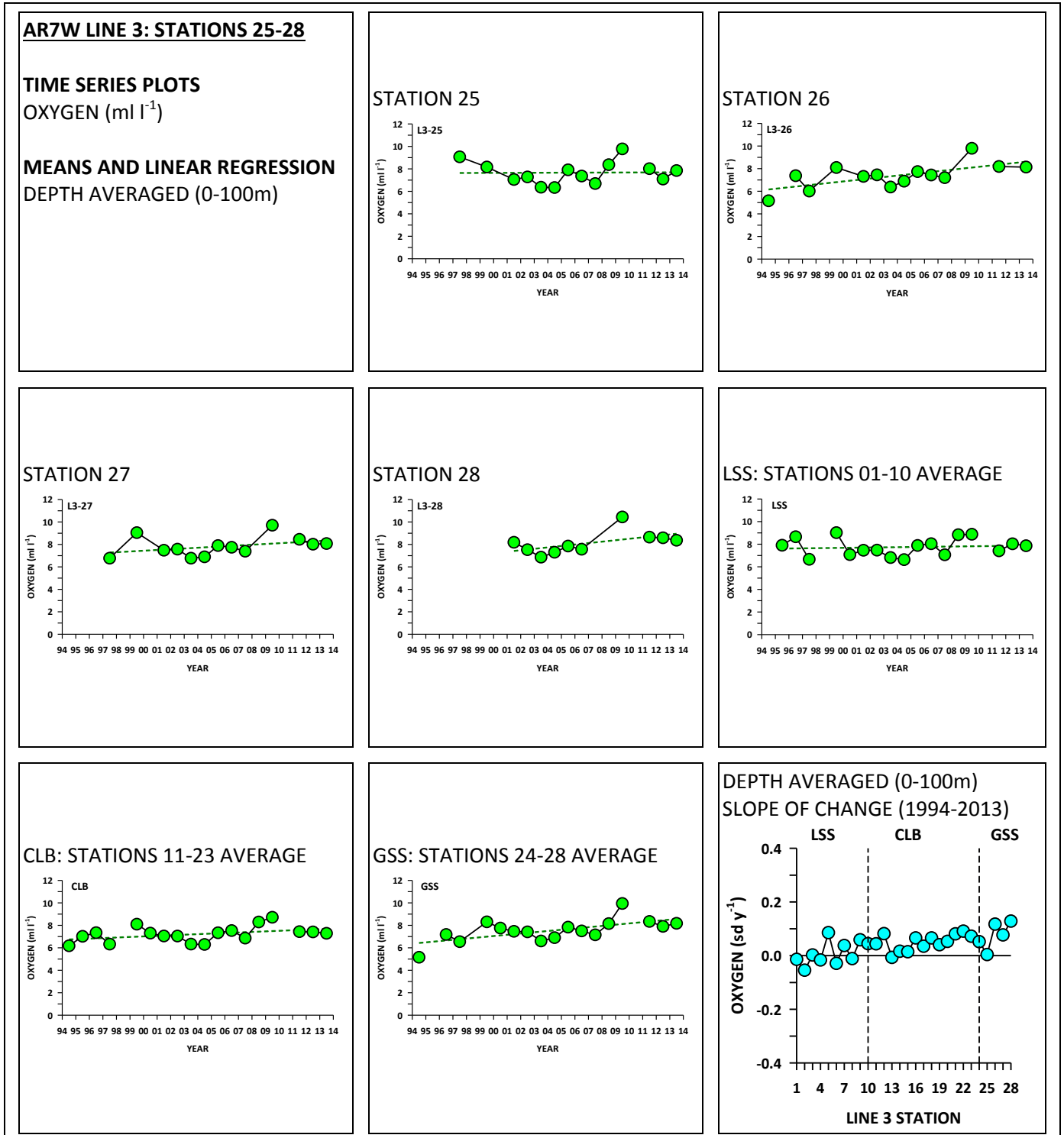


Figure 47

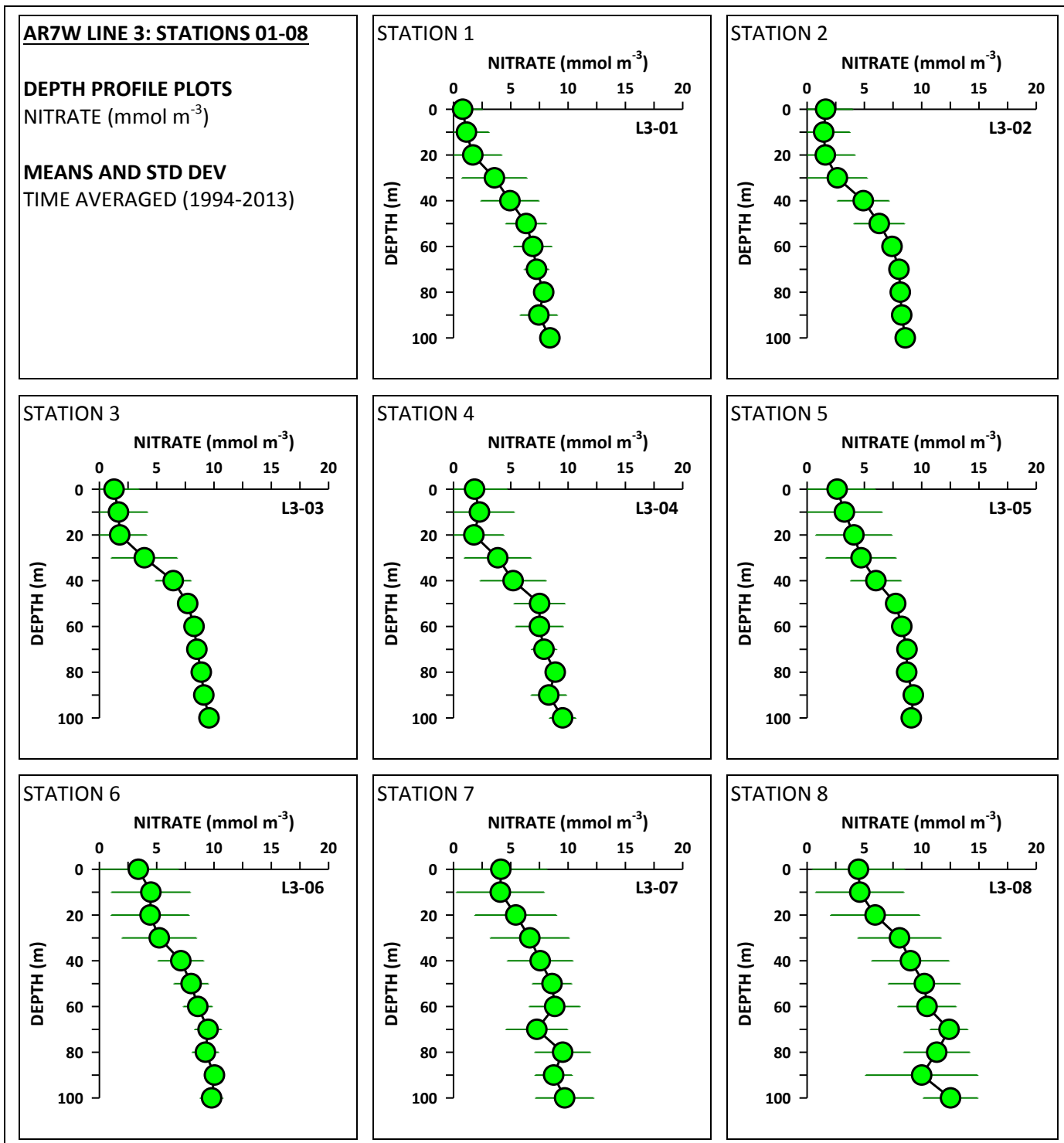


Figure 48

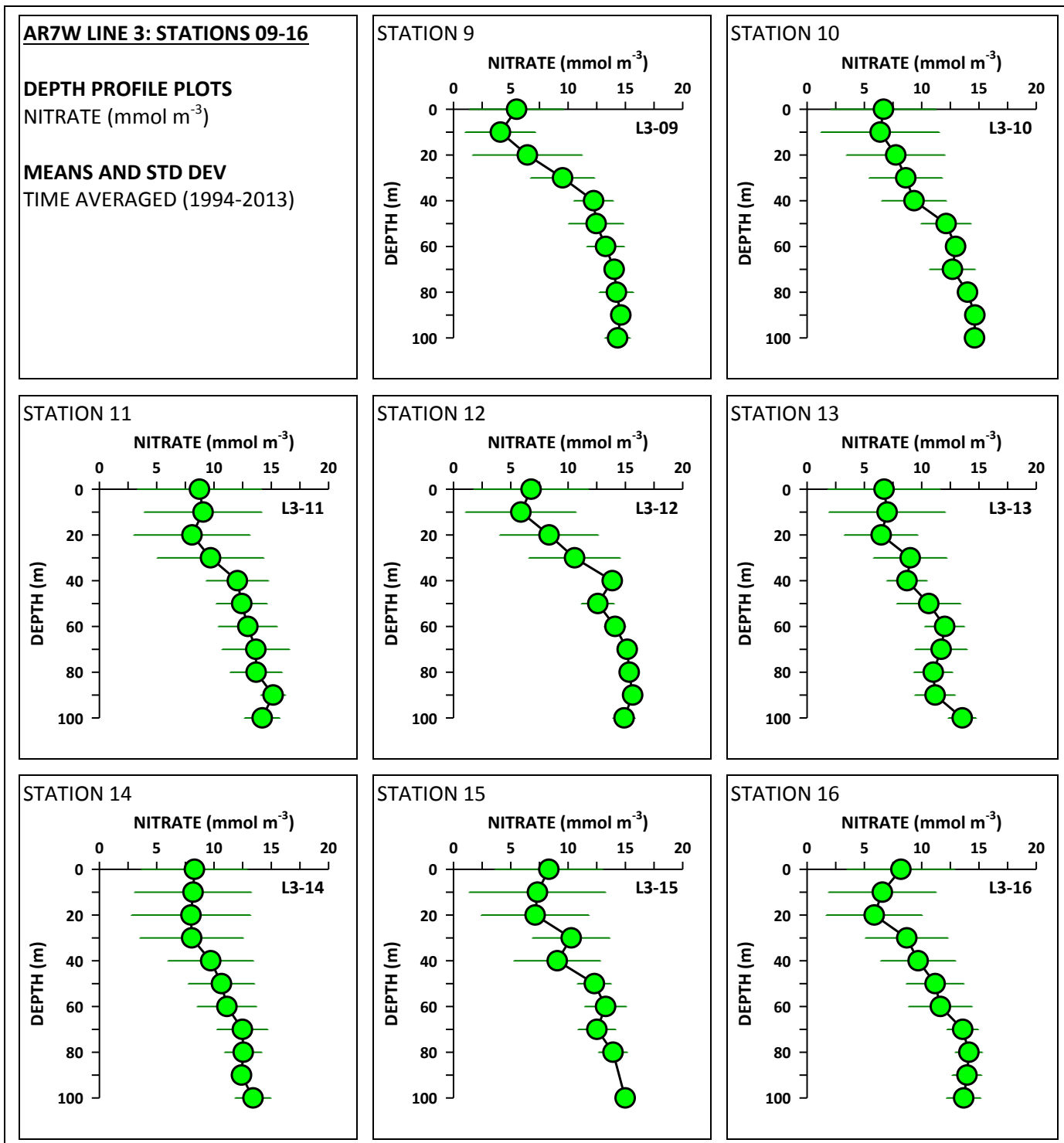


Figure 49

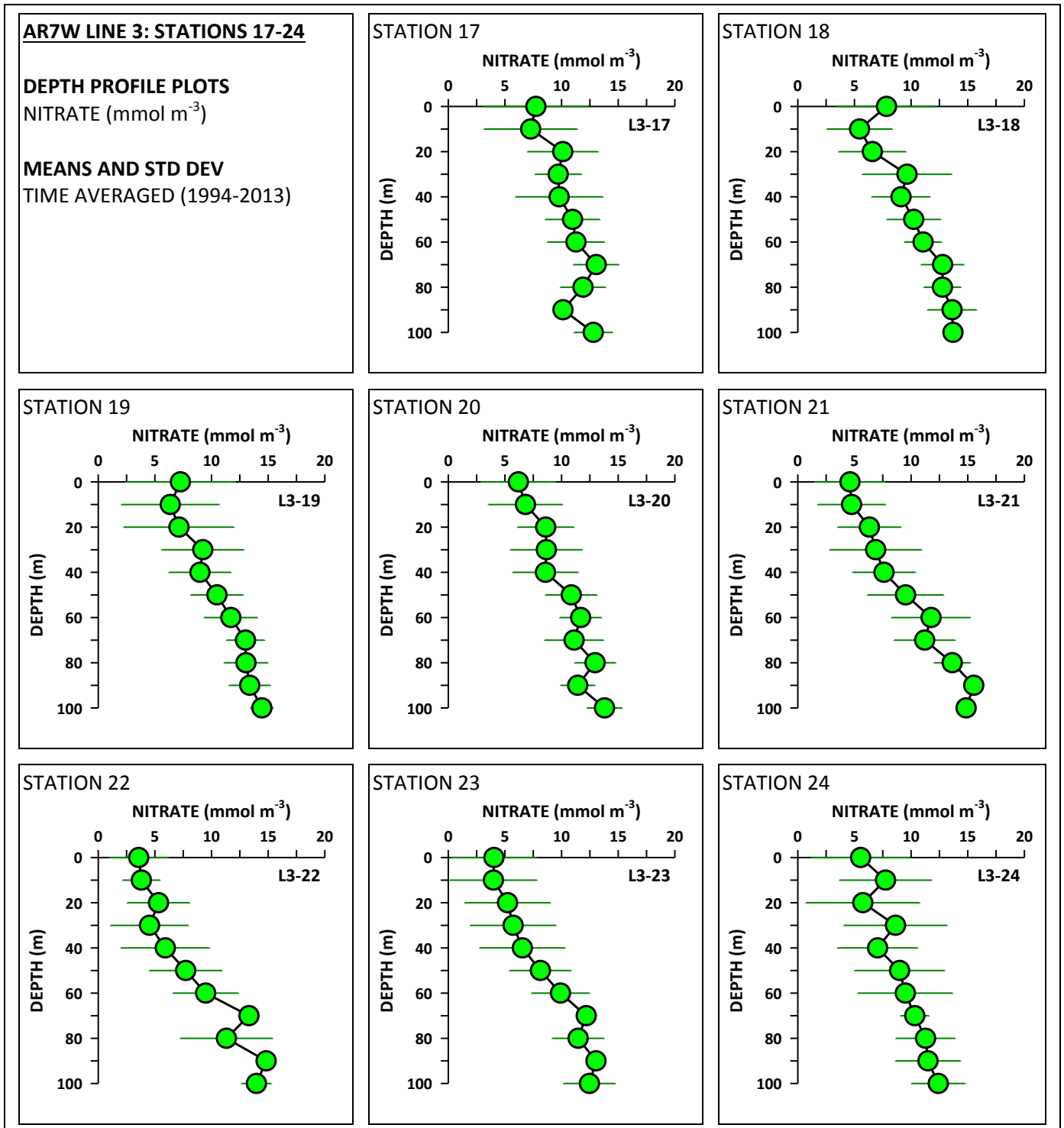


Figure 50

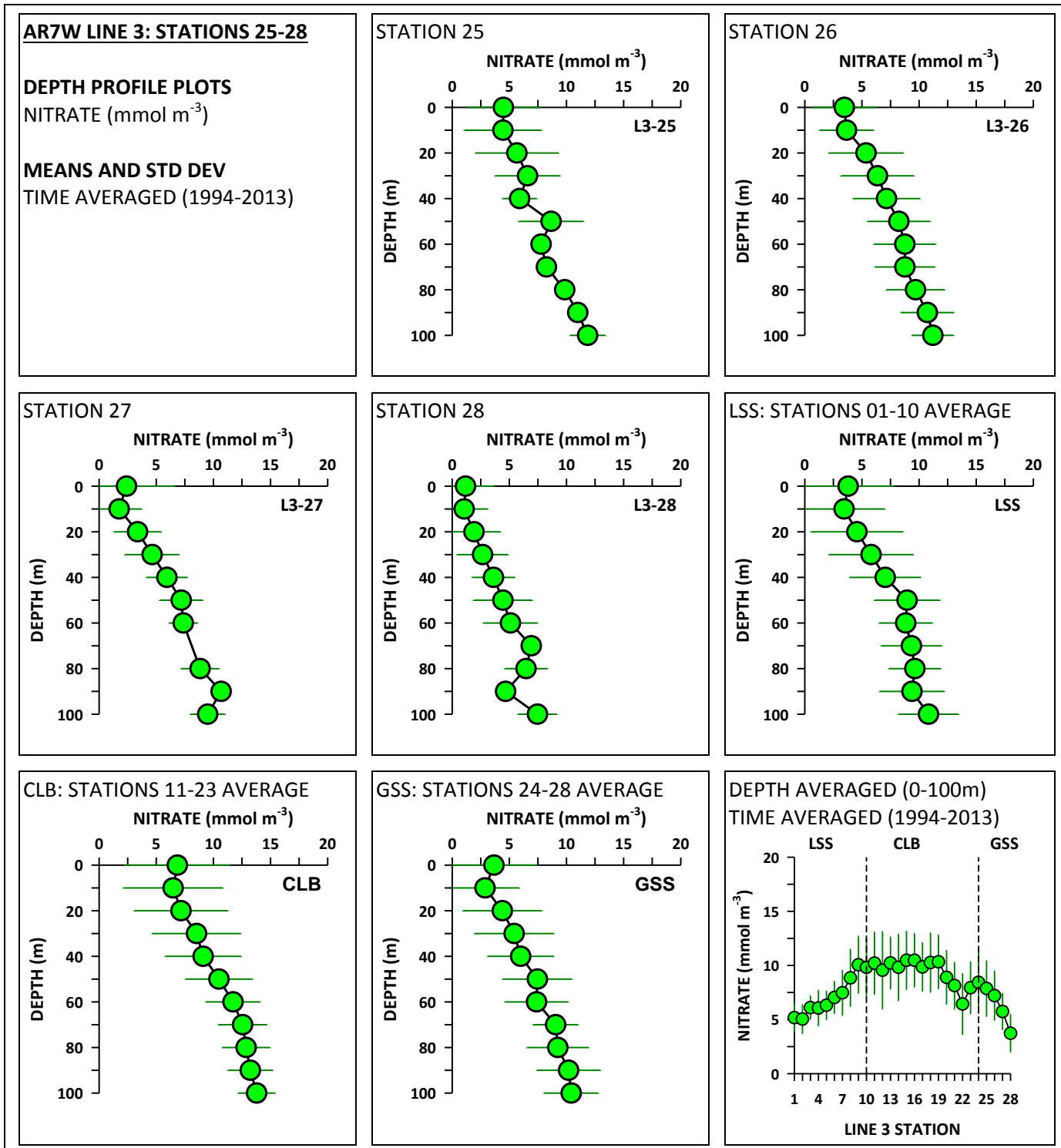


Figure 51

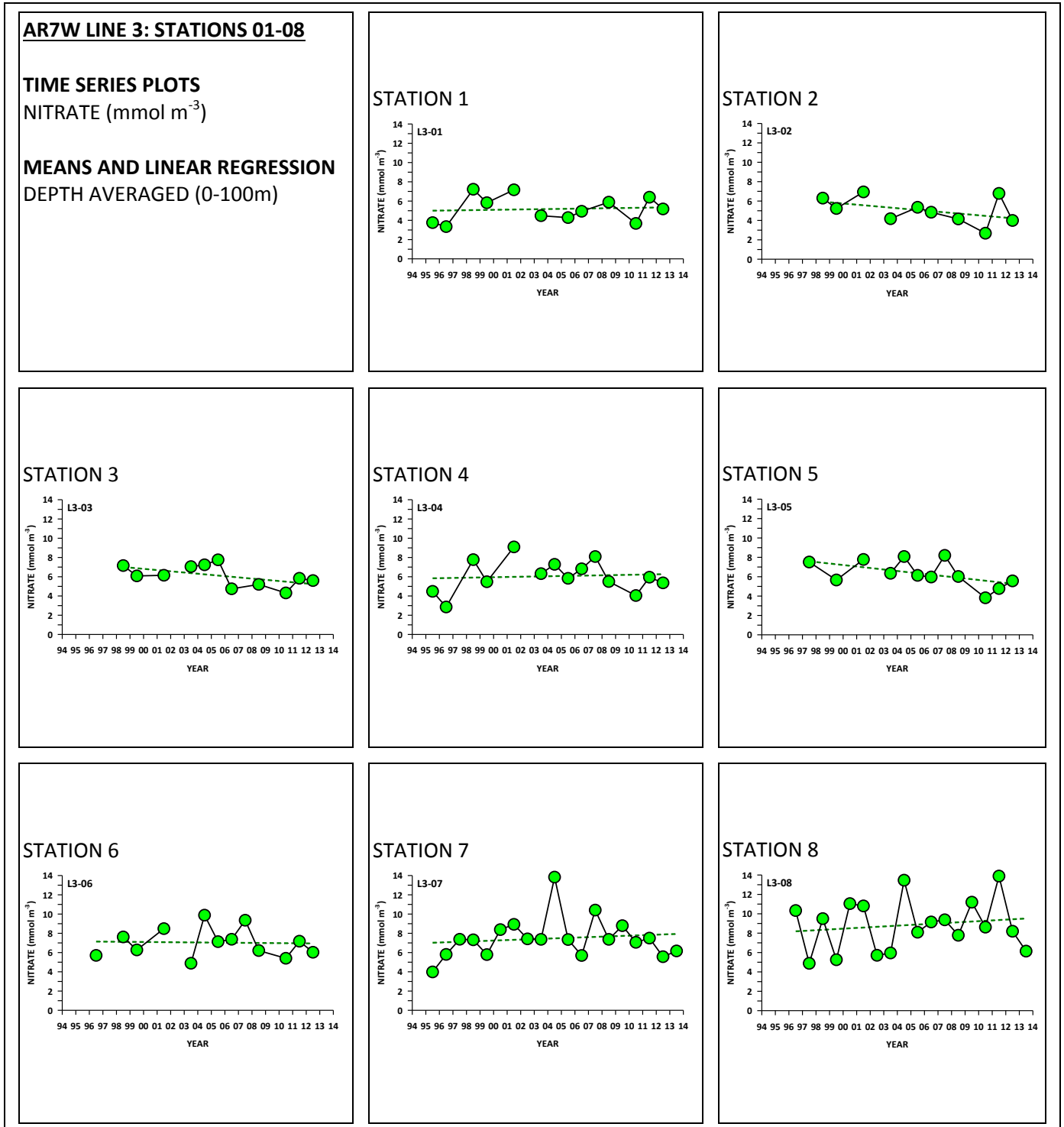




Figure 52

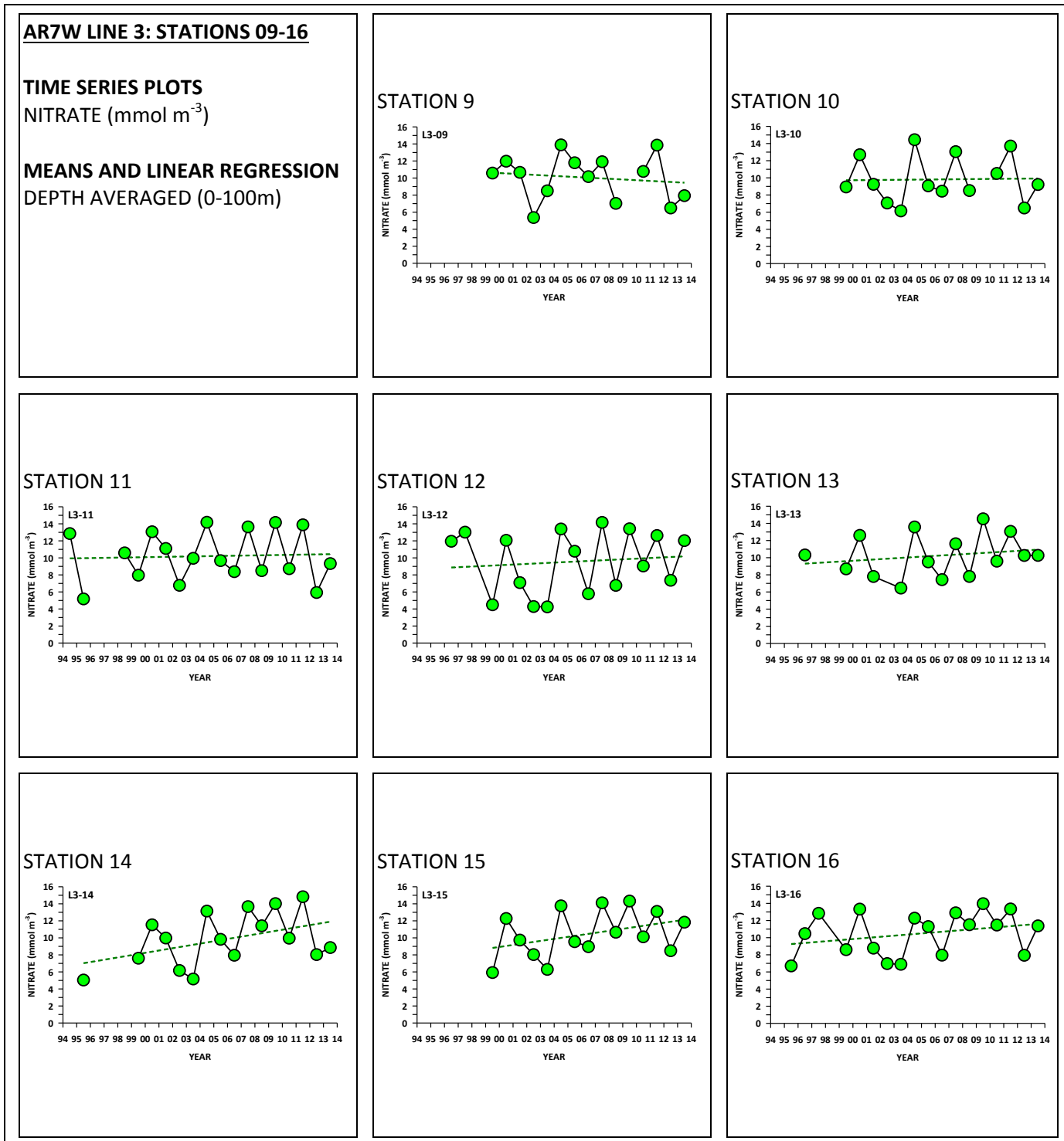


Figure 53

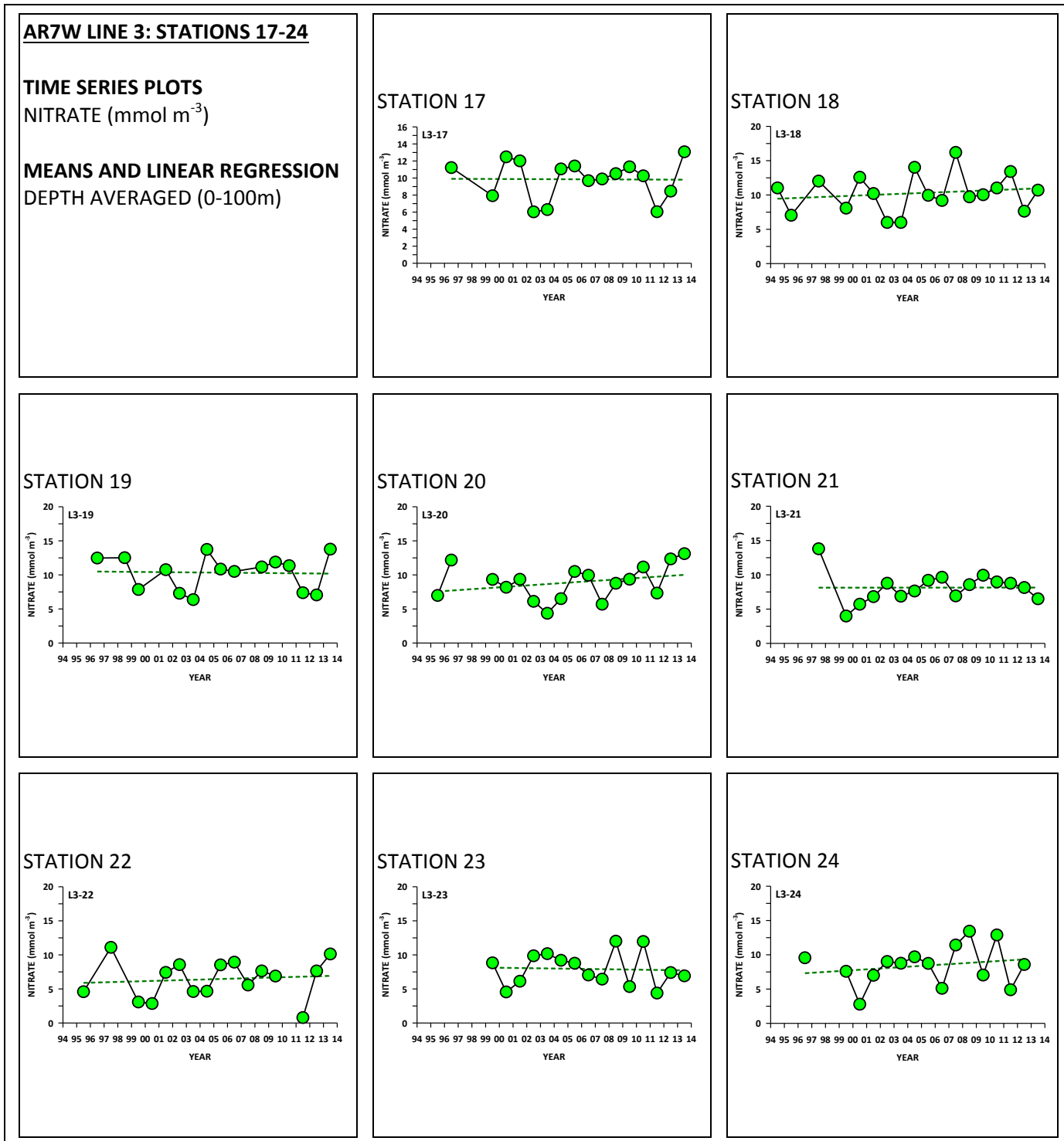


Figure 54

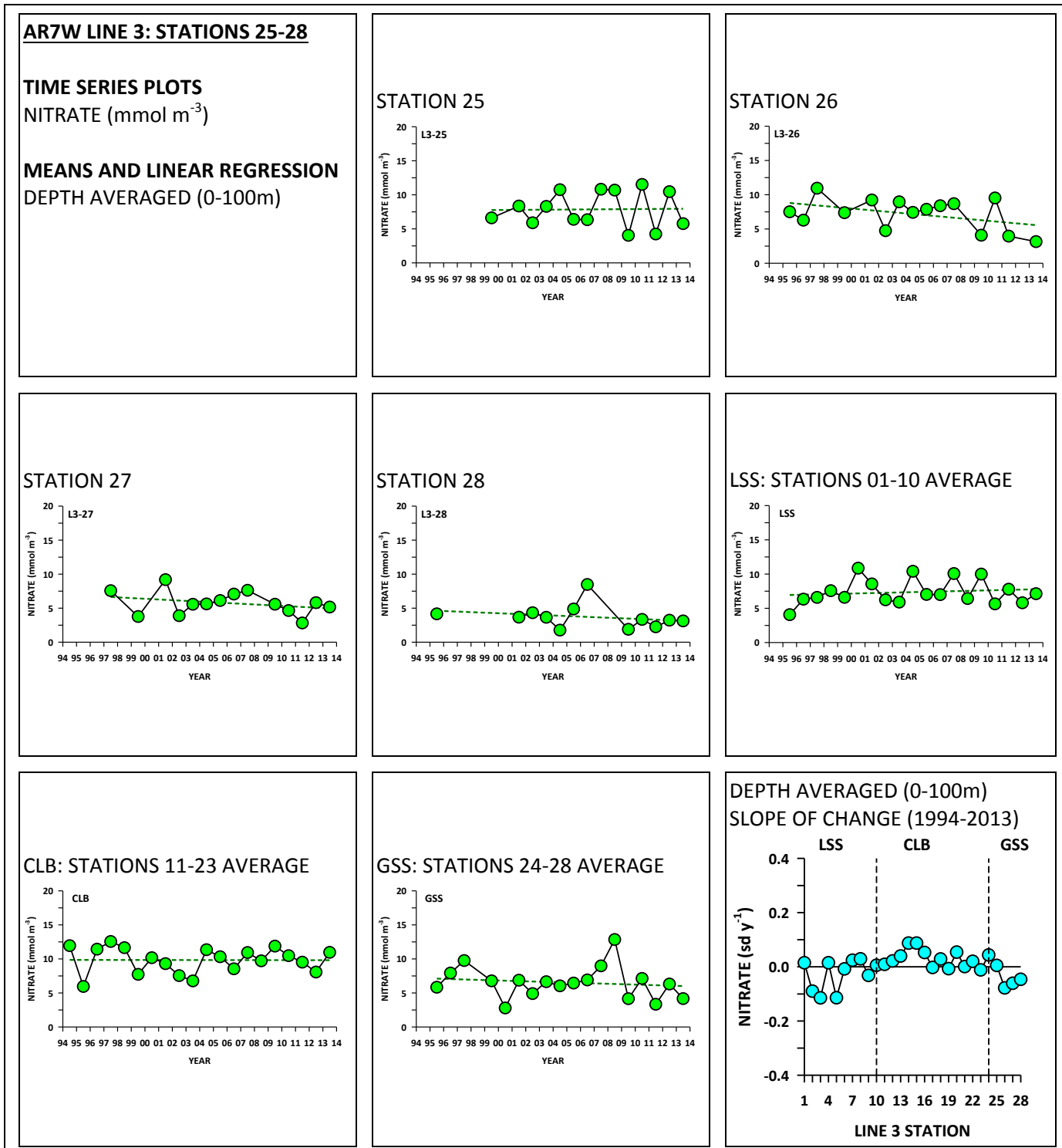


Figure 55

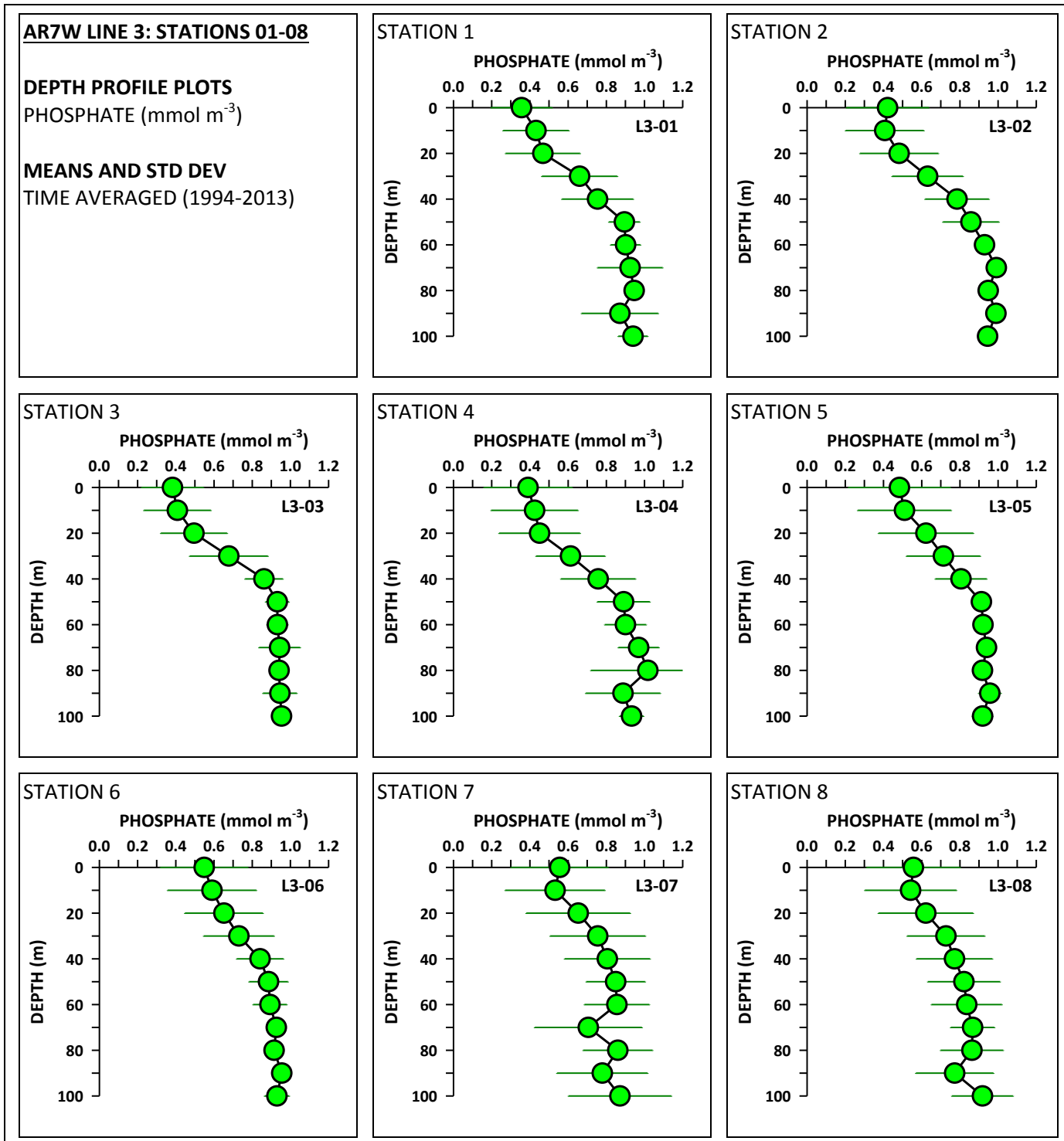


Figure 56

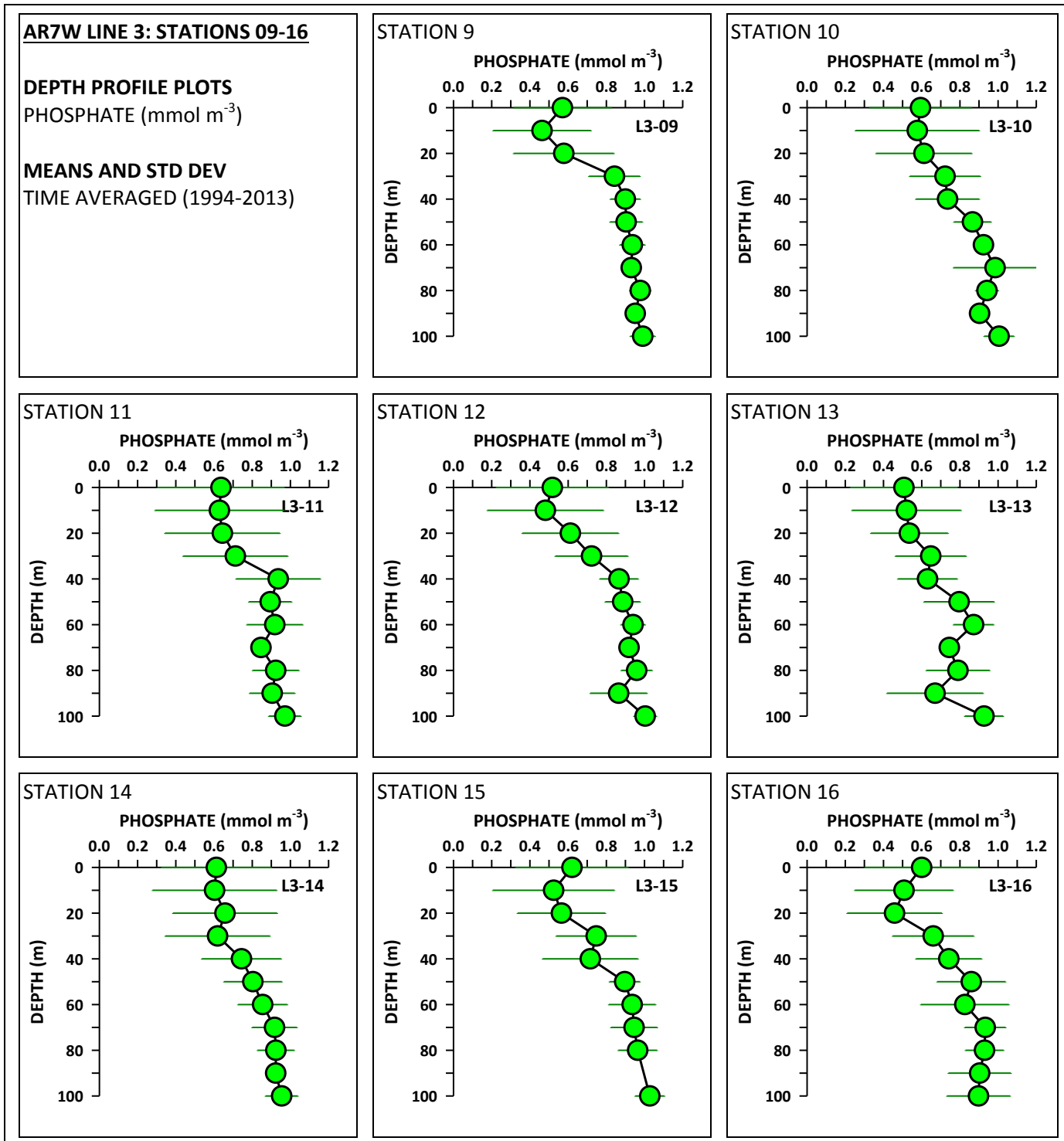


Figure 57

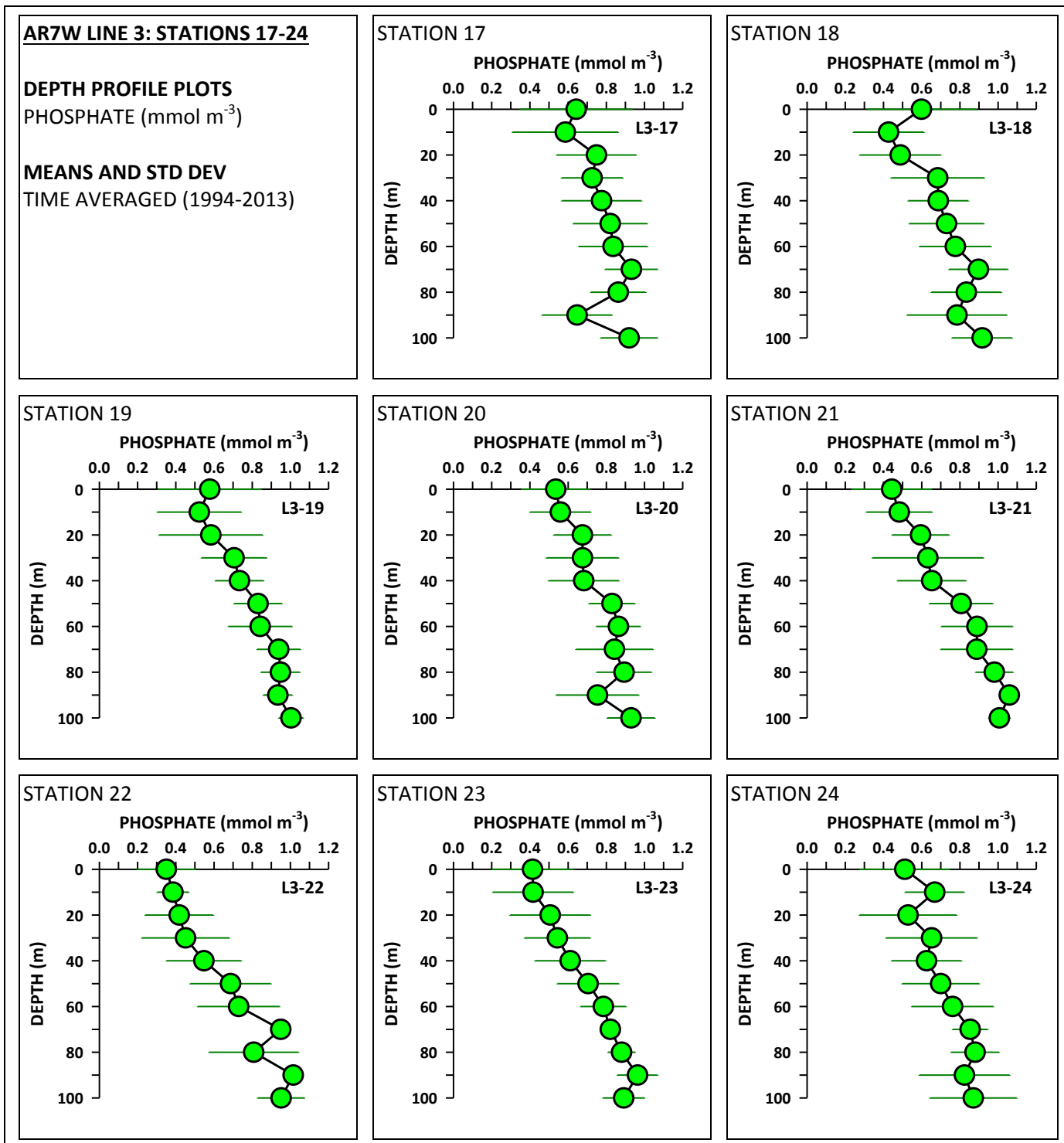


Figure 58

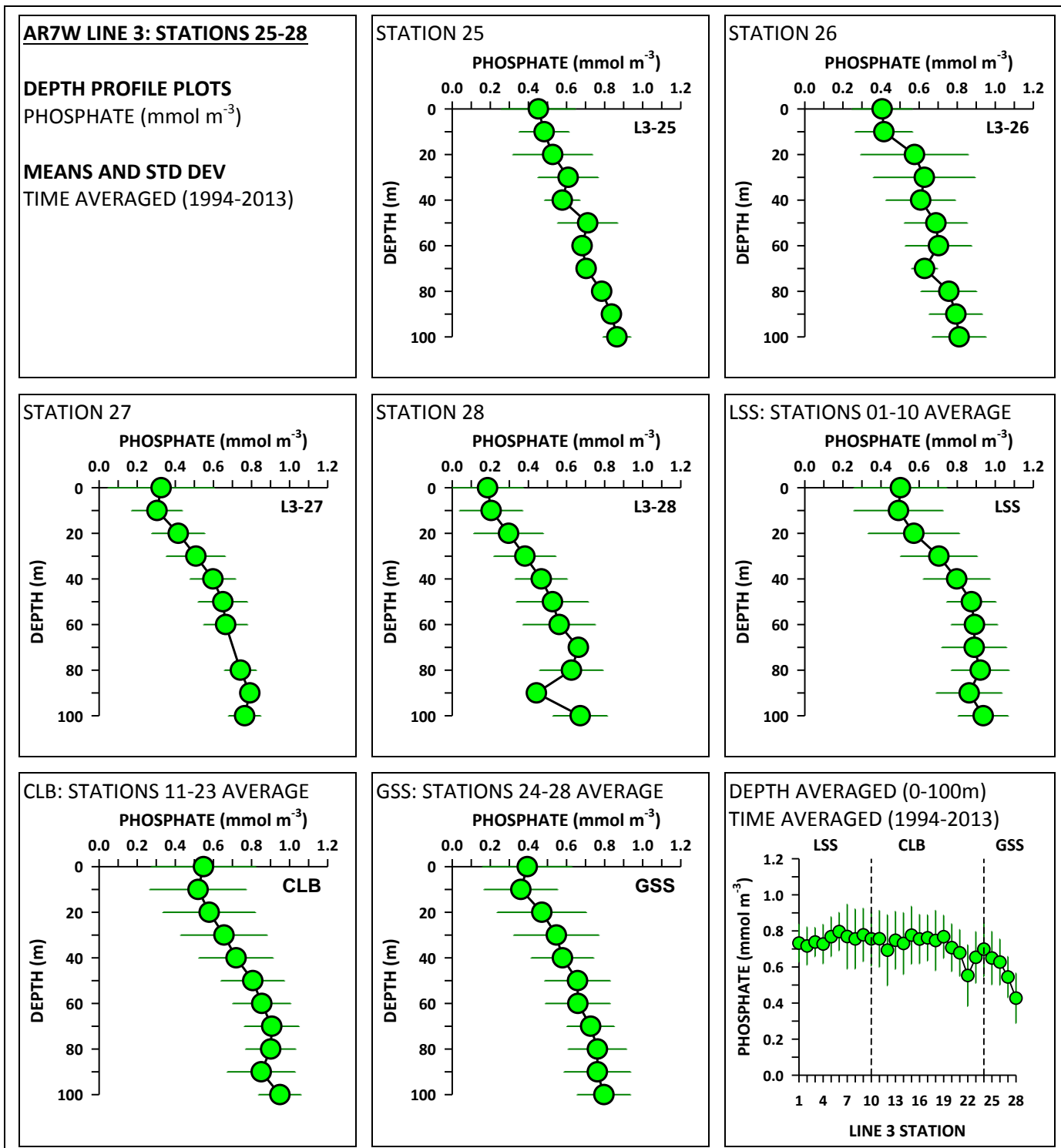


Figure 59

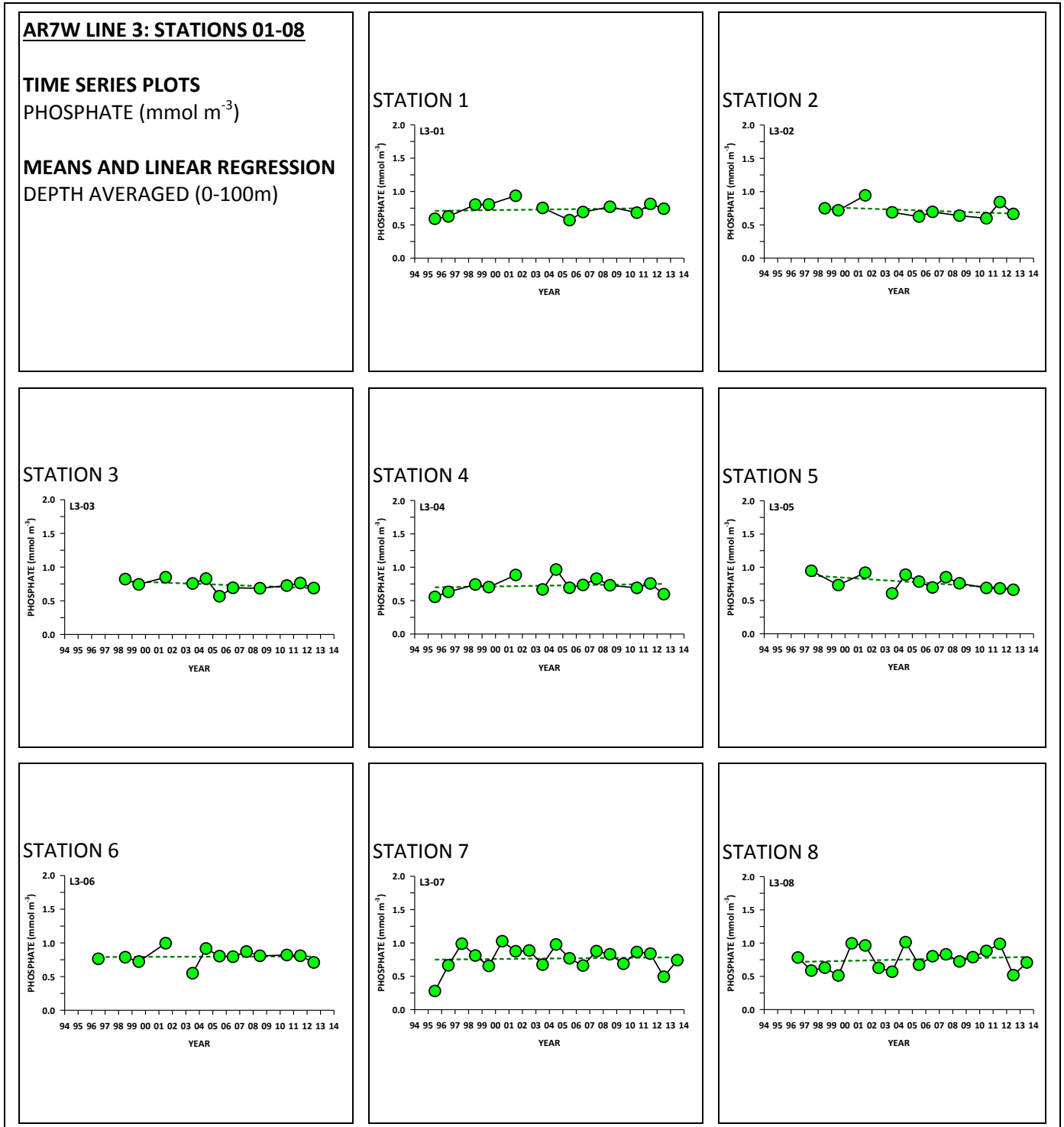




Figure 60

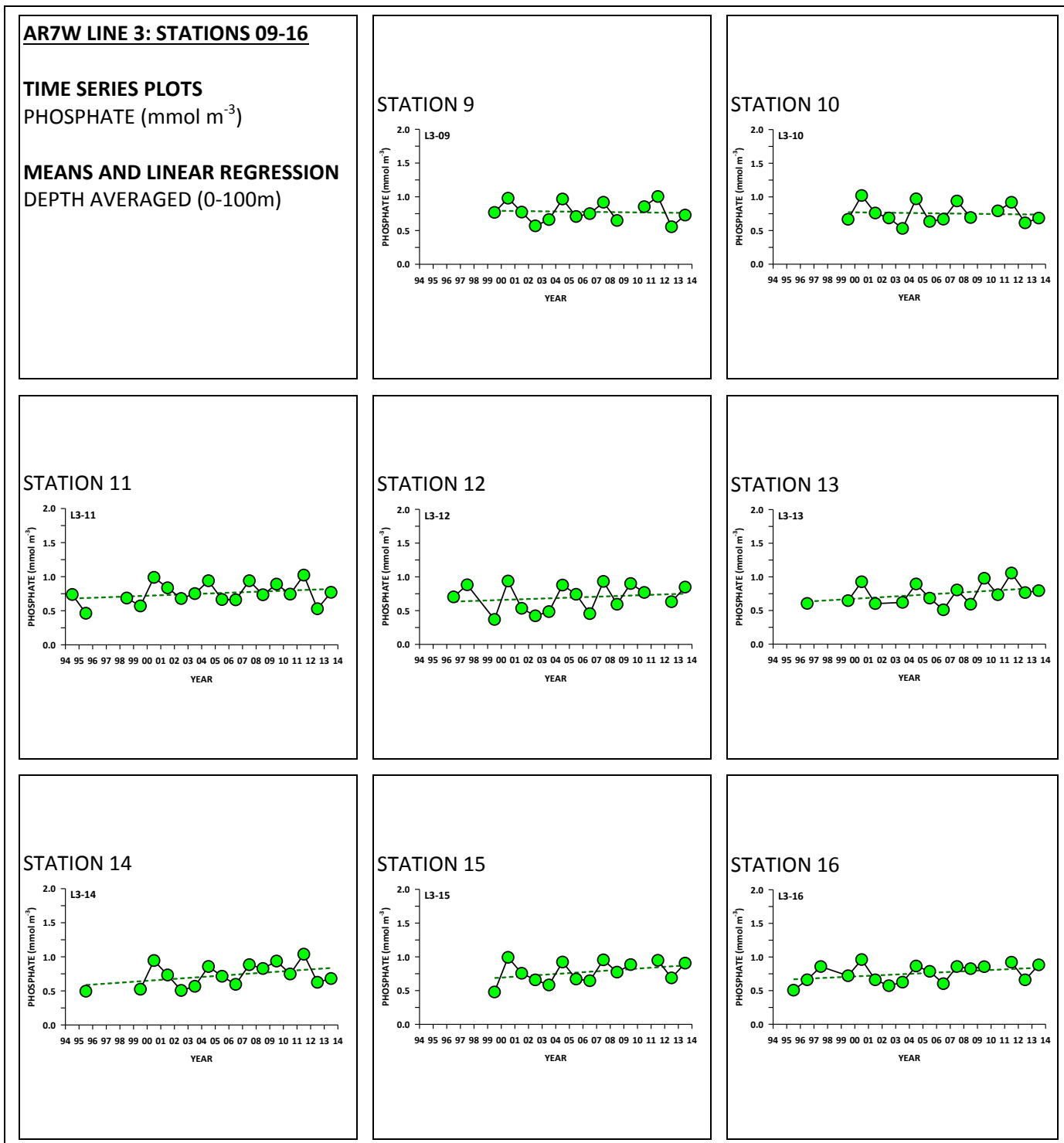


Figure 61

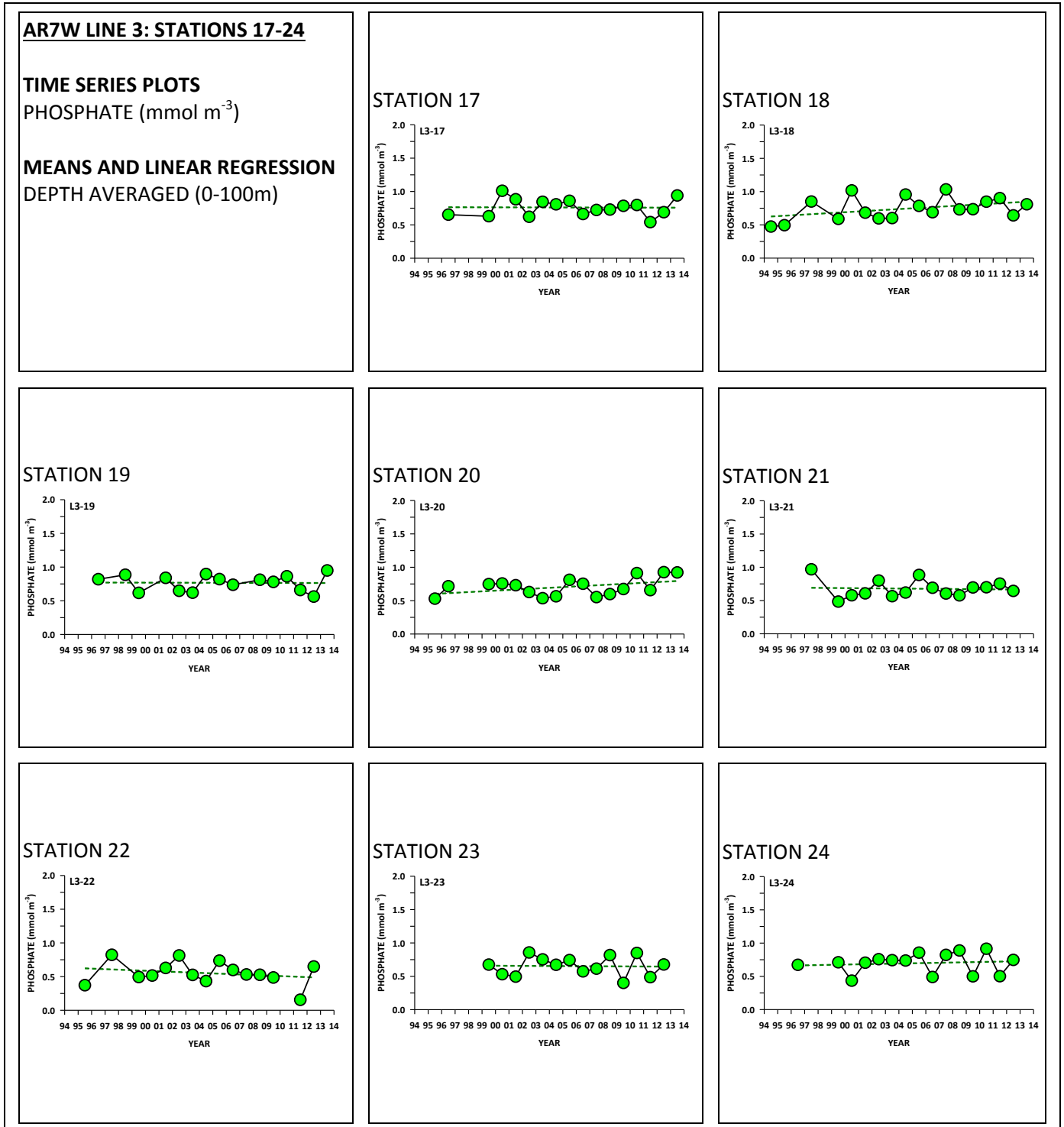


Figure 62

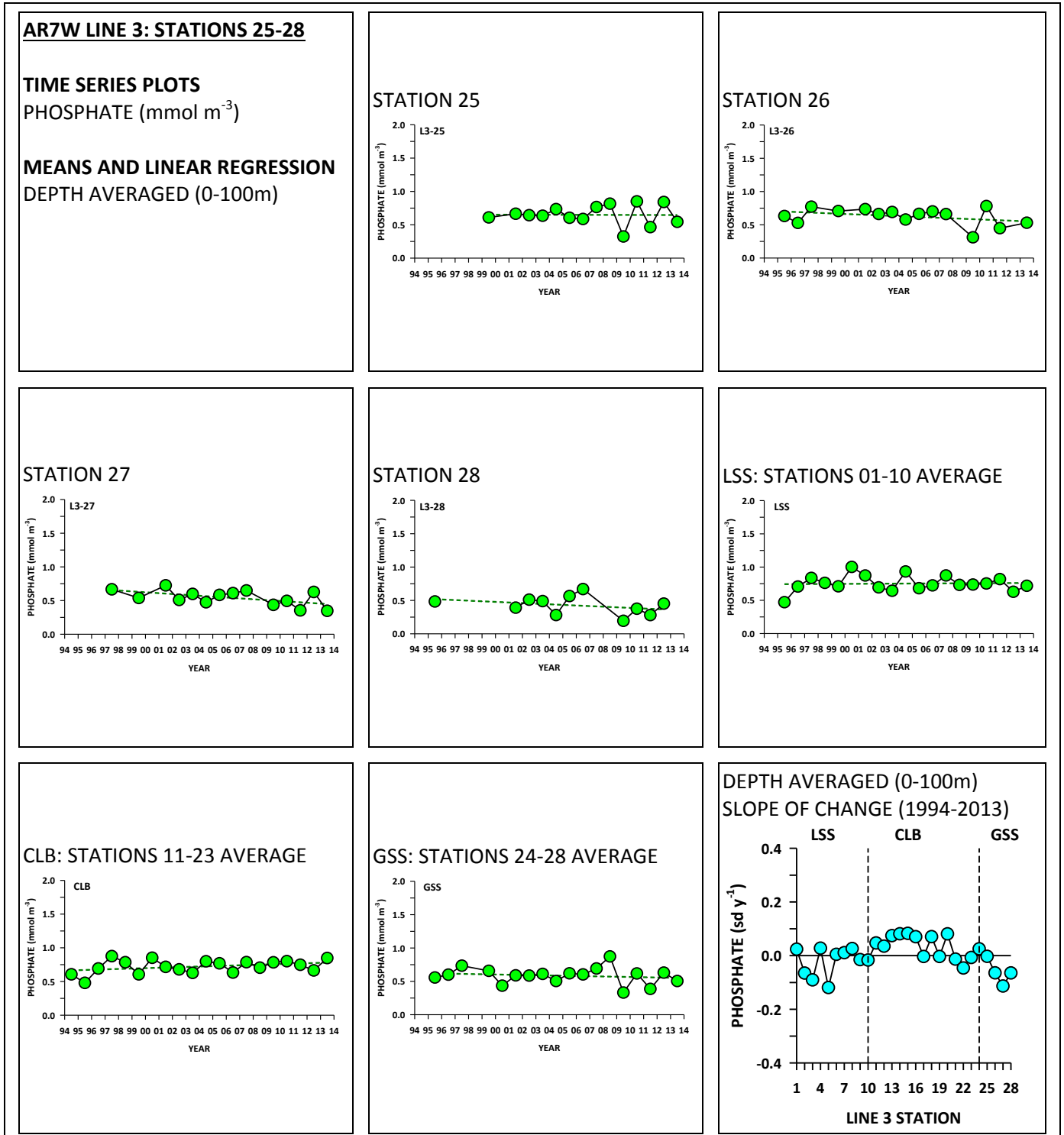


Figure 63

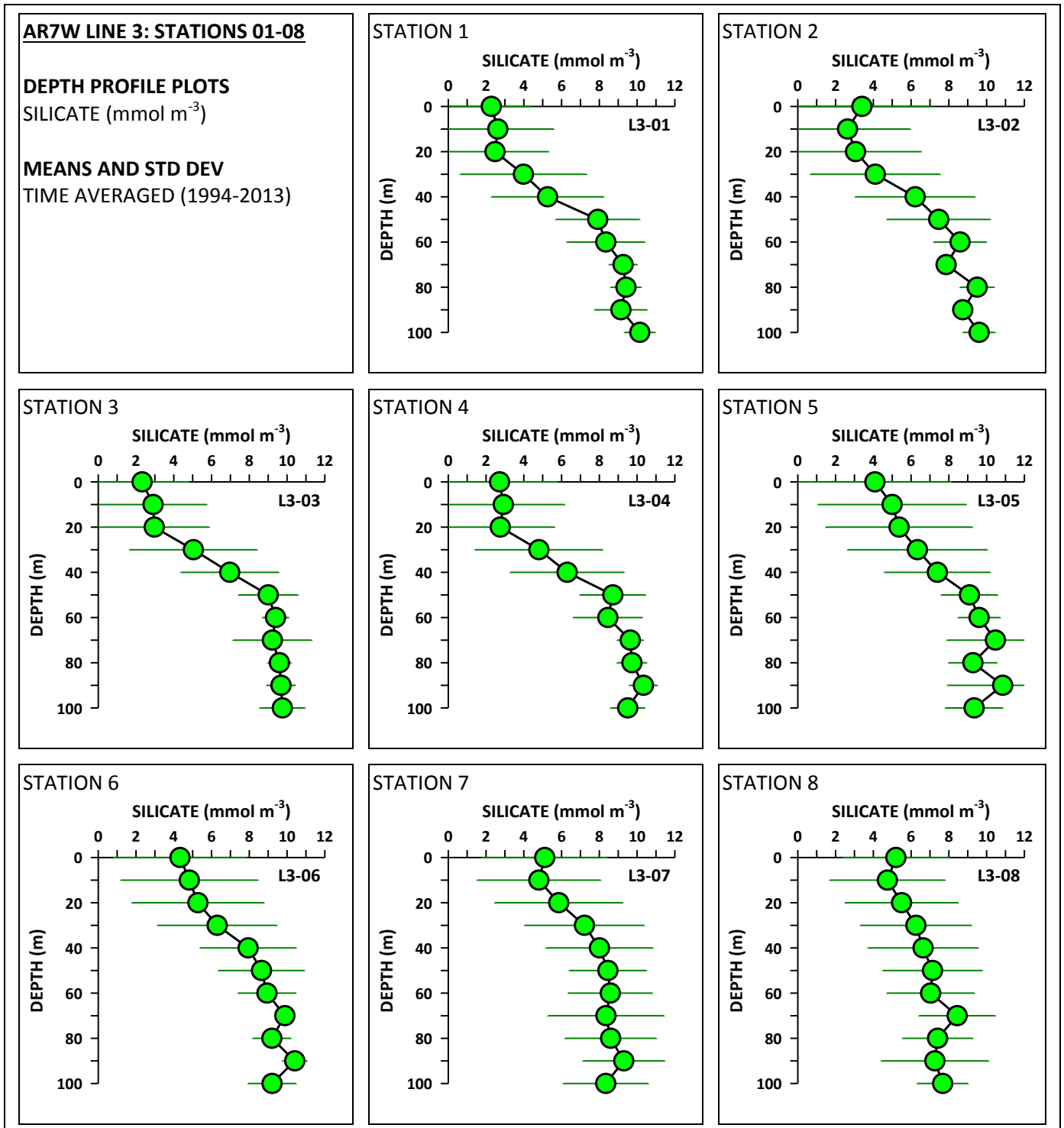


Figure 64

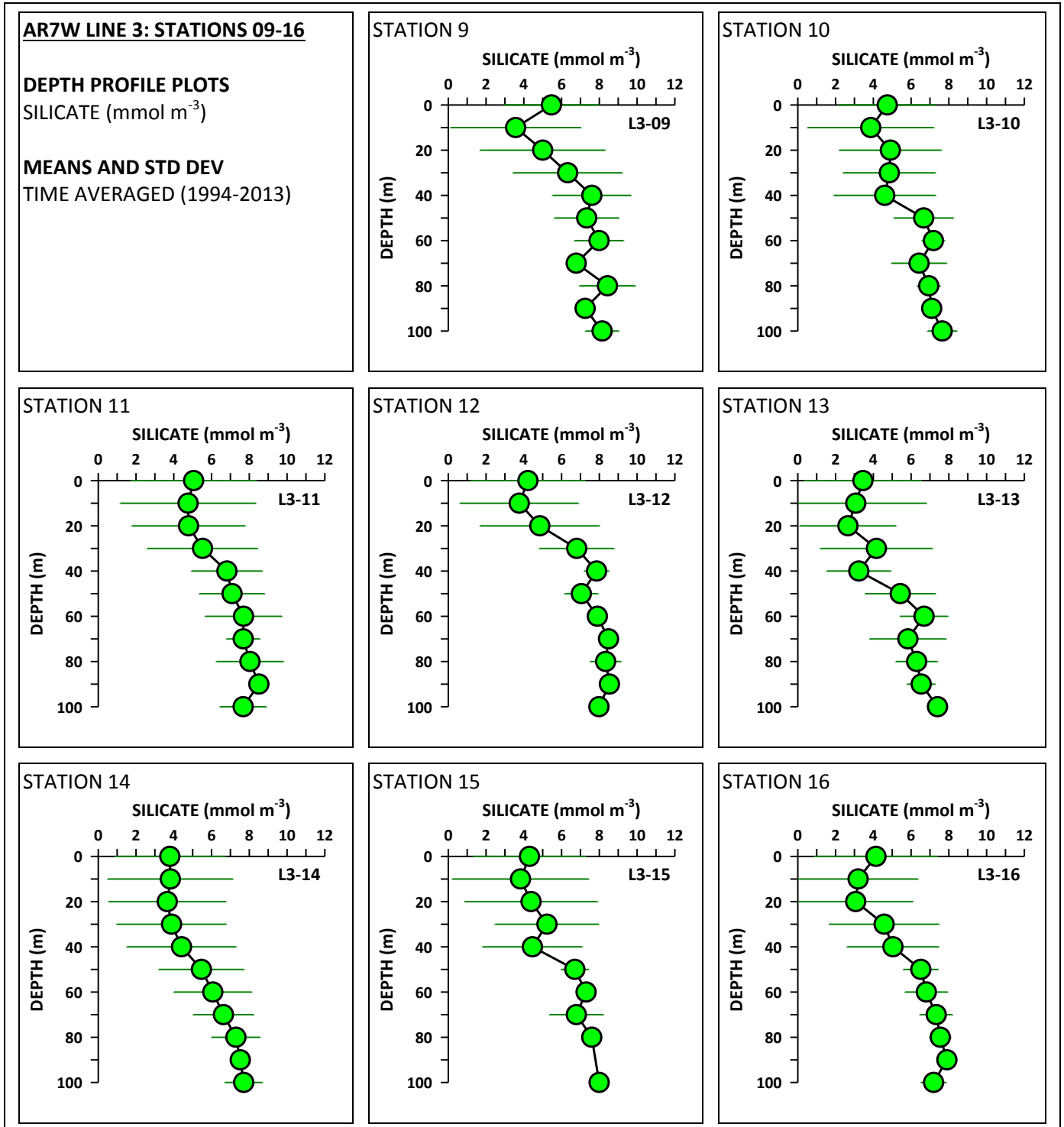


Figure 65

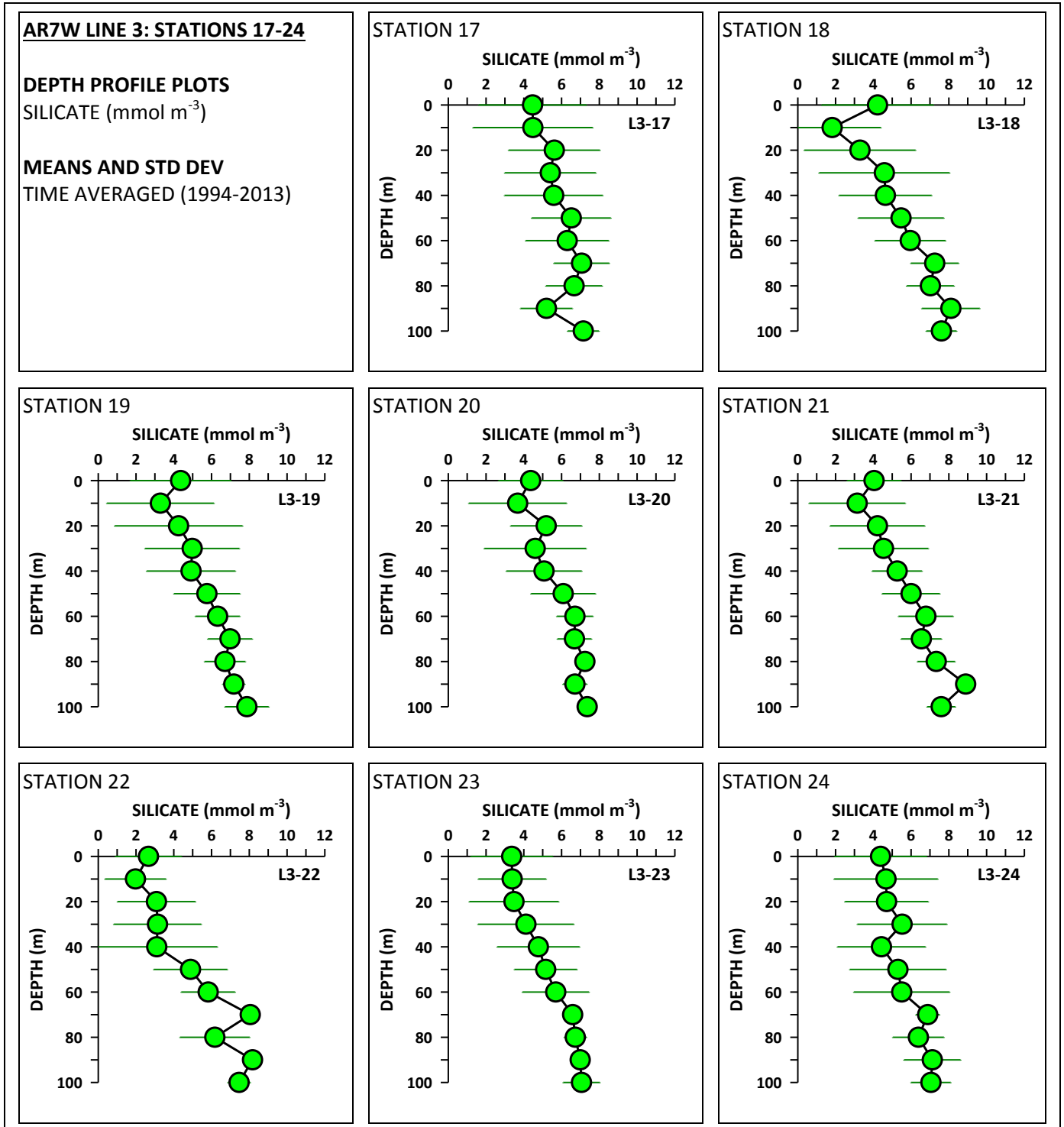


Figure 66

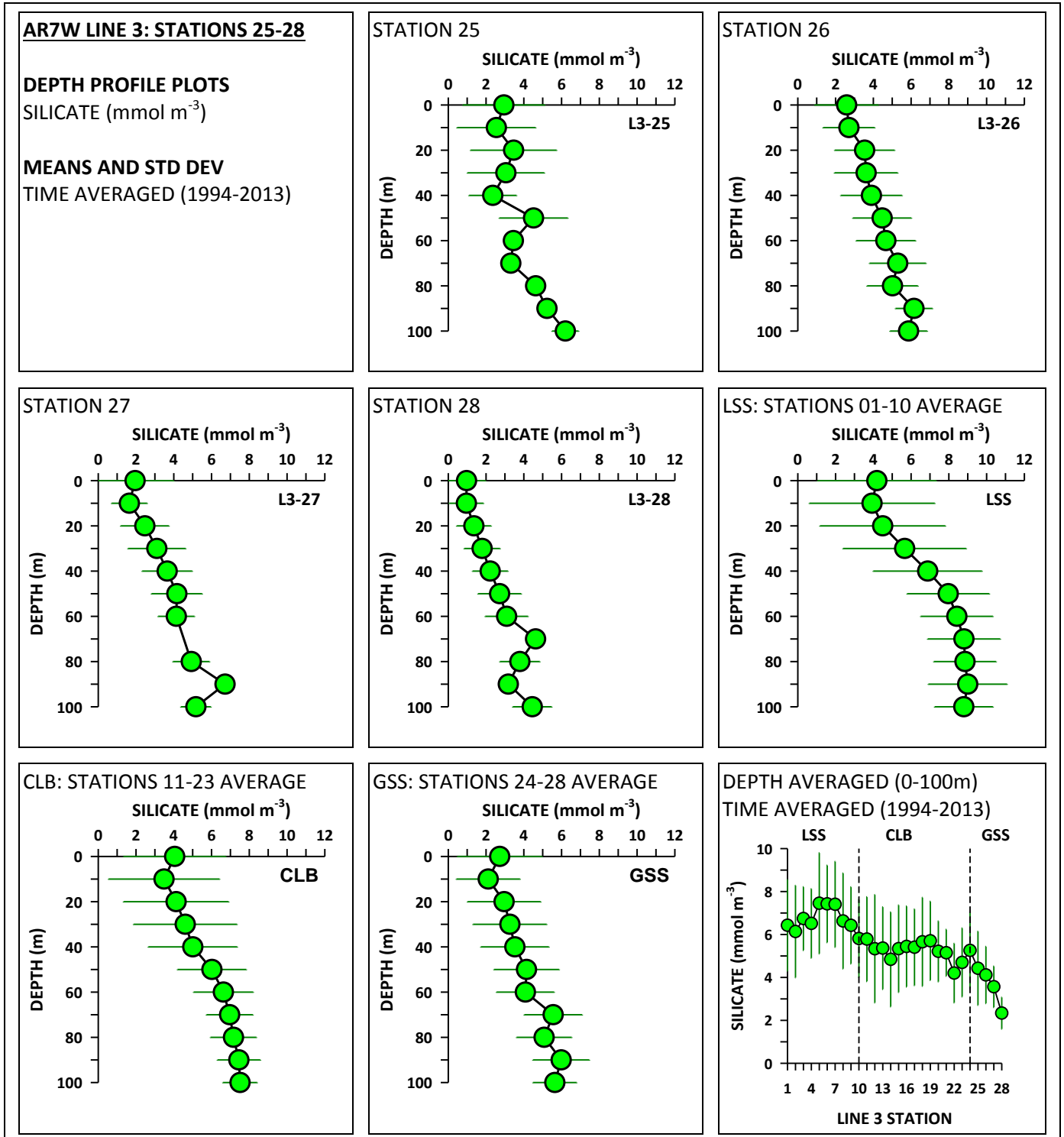


Figure 67

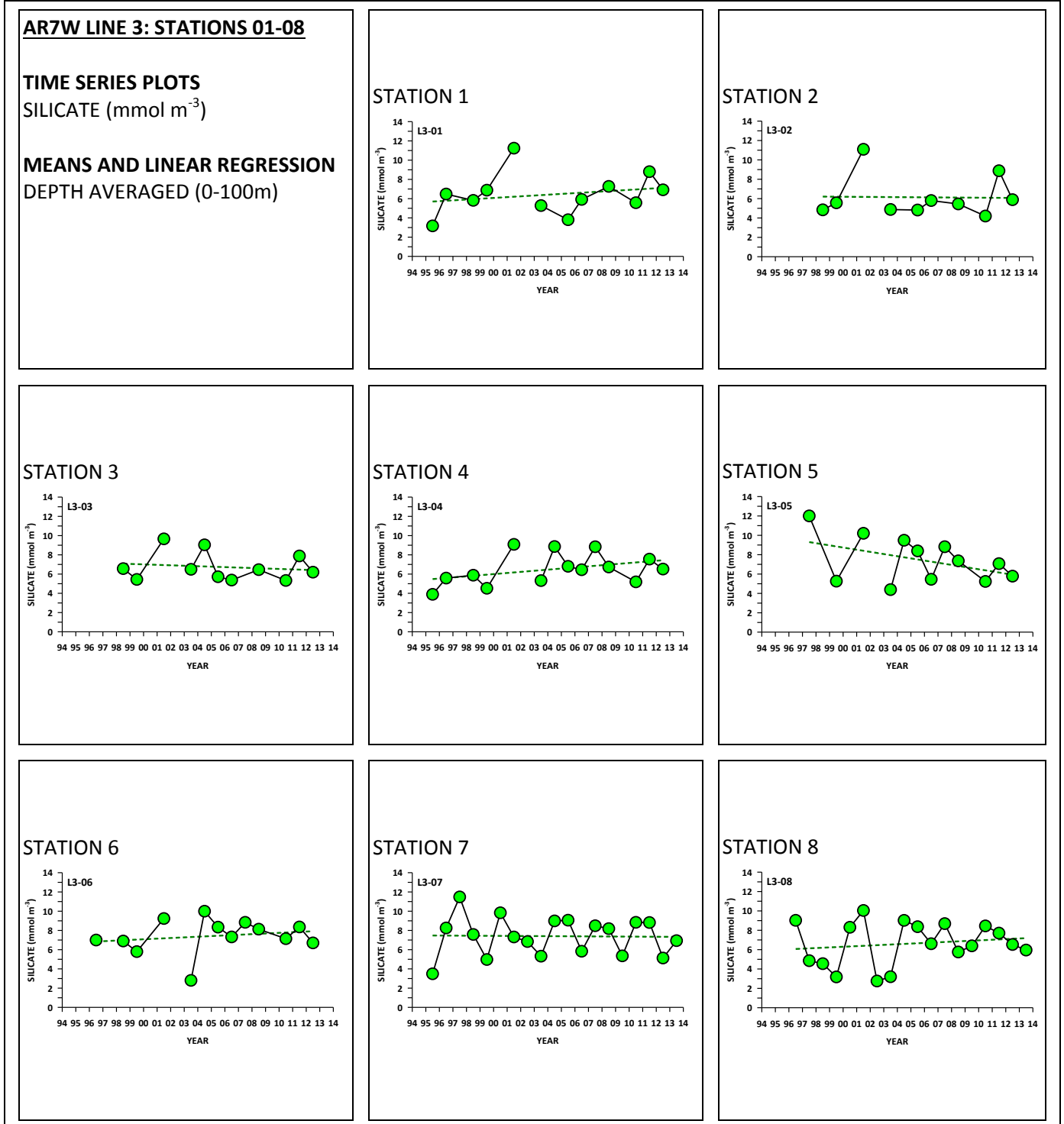




Figure 68

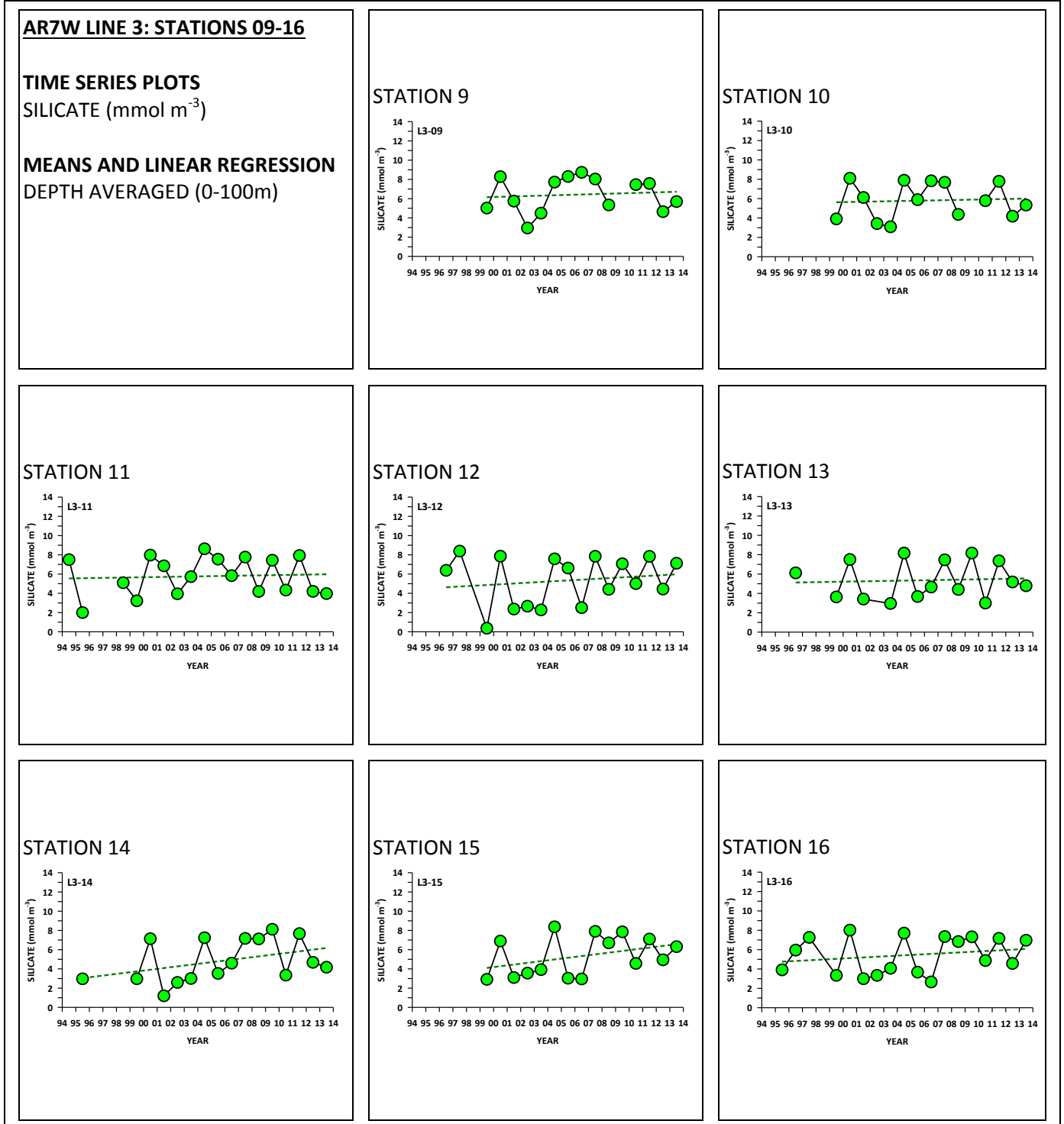


Figure 69

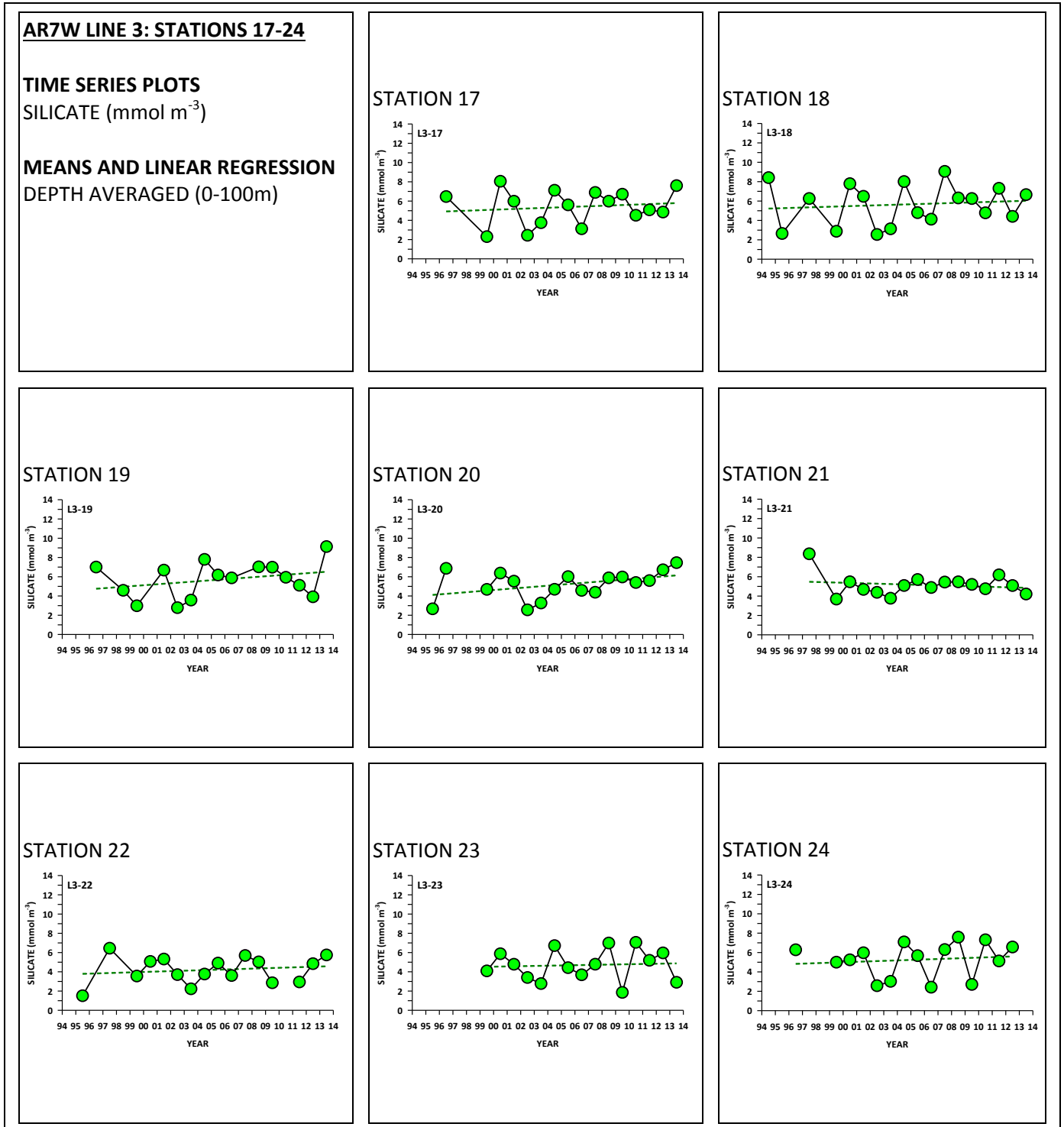


Figure 70

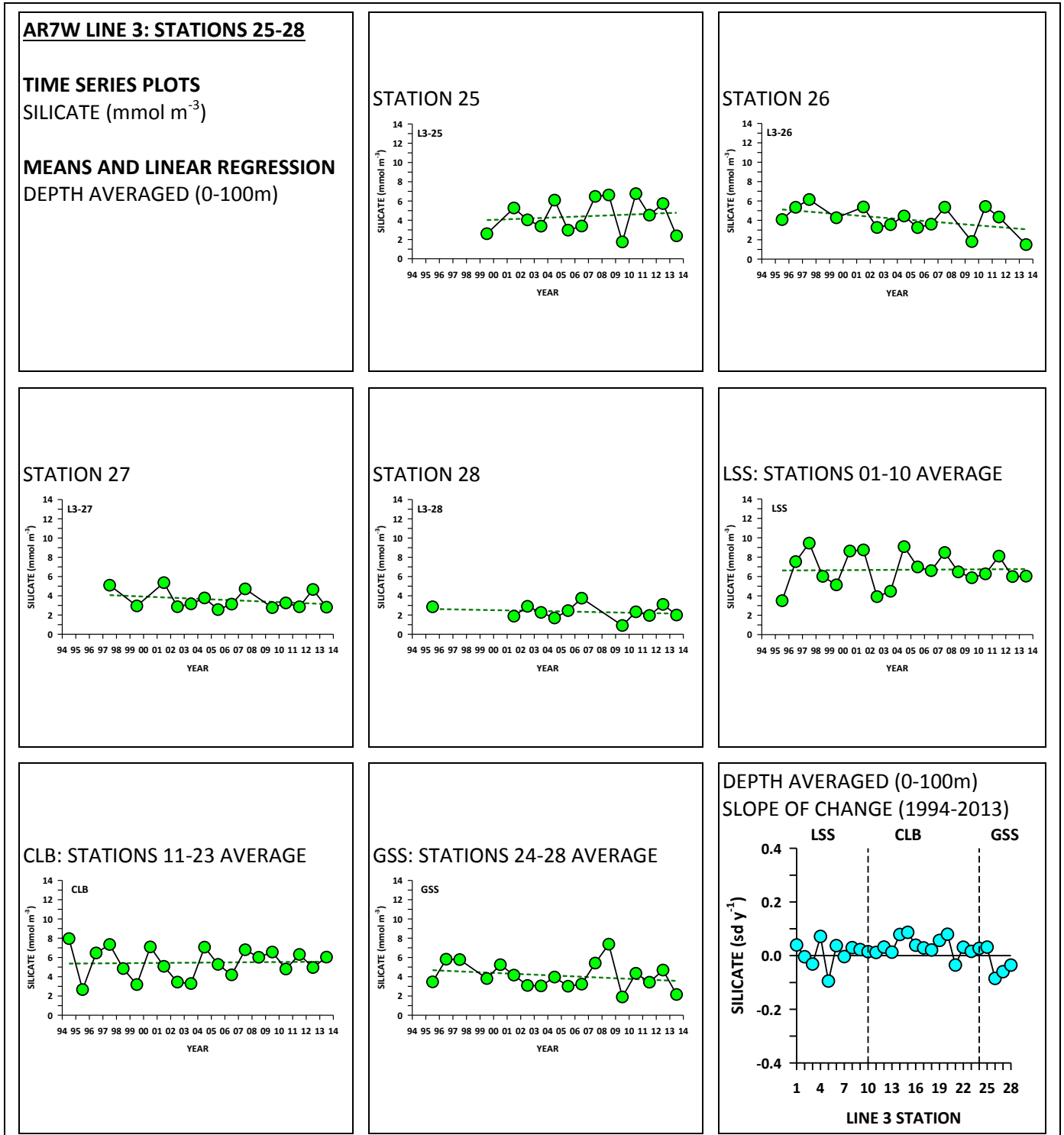


Figure 71

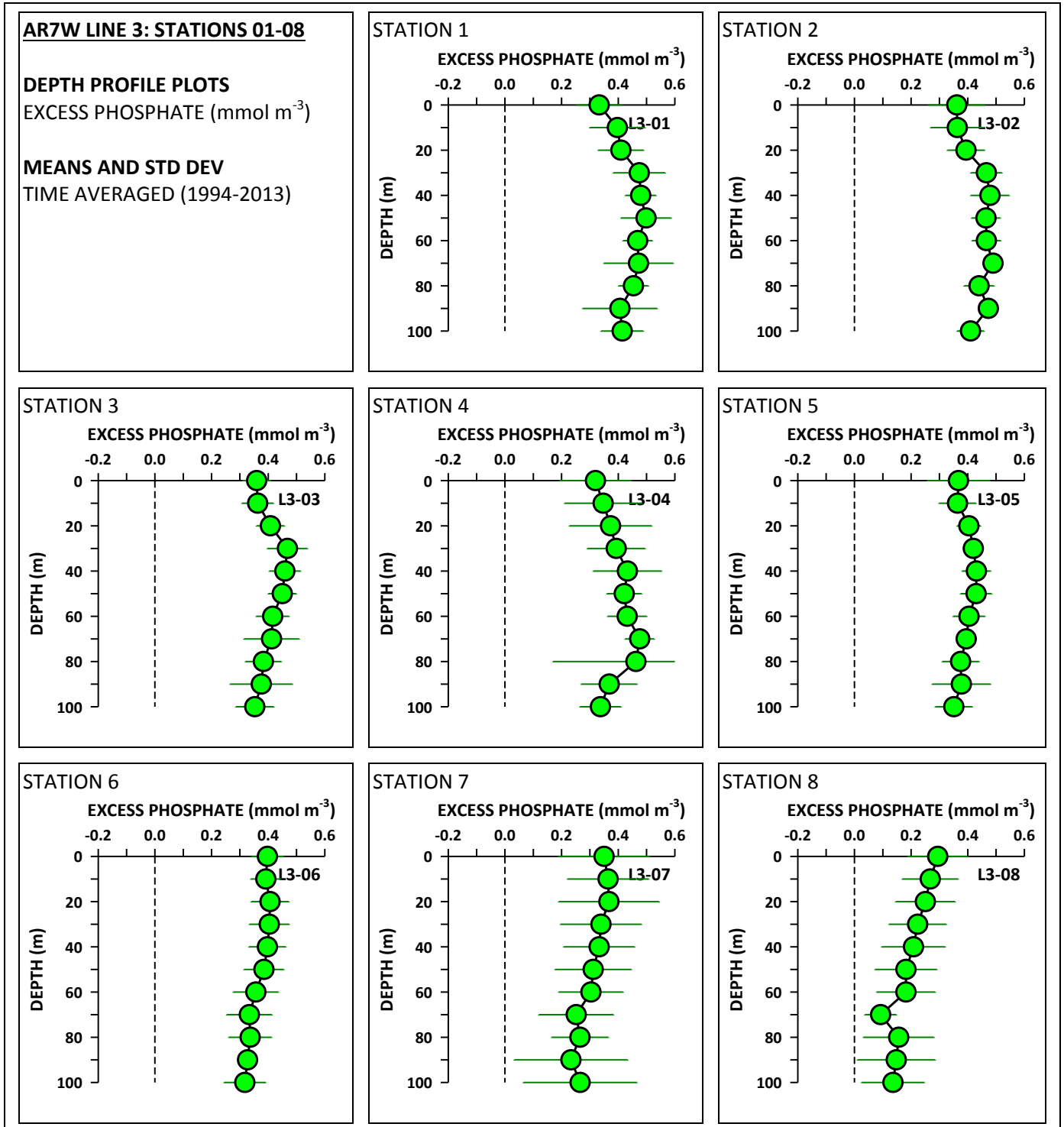


Figure 72

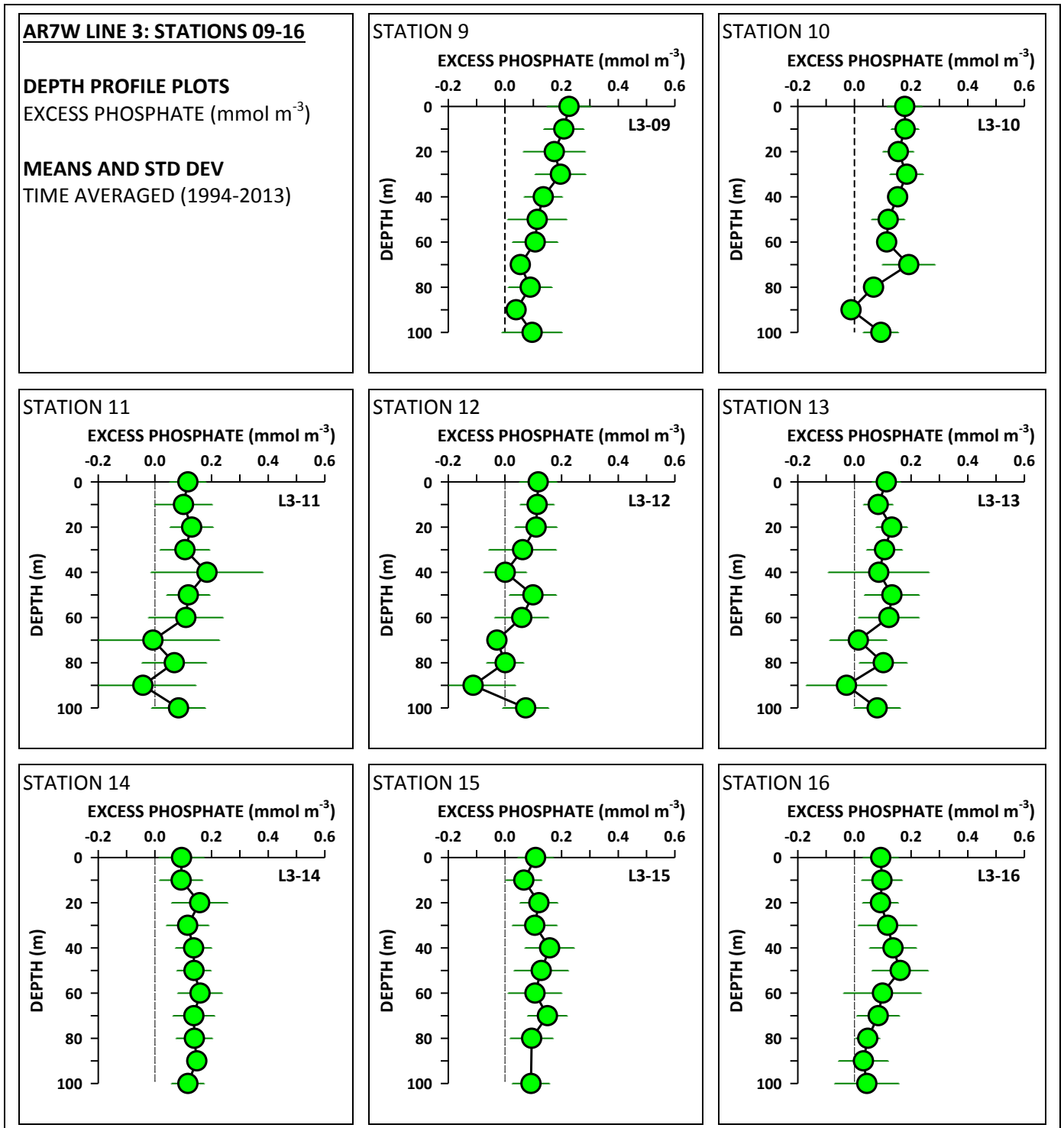




Figure 74

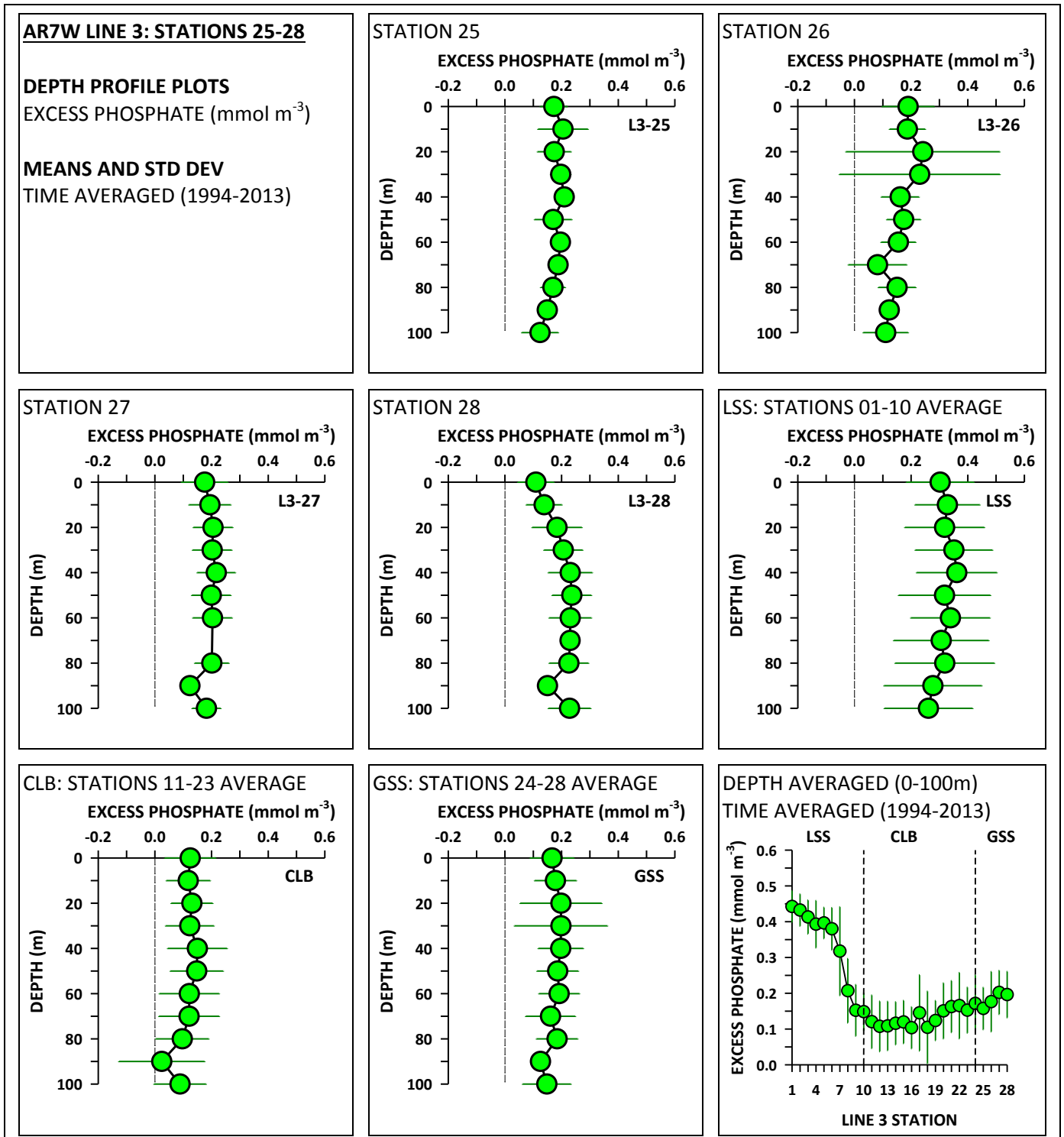


Figure 75

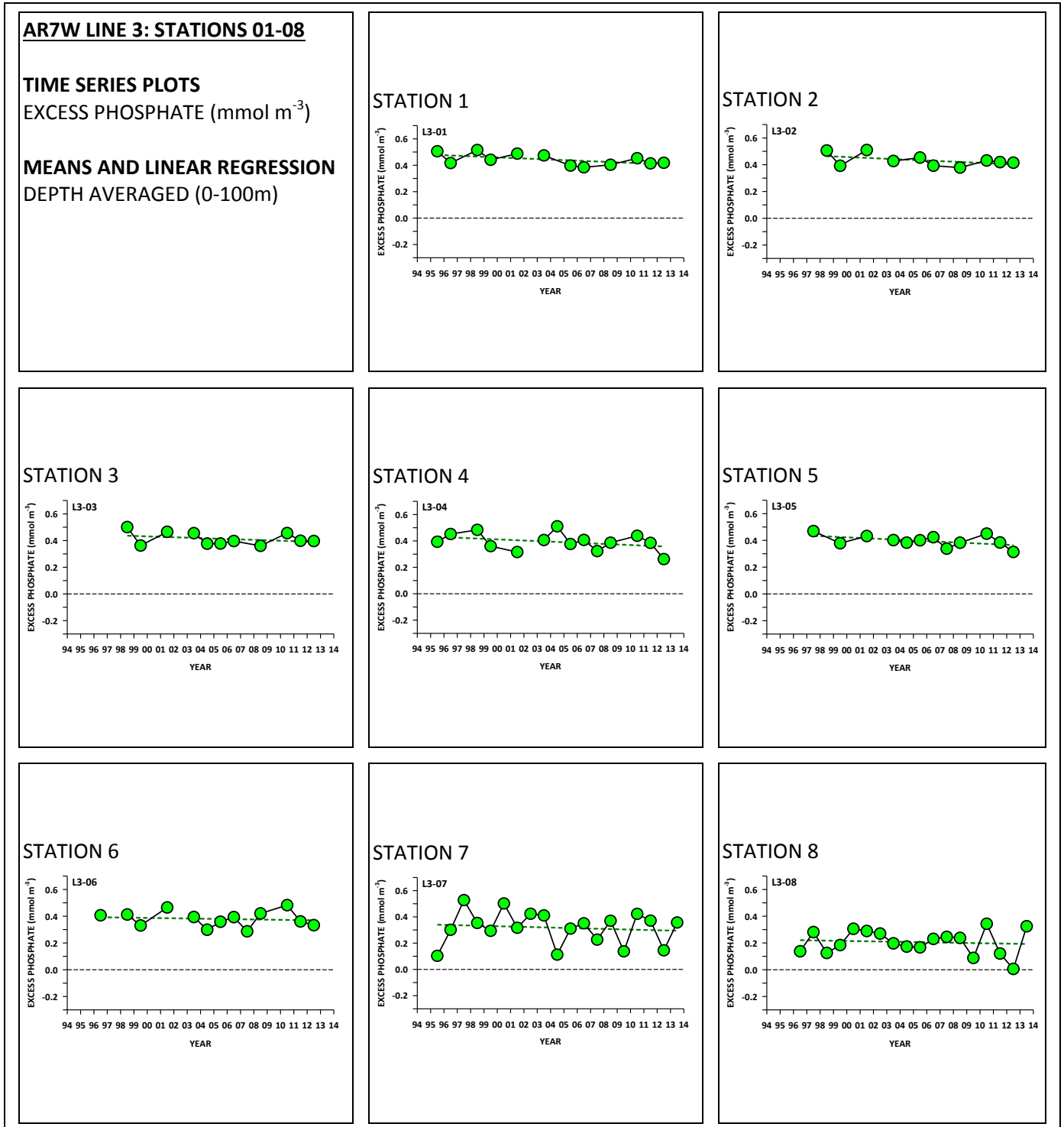




Figure 76

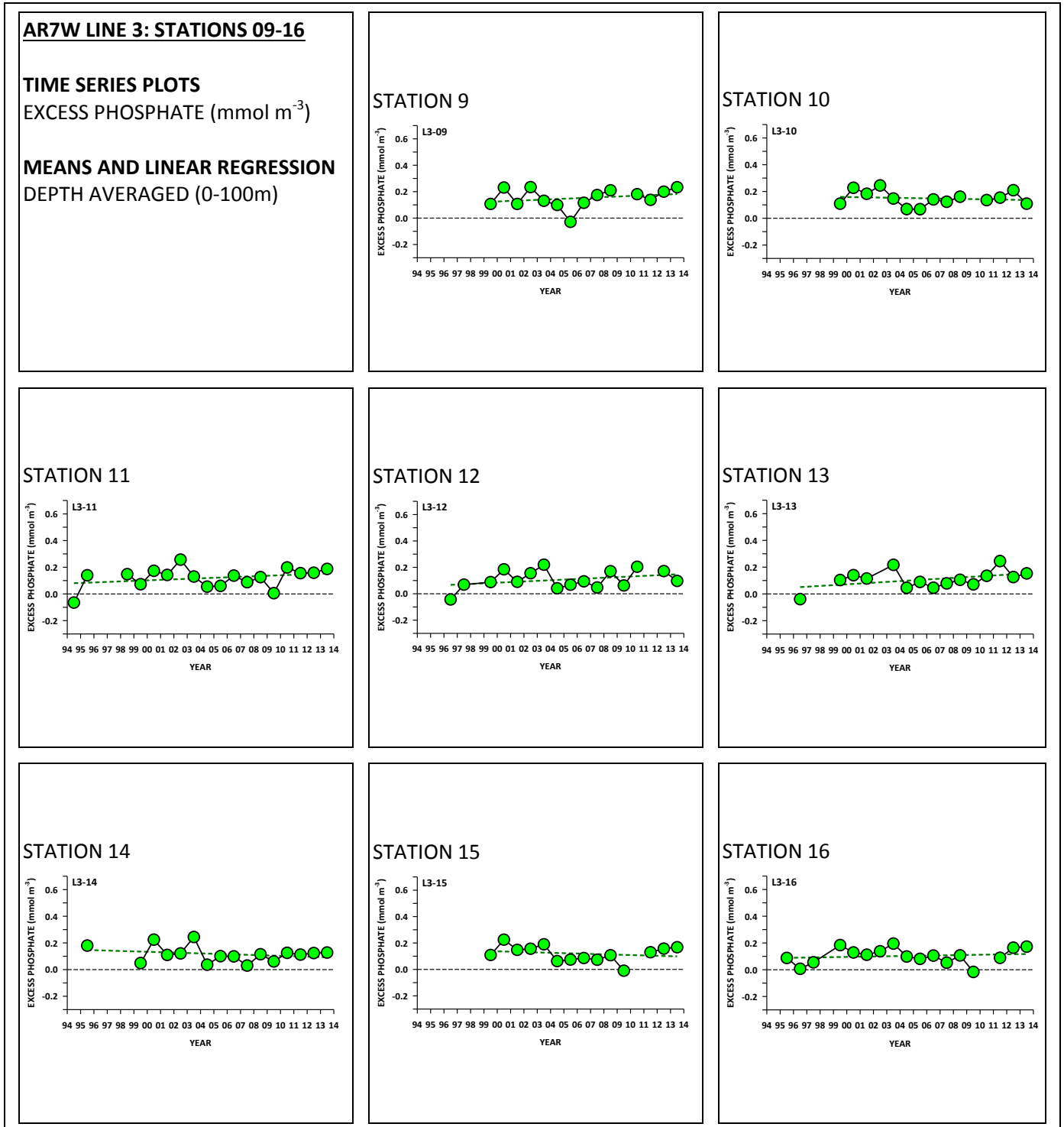


Figure 77

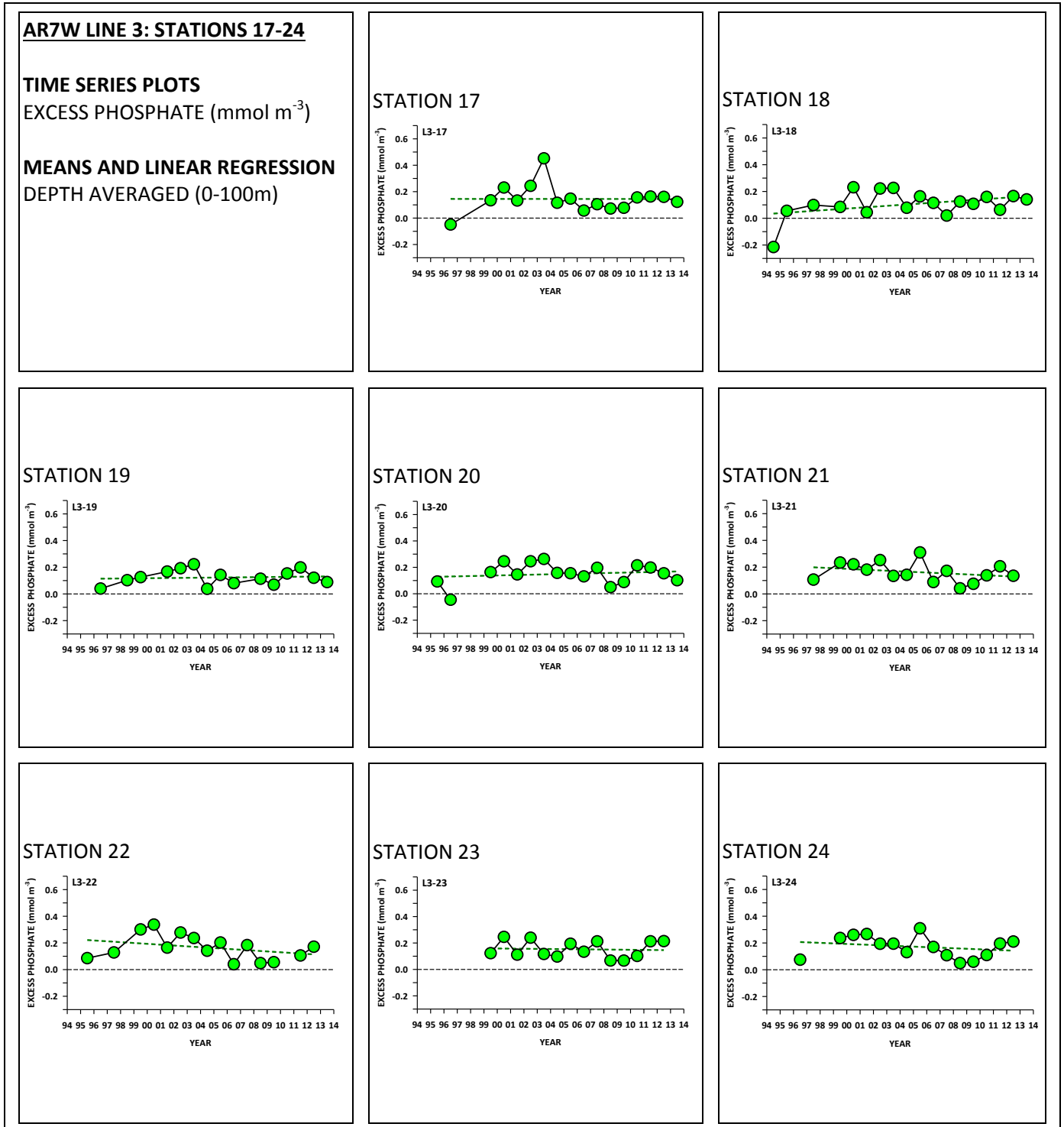


Figure 78

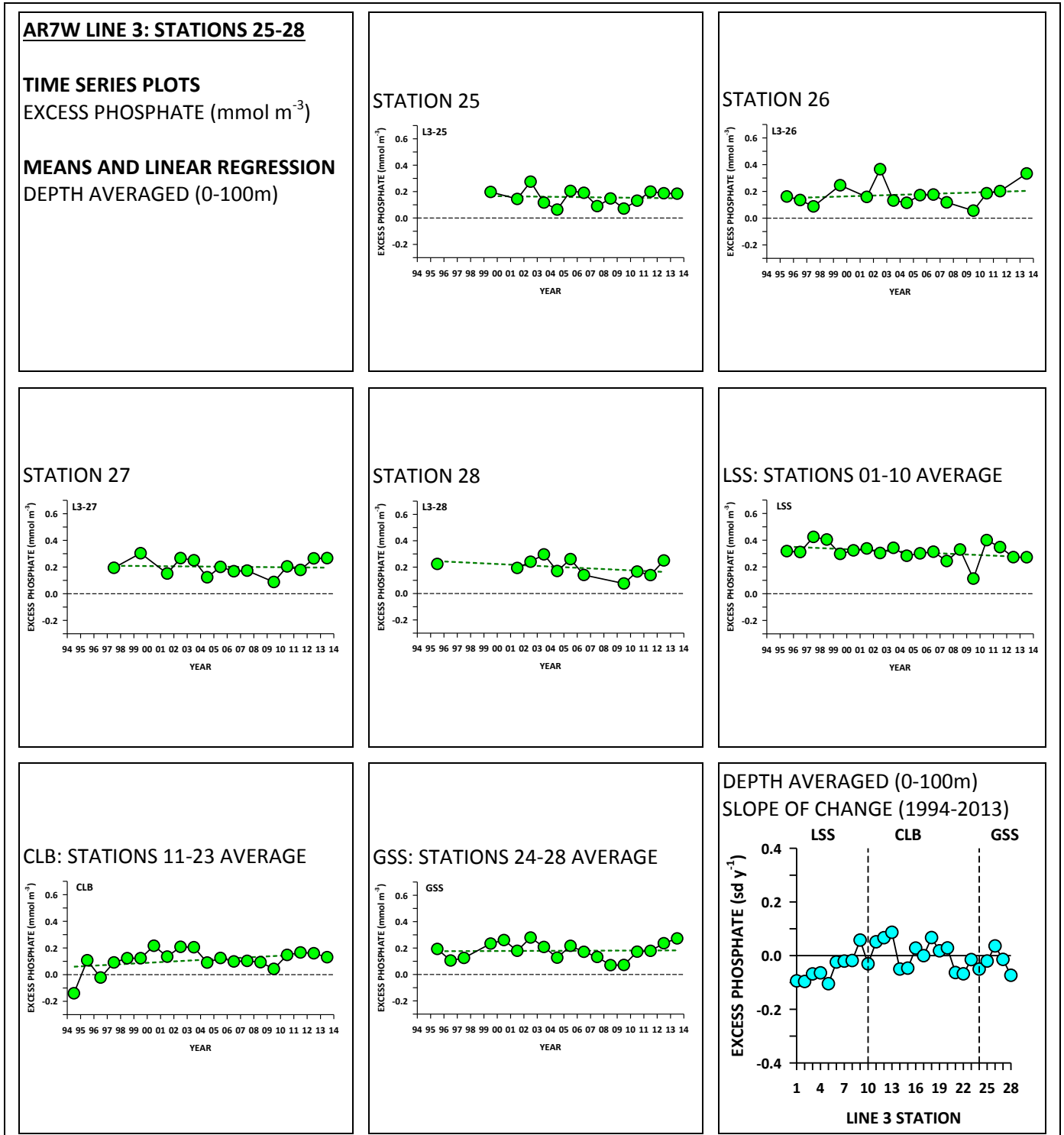




Figure 80

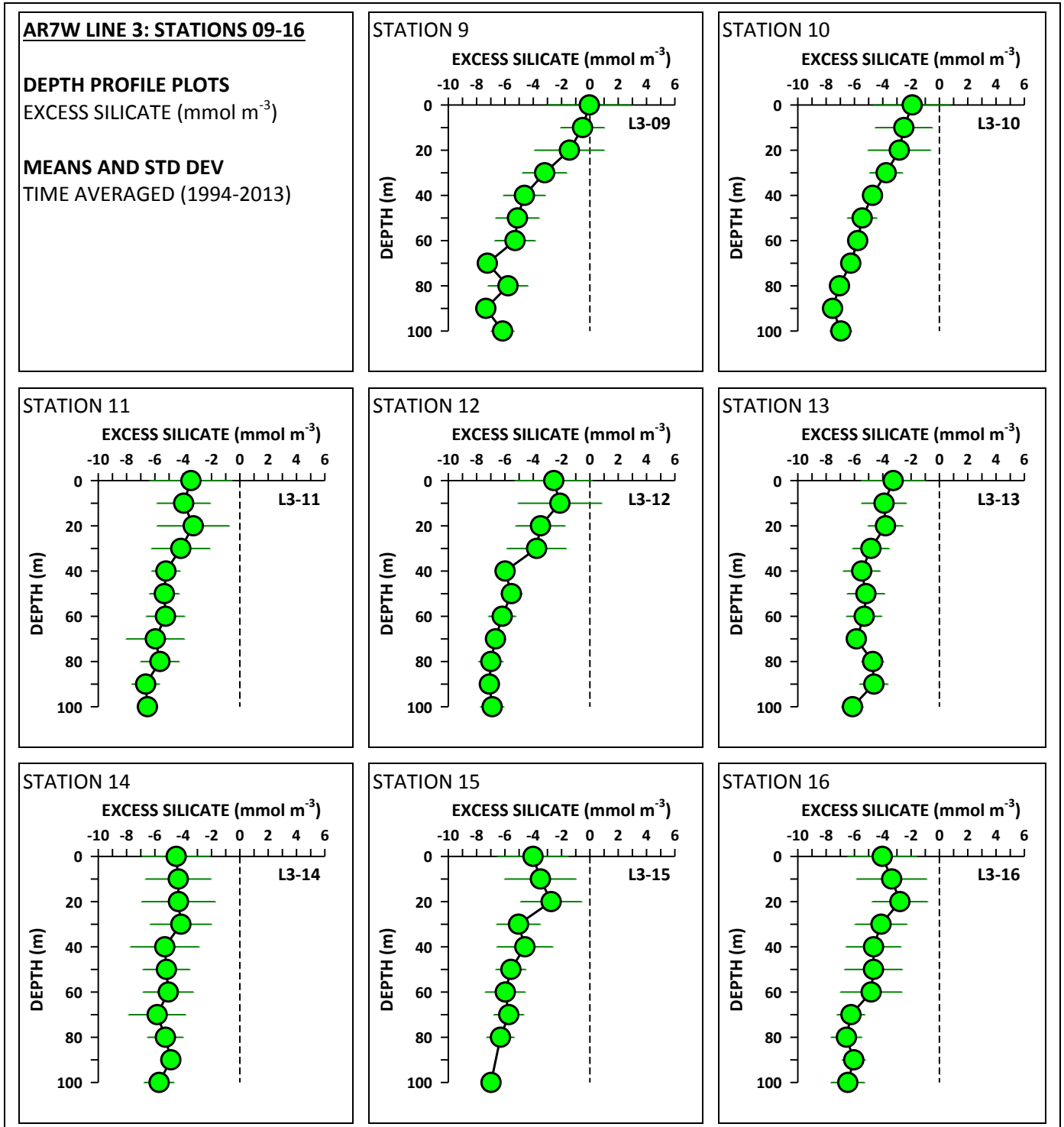


Figure 81

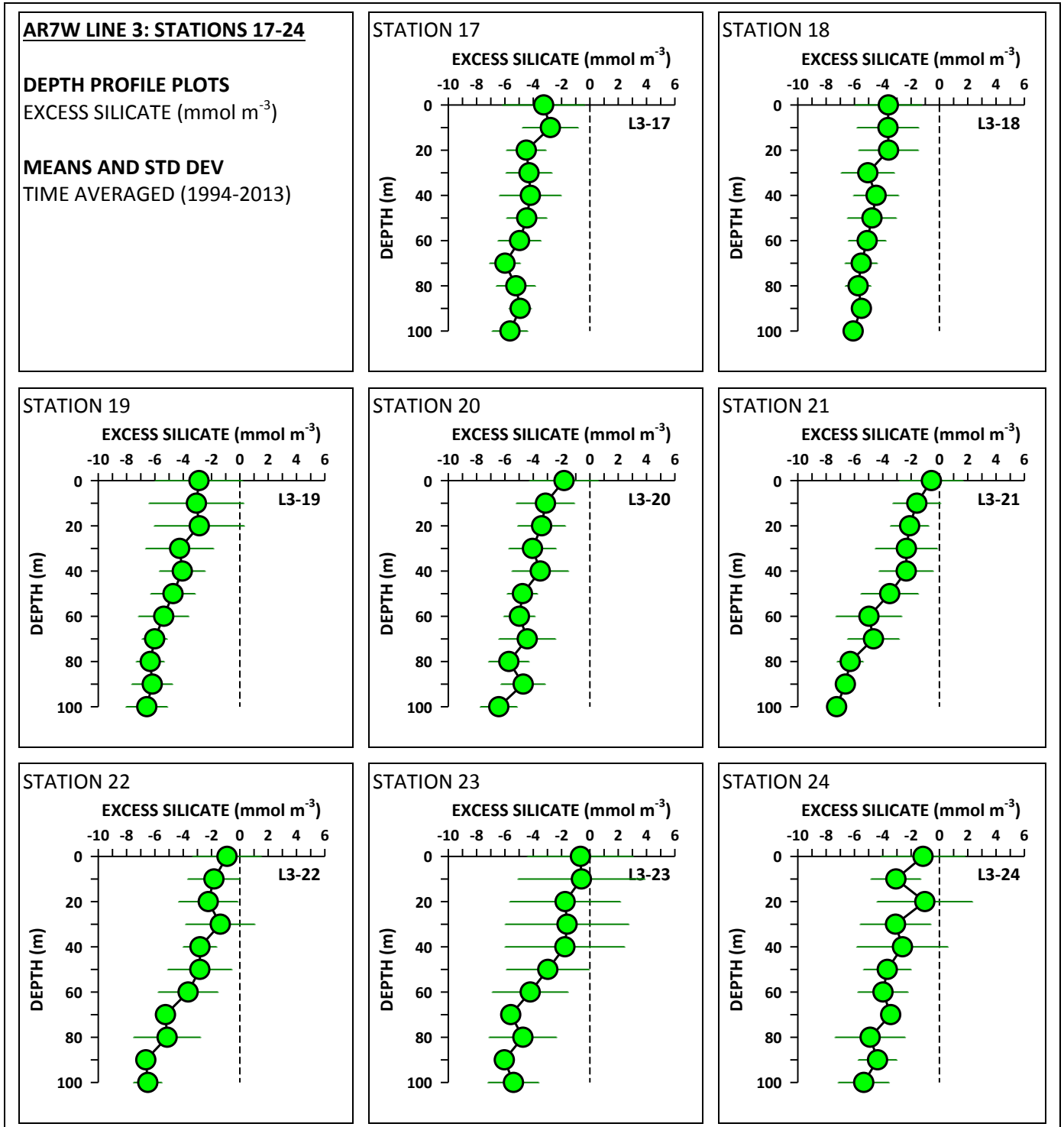


Figure 82

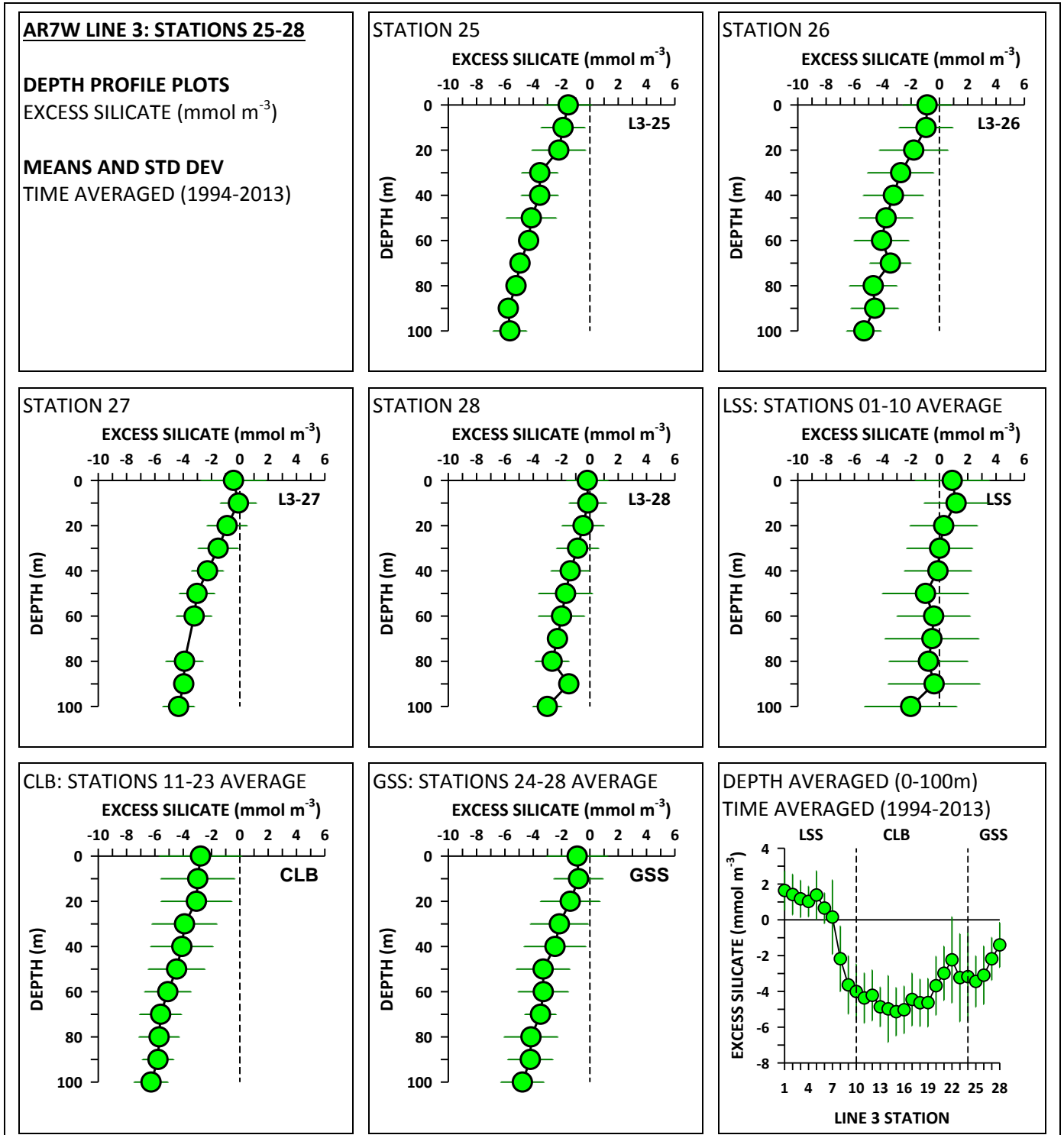


Figure 83

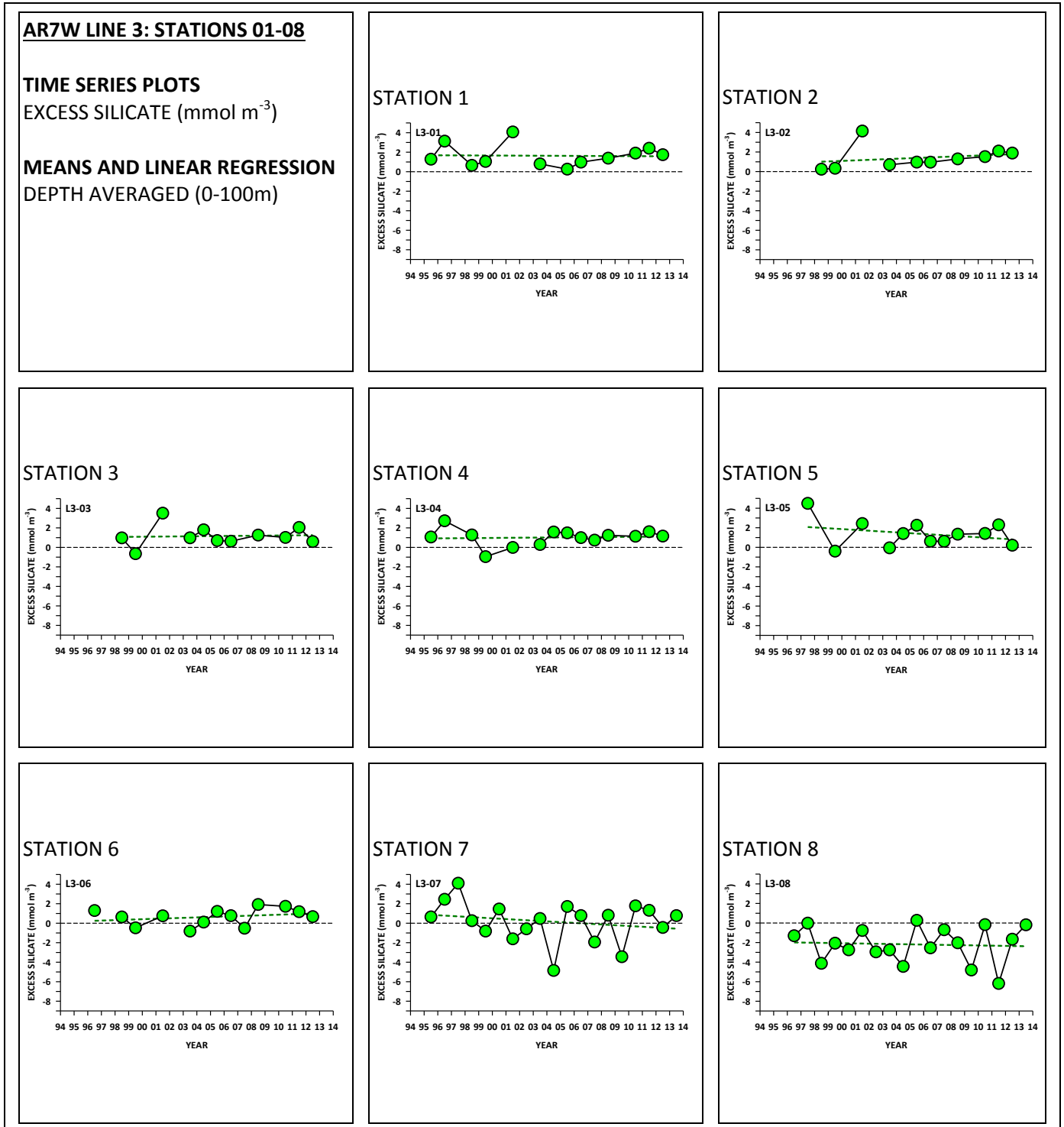




Figure 84

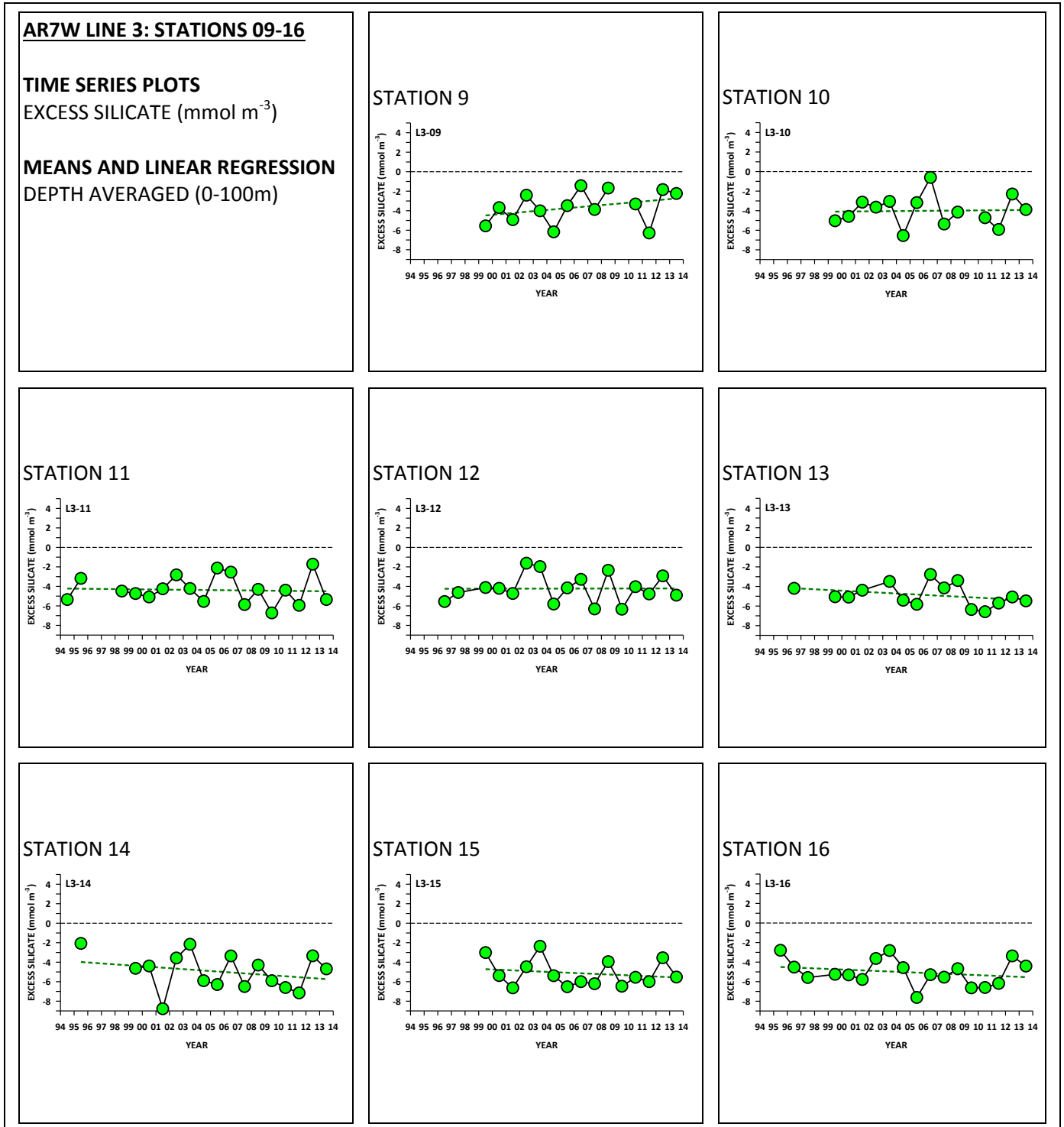


Figure 85

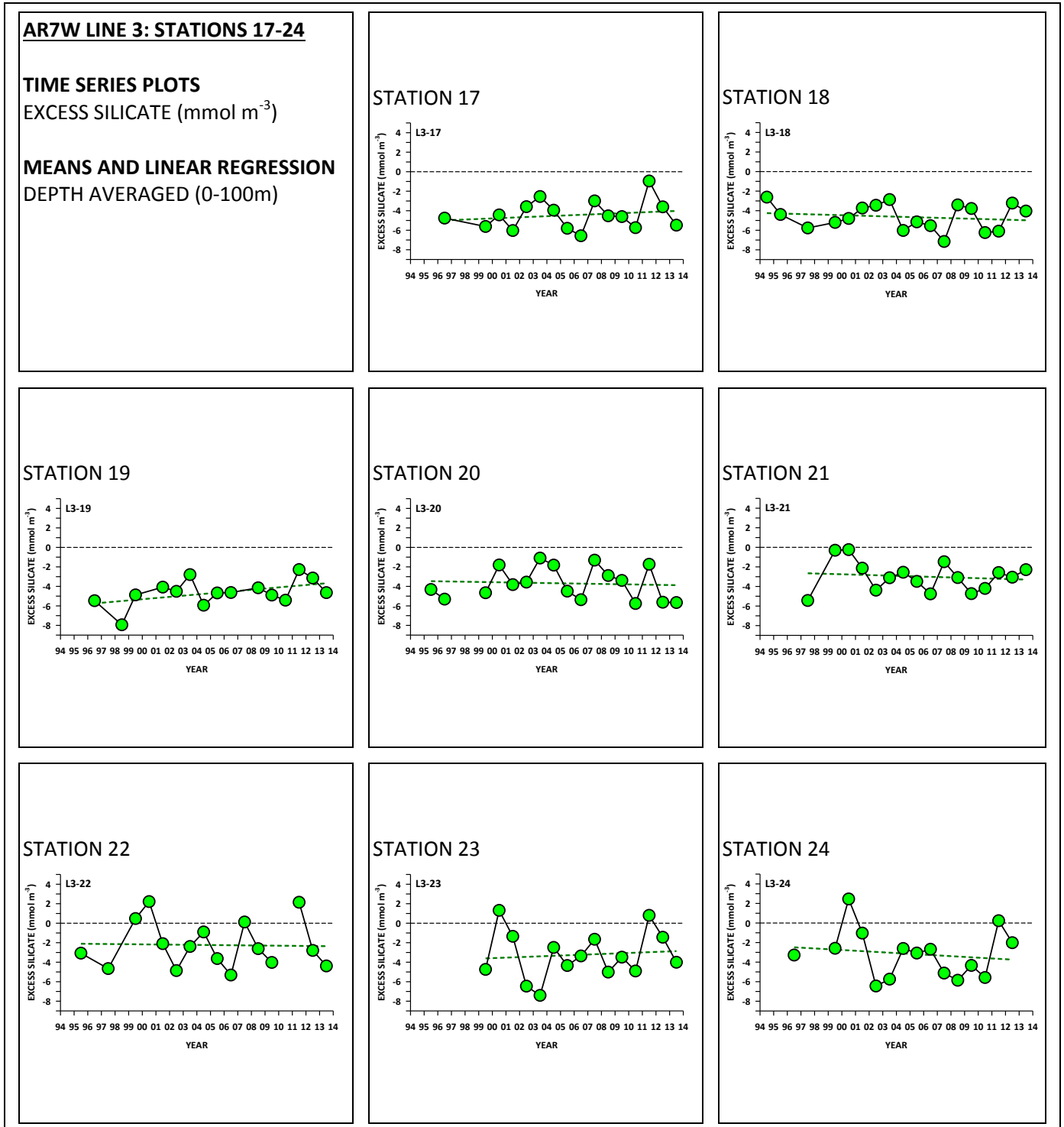


Figure 86

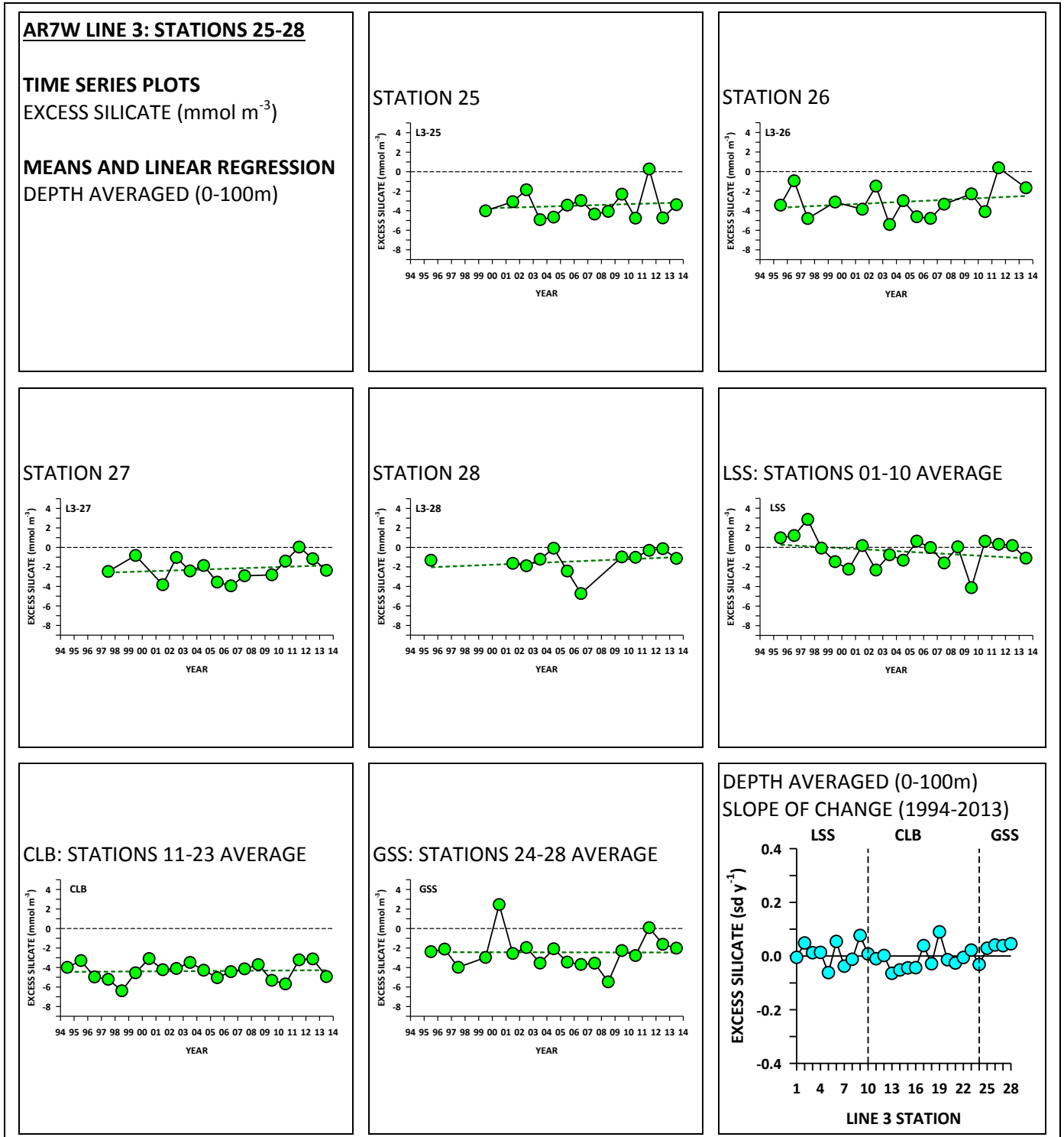


Figure 87

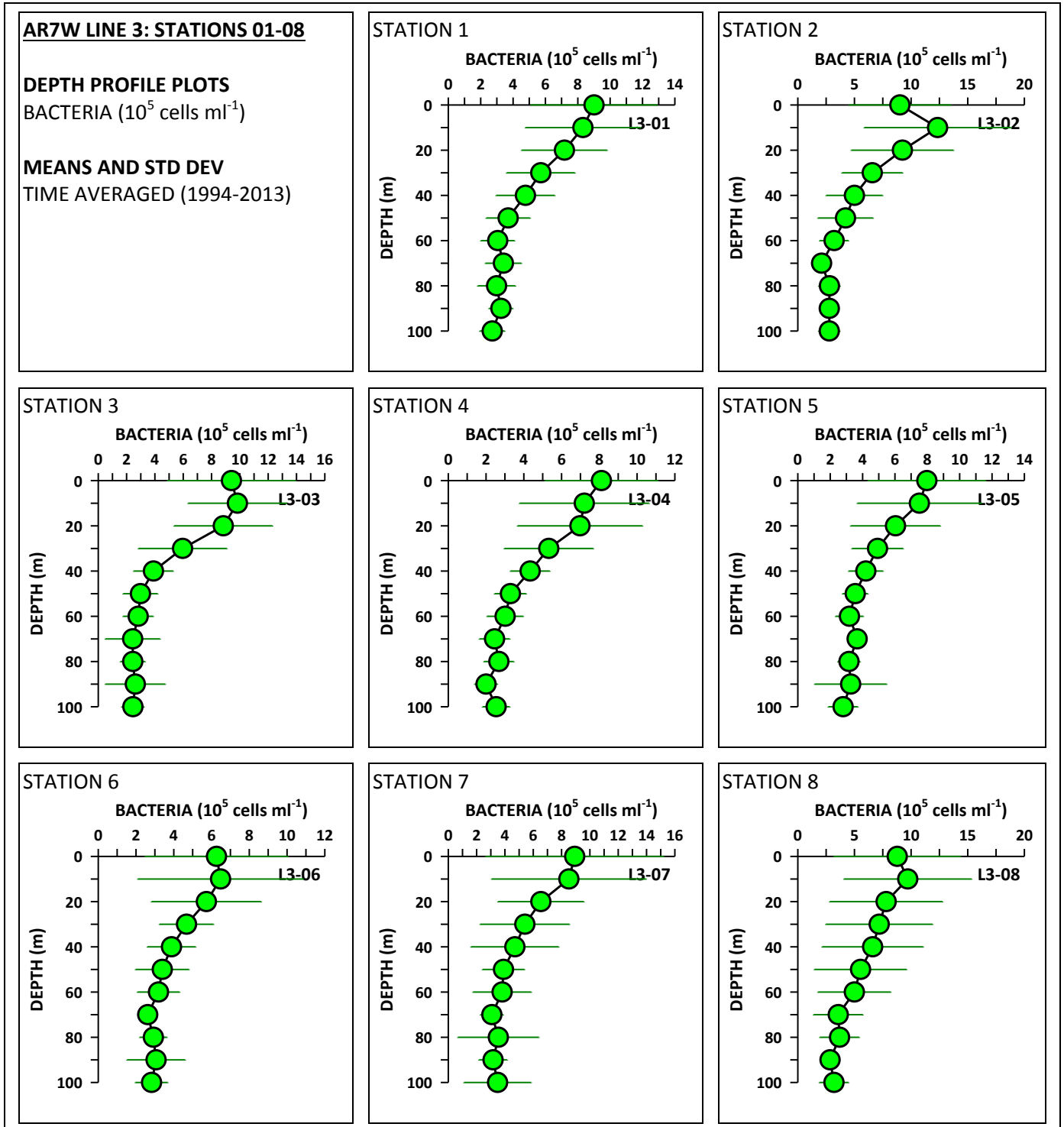


Figure 88

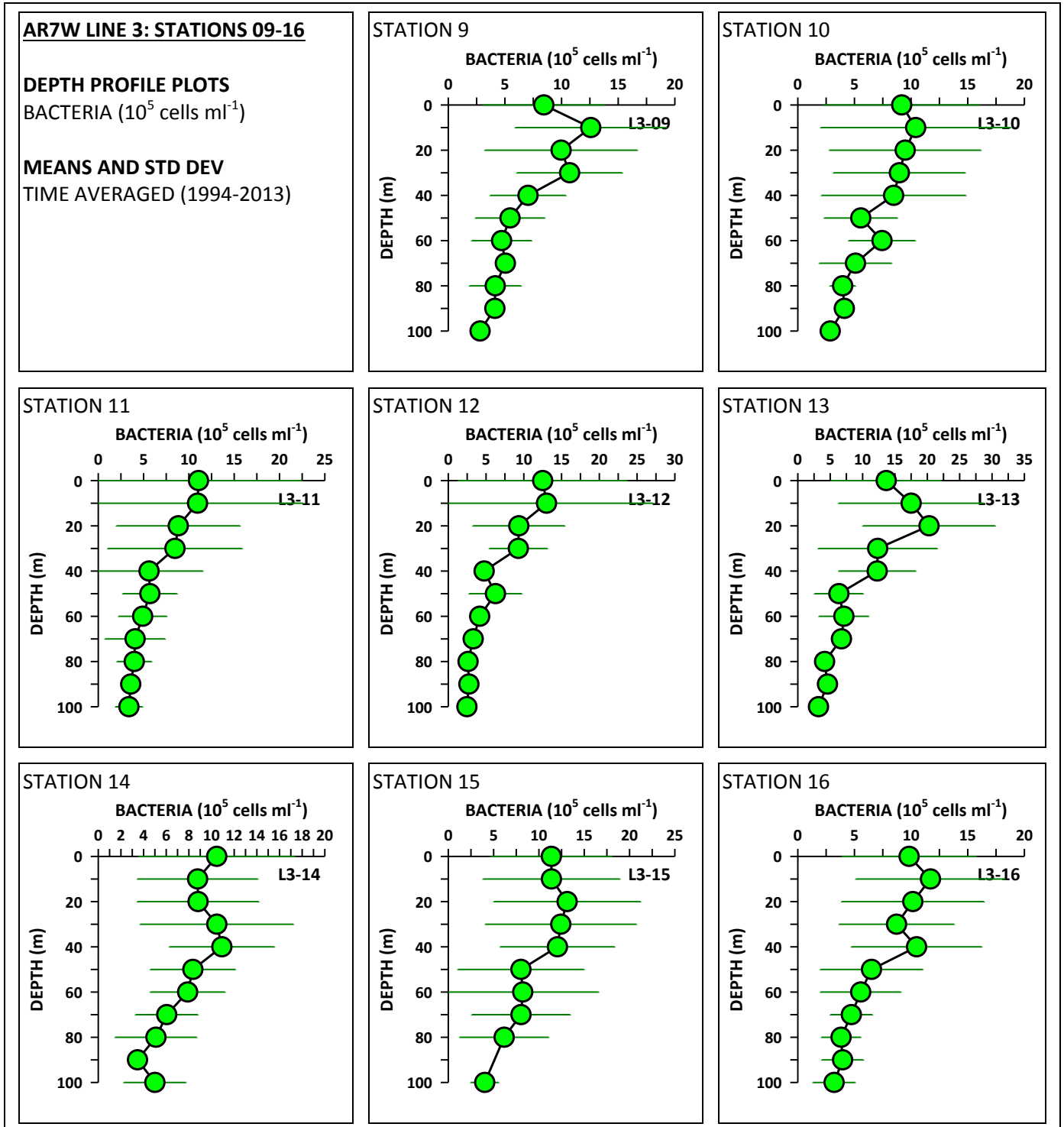


Figure 89

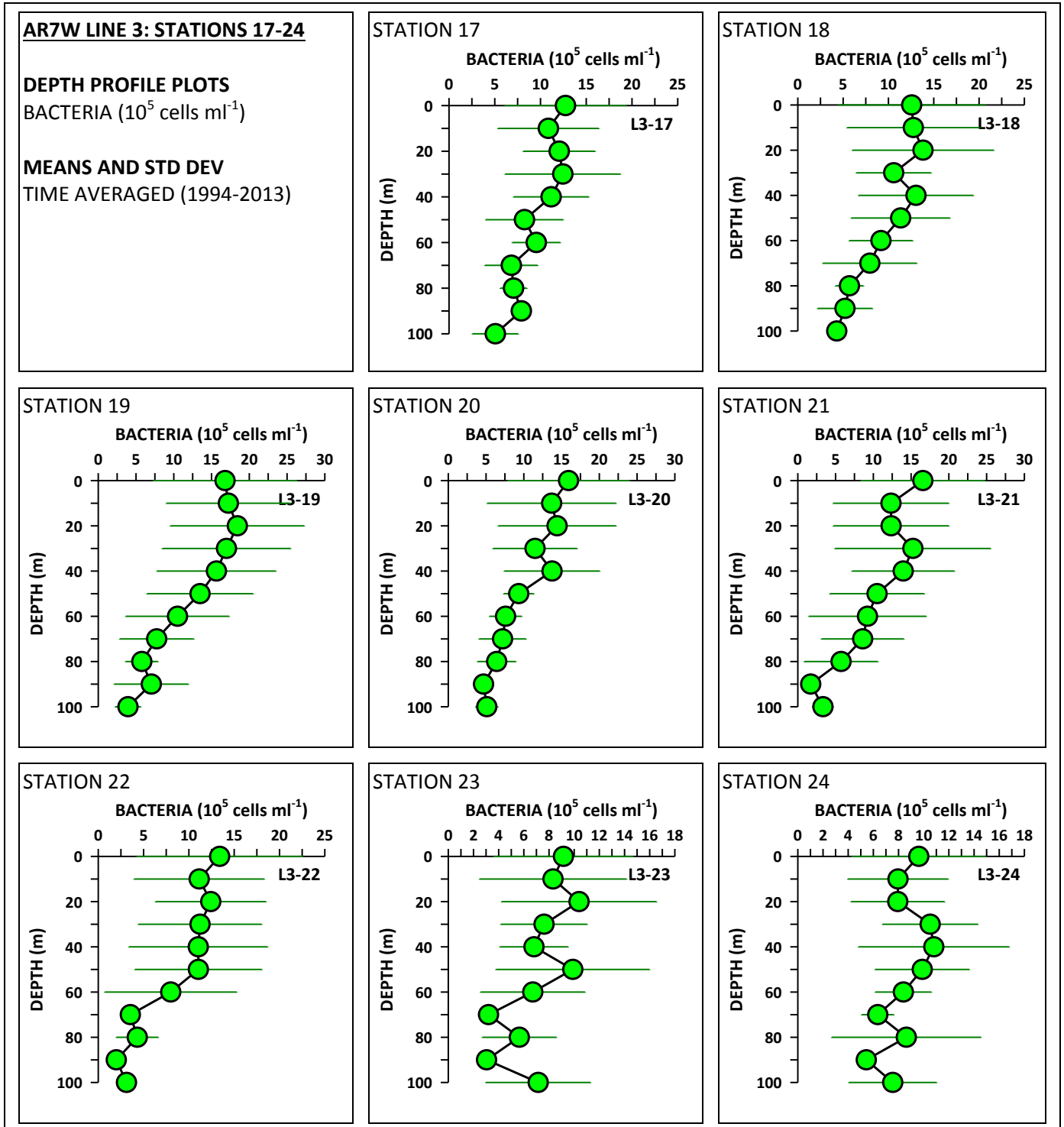


Figure 90

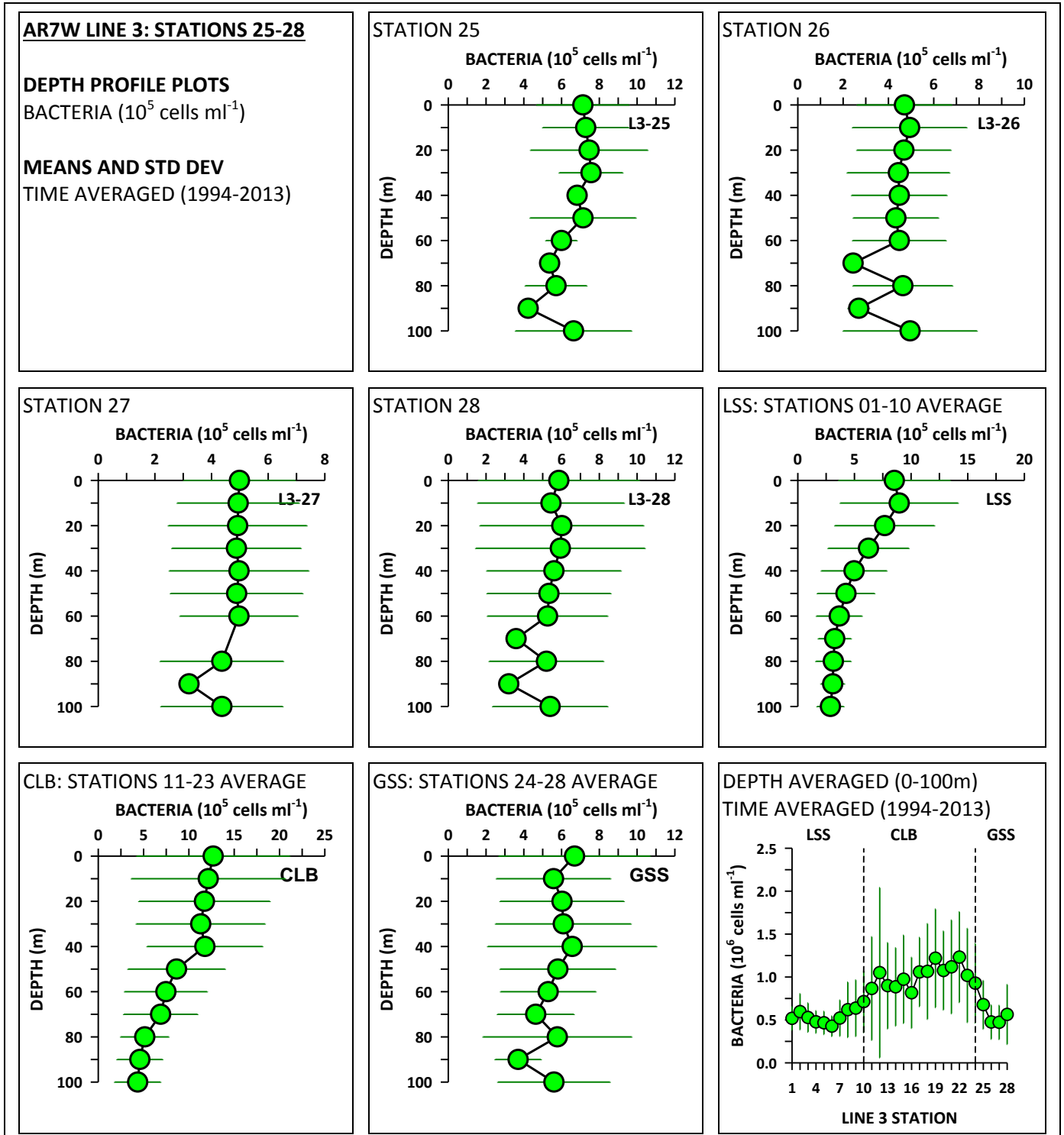


Figure 91

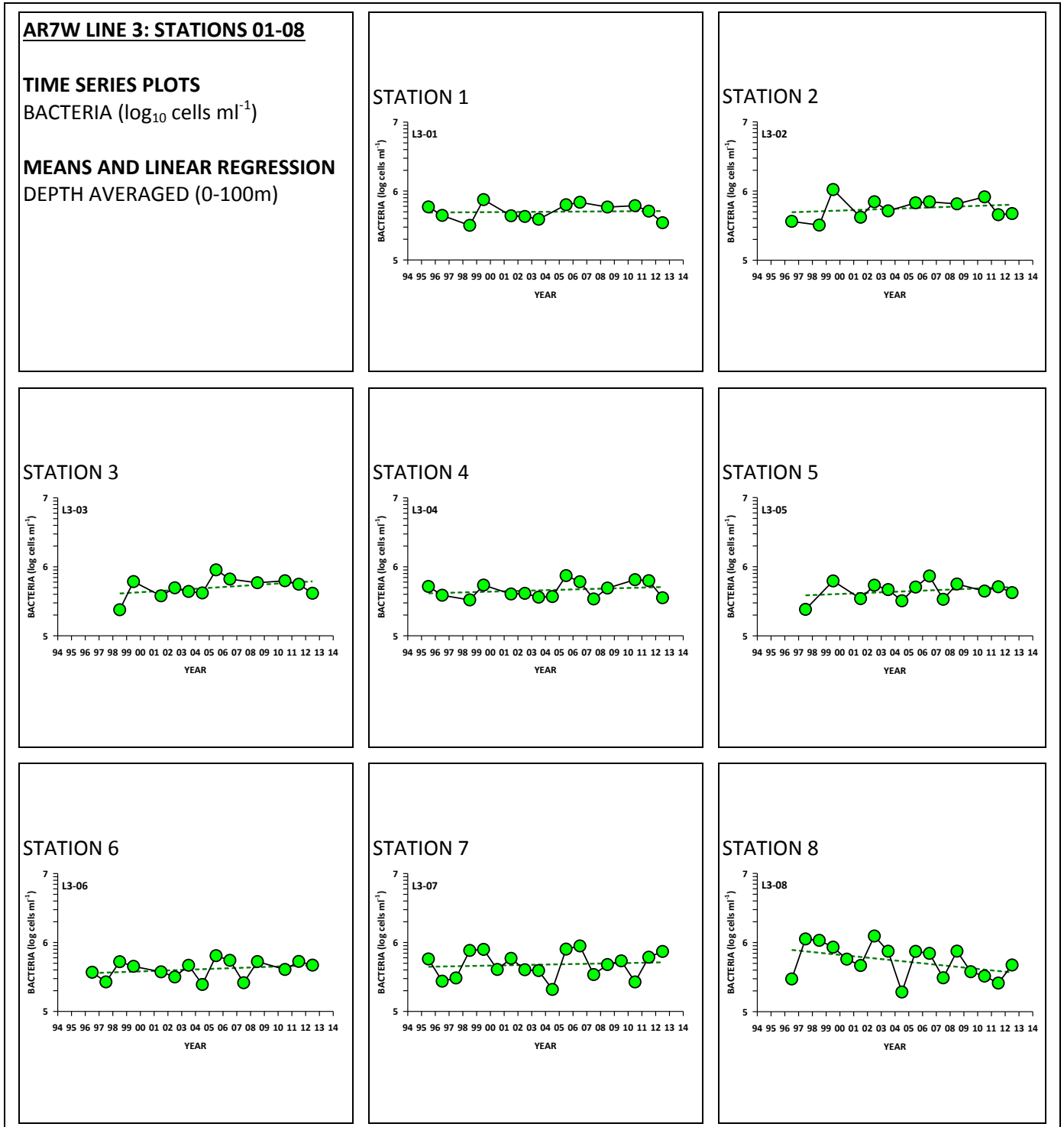




Figure 92

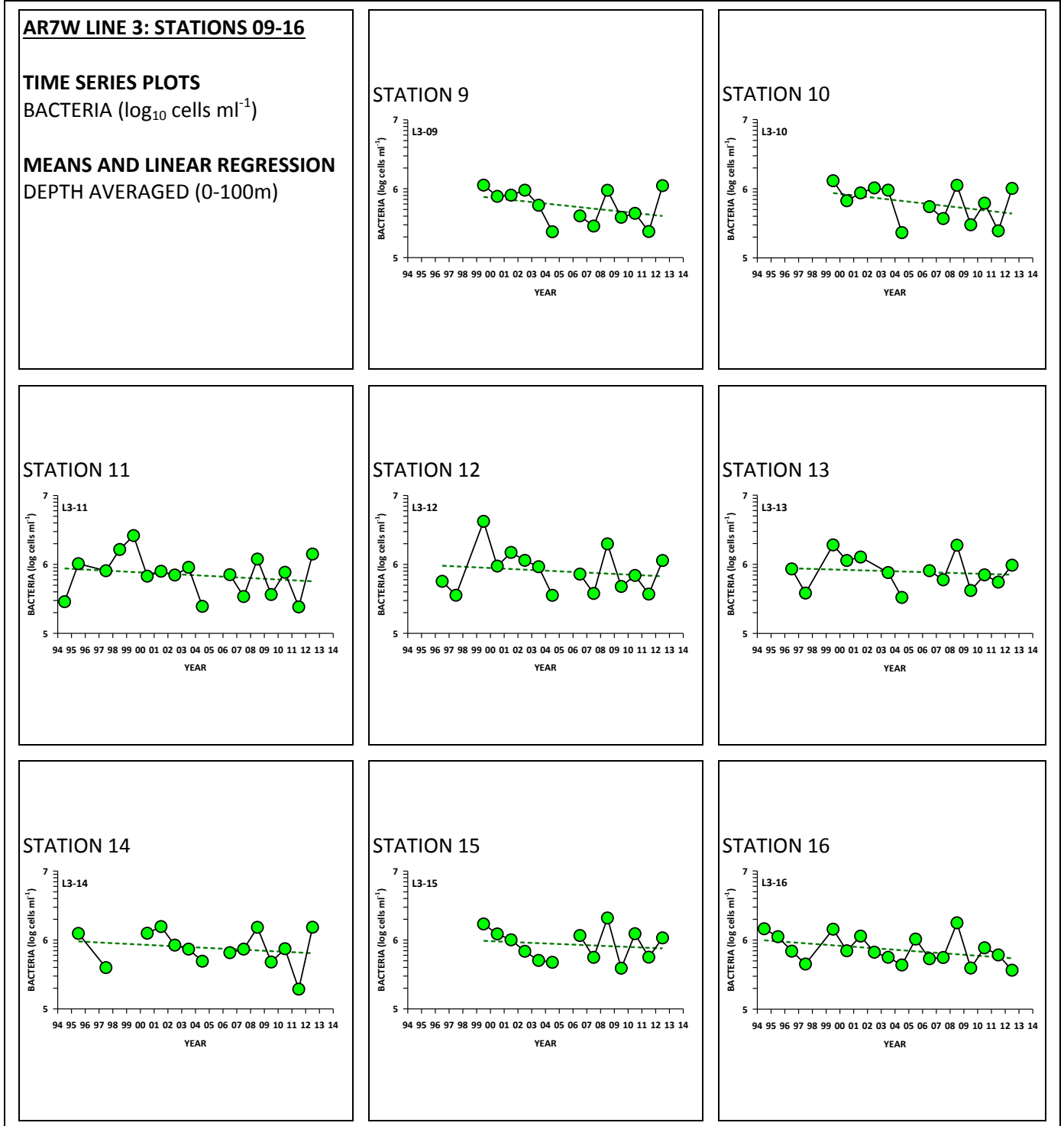


Figure 93

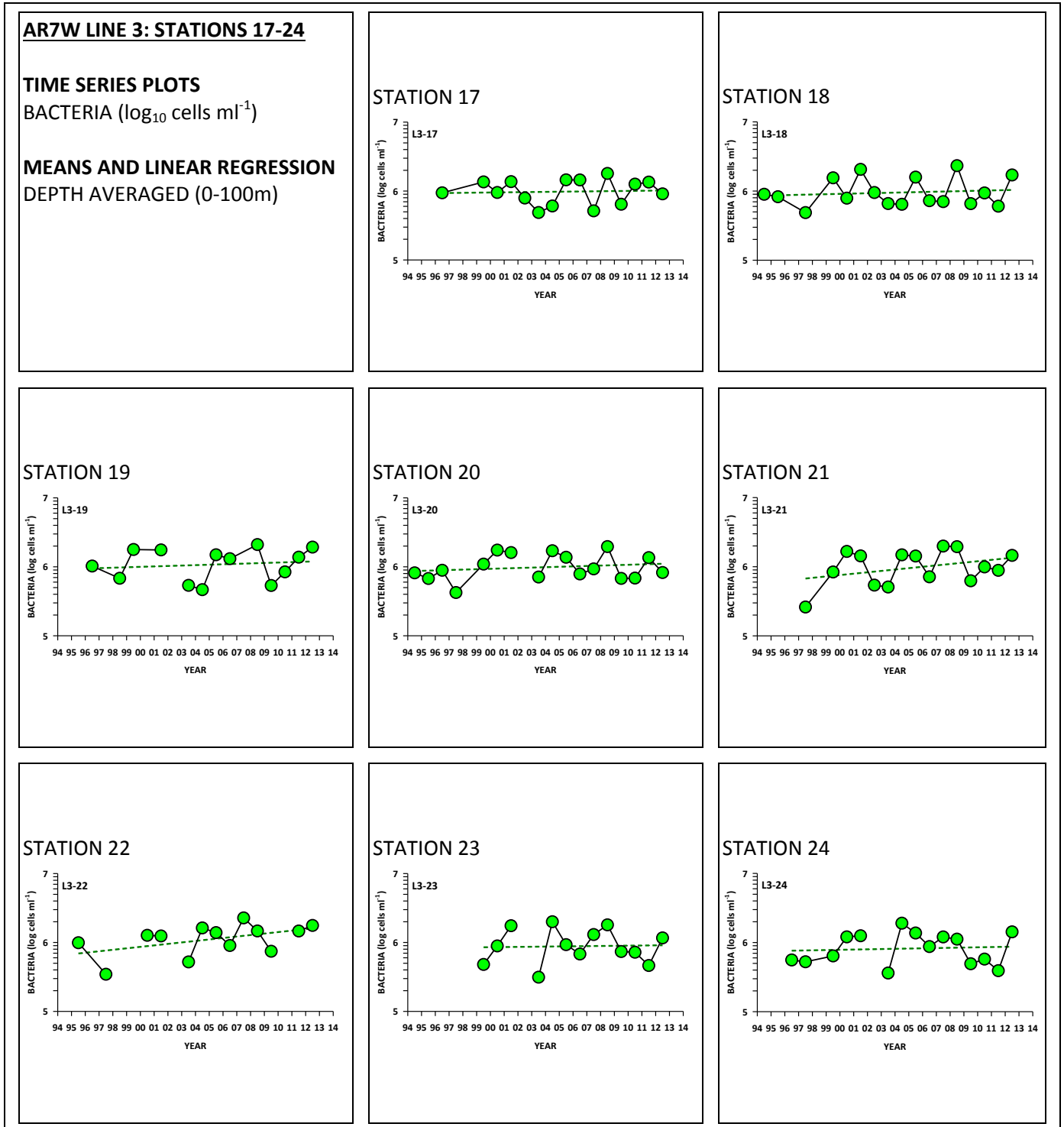


Figure 94

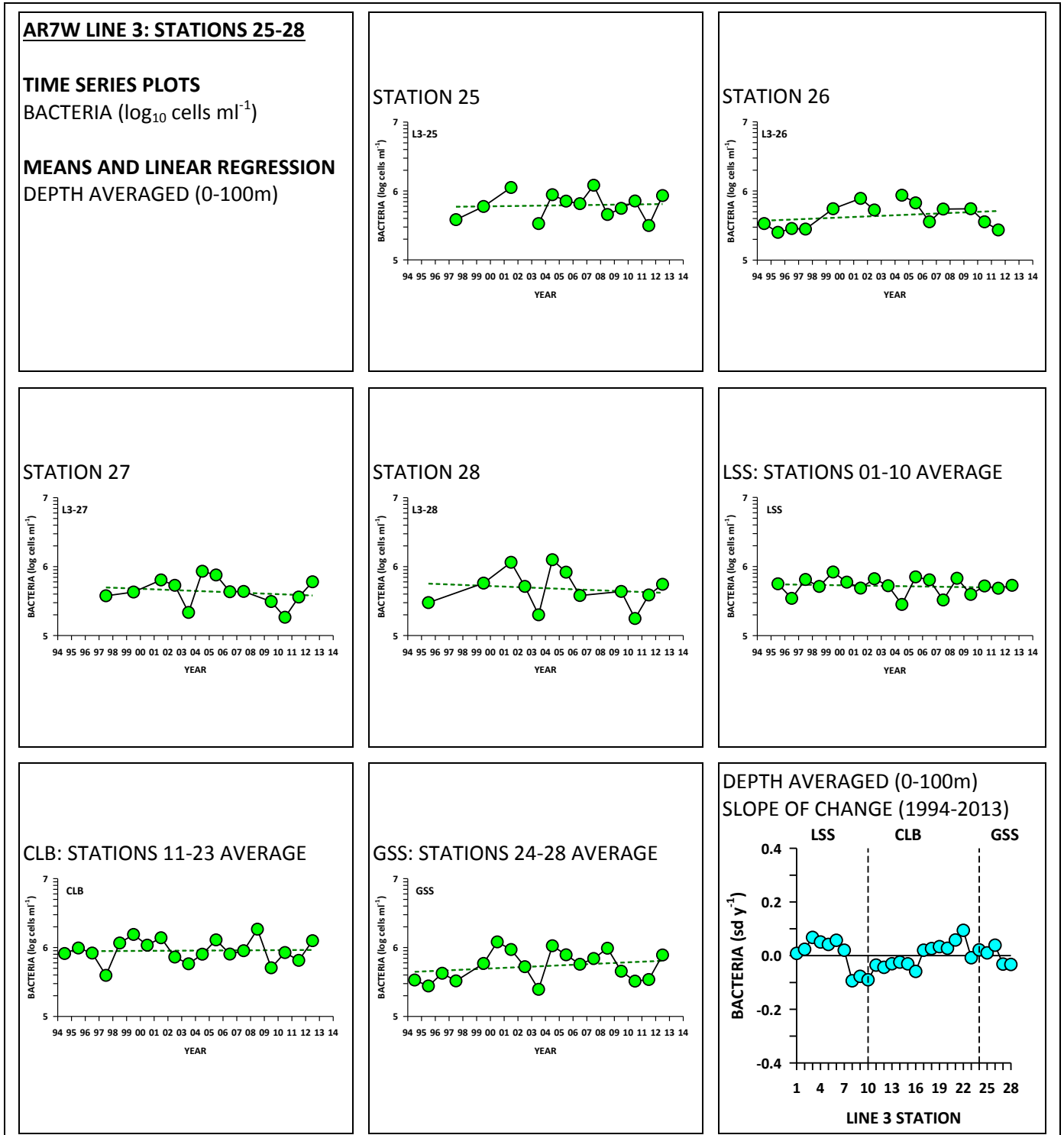


Figure 95

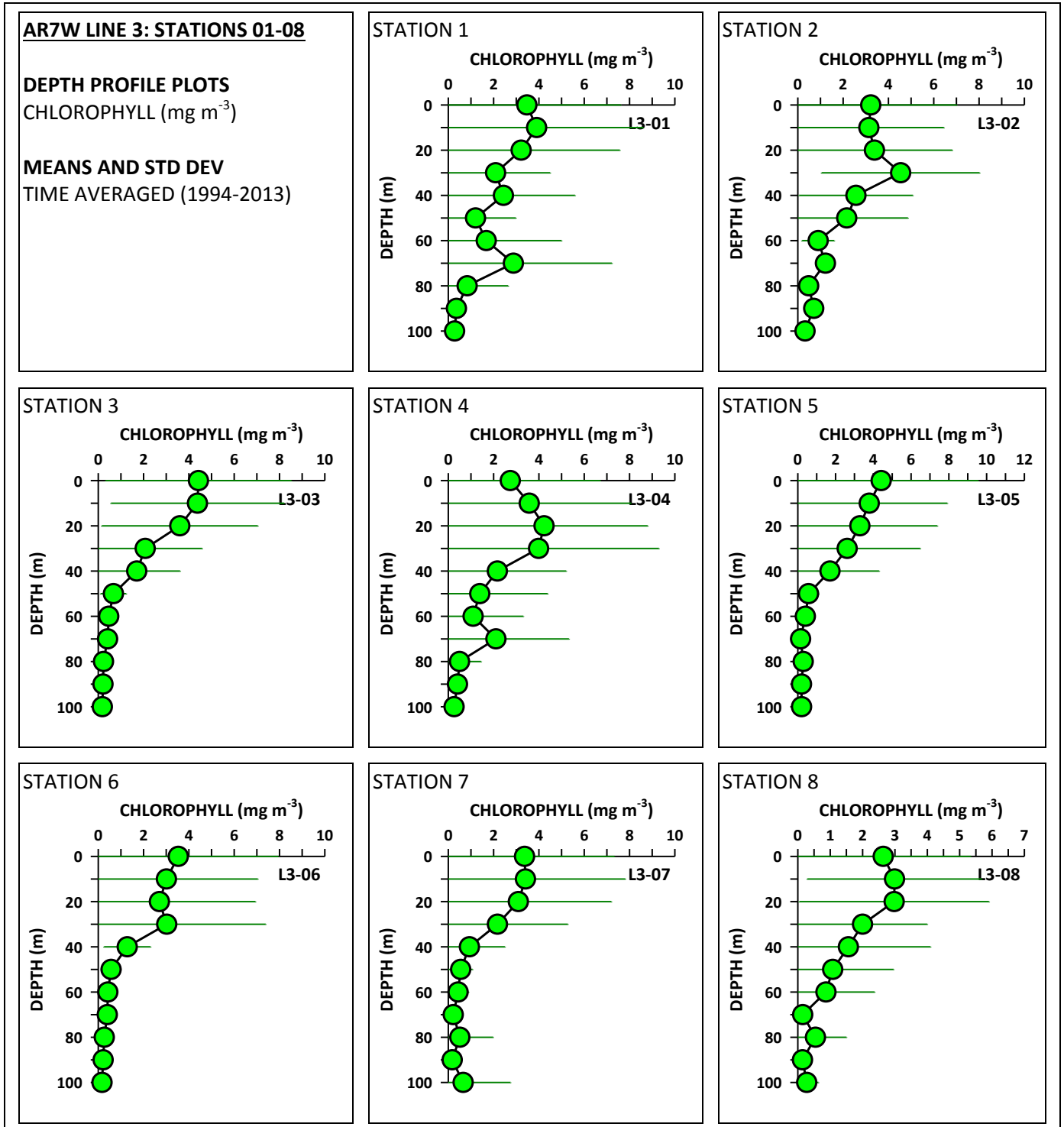


Figure 96

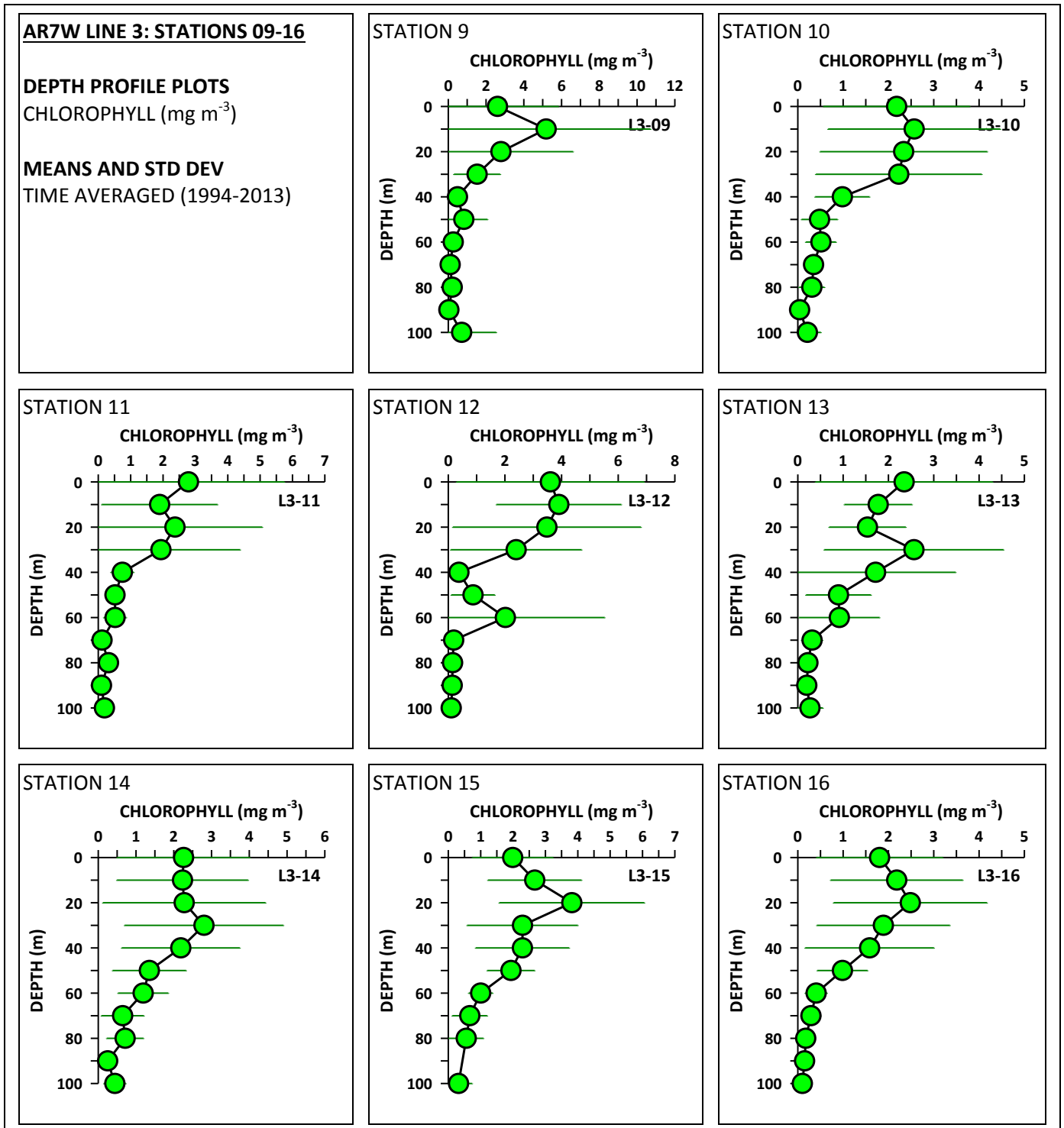


Figure 97

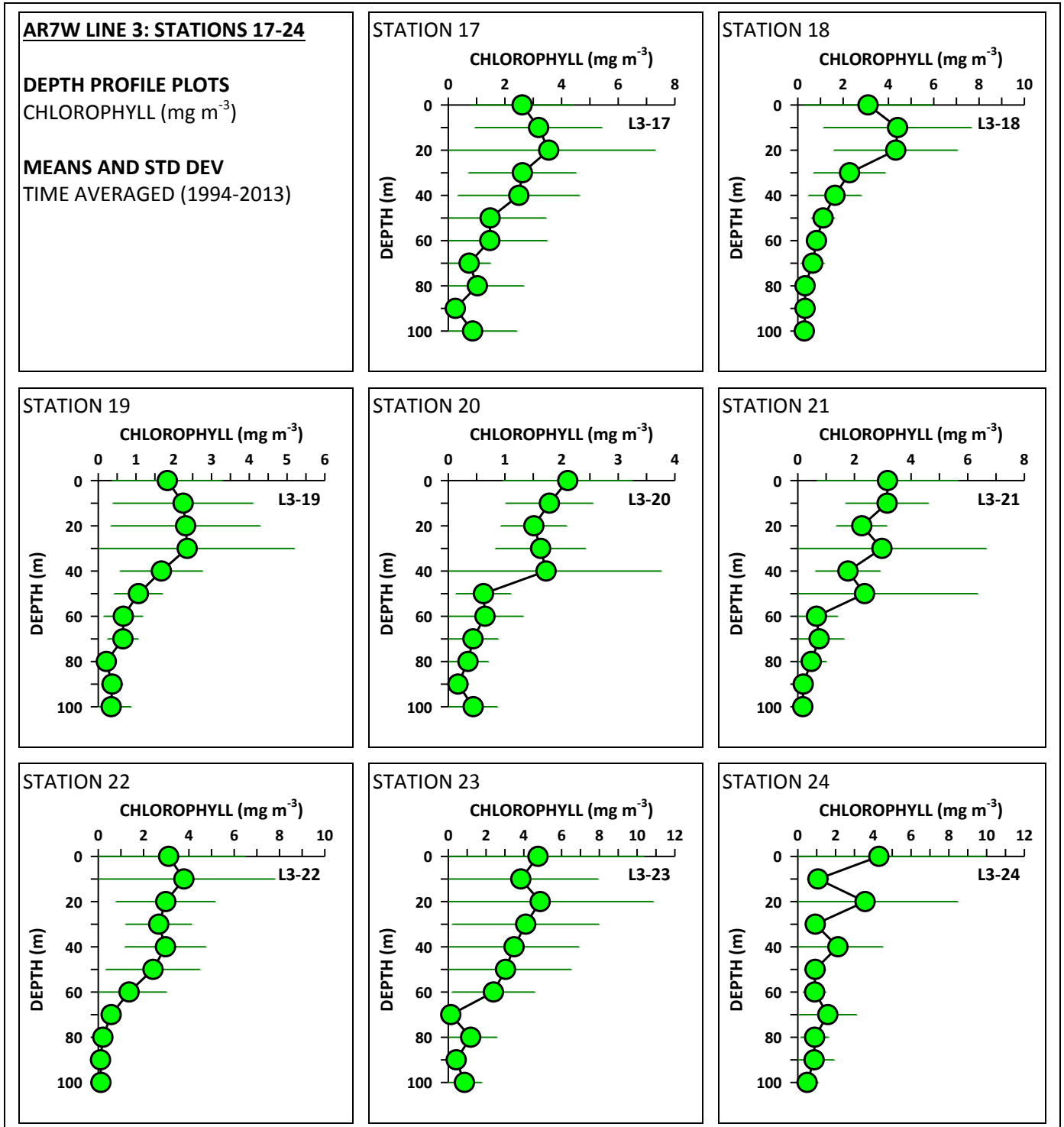


Figure 98

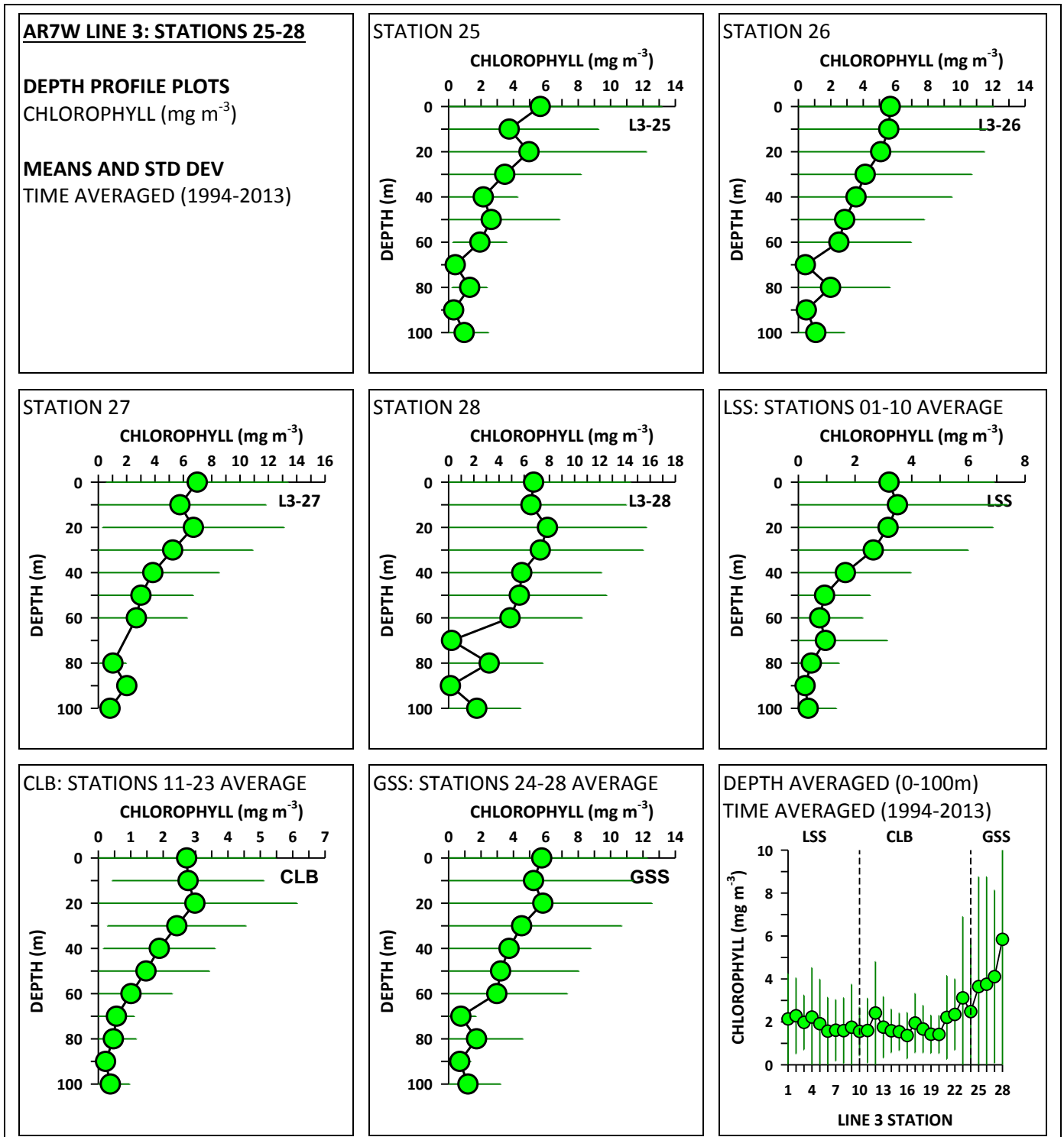


Figure 99

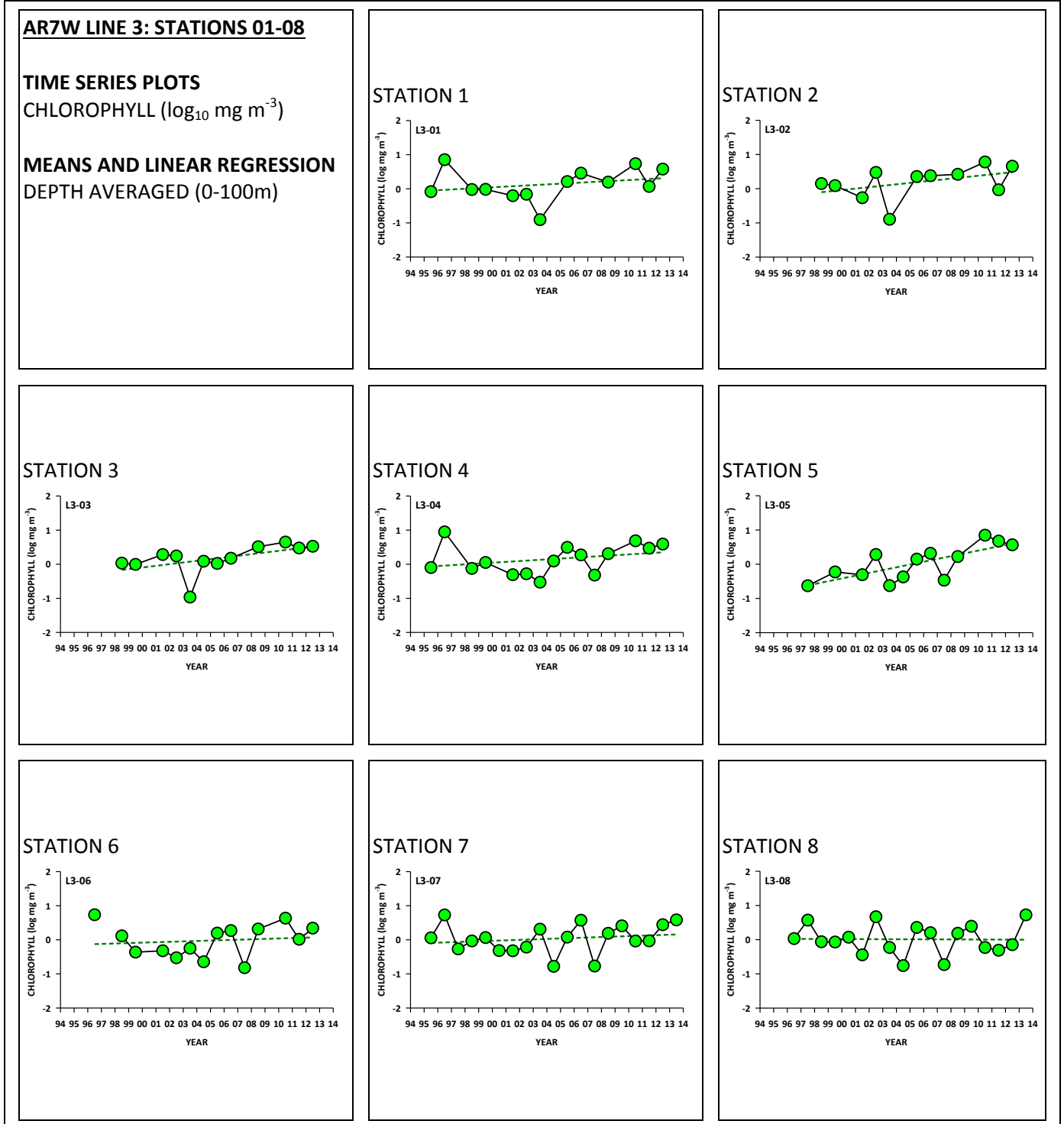




Figure 100

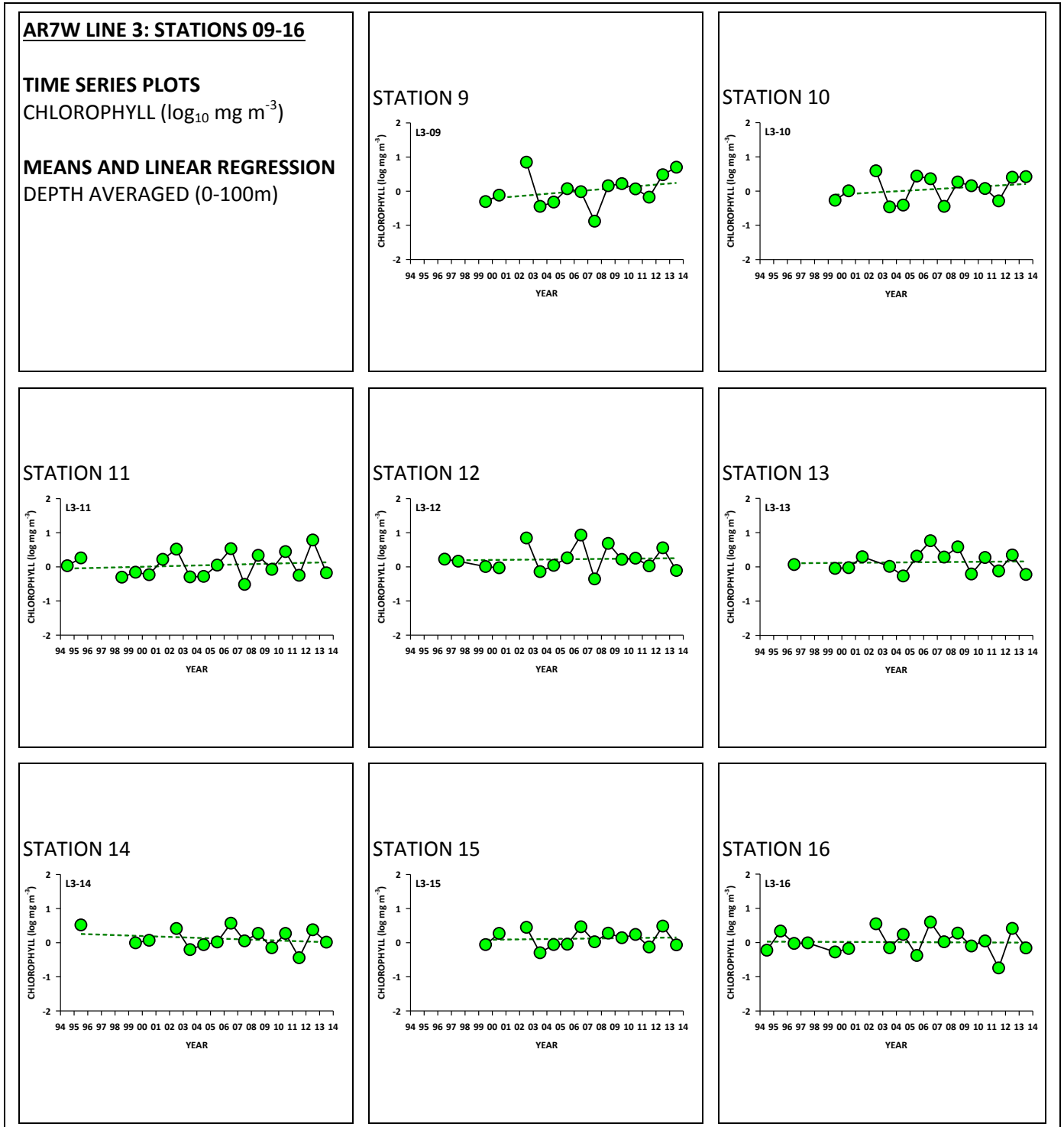


Figure 101

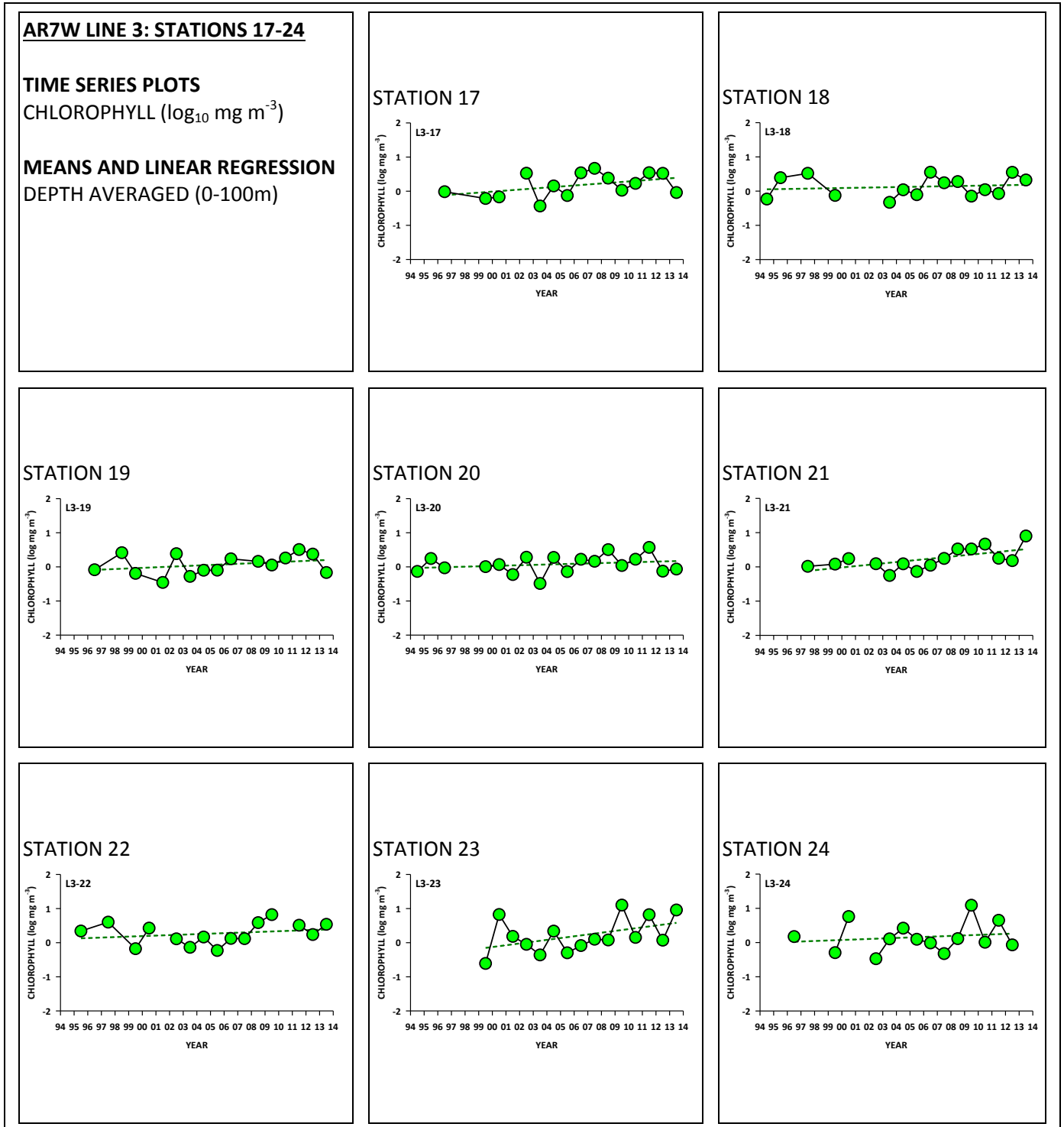


Figure 102

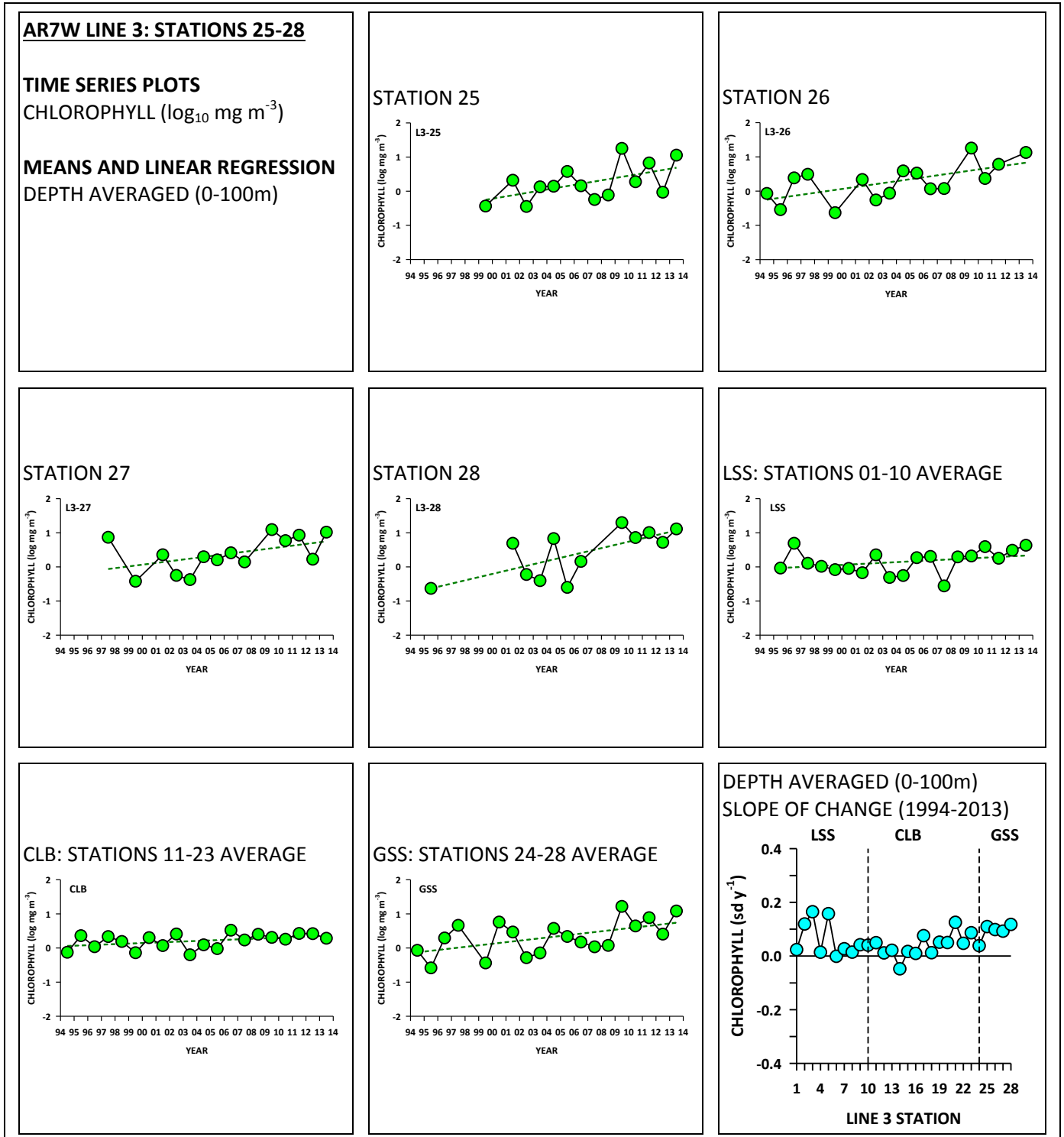


Figure 103

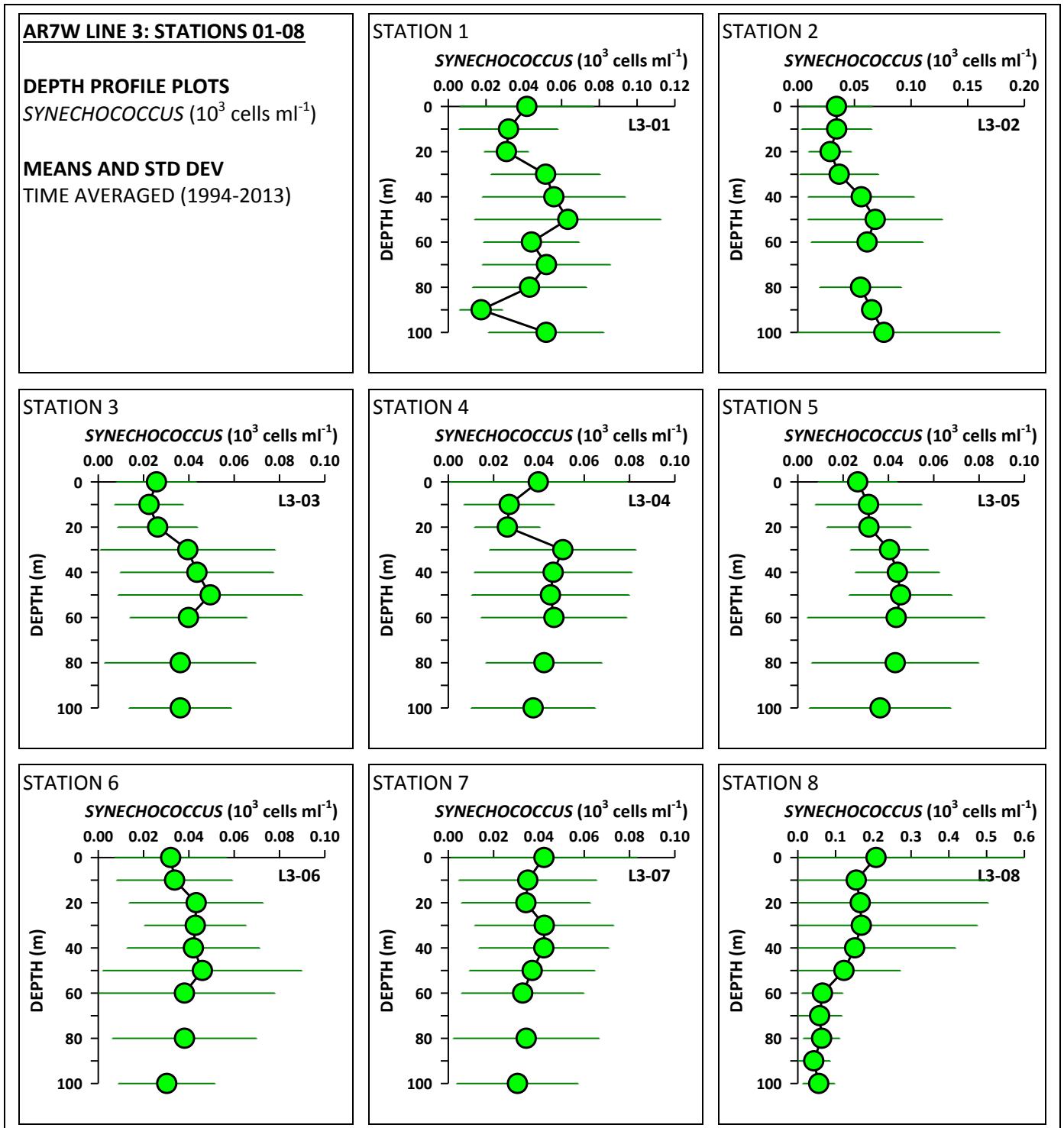


Figure 104

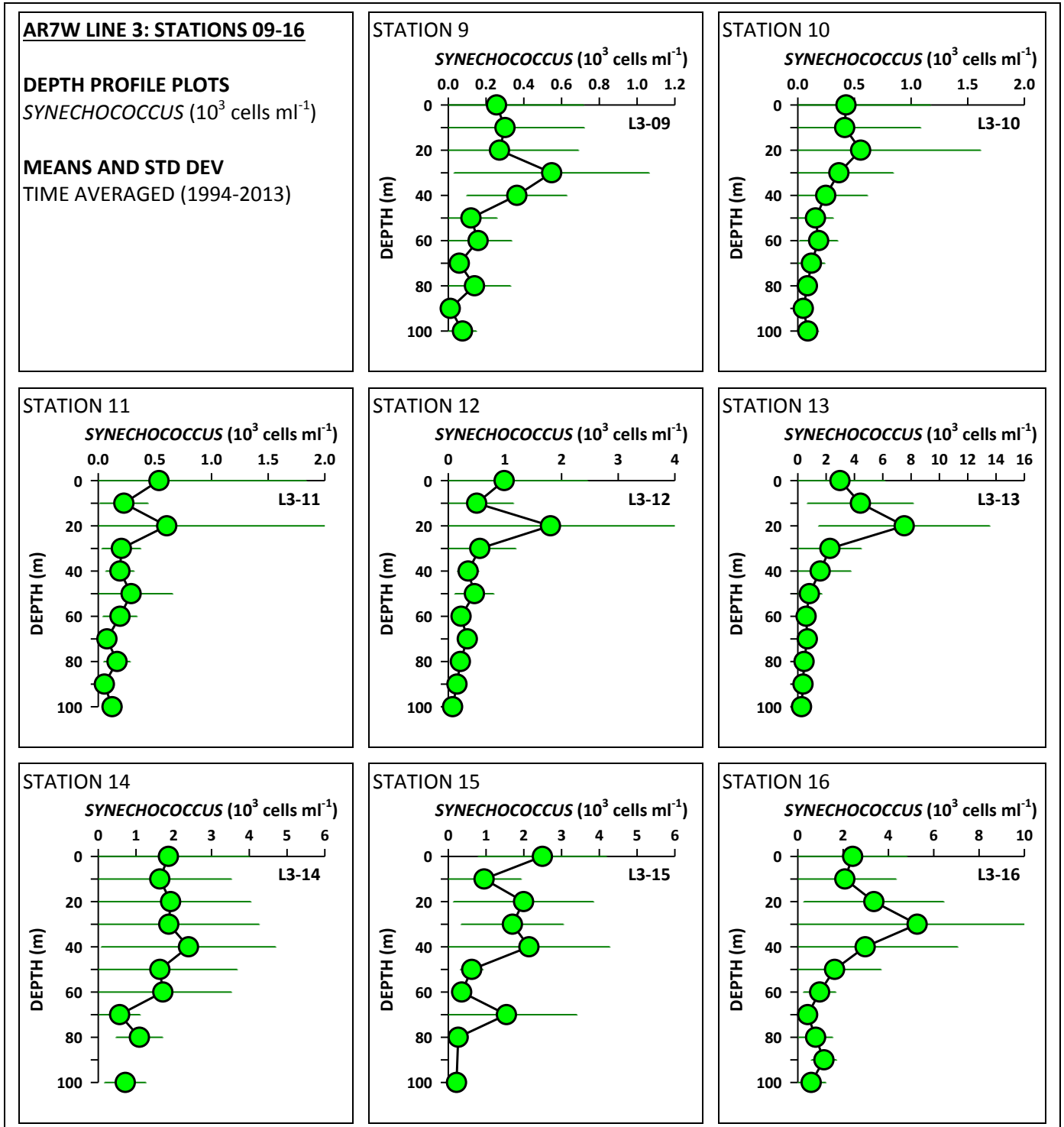


Figure 105

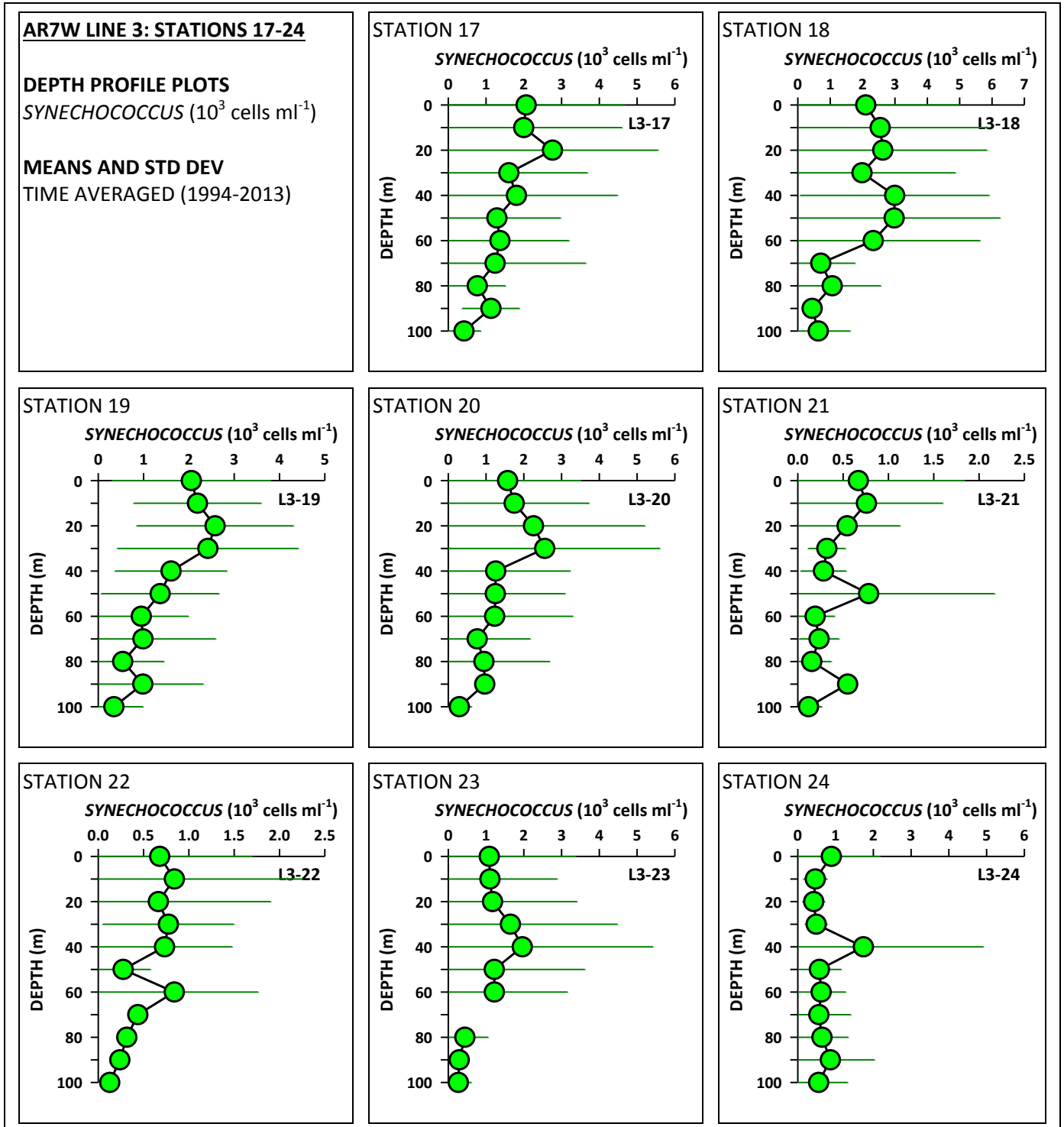


Figure 106

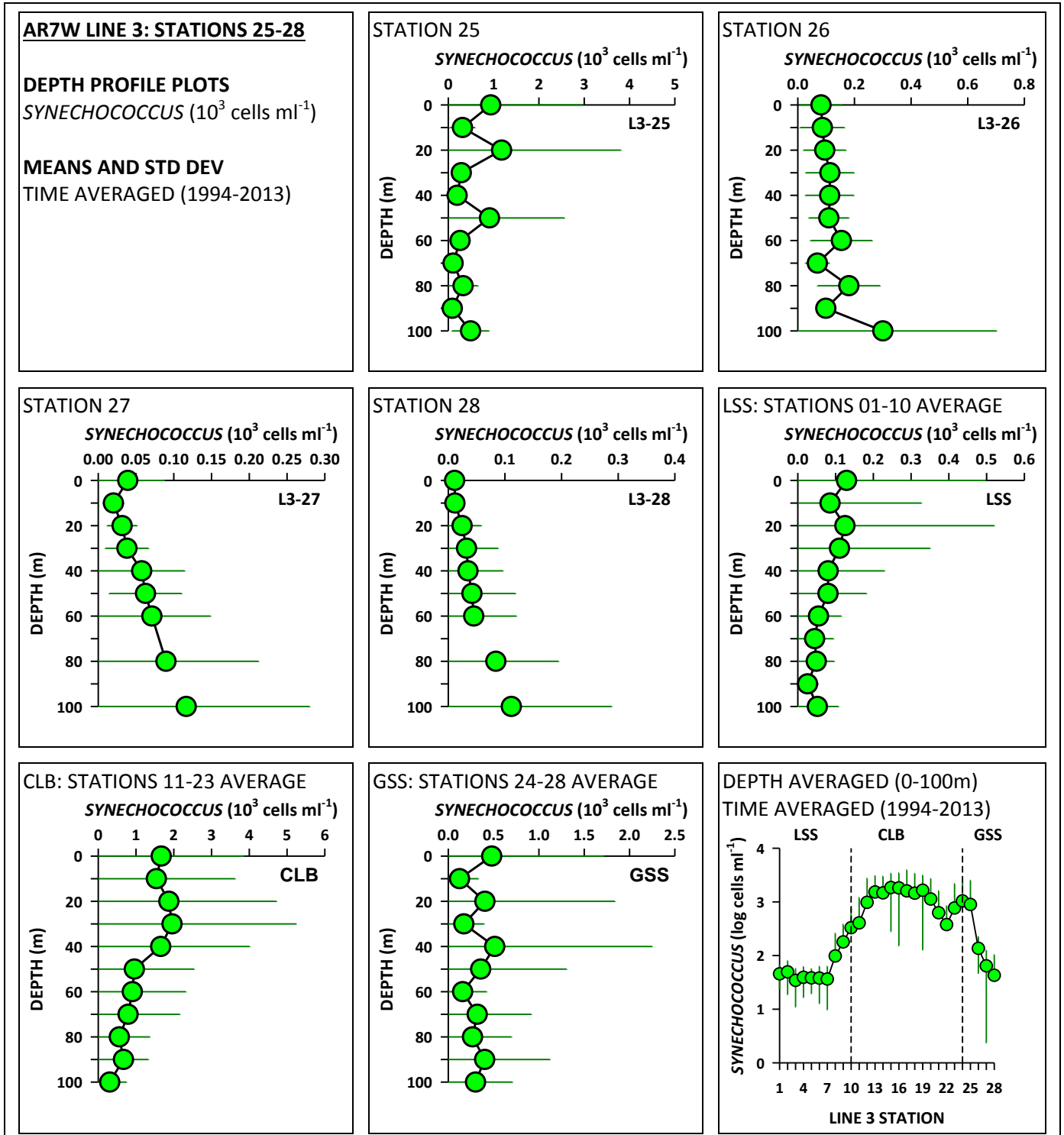


Figure 107

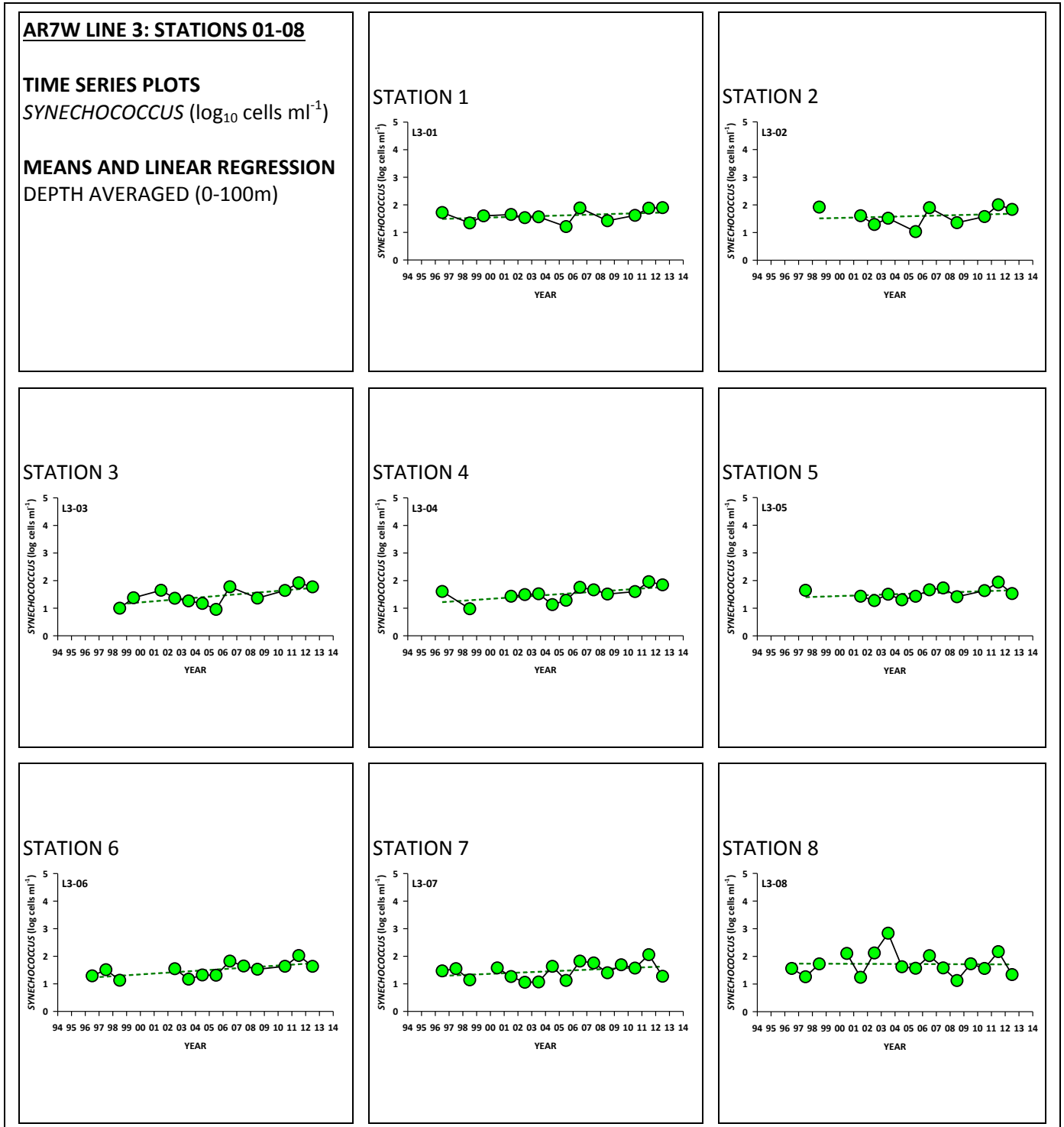




Figure 108

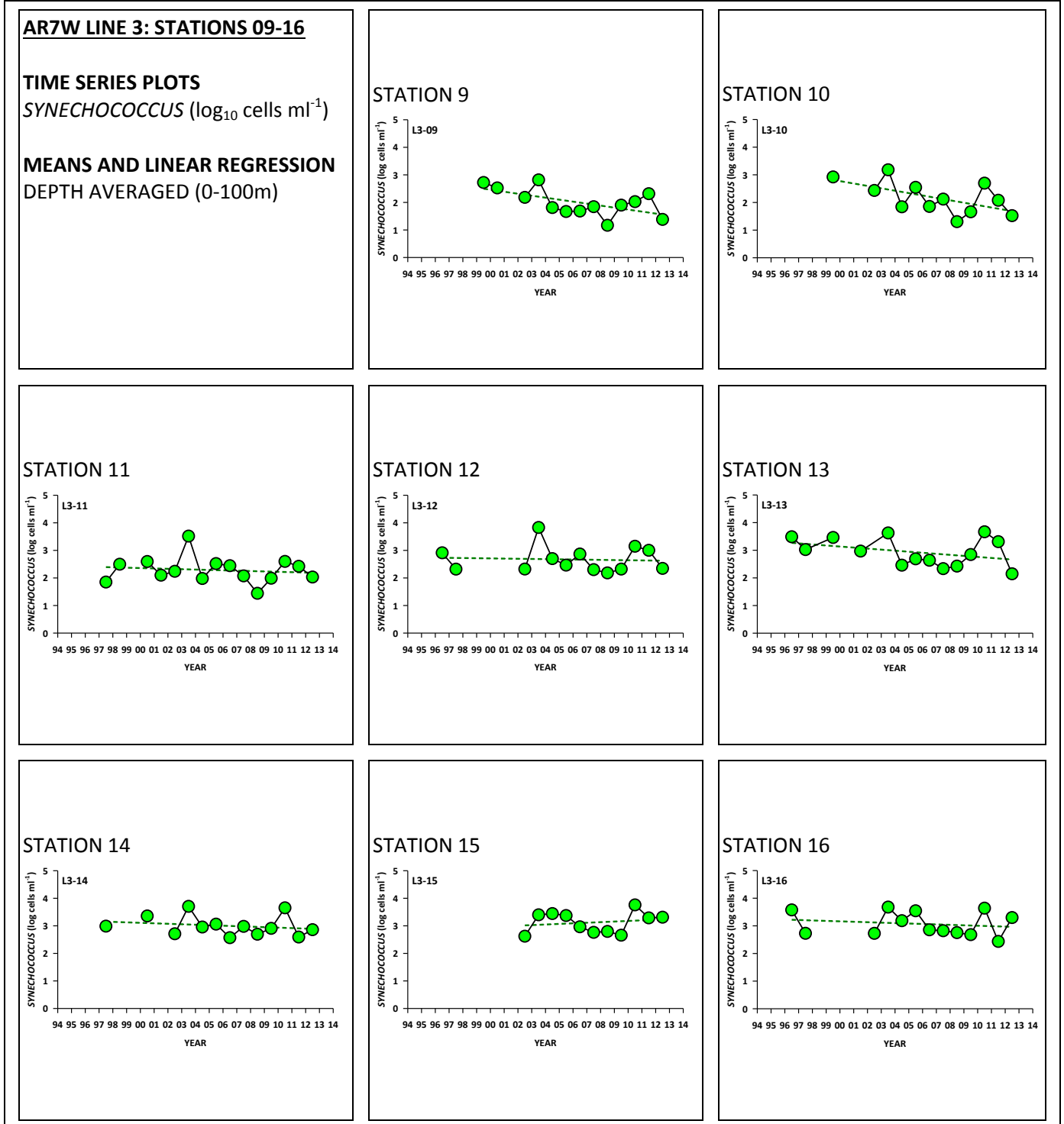


Figure 109

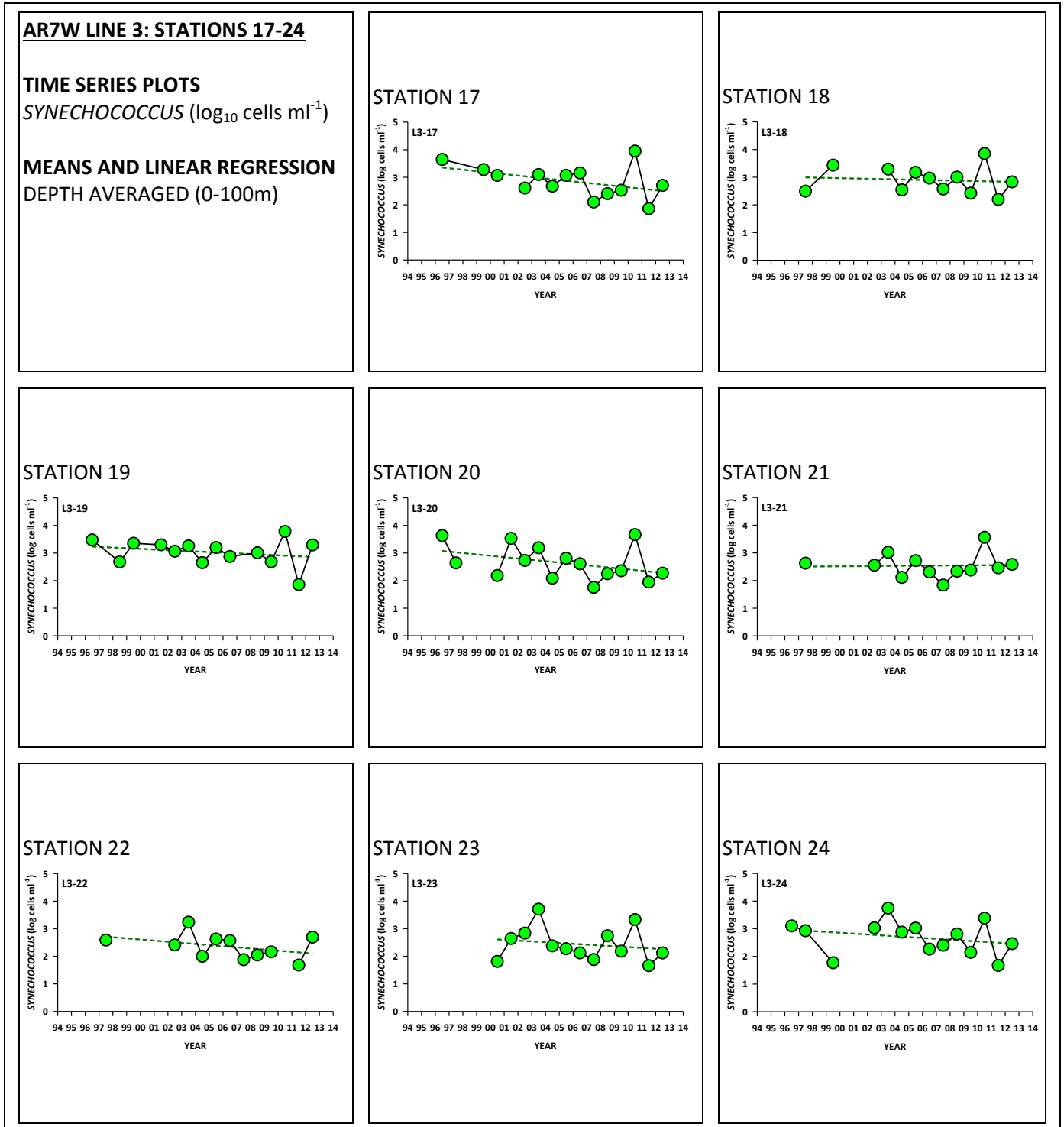


Figure 110

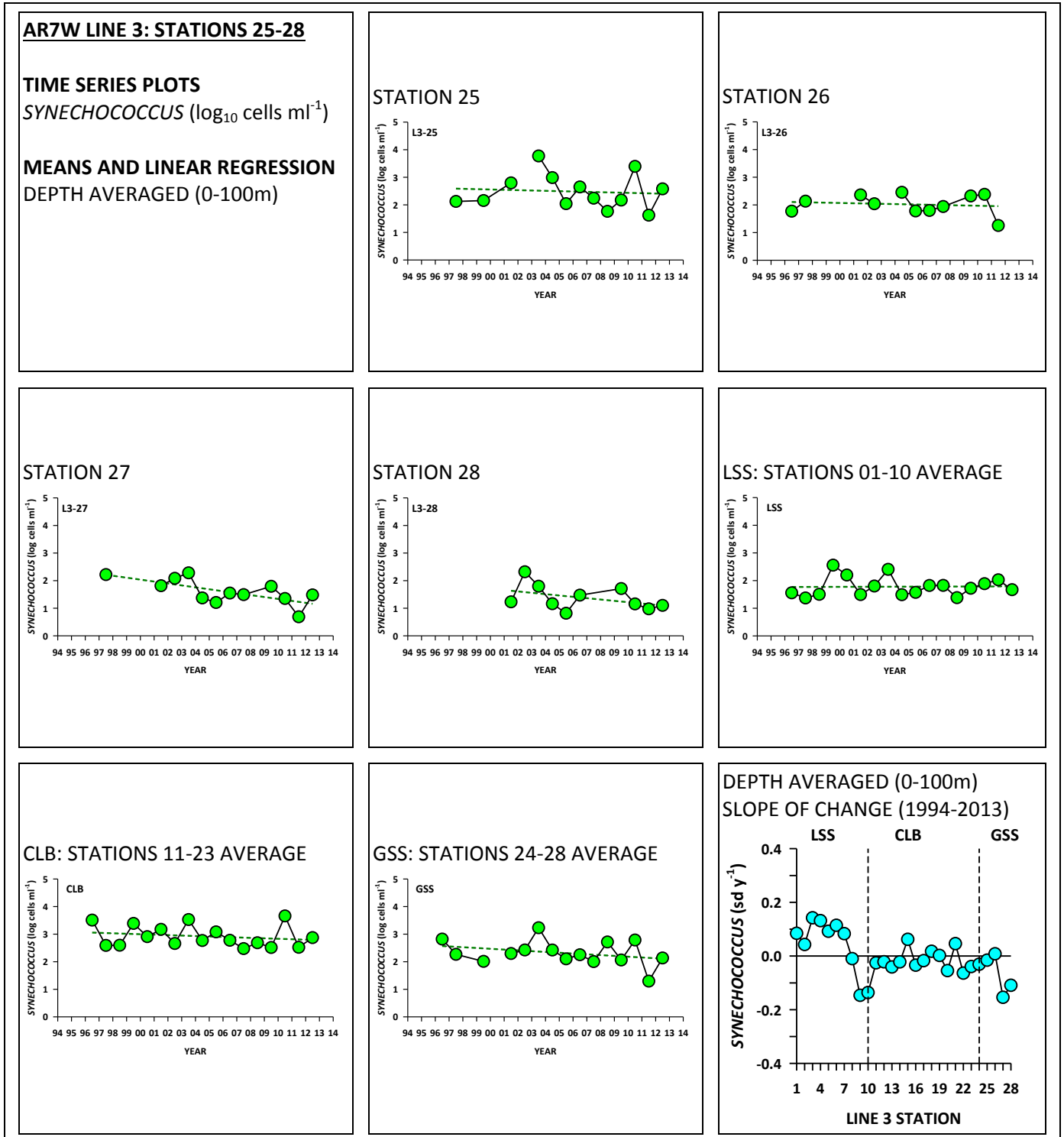


Figure 111

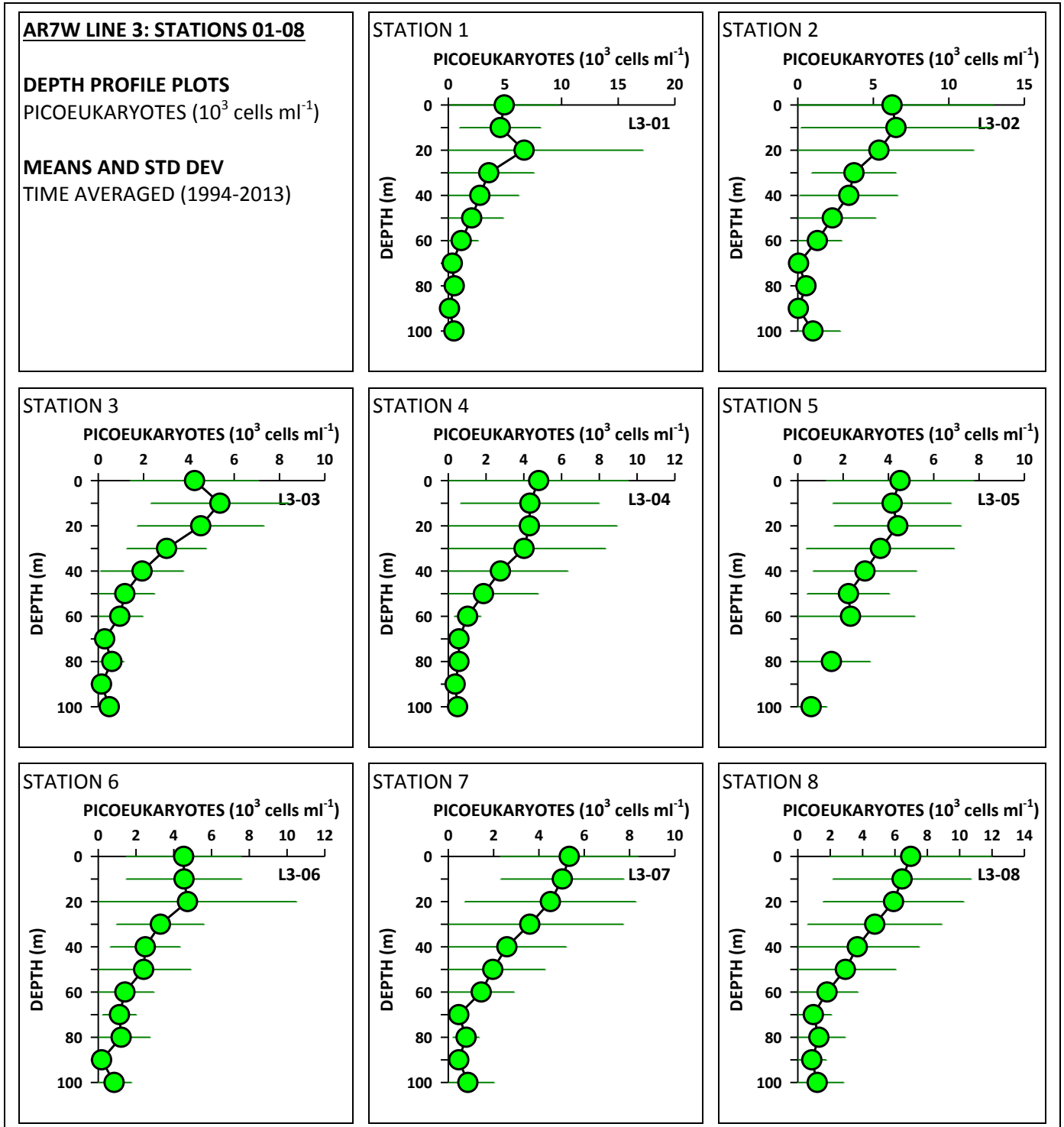


Figure 112

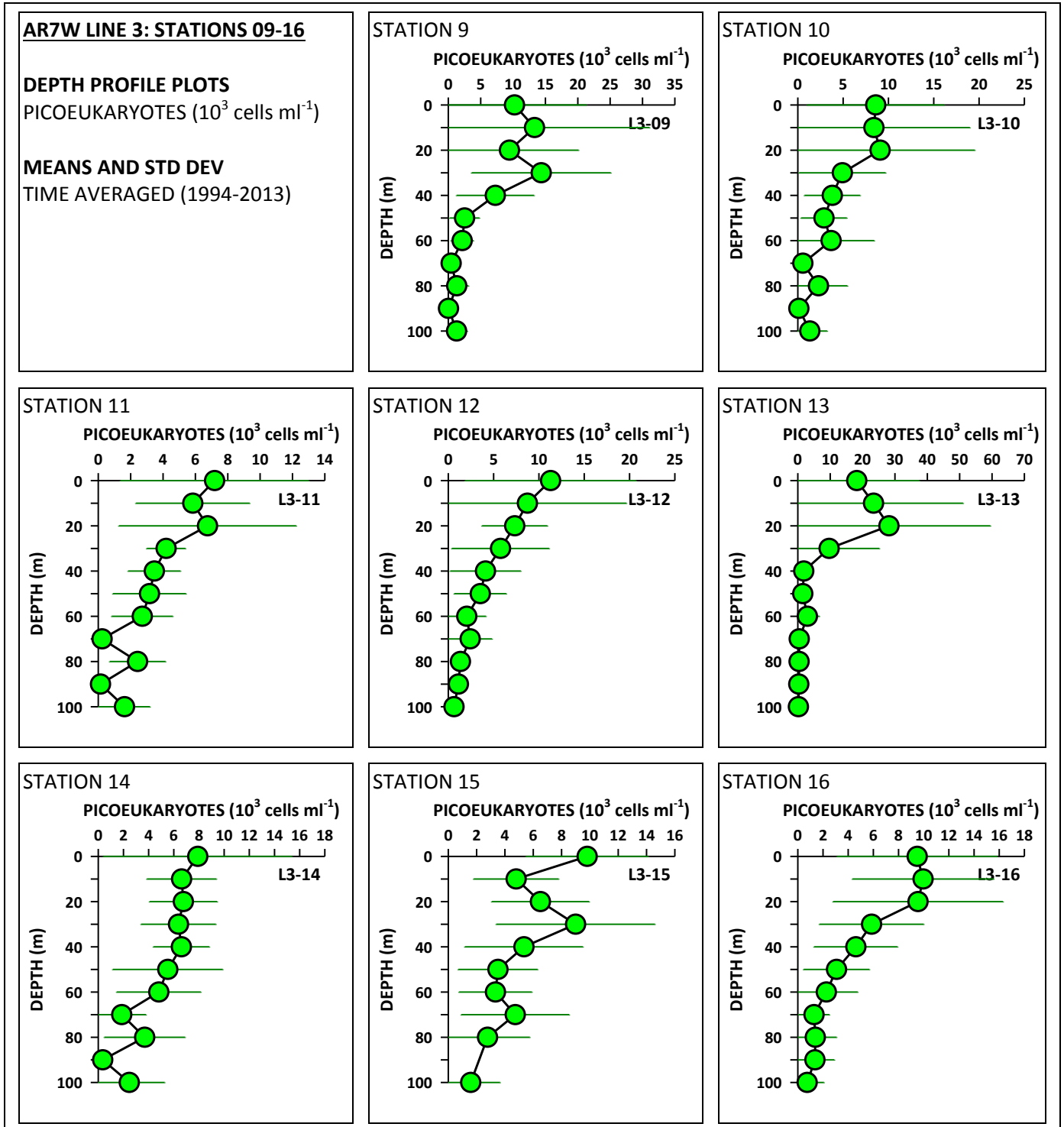


Figure 113

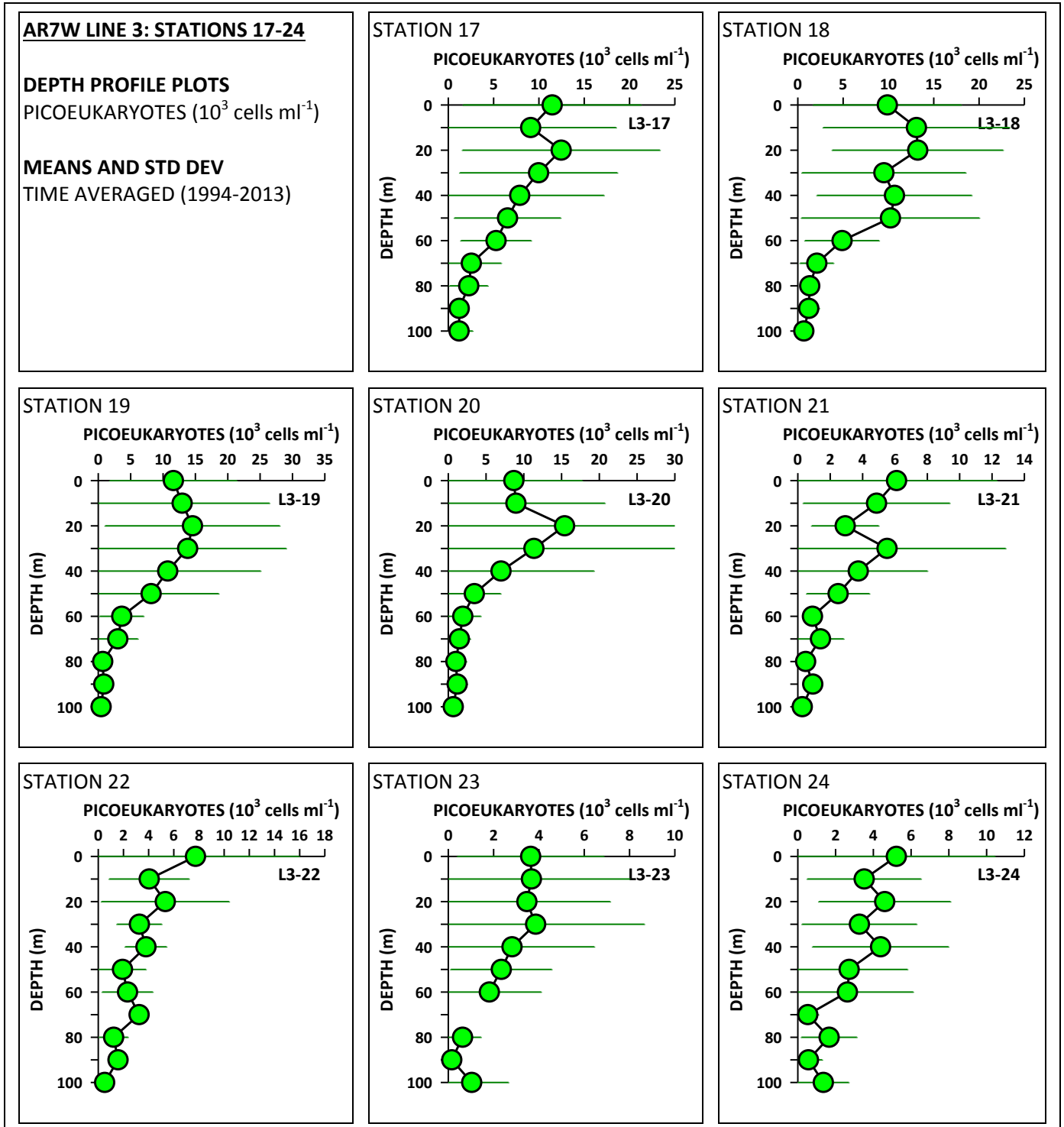


Figure 114

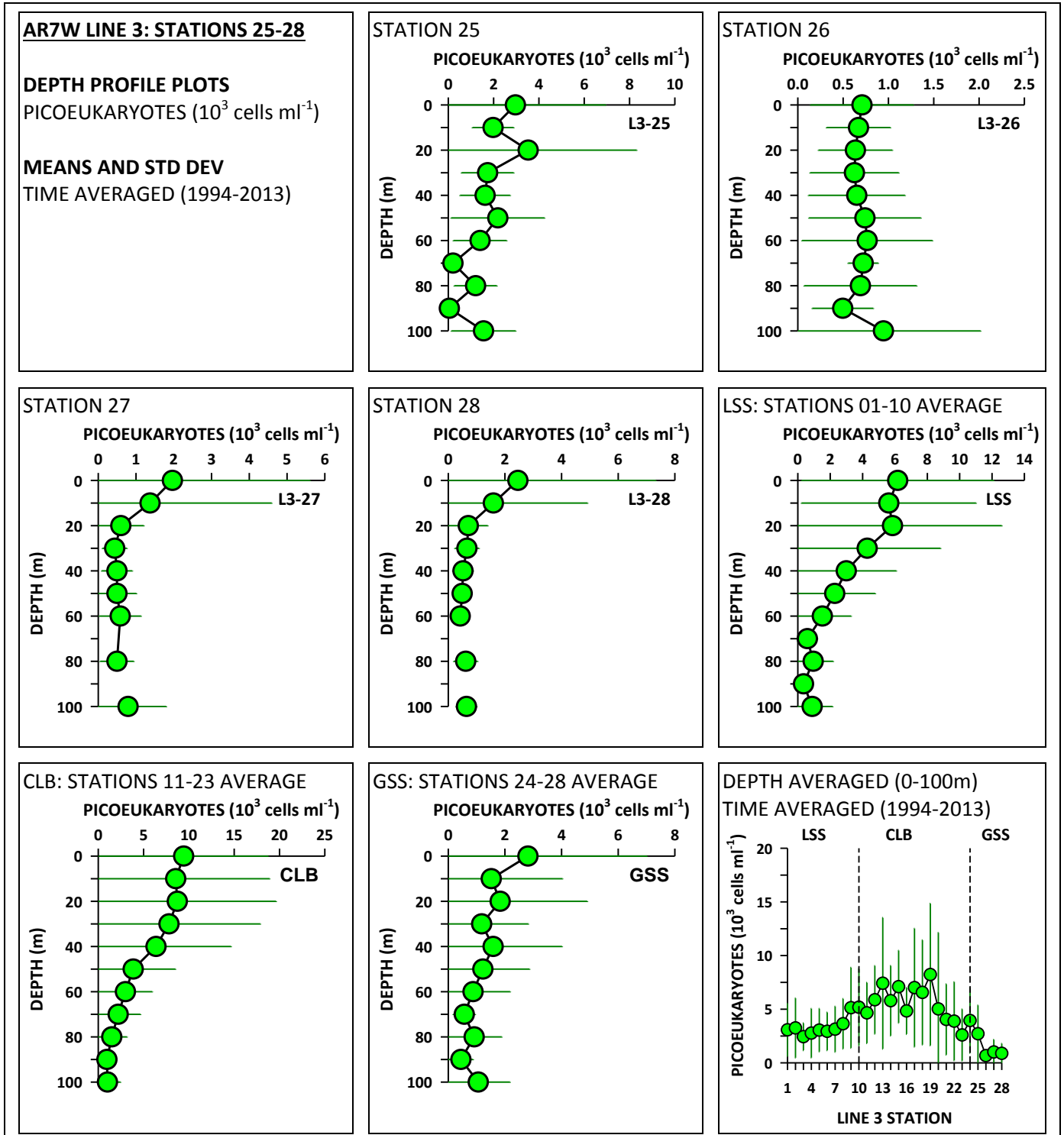


Figure 115

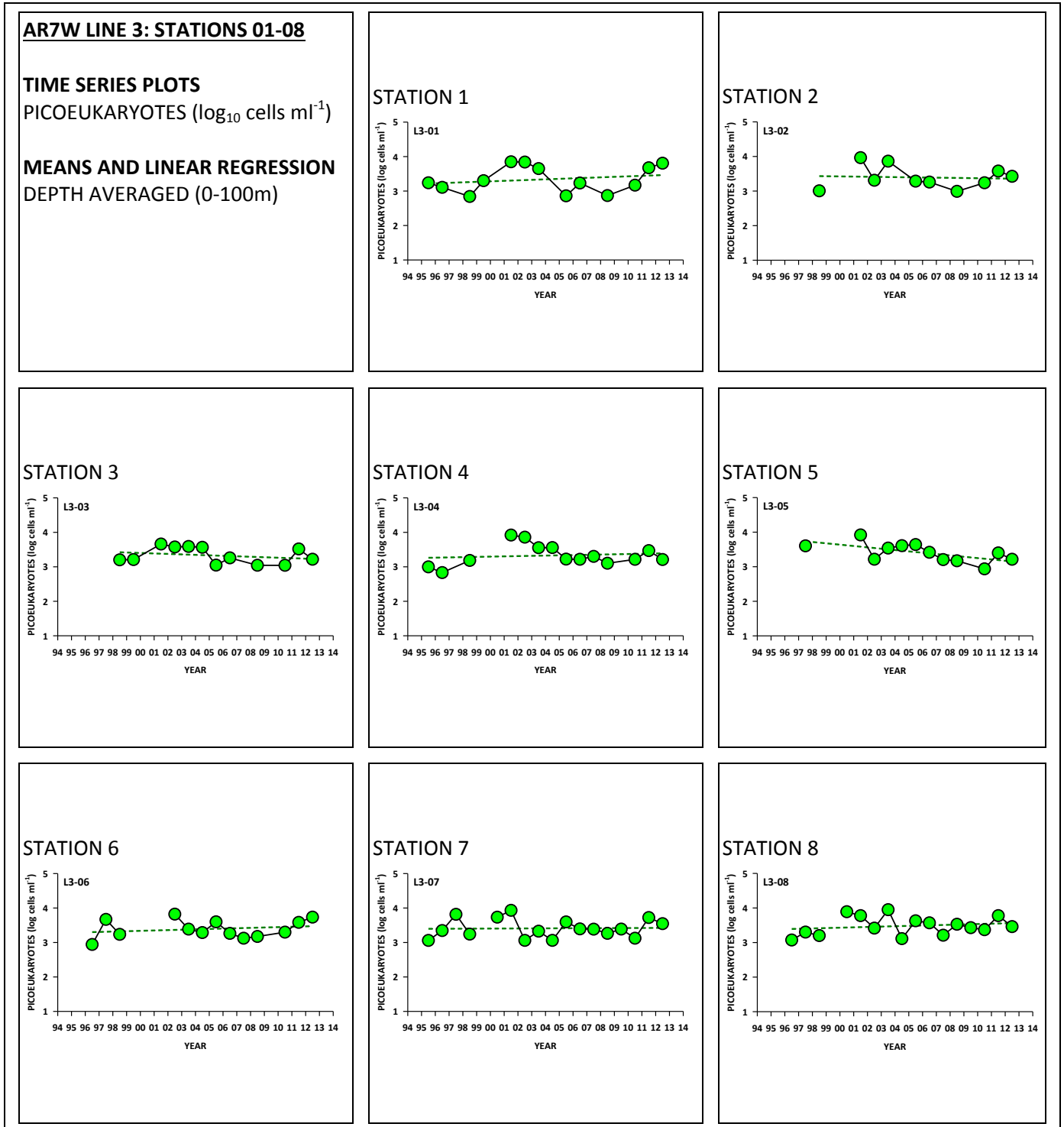




Figure 116

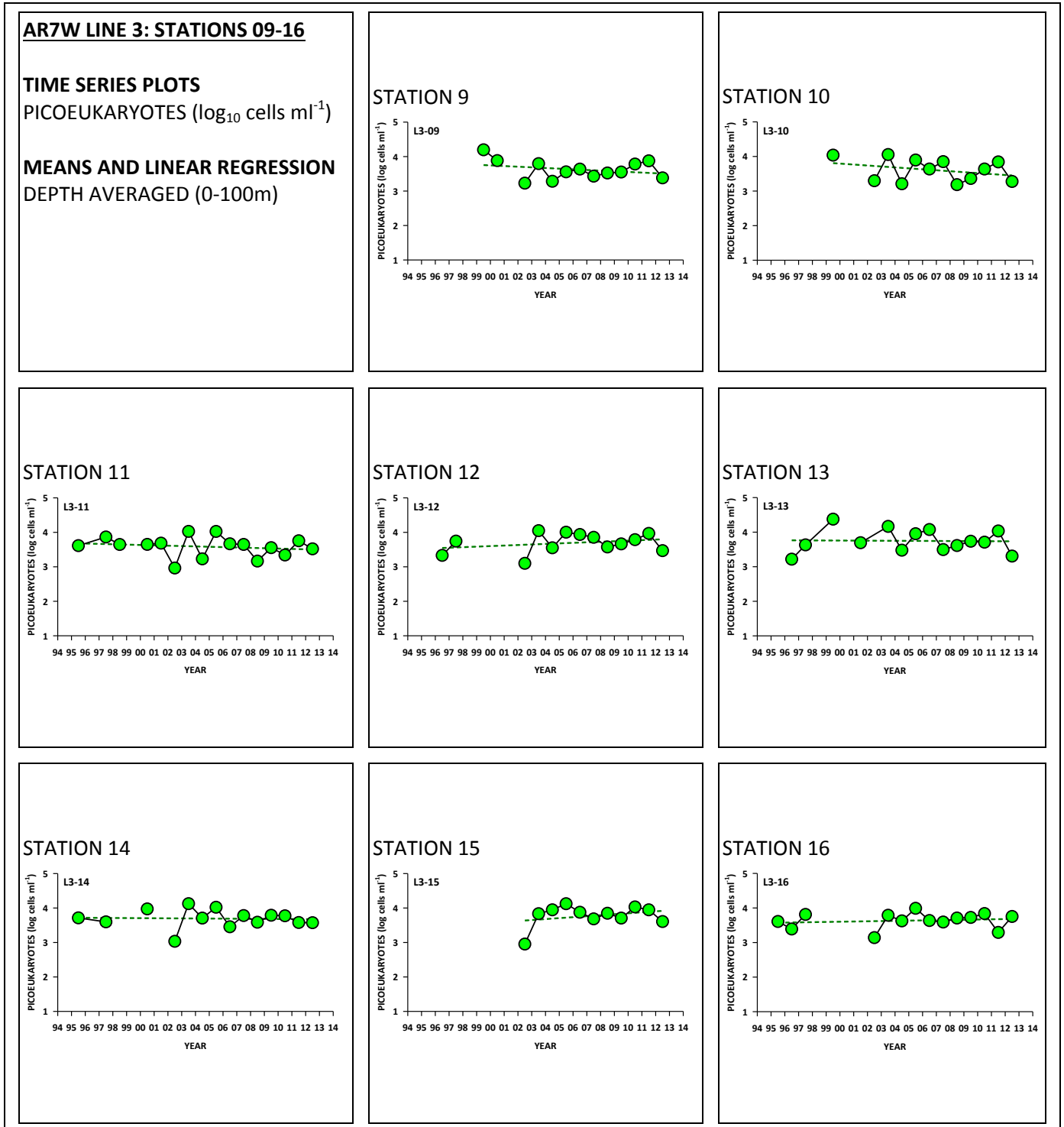


Figure 117

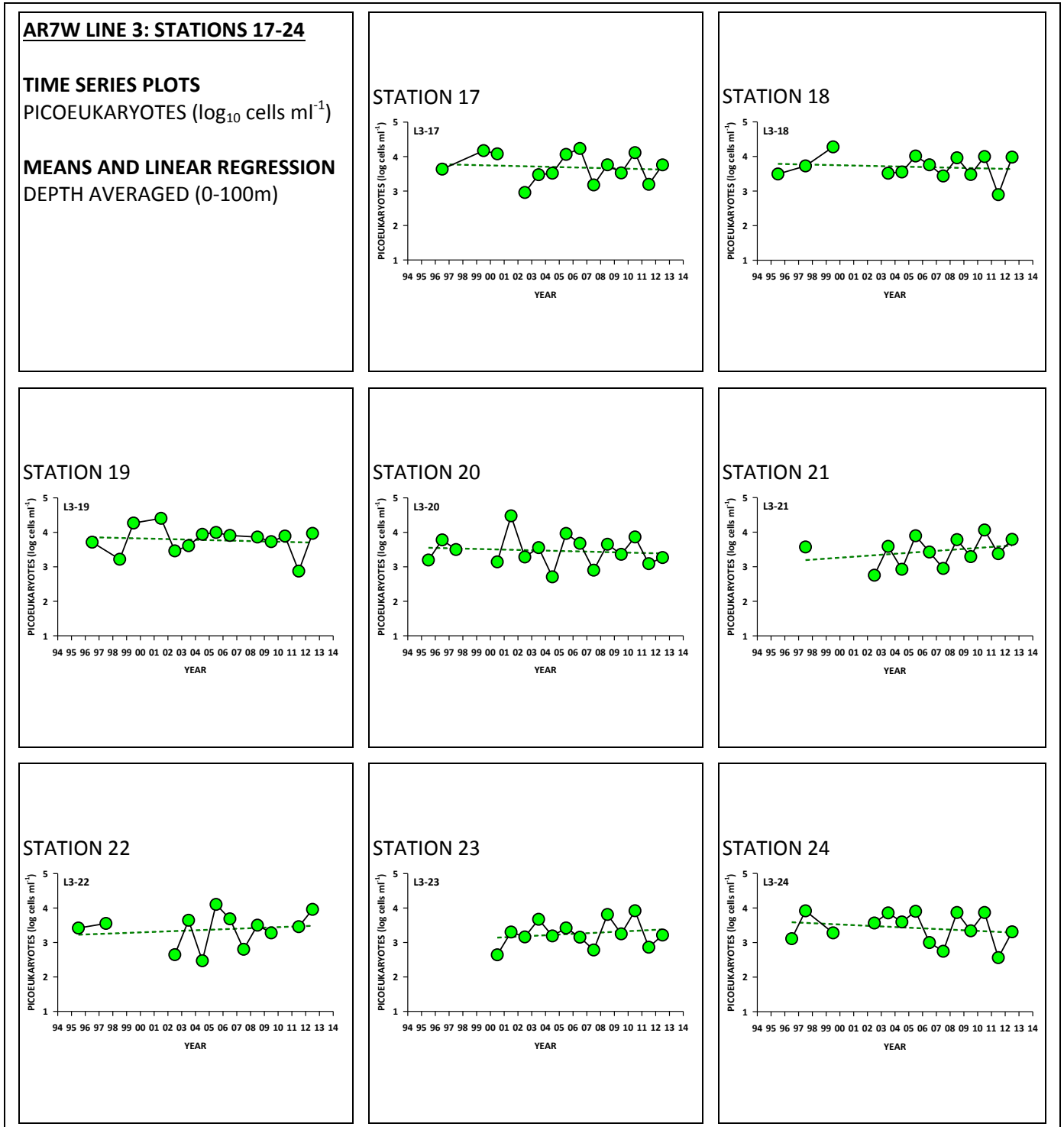


Figure 118

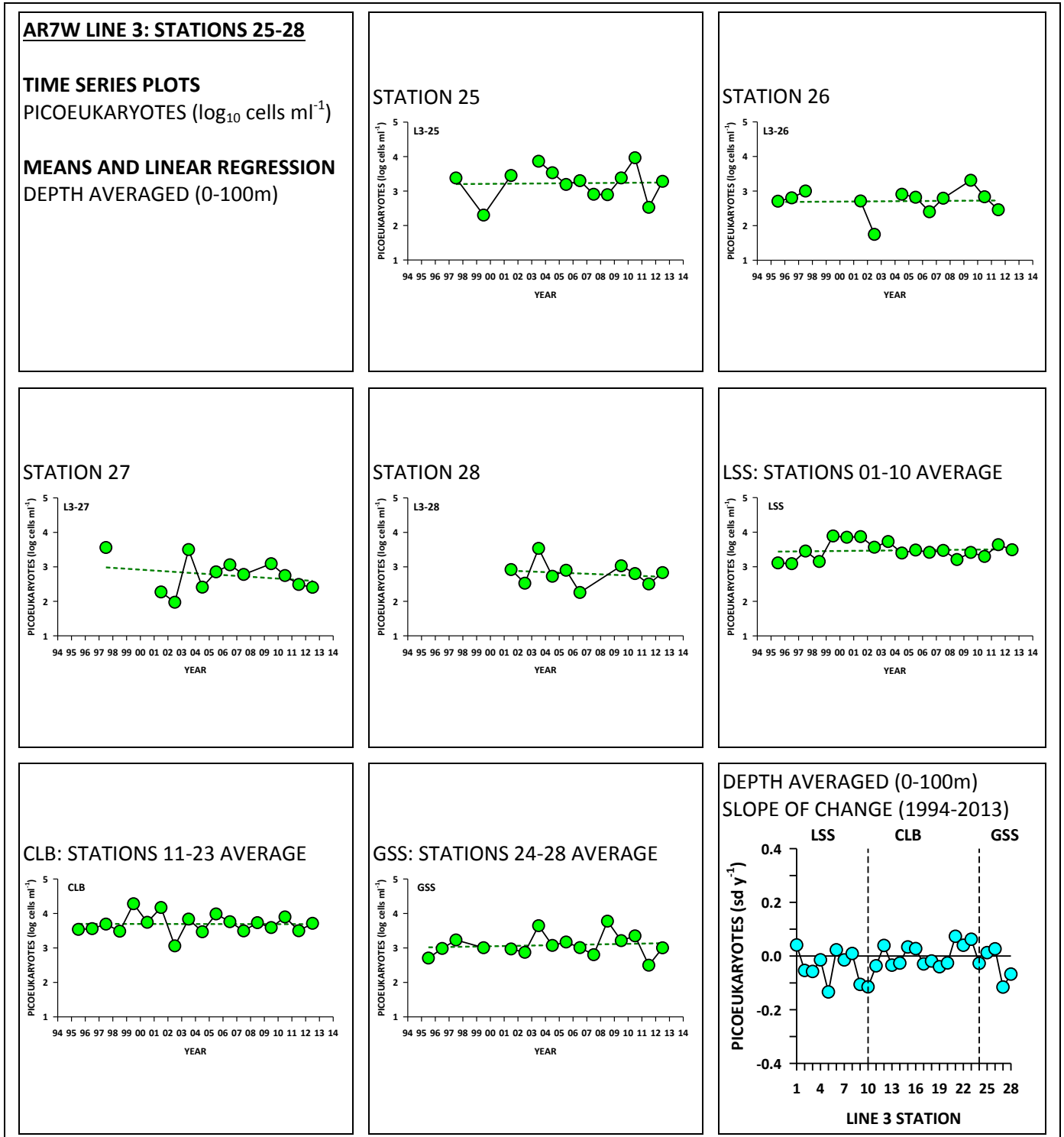


Figure 119

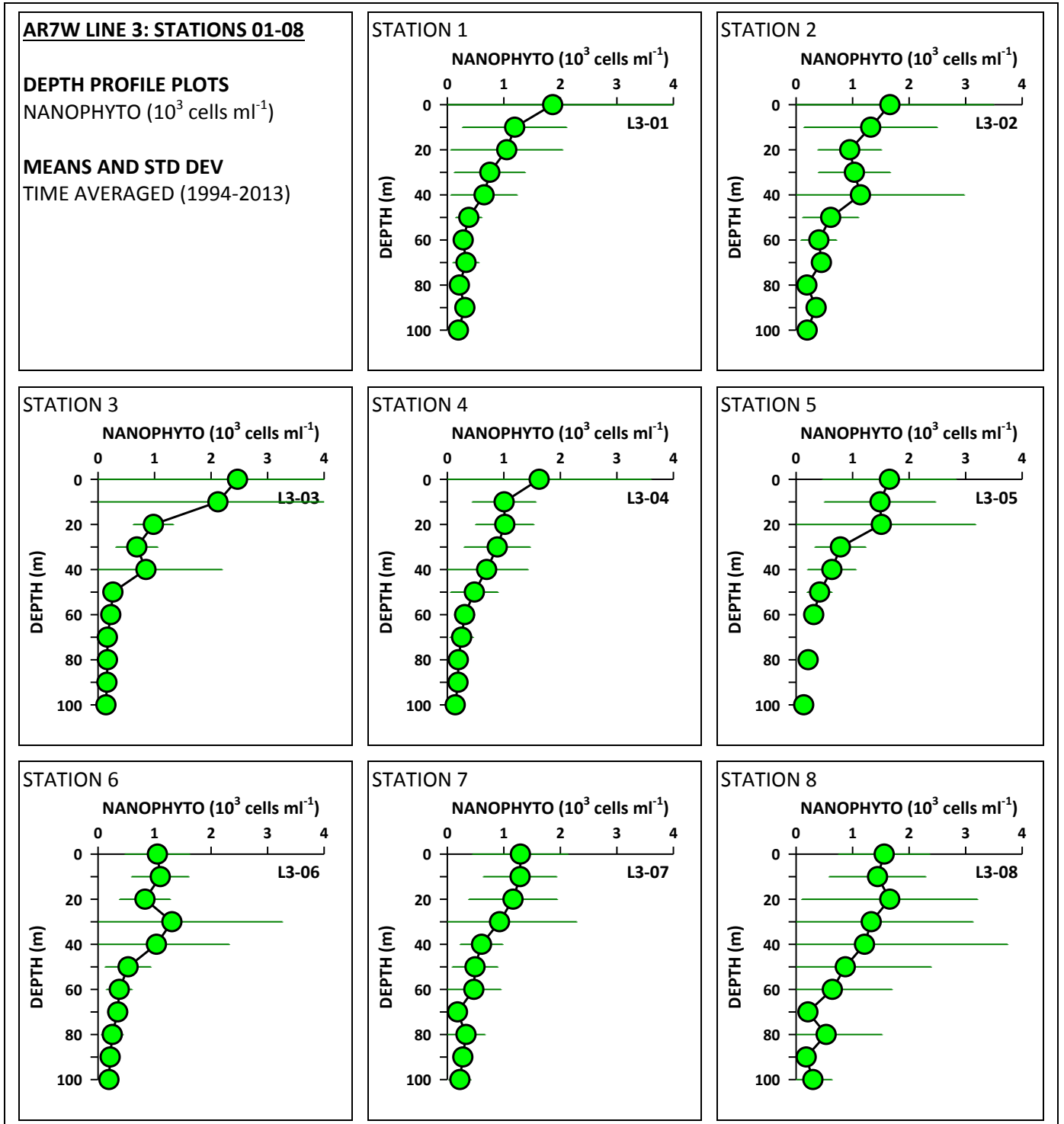


Figure 120

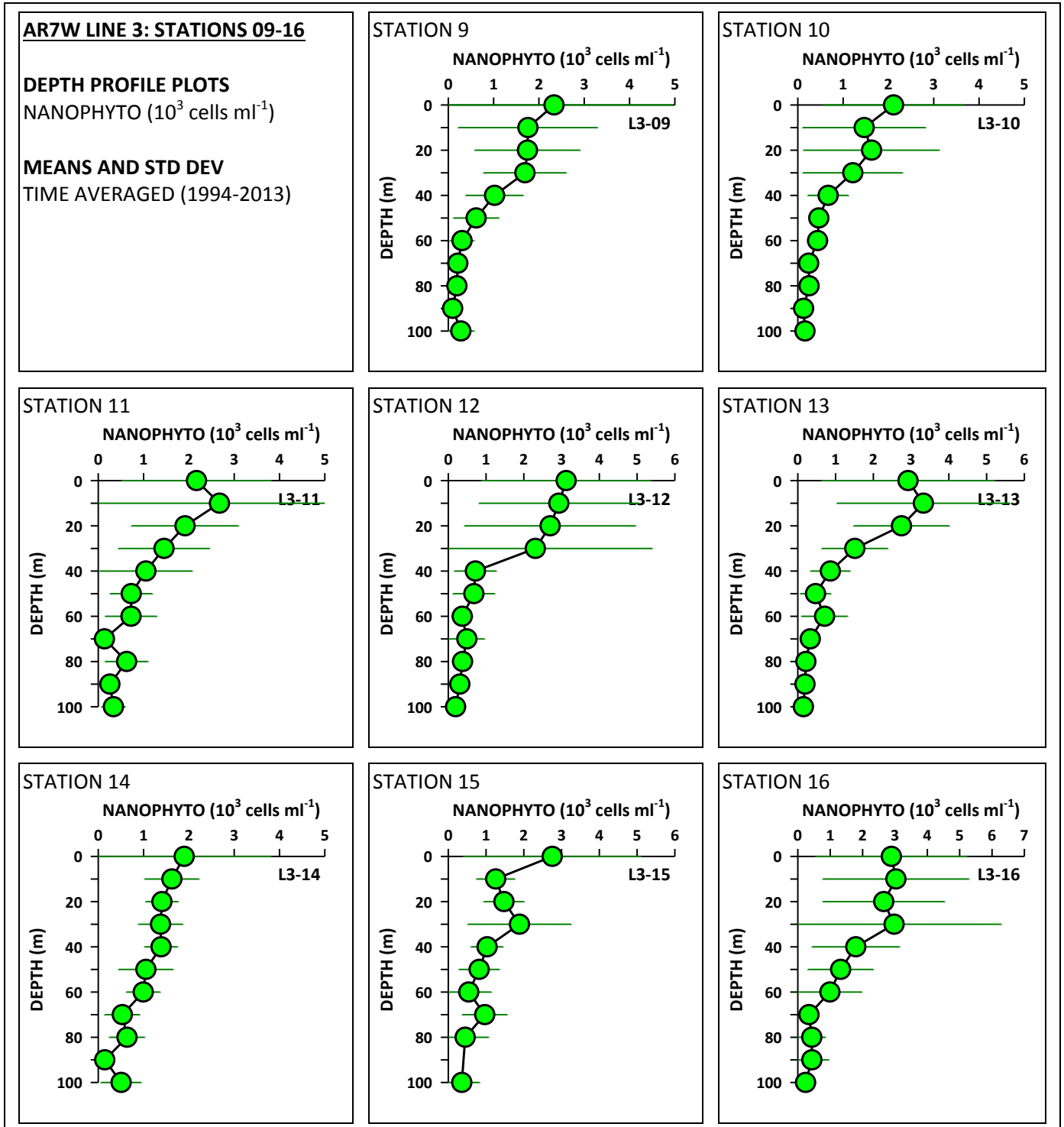


Figure 121

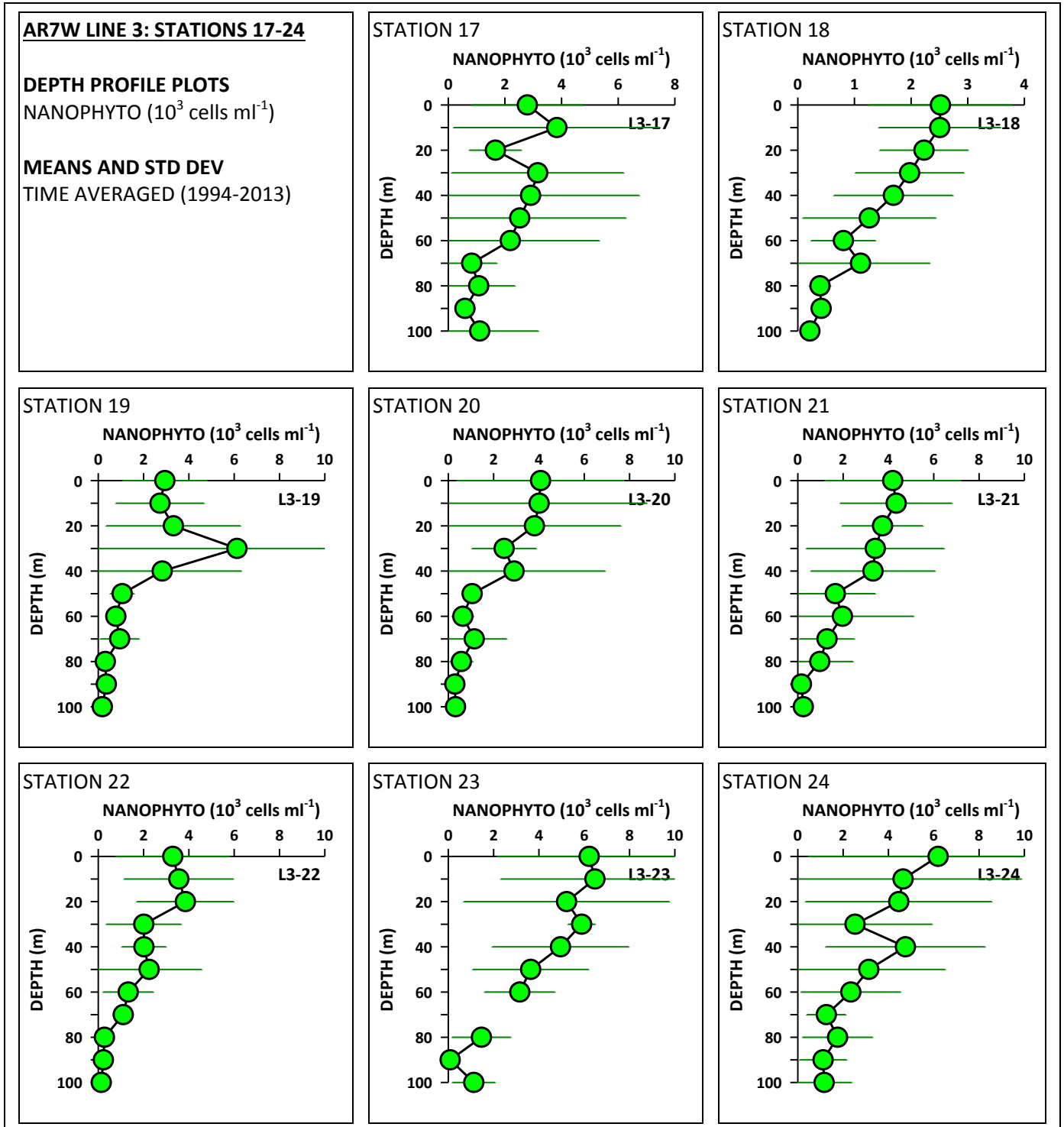


Figure 122

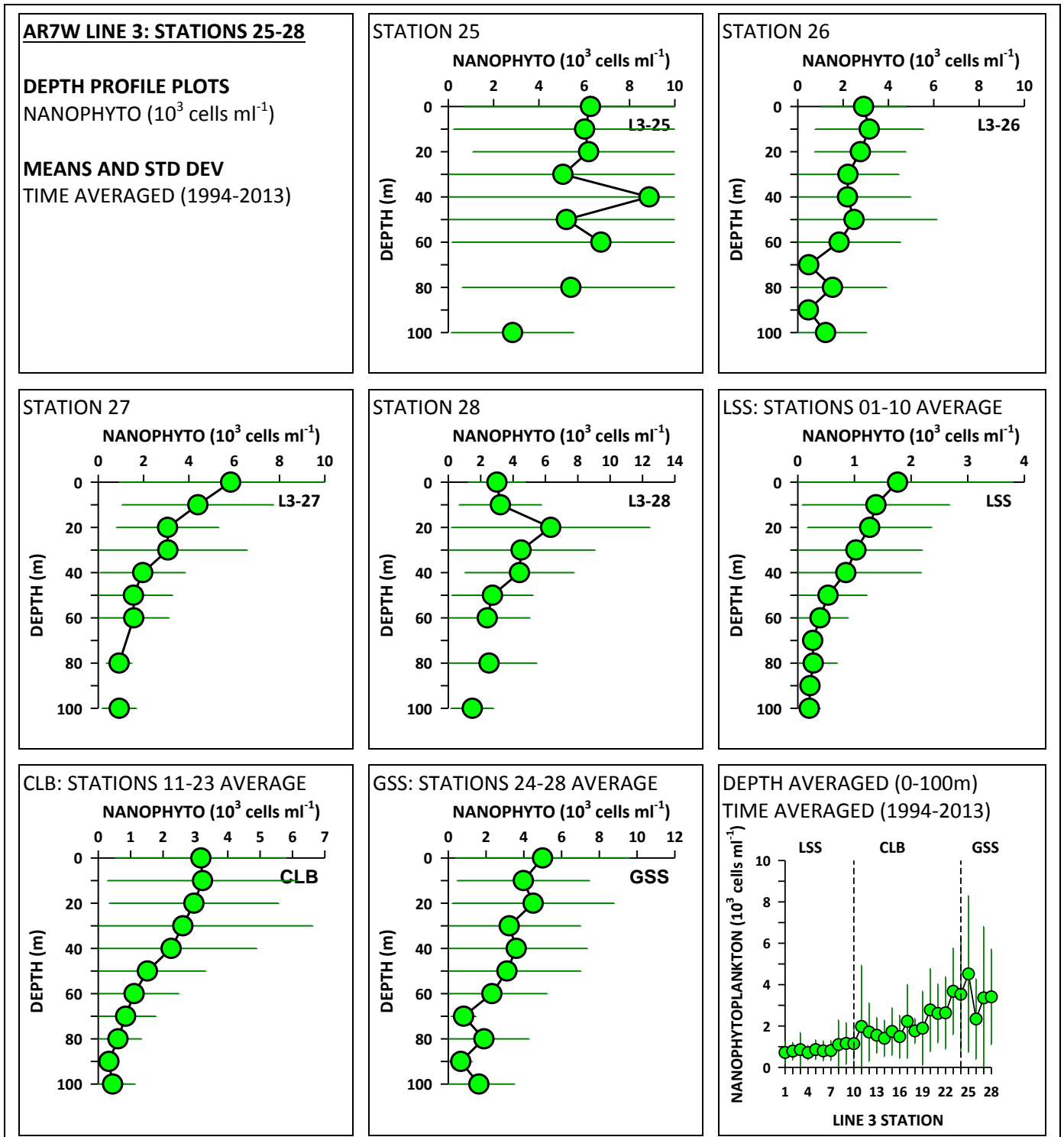


Figure 123

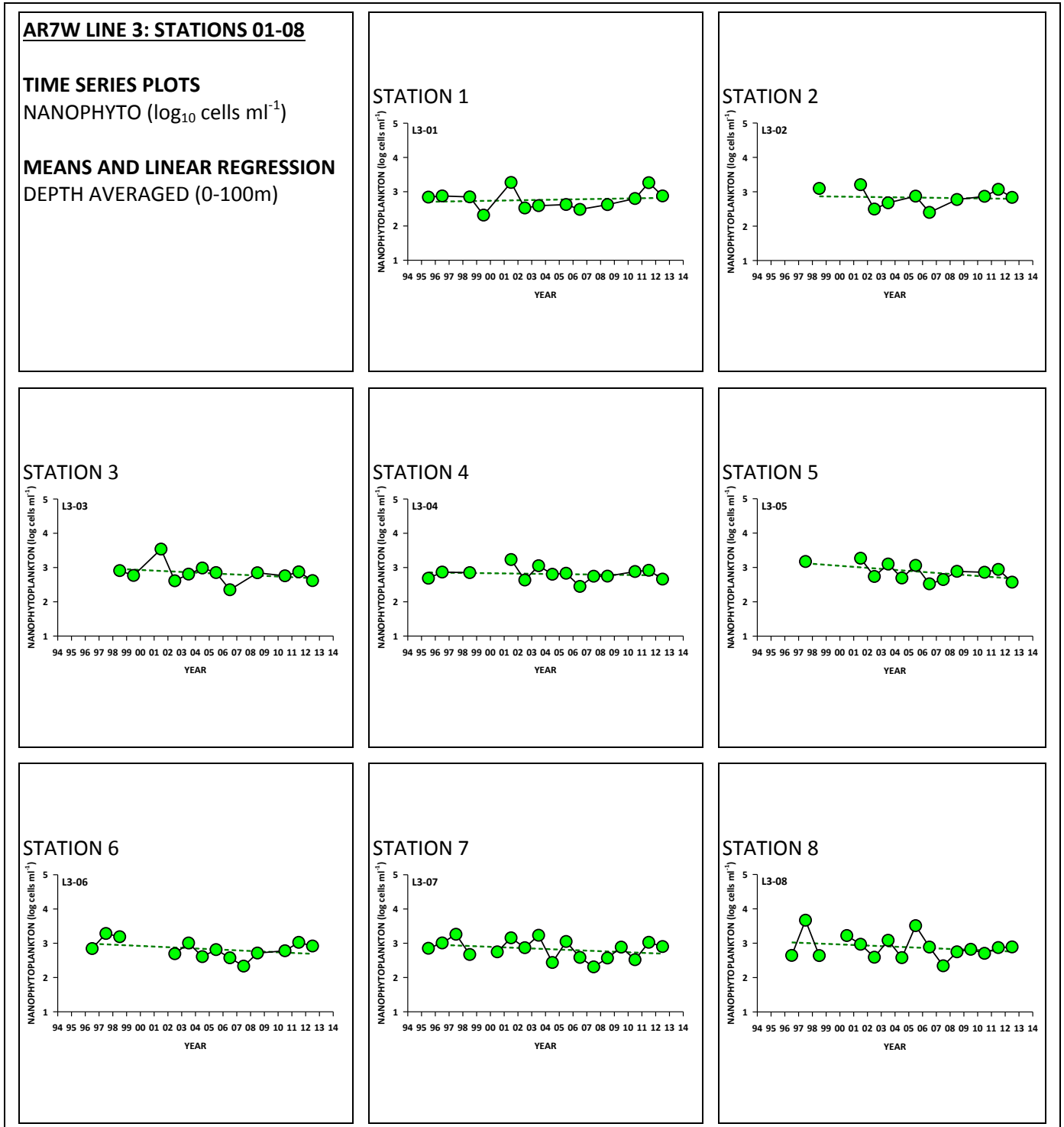




Figure 124

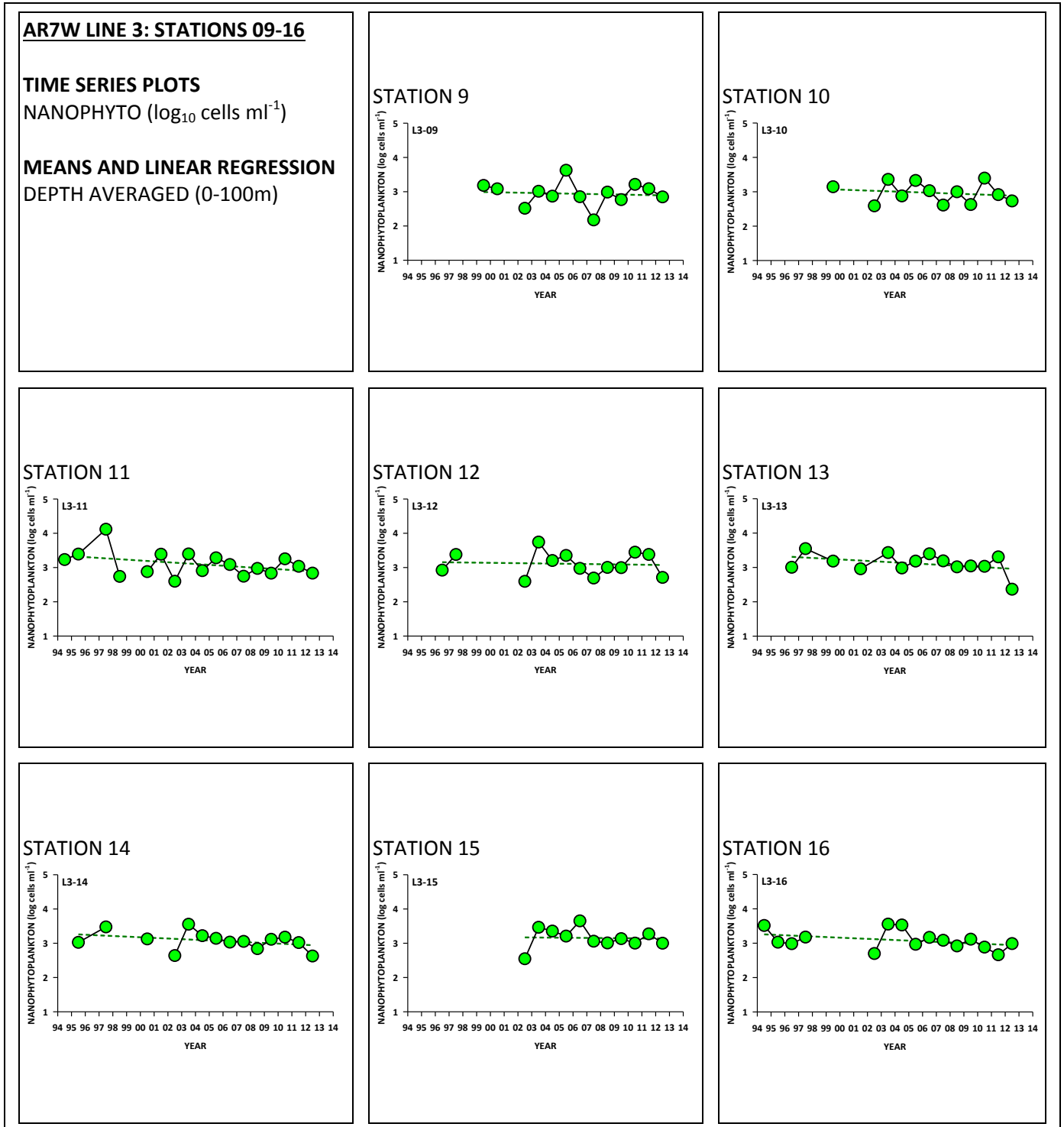


Figure 125

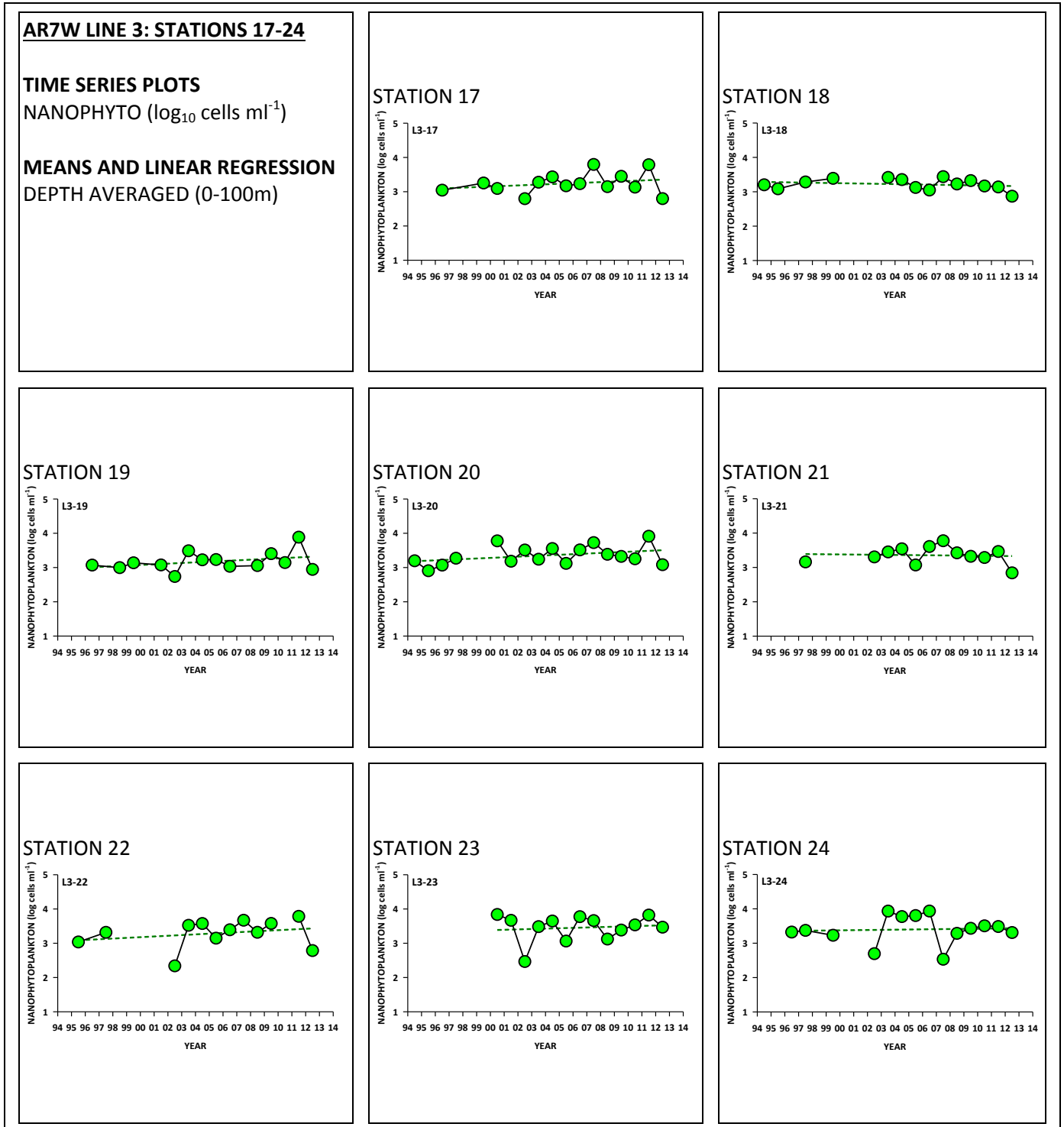


Figure 126

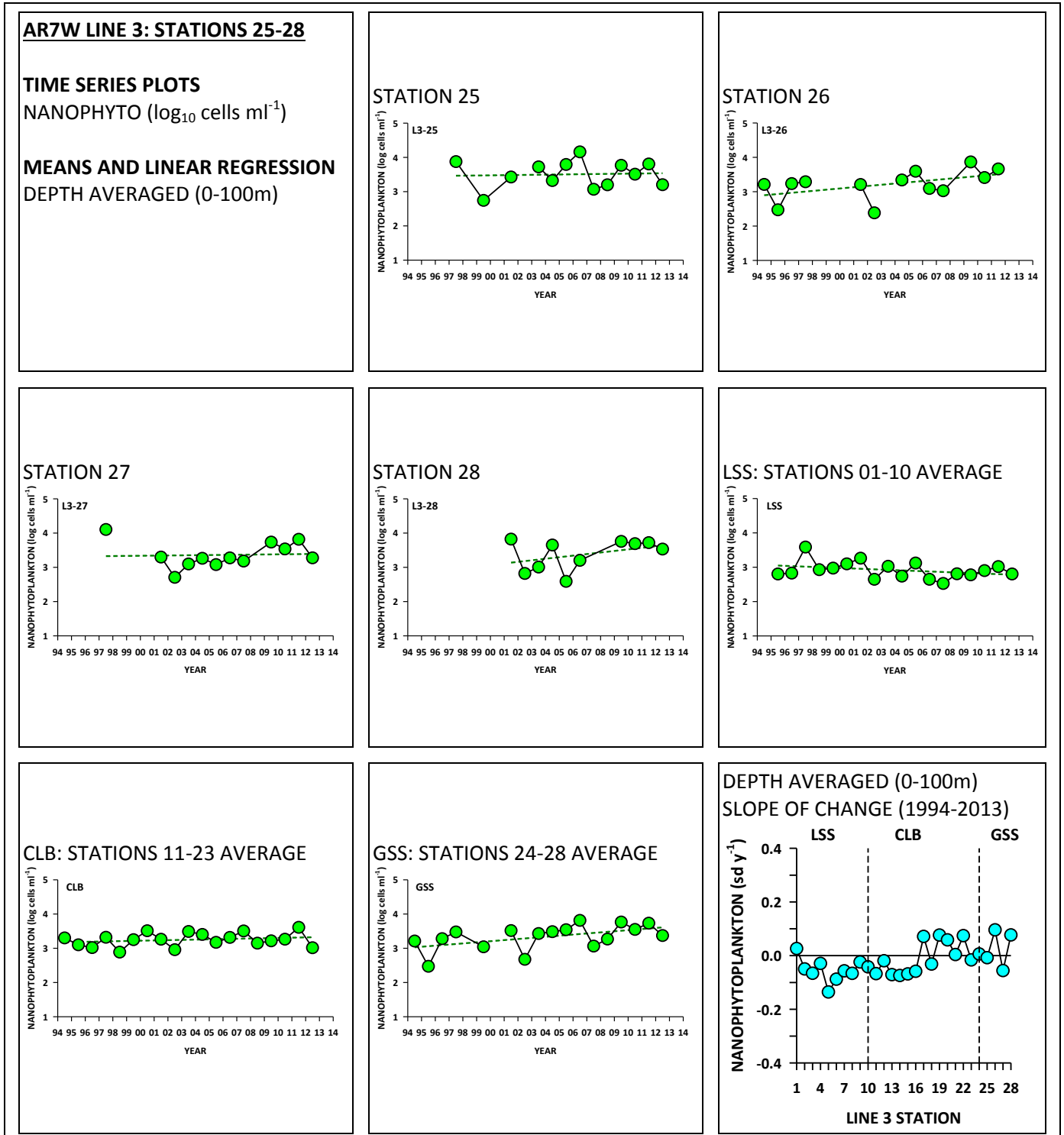


Figure 127

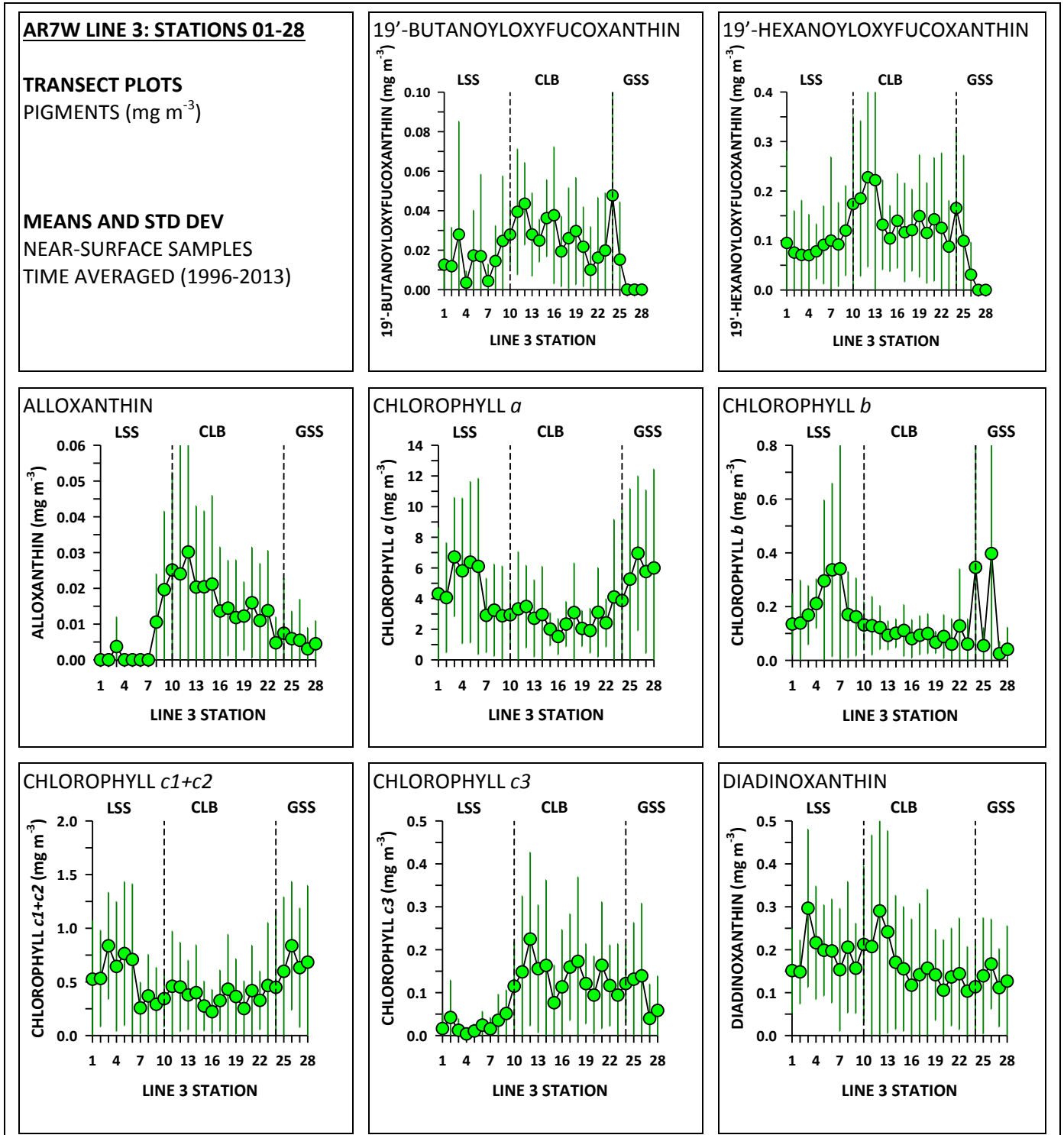


Figure 128

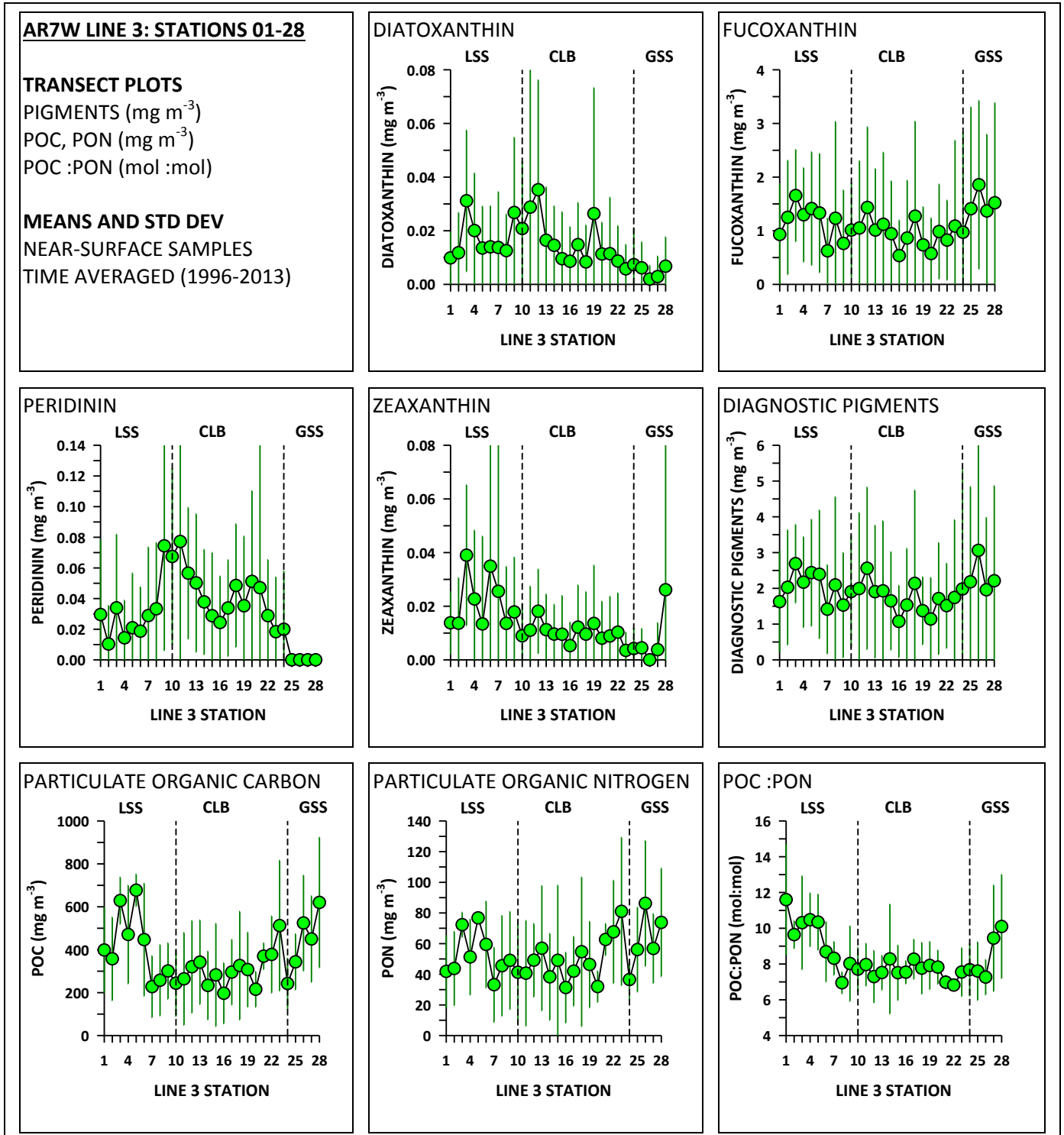


Figure 129

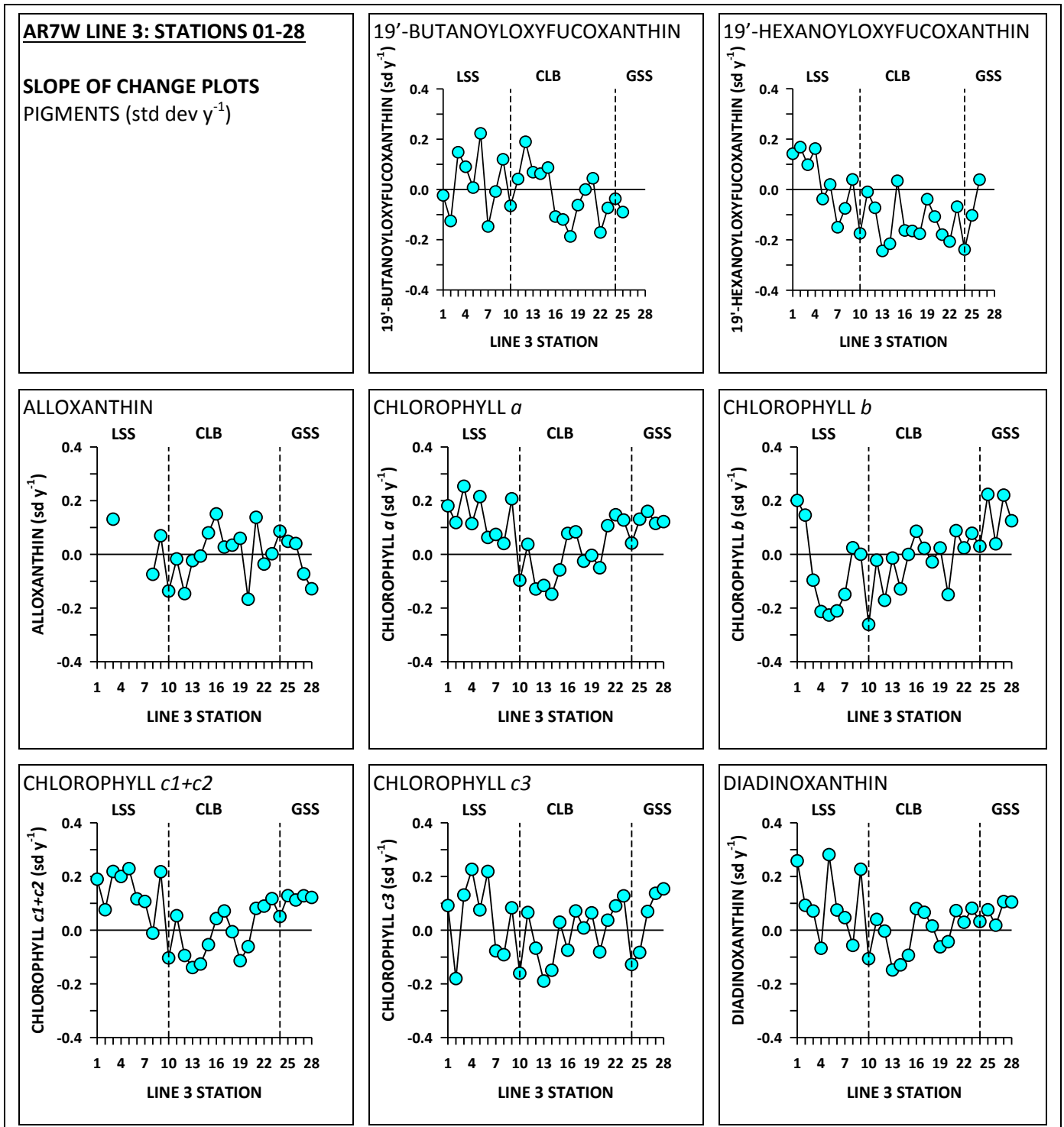


Figure 130

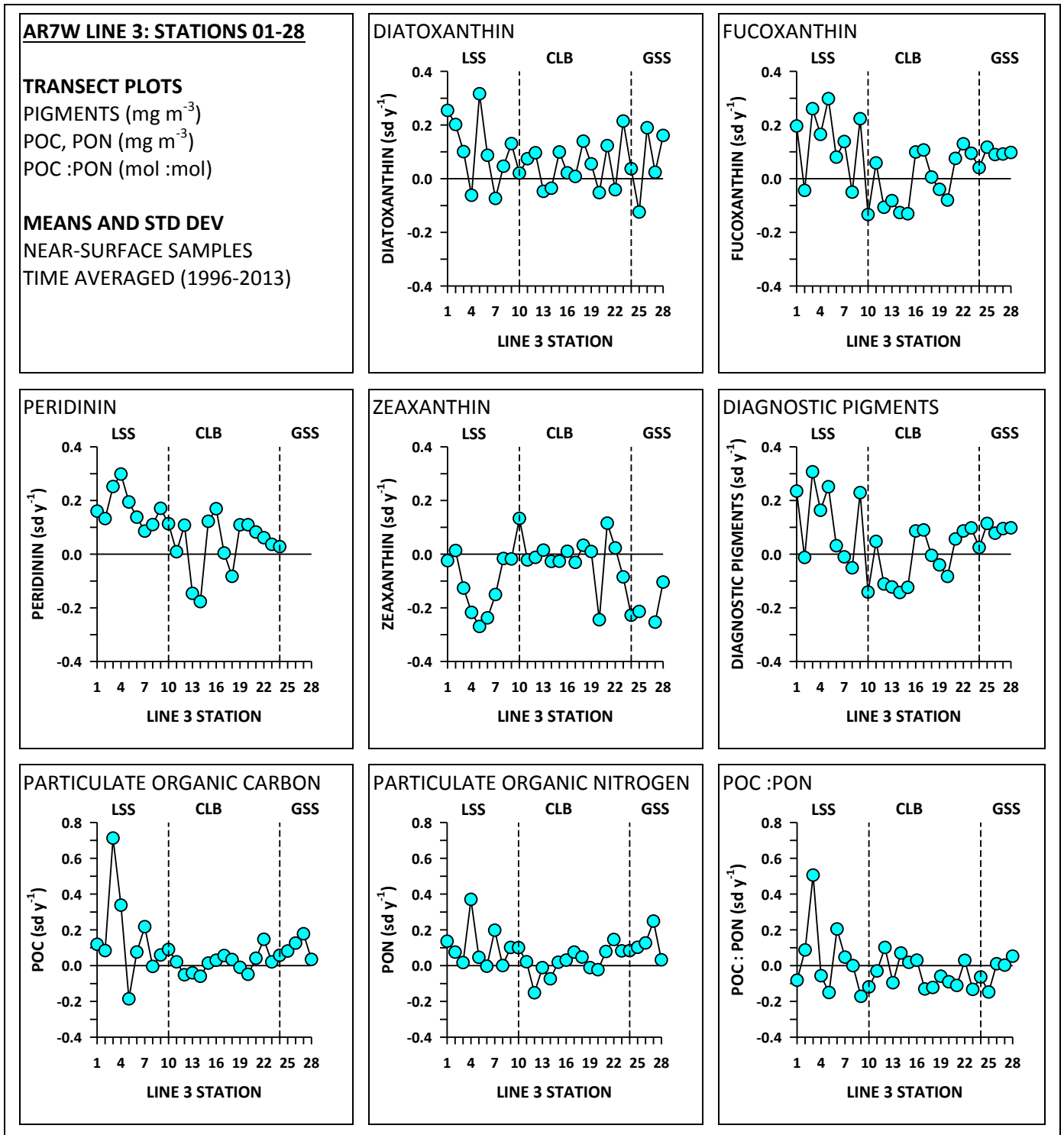


Figure 131

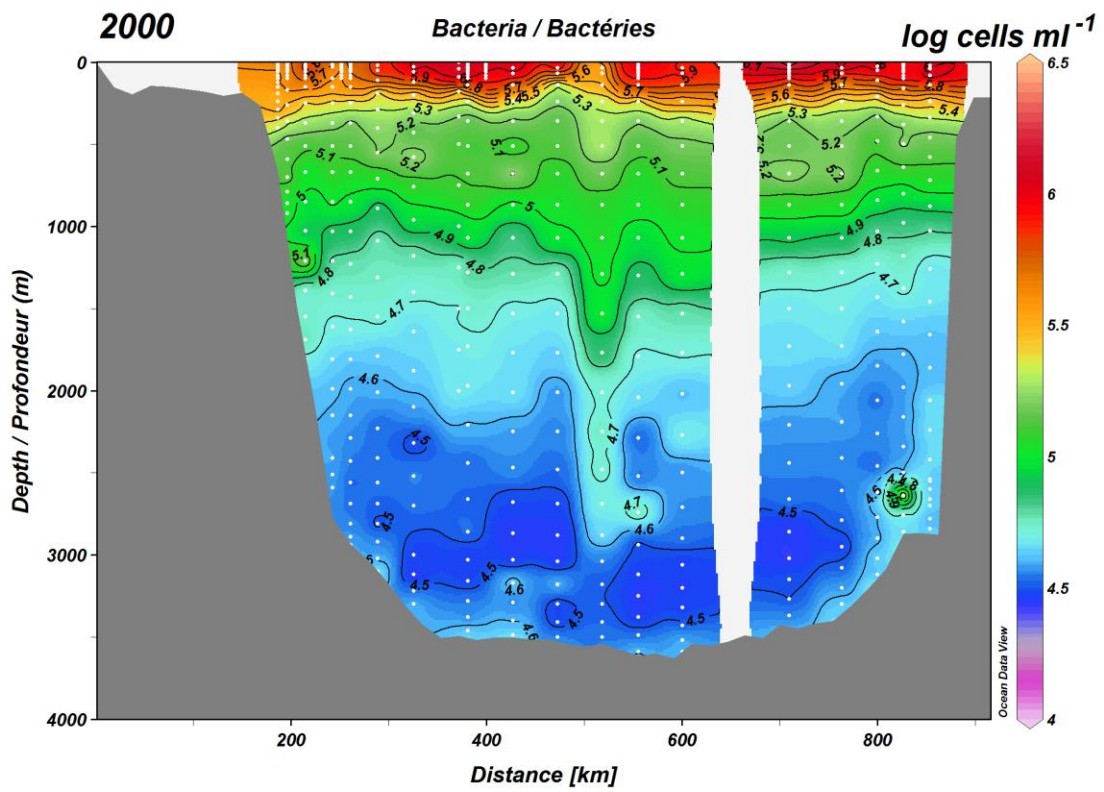
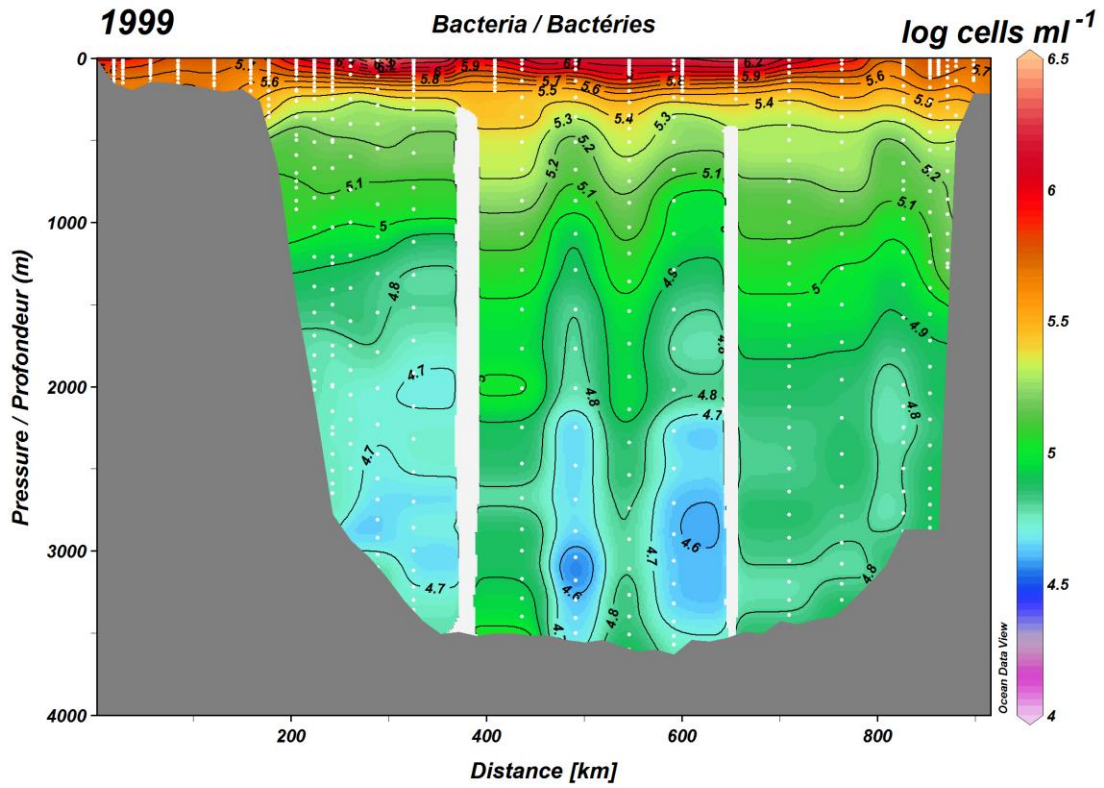




Figure 132

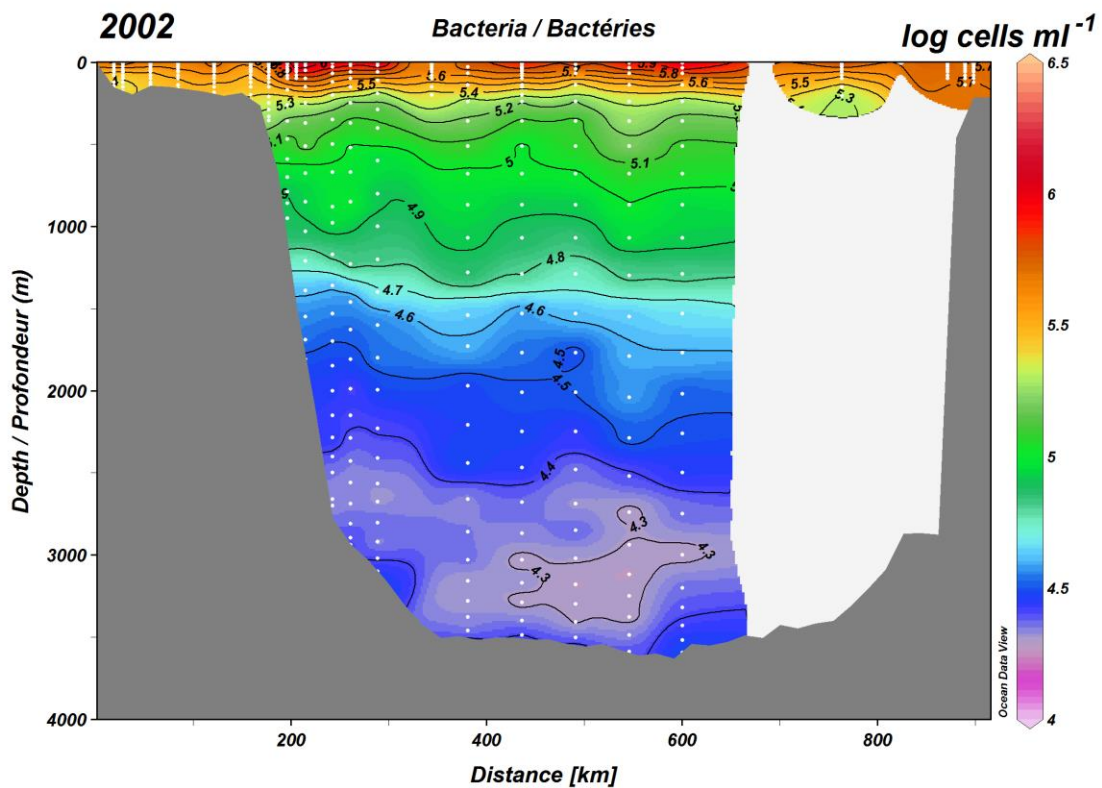
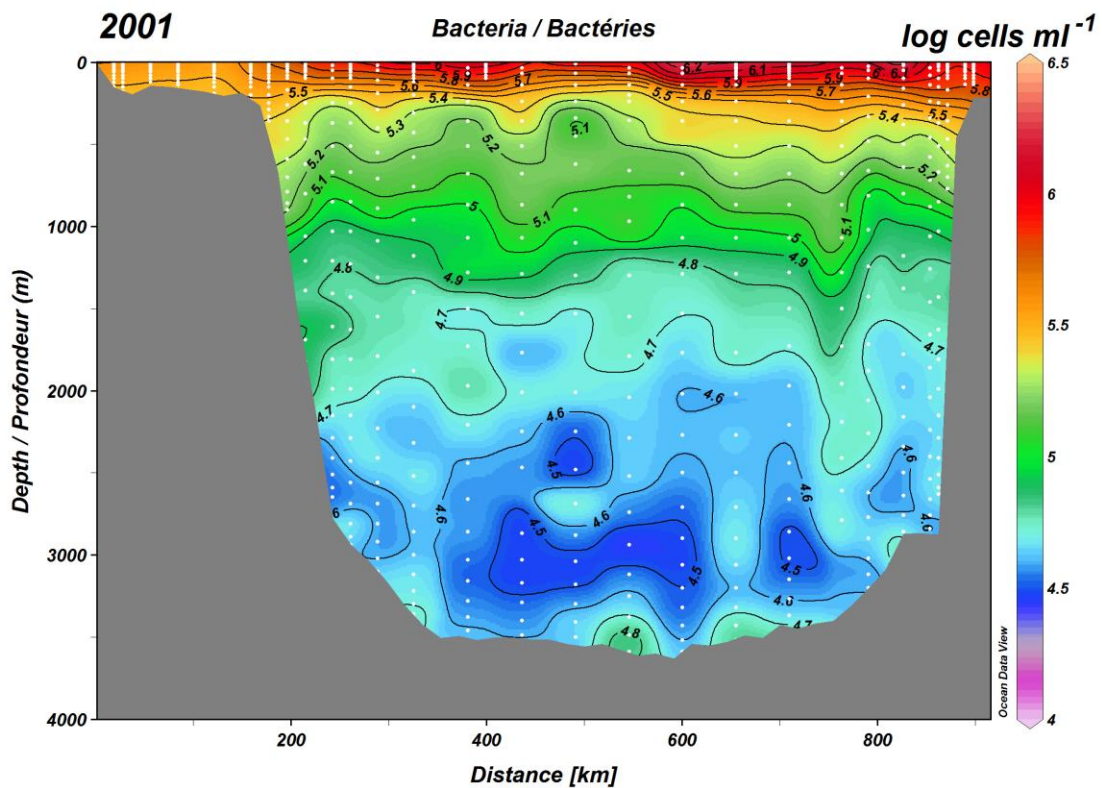


Figure 133

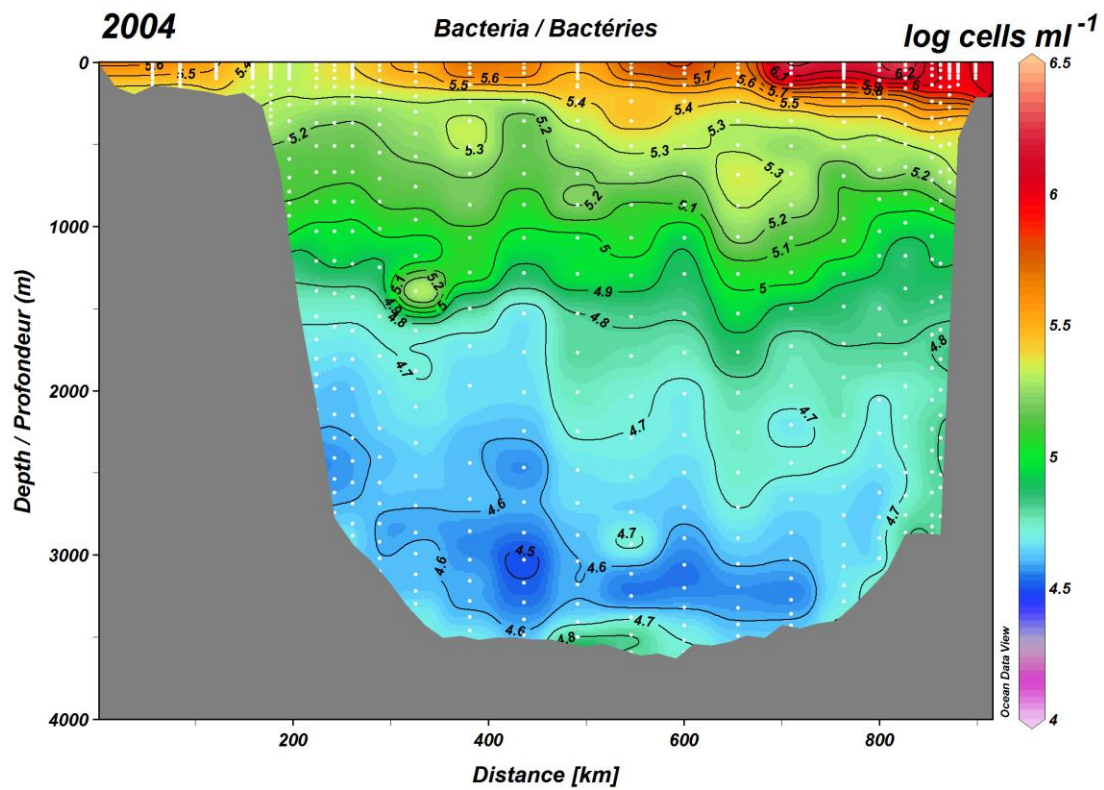
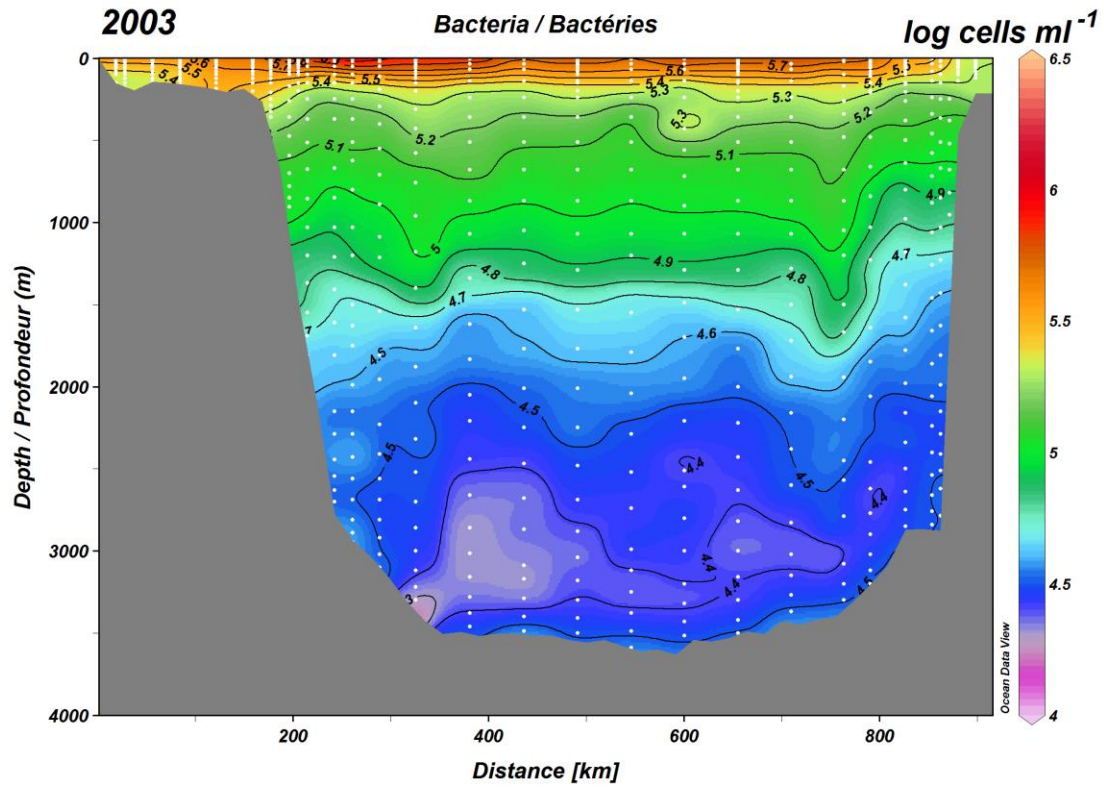


Figure 134

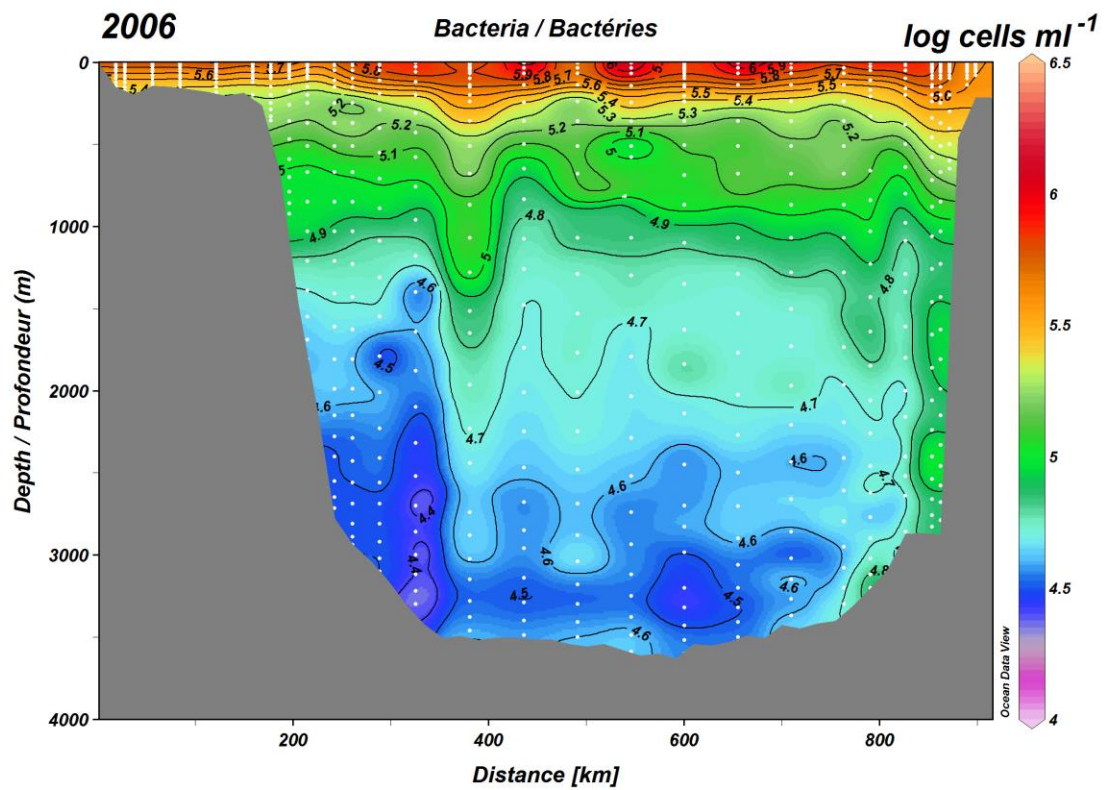
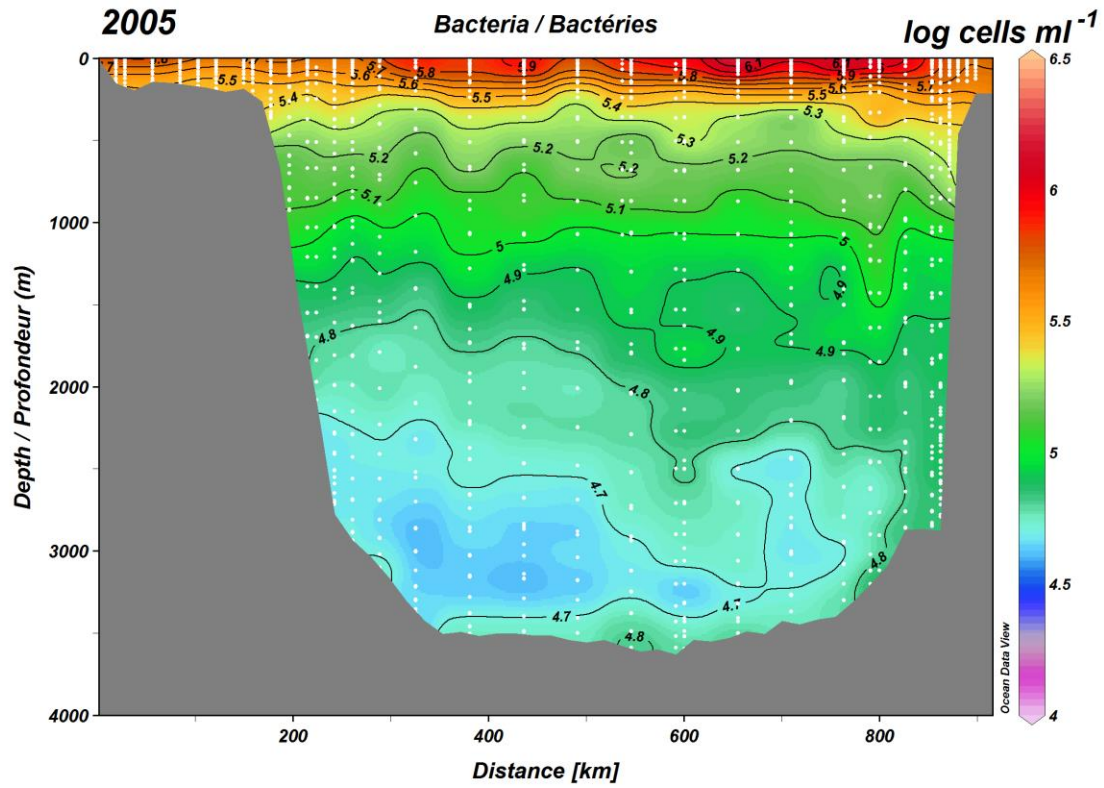




Figure 135

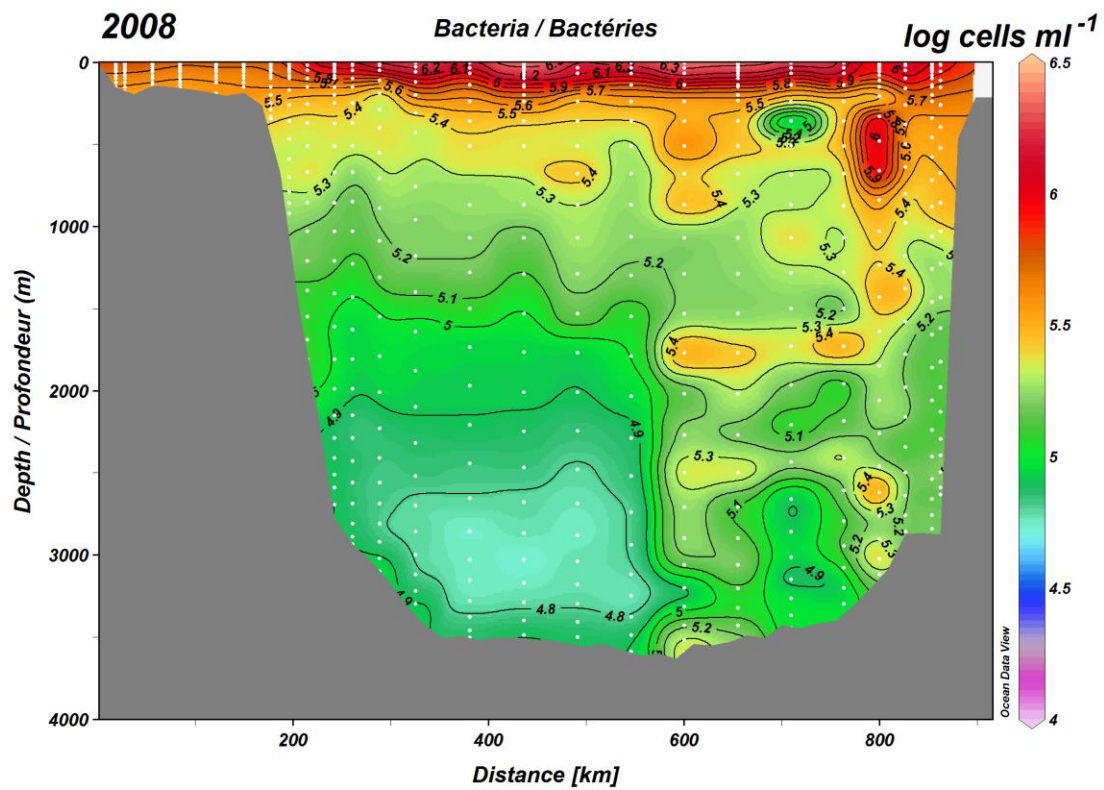
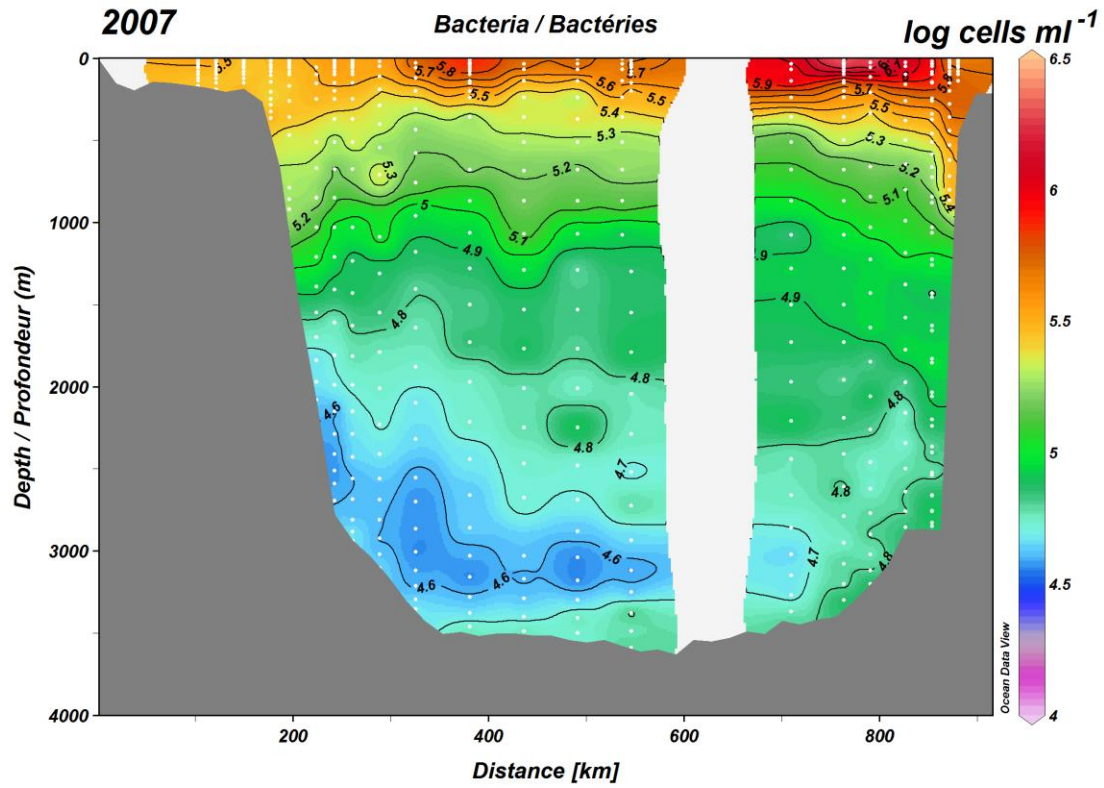


Figure 136

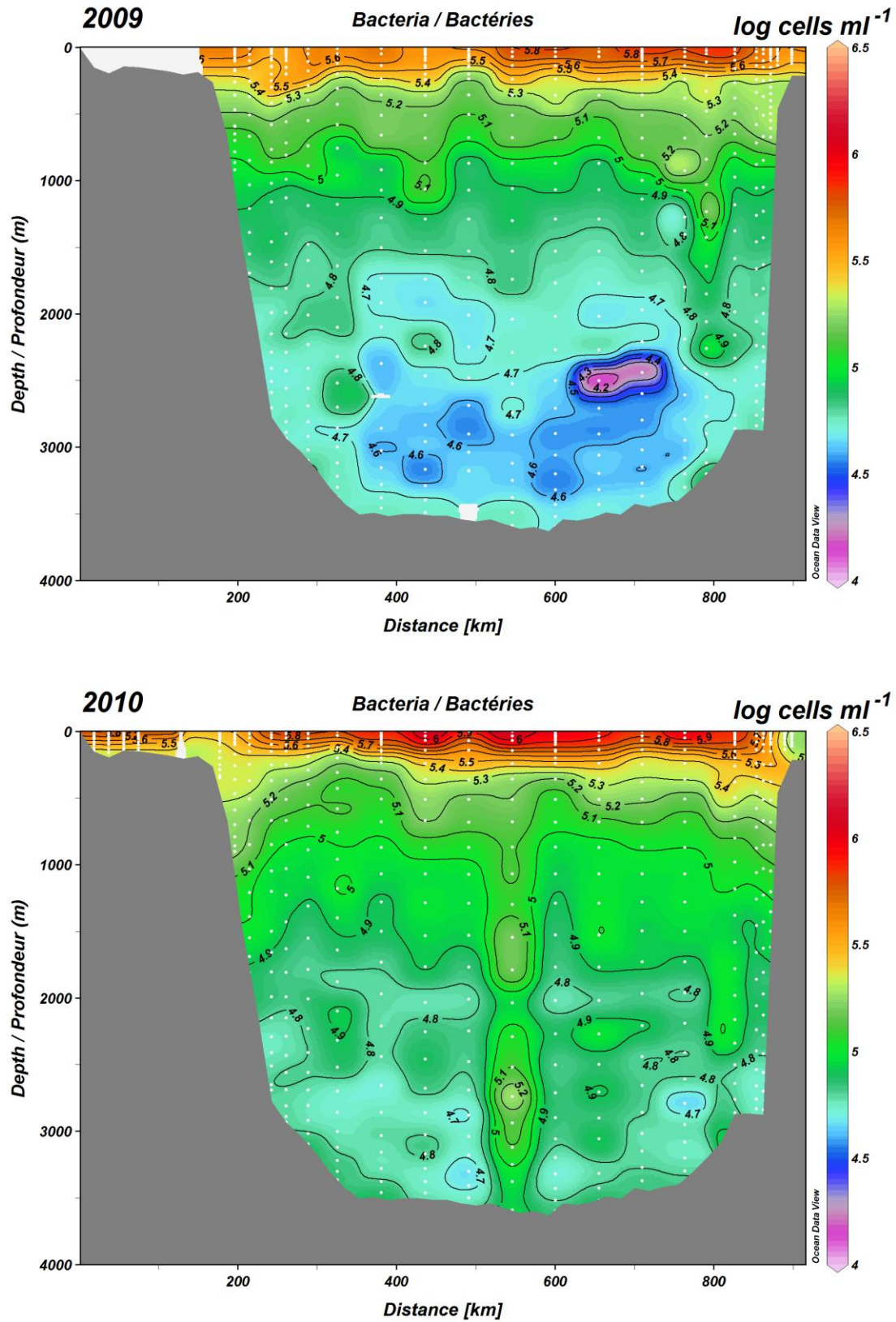




Figure 137

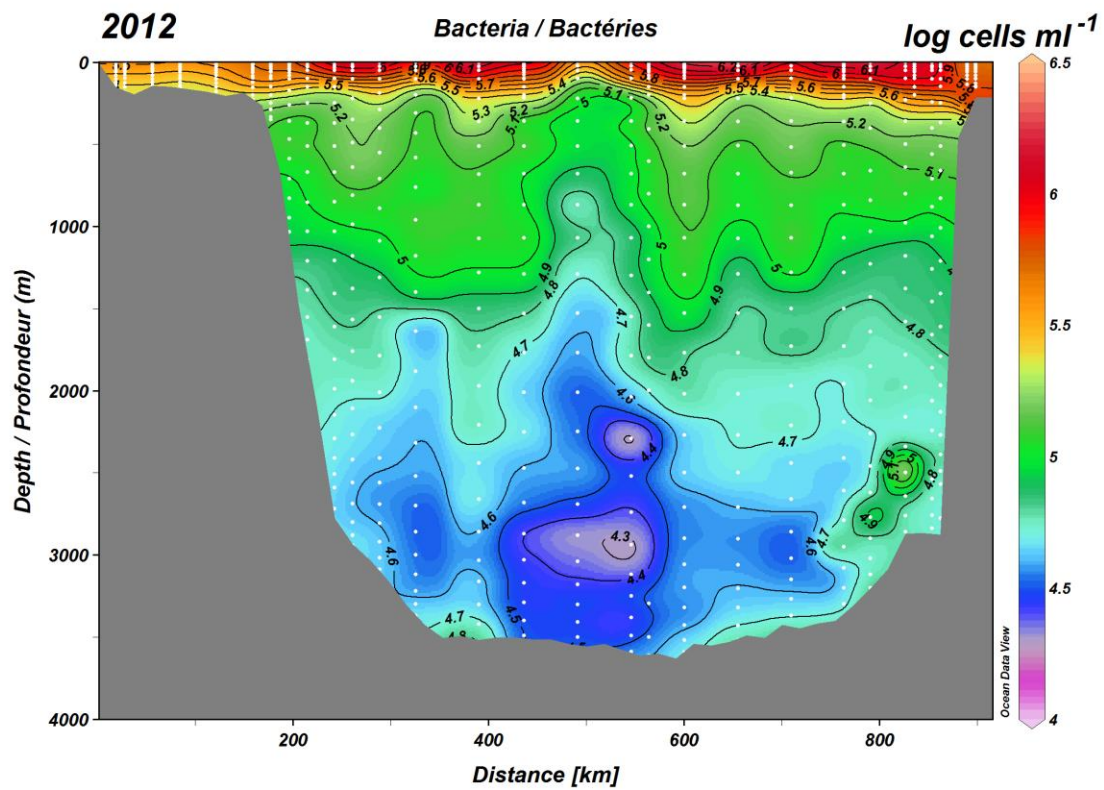
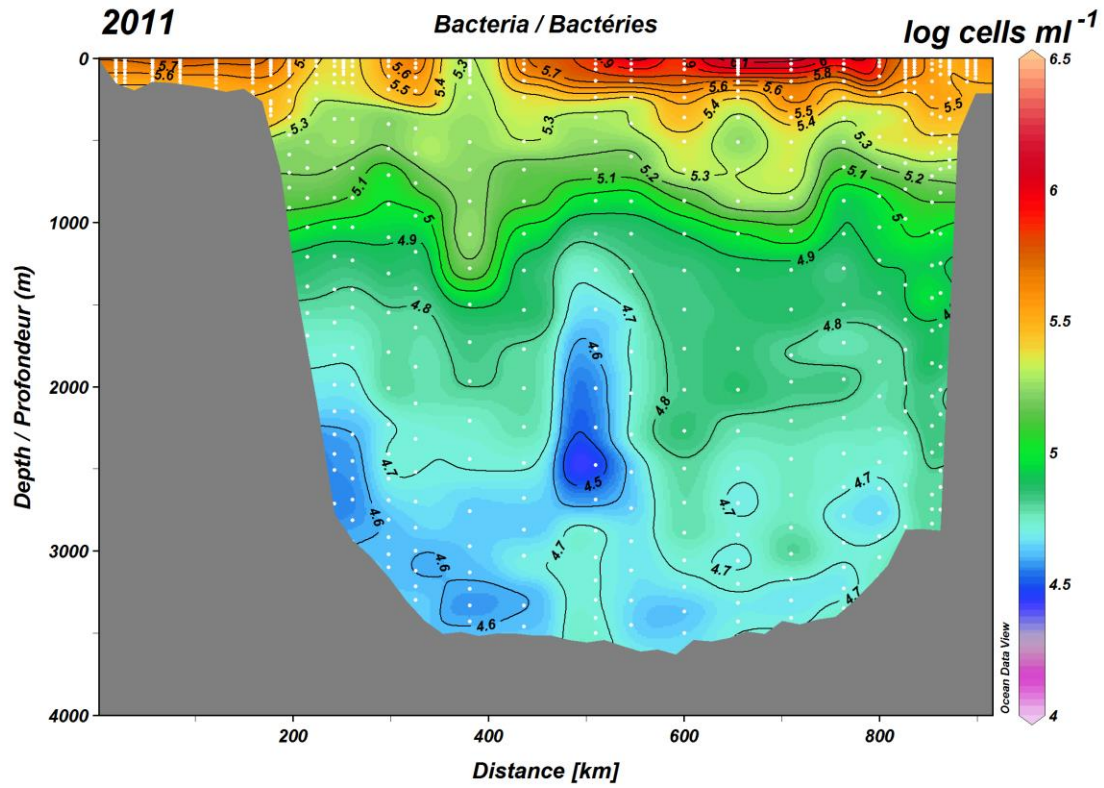


Figure 138

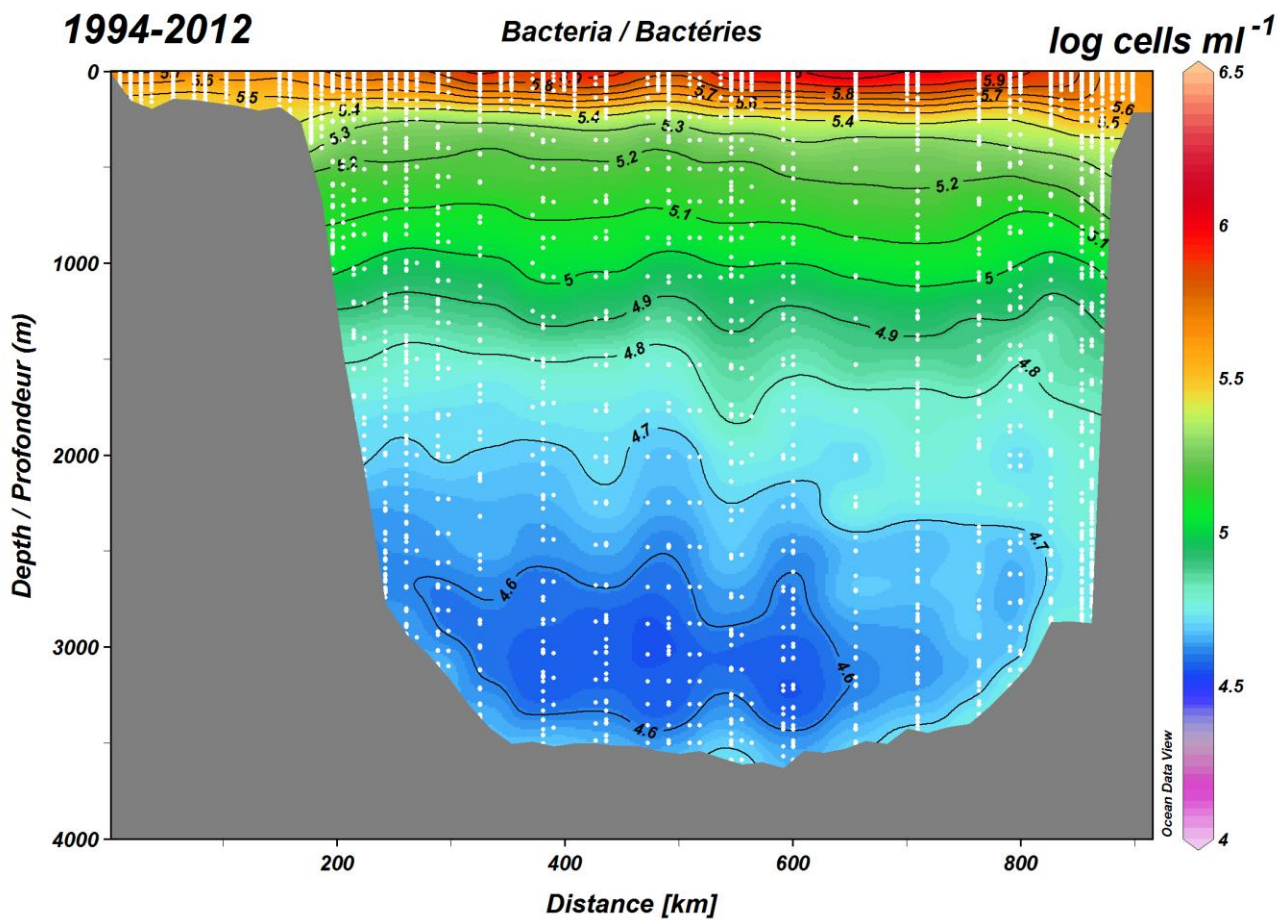


Figure 139

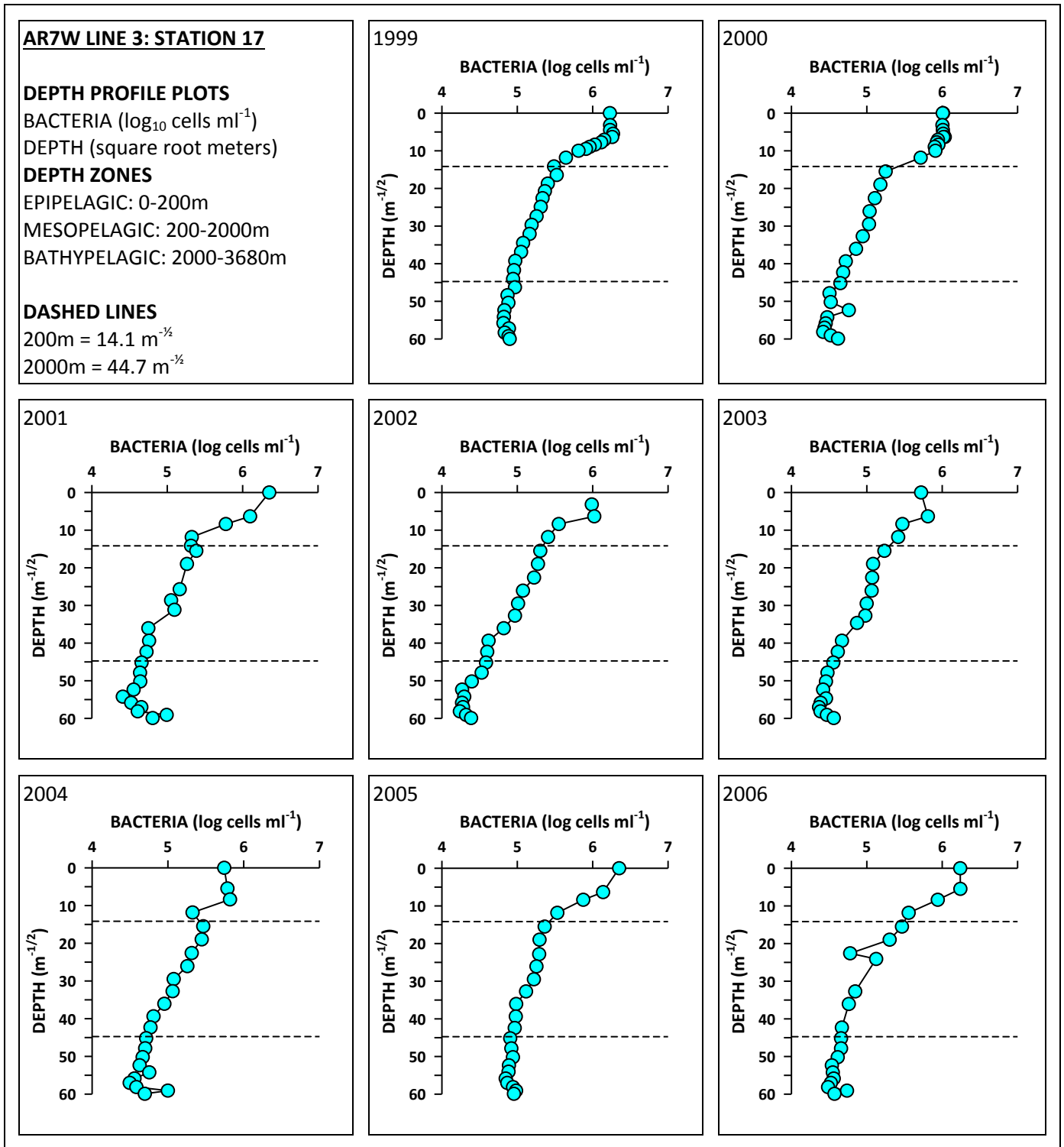




Figure 140

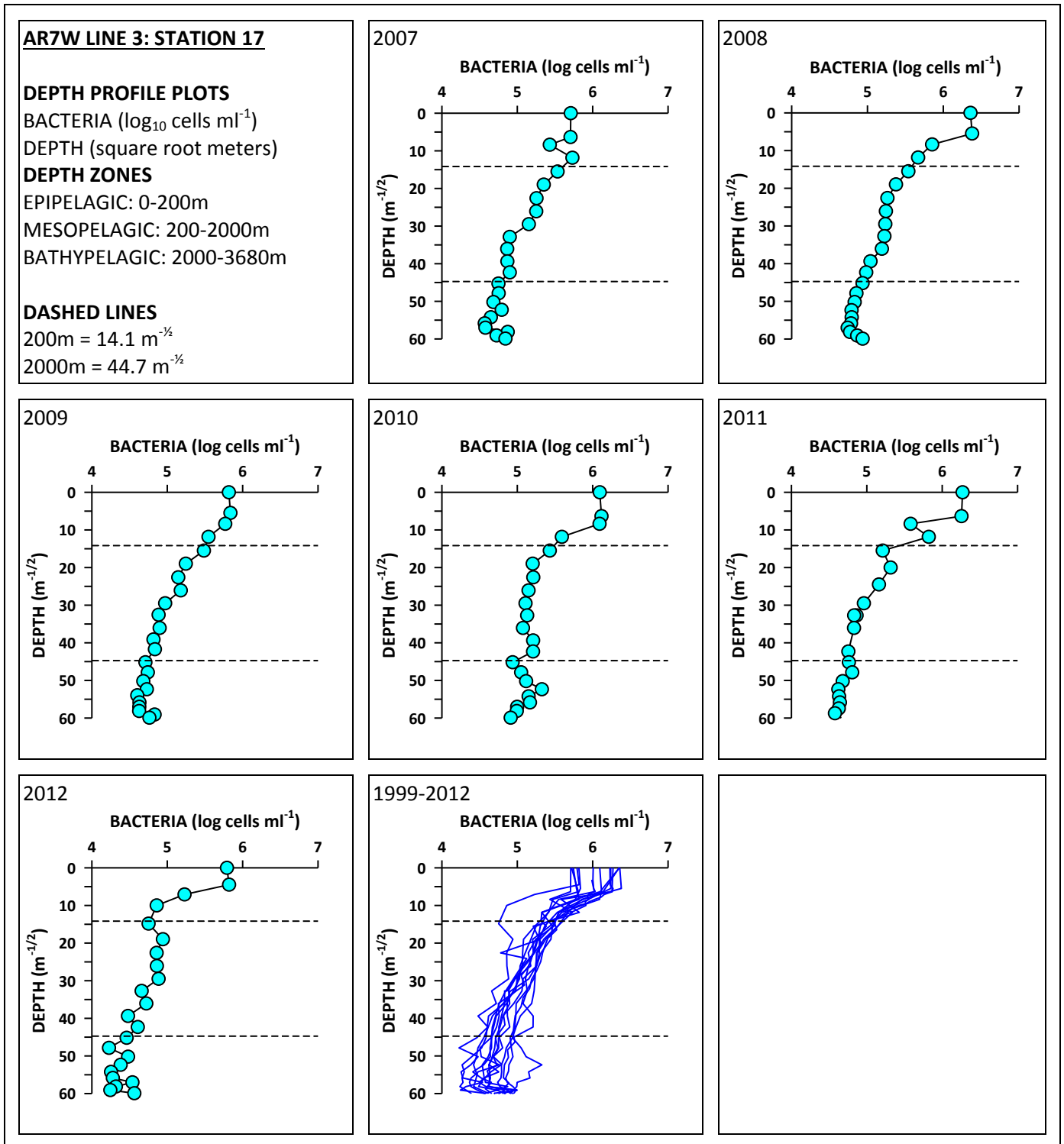


Figure 141

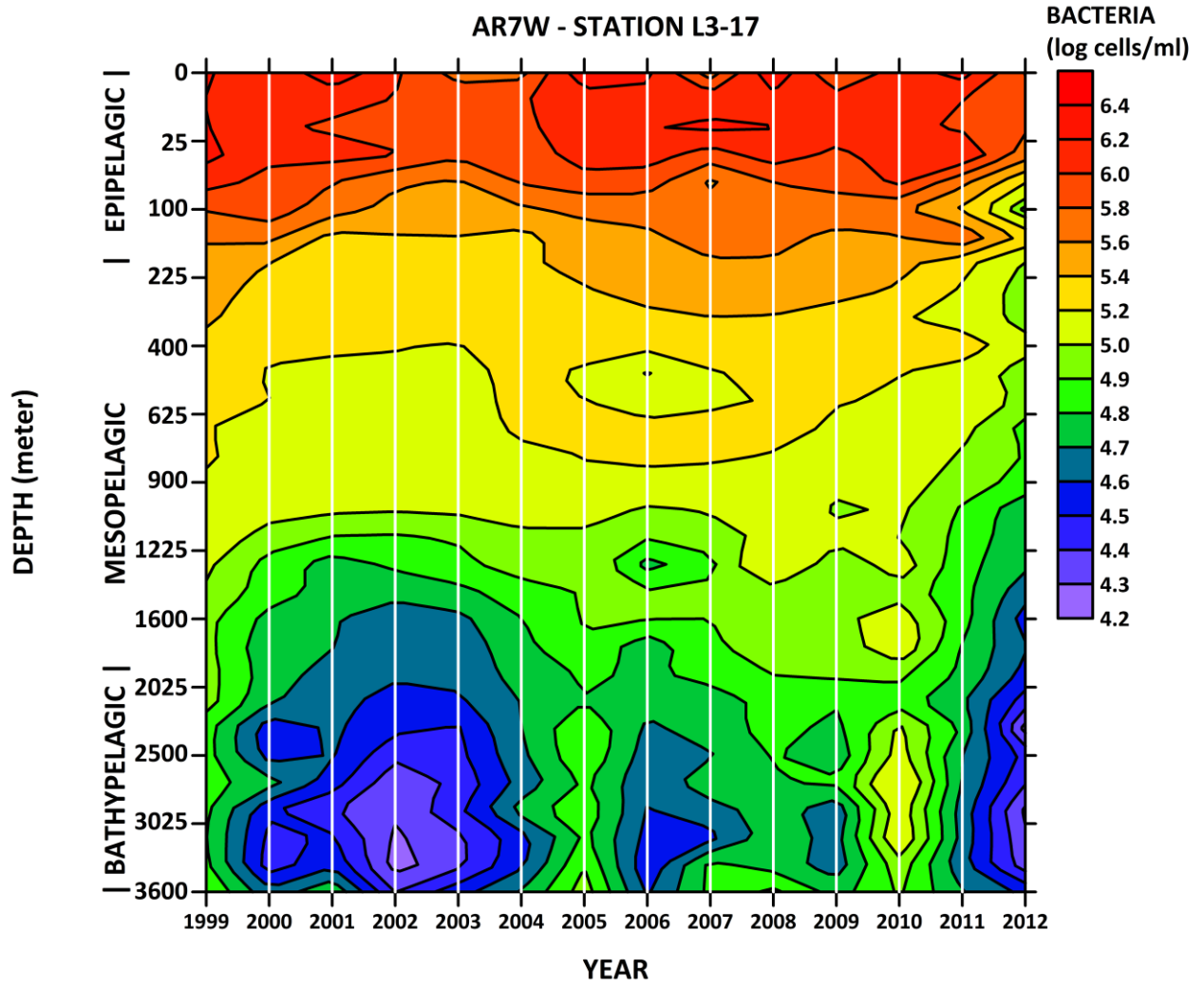


Figure 142

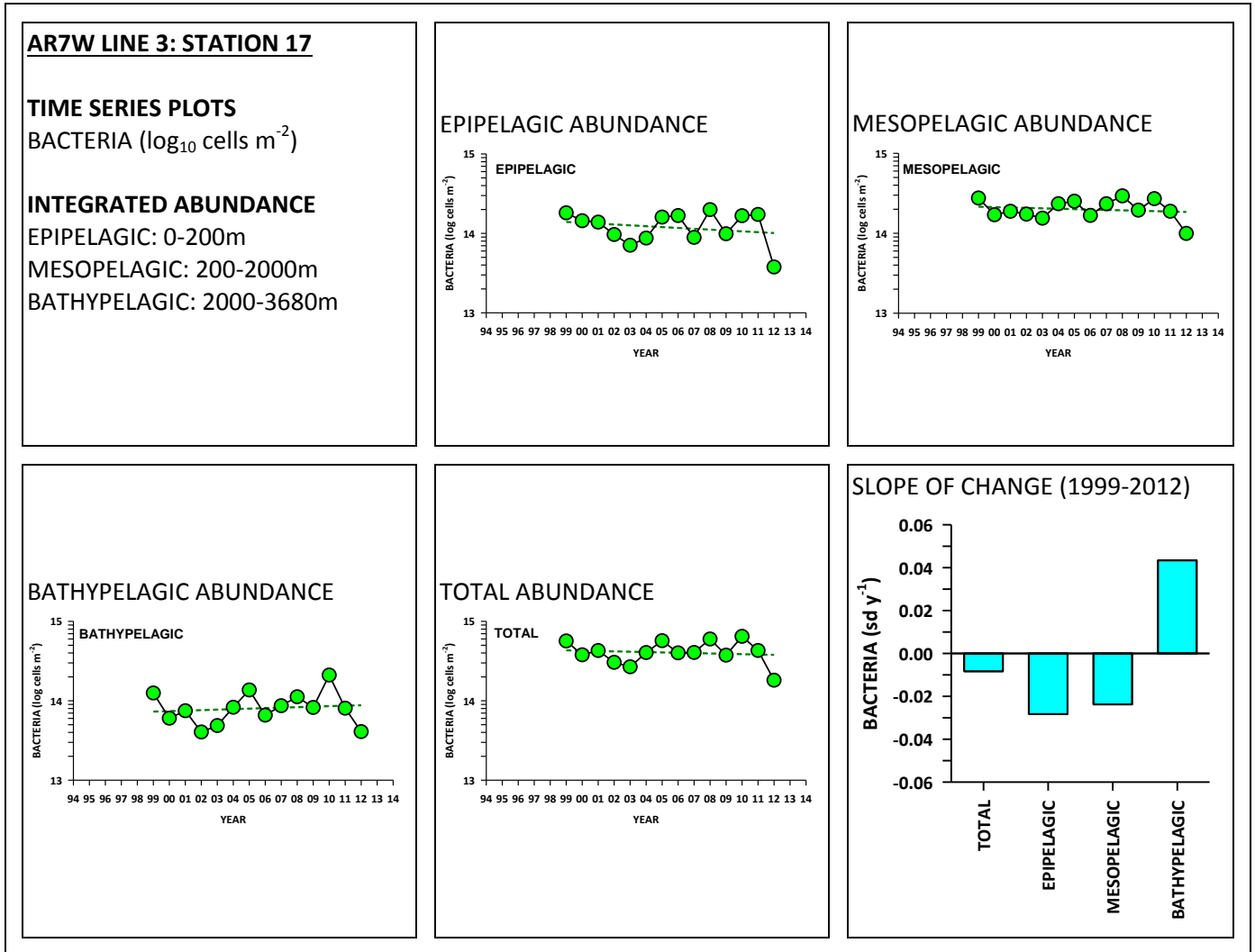


Figure 143

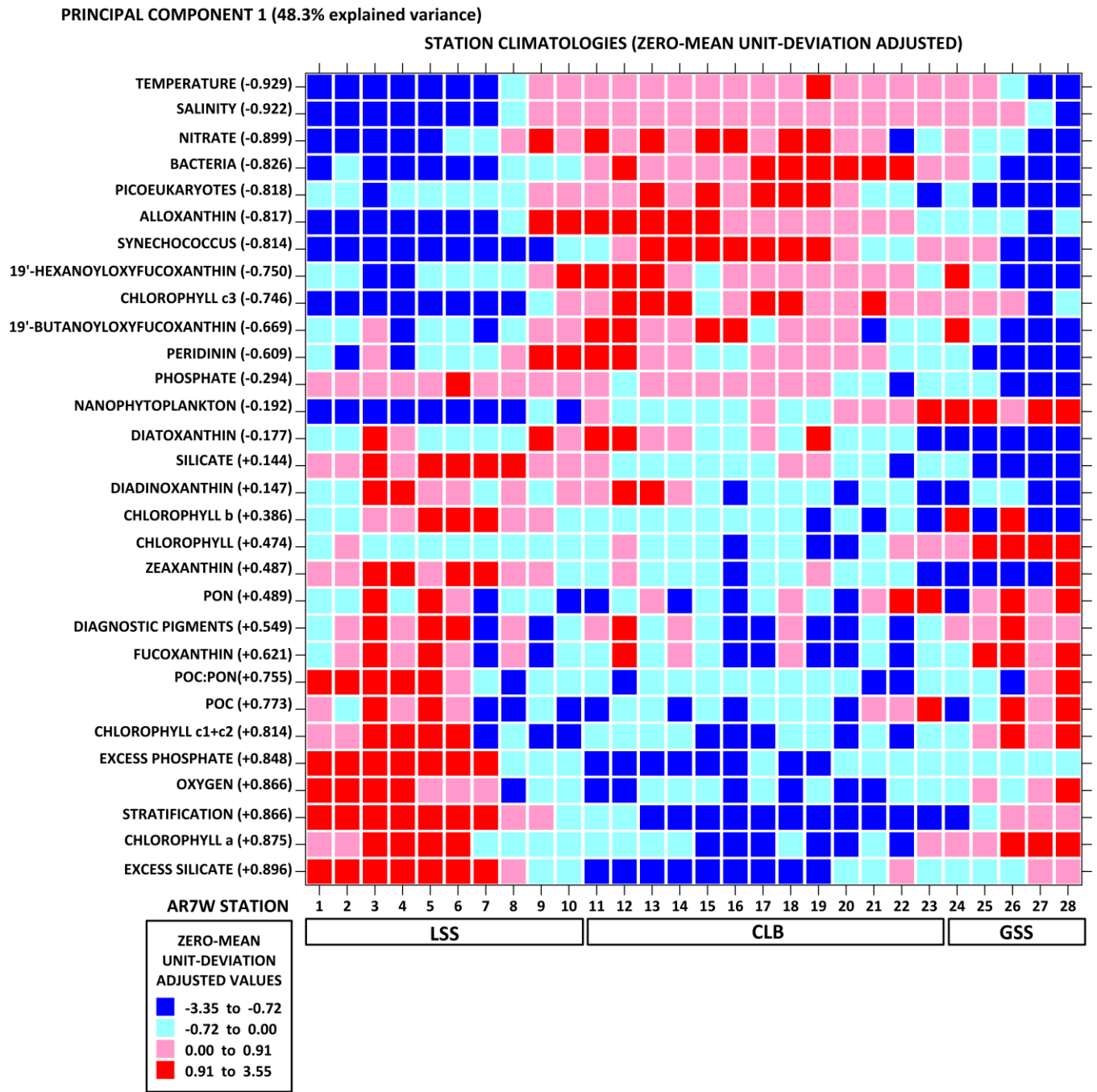


Figure 144

